Air pollution impacts on European forest soils: Steady-state and dynamic modelling

Gert Jan Reinds

Thesis committee

Thesis supervisor
Prof. Dr. R. Leemans
Professor of Environmental Systems Analysis
Wageningen University

Thesis co-supervisors
Dr. Ir. W. de Vries, Senior Scientist, Alterra, Wageningen UR
Dr. M. Posch, Senior Policy Researcher, Coordination Centre for Effects, PBL, Bilthoven

Other members
Prof. Dr. M. Forsius, Finnish Environment Institute, Helsinki, Finland
Prof. Dr. J. Aherne, Trent University, Canada
Prof. Dr. C.J.F. ter Braak, Wageningen University
Prof. Dr. J.W. Erisman, VU University, Amsterdam

This research was conducted under the auspices of the Wageningen Institute for Environment and Climate Research (WIMEK)

Air pollution impacts on European forest soils: Steady-state and dynamic modelling

Gert Jan Reinds

Gert Jan

Thesis
submitted in partial fulfilment of the requirements for the degree of doctor
at Wageningen University
by the authority of the Rector Magnificus
Prof. dr. M.J. Kropff,
in the presence of the
Thesis Committee appointed by the Doctorate Board
to be defended in public
on Wednesday 16 December 2009
at 11 AM in the Aula.

Gert Jan Reinds
Air pollution impacts on European forest soils:
Steady-state and dynamic modelling
223 pages

Thesis Wageningen University, Wageningen, NL (2009)
With references, with summaries in Dutch and English

ISBN 978-90-8585-520-0

Abstract

Reinds, G.J. 2009. Air pollution impacts on European forest soils: Steady-state and dynamic modelling. Thesis, Wageningen University and Research Centre, 223 pp.

This thesis describes the development, calibration, uncertainty analysis and application of a dynamic model for soil acidification, in combination with the use of comprehensive European environmental data sets. The model (VSD) was developed as a dynamic extension of the steady-state Simple Mass Balance (SMB) model that has been widely used to compute critical loads for Europe for sulphur (S) and nitrogen (N), i.e. depositions that do not cause harmful effects on ecosystems in the long-term. The VSD model was calibrated on 122 intensively monitored forest sites in Europe, using Bayesian calibration. Soil solution measurements were used to determine how well the model was able to reproduce field observations. The calibration improved the accuracy of the model when model results were compared with soil and soil solution measurements at 60 validation plots.

An uncertainty analysis was performed for critical loads and target loads (i.e. depositions that lead to a desired chemical soil status in a prescribed year) using the posterior parameter distributions from the calibration. Inputs of base cations (Bc) by weathering and deposition, and the parameters that determine the equilibrium between protons and aluminium (Al) in the soil solution mainly determined the uncertainty in critical loads for S. The uncertainty in critical loads for the eutrophying effect of N is caused by uncertainty in the N immobilisation and uptake.

Critical limits have a strong impact on critical loads. In an analysis for Europe and Northern Asia we showed that the use of a critical Acid Neutralizing Capacity (ANC) of zero would protect the ecosystems to both unfavourable Al concentrations as well as to high Al/Bc ratios. The use of a single critical limit for base saturation, suggested as an alternative for the criticised Al/Bc ratio, leads to unrealistic results. The concept of equivalent criteria, i.e. the values that need to be used for each of the criteria to obtain the same critical load function has proven valuable in judging the consequences of the use of different criteria.

Recovery of almost all acidified forest ecosystems in Europe can be achieved by 2050 if all currently available emission abatement technologies are used, but even with current policy plans violation of critical soil limits strongly declines in the future. More effort is needed to reduce the eutrophying effects of nitrogen. In our model simulations, climate change has a minor (generally positive) effect on recovery from acidification, and therefore current emission abatement policies need not be revised in view of climate change. The VSD model, however, was not

designed to incorporate all climate effects, so this conclusion should be substantiated by other more elaborate modelling studies.
The analysis of the data from the combined EU/UNECE Forest Intensive Monitoring programme has proven that these data support the parameterisation and use of a model which was specifically designed for policy relevant regional assessment.

Keywords: Acidification, forest soils, critical loads, target loads, dynamic modelling, climate change.

Preface

The first notes on this thesis date from May 2001. On the roof-terrace of a hotel in Rome, covered with fluorescent-green artificial grass and with a splendid view over the city, I noted down the first ideas on the content of this thesis in a small notebook. I made some notes on the title, which chapters it could contain and even wrote down a few propositions. Meanwhile, more than eight years have passed, the notebook has crumbled at the edges and the original planning of three to four years for writing this thesis has proven to be rather optimistic… There have been times when hardly anybody dared to ask if there was any progress. The title as well as the content of this thesis has changed several times during these eight years, but, remarkably, some of the initial propositions have remained unchanged.

A long-lasting process requires a supervisor with patience, and Rik Leemans turned out to be exactly that. Patient when there was little progress, but enthusiastic and supportive if, for example, comments on draft papers was required. Rik's pragmatic and constructive attitude has been of great help. His extensive knowledge of climate change strongly improved the last chapter in this thesis on the interaction between soil acidification and climate change.

As co-supervisor and colleague since almost two decades, Wim de Vries has contributed to the structure and contents of this thesis. During fruitful discussions with Wim, the content was shaped and the connection between the various chapters safeguarded. Many of the topics discussed in this thesis have their roots in research by Wim. His extensive knowledge of soil acidification has helped to solve many conceptual problems.

Max Posch of the Coordinating Centre for Effects (CCE) in Bilthoven has acted as second co-supervisor and strongly contributed to the contents of various chapters. The core of the VSD model that plays such an important role in this thesis, was developed by Max. His detailed comments on all chapters has certainly improved the text and eliminated, hopefully, even the smallest typos in the references. Much of the work and programming for the work described in this book took place during one of his numerous Friday-visits to Wageningen, often concluded with a diner at my place. Even though the thesis is finished now, I expect that we can continue our very pleasant collaboration and diners in the coming years.

I owe a special word of thanks to the one who initially was my supervisor for this thesis, Jean-Paul Hettelingh of the CCE. Even after he finished his professorship in

Leiden, Jean-Paul has always remained interested in this thesis, which covers topics within the working area of the CCE. Without the CCE this thesis could not have been written: a substantial part of the research was funded and supported by the CCE. I sincerely hope that we can continue our long-lasting cooperation.

Marcel van Oijen of CEH Edinburgh is gratefully acknowledged for his contribution to chapter 3. It was Marcel who put me on the track of Bayesian model calibration, which plays an important role in two chapters. Gerard Heuvelink has strengthened some chapters through his knowledge of (geo-) statistics. His prompt and valuable comments on chapter 4 have been very helpful. My colleague Hans Kros made valuable contributions to the chapters on the Bayesian calibration and uncertainty analysis.

My paranymphs, Janet Mol and Bert Jan Groenenberg have been my consecutive roommates at Staring Centre and Alterra during the last 20 years. As such, they strongly contributed to my well-being at work. Metaphorically, they represent both sections in my Alterra Soil Chemistry and Nature team. I also thank the other members of the team for creating and maintaining the very pleasant atmosphere and good cooperation within the team, which makes it such a wonderful group.

The cover of this thesis was designed in close (and very pleasant) cooperation with Martin Jansen.

The best supporter over the last eight years has been Cobi Izeboud. She never doubted that I would be able to finish this thesis. Such confidence has helped me through times when I wondered if I would be able to find the time and inspiration needed to write this book. Fortunately, my private life did not suffer much from the work for this thesis, so I need not apologize to my children Michiel en Ida for being absent as a father; most of the writing took place during working hours or the hours when they were asleep.

Contents

Contents

Introduction

Air pollution effects on forest ecosystems

Towards the end of the 1970s concern arose about forest decline in parts of central Europe (Ulrich et al., 1979; Ulrich and Pankrath, 1983). Some of the areas with reduced forest vitality coincided with areas that had high concentrations of air pollutants, such as sulphur dioxide. Initially, hypotheses were raised in which reduced forest vitality was attributed to air pollutants alone, mainly considered to be the result of the subsequent release of toxic aluminium by soil acidification (Ulrich, 1983; Hutchinson et al., 1986; Cronan et al., 1989). However, it soon became evident that a complex system of anthropogenic and natural stress factors as well as forest management determined the health of forest ecosystems (e.g. Schulze, 1990; Landmann, 1995). Only in areas with very high pollutant concentrations, direct effects on forest health were observed in the form of damage to needles and leaf tissue and increased needle shedding (e.g. Smith, 1981; Kukkola et al., 1997; Lamppu and Huttunen, 2001).

It is now widely accepted that high input of sulphur and nitrogen leads to soil acidification in forests that is much more rapid than under natural conditions (Van Breemen et al., 1983; Van Breemen et al., 1984; De Vries and Breeuwsma, 1986; De Vries and Breeuwsma, 1987). Acidification of acid sensitive soils with a low base saturation leads to the release of aluminium in the soil solution (Mulder et al., 1987; De Vries et al., 1995). There is strong evidence that leaching of aluminium from soils due to acidification has lead to widespread acidification of streams and lakes in (especially) northern Europe where sensitive organisms, such as salmonids, have been lost (Jensen and Snekvik, 1972; Dickson, 1978; Overrein et al., 1980). Laboratory experiments showed that aluminium can also be toxic to tree roots (Rost-Siebert, 1983; Van Scholl et al., 2004) but field evidence on the effects of aluminium on forest vitality or forest growth in mature forest stands is often lacking (De Wit et al., 2001; Göransson and Eldhuset, 2001; Nyberg et al., 2001; Nygaard and De Wit, 2004). Nevertheless, a critical aluminium to base cation ratio (Al/Bc) has become one of the basic concepts for defining thresholds for acid inputs in many countries.

Apart from acidification, the elevated input of nitrogen may have various other negative effects on natural ecosystems (Bobbink et al., 2002; De Vries et al., 2007a; De Vries et al., 2009). In forests, excess N input can lead to nutrient imbalances and relative phosphorus and base cation deficiencies in foliage, of which Mg deficiency is mentioned most often (Roberts et al., 1989). This deficiency can be caused by competition between base cations and phosphorus in soil solution on the one hand and ammonia on the other hand (Roelofs et al., 1985; Boxman et al., 1986) or because of the toxic effects of aluminium on tree roots leading to decreased base

cation uptake (Hutchinson et al., 1986; Cronan et al., 1989). Excess nitrogen input may also influence macrofungi and mycorrhiza in the forest soil that play in important role in nutrient uptake. Elevated nitrogen input to forests can also affect the species composition of the ground vegetation, leading to an increased abundance of nitrophilous and acid-tolerant species. Changes in forest ground vegetation towards nitrophilous species have been observed in many European countries with significant N inputs such as the Netherlands, Sweden, Germany, Switzerland, Belgium and France (Falkengren-Grerup, 1986; Kuhn et al., 1987; Dirkse and Van Dobben, 1989; Thimonier et al., 1992; Lameire et al., 2000; Kraft et al., 2003). Long periods of elevated N input can lead to nitrogen saturation in forest ecosystems, and to increased nitrate leaching as observed on a number of experimental sites (Aber et al., 1989; Gundersen et al., 2006). Increased N leaching, in turn, can cause stream-water acidification and eutrophication (Bergström and Jansson, 2006). Analysis of European datasets from monitoring plots revealed that there is a strong correlation between N input and N leaching (Gundersen et al., 2006; De Vries et al., 2007b; Dise et al., 2009).

Generally it is assumed that the increase in nitrogen deposition has also lead to an increased forest growth in those regions in Europe where N was the limiting factor (Spiecker et al., 1996; Rehfuess et al., 1999). There is evidence from long-term N addition experiments in N-limited sites that elevated N inputs leads to increased stem volume increment, but that above an optimum value growth will decrease (Tamm et al., 1995; Högberg et al., 2006). At very high N inputs N contents in needles increases and stem volume growth can decline (Magill et al., 2004; Högberg et al., 2006). Current hypotheses also suggest that N deposition may lead to an augmented C and N fixation in the soil, through increased litterfall resulting from growth increase and because of reduced decomposition of old organic matter (Berg and Matzner, 1997). Nitrogen deposition may thus lead to a higher C sequestration in forest ecosystems and thus increase the CO_2 sink. The evidence for reduced decomposition of organic matter is, however, not conclusive as also increased mineralisation with increasing N content has been observed (e.g. Vesterdal, 1999; Lorenz et al., 2004) as well as no effect at all (Melillo et al., 1982; Murphy et al., 1998). Whether the increase in C sequestration due to increased N deposition is significant compared to effects of increased temperature, changes in forest management or aging processes in general, is subject to research and discussion (Nadelhoffer et al., 1999; De Vries et al., 2006; Magnani et al., 2007; De Vries et al., 2008).

As a result of the observed relationship between air pollution and acidification of soils and waters, in 1979 the United Nations Economic Commission for Europe (UNECE) initiated the Convention on Long-range Transboundary Air Pollution

(LRTAP). Under this convention a number of working groups were established, to investigate all relevant aspects of air pollution and its effects on ecosystems, crops, human health and materials; each of the working groups has an associated 'International Cooperative Programme' (ICP) (Bull et al., 2001). Under the Working Group of Effects (WGE), the ICP on Modelling and Mapping of Critical Levels and Loads and Air Pollution Effects (ICP M&M) is responsible, inter alia, for the assessment of regional critical loads. Critical loads are the maximum tolerable inputs of sulphur and nitrogen that, on an infinite time scale and according to current knowledge, will not lead to significant harmful effects on the ecosystem (Nilsson and Grennfelt, 1988). Critical loads for acidity are commonly modelled with a simple mass balance (SMB) model (Sverdrup and De Vries, 1994). Critical loads for nutrient nitrogen can be computed with SMB as well, but have also been derived from N addition experiments in the field (empirical critical loads).

Models for critical loads and scenario evaluation; the ICP Modelling and Mapping

The major aim of the ICP M&M is to develop methodologies and databases of maximum allowable deposition levels (i.e. critical loads) of sulphur and nitrogen that are used in the assessment of cost-effective emission-abatement alternatives in support of European policies to curb air pollution (Gregor et al., 2001). The first Sulphur Protocol was signed in 1985 and aimed at a flat rate reduction of at least 30% in sulphur emissions by 1993 compared to 1980, for all countries under the Convention. A flat-rate reduction of sulphur emissions is not the most cost-effective way to abate air-pollution. Reducing sulphur input to areas with soils not sensitive to acidification, for example, cannot be considered very efficient. The same is true for carrying out high-cost emission reductions in a country where many technologies have already been implemented, compared to low-cost reductions in an adjacent country using old-fashioned coal burning technology producing high emissions. In the NO_x Protocol of 1988, it is therefore stated that the parties to the convention for future N-emission reductions should take "into account the best available scientific and technological developments, internationally accepted critical loads and other elements resulting from the work programme undertaken…". It is also stated that the parties shall "develop, in the context of an approach based on critical loads, methods to integrate scientific, technical and economic data in order to determine appropriate control strategies."
Following these obligations laid down in the 1988 NO_x Protocol, the 1994 Protocol on further abatement of Sulphur was the first protocol based on computations that

provided the most cost-effective measures based on ecosystem vulnerability (expressed by critical loads) and emission abatement costs, optimized in an European framework. It aimed at a 60% closure of the gap between deposition in 1994 and the critical load by the year 2000 (2010 for some countries). In 1999 the so-called multi-effect multi-pollutant protocol (also known as the Gothenburg Protocol) was signed that included sulphur (S), nitrogen oxides (NO_x), ammonia (NH_3) and volatile organic compounds (VOCs). At the European Union (EU) level, national emission ceilings (NEC) have been defined to abate air pollution. These levels agreed upon by the EU countries are close to the ones resulting from the Gothenburg protocol.

The emission reduction protocols have been successful: compared to 1980, the emissions in 2010 in Europe of SO_x under the Gotherburg protocol will be reduced by more than 60%, emissions of NO_x by about 40% and those of ammonia by 17% (EMEP 2004, see Figure 1).

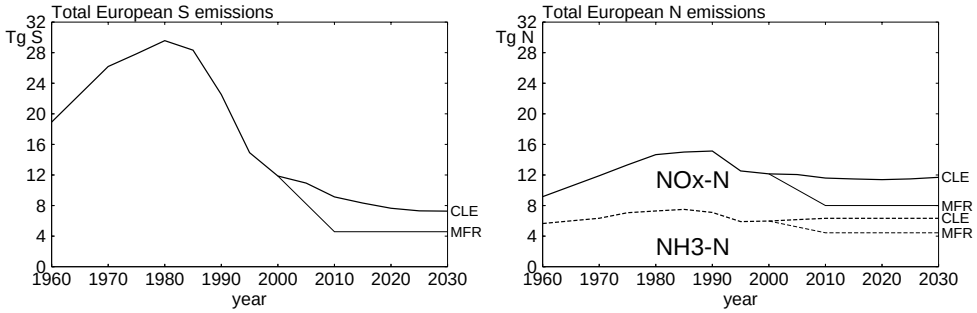

Figure 1. Emission histories and scenarios for S, NO_x and NH_3; CLE=Current Legislation (Gothenburg protocol), MFR = Maximum Feasible Reductions with current abatement technologies (from Reinds et al. (2009)

Although critical loads give the maximum allowable deposition that, on an infinite time scale, protects an ecosystem, it does not provide information on the time development of pollution induced stress and its effects on the ecosystem. Furthermore, if a critical load is currently exceeded (or was exceeded in the past), neither the critical load nor its excess can be used to estimate the time delay before a criterion, i.e. the critical value of a geochemical indicator associated to a biological effect, is violated (e.g. the Al/Bc ratio in the soil solution). Nor can one estimate from the critical load the time delay to geochemical recovery if deposition is reduced to or below the critical load (Posch et al., 2003). Therefore, interest has nowadays shifted from critical loads alone towards the use of dynamic acidification models for soils and surface waters, that are capable of simulating the

change in time of the chemical ecosystem status as a function of changing deposition (Grennfelt et al., 2001; Posch et al., 2003). Models that can simulate dynamics in soil (solution) chemistry as a function of atmospheric deposition have been developed over the last decades, and range from complex models for site applications such as ForSVA (Arp and Oja, 1997) and NUCSAM (Groenenberg et al., 1995) to simpler models designed for applications on a regional scale, such as SMART (De Vries et al., 1989; Posch et al., 1993) and SAFE (Warfvinge et al., 1993) for terrestrial ecosystem and the MAGIC model (Cosby et al., 1985a; Cosby et al., 2001) for stream water chemistry. To have a model that is fully compatible with critical loads, the VSD model was developed (Posch and Reinds, 2009) that extends the SMB model by incorporating cation exchange and time-dependent N immobilization. The VSD model requires a minimum set of input data and is designed for application on the European and continental scale. It is capable of simulating the effects of critical load exceedances in terms of time delays to 'damage' (exceeding the critical value of a geochemical indicator) and, in the case of sufficient deposition reduction, to 'recovery' (reducing a geochemical indicator to its critical value) and can be used to set deposition targets for the short to medium term, called target loads. To calibrate and test such model, data on the chemical response of forest soils to acid deposition are a prerequisite. Such data can be obtained from forest soil monitoring programmes such as performed within the EU/UN context.

Forest monitoring data: EU/ICP Forests monitoring

The ICP Forests is responsible for the large-scale monitoring of forest condition in Europe and for intensive monitoring aimed at finding cause-effect relationships between environmental factors and forest condition. Defoliation (leaf/needle loss) and discolouration have been monitored since 1986 on a systematic 16×16 km grid over Europe on a total of about 6000-7000 plots (Müller-Edzards et al., 1997; Lorenz et al., 2008). These plots are referred to as 'Level I' plots within the ICP-Forests. From 1986/87 to 1991 forest monitoring at Level I was carried out and reported parallel to the identical forest health monitoring carried out under the umbrella of the EU scheme on the protection of the Community's forests against atmospheric pollution (Council Regulation Nº. (EEC) 3528/86). Since 1992, a joint EU/ICP-Forest annual report has been produced. In 1995 a survey of soil condition was also carried out at the majority of the plots (Van Mechelen et al., 1997) and an analysis of the chemical condition of the foliage at about 10-15% of the plots (Stefan et al., 1997). It became evident that the yearly inventory of forest health in Europe

provided information on the geographical patterns of forest damage and their time-trends, but did not reveal any causes of forest damage nor provided insight in the relationship between air pollution and forest health. It was therefore decided to establish a second level ('Level II') of forest monitoring. This Intensive Monitoring programme consists of about 800 plots in Europe and is carried out as a joint UNECE/EU effort. It comprises a more intensive monitoring of ecosystems to provide insight into cause-effect relationships between air pollution and other natural and anthropogenic stress factors on the one hand and the health of the forest ecosystems on the other hand. Initially, surveys were carried out on crown condition, soil and foliar chemistry and forest growth on all plots, and on deposition and soil solution chemistry at part of the plots. Later, optional surveys on meteorology, ground vegetation and ambient air quality were added to the programme (De Vries et al., 2003d). At about 200 of the Intensive Monitoring plots both the input of acid deposition as well as the soil solution composition is measured on bi-weekly or monthly basis (De Vries et al., 2003c). These plots are thus very suitable for calibrating parameters used in the critical load- and dynamic models, because measured effects of (changes in) acid deposition on soil solution concentrations are available.

Problem description

To support the air pollution policy in Europe, use is made of critical loads supplied by National Focal Centres. Critical loads for acidity are normally computed using steady-state models, while critical loads for nitrogen as a nutrient can also be derived from experimental data (empirical critical loads). Dynamic models are used to evaluate the effectiveness of emission reduction plans. These models are mostly applied to large sets of computational units (receptors; being combinations of, for example, soil, climate and vegetation) and use regionalized (generalized) data that stem from national surveys or data that are directly taken from literature or maps (Posch et al., 1995; Posch and Hettelingh, 2001; Hetteling et al., 2008). This means that the resultant critical loads contain a substantial uncertainty.
In a way these uncertainties are inevitable since there is a trade-off between accuracy of the process descriptions and associated parameterisation of the critical loads equations and their regional applicability. Because critical loads should be computed for all relevant ecosystems in a country, a large number of computation units (for some countries more than 100000) is needed to accurately represent the geographical variation of ecosystems in a country. If one only uses receptors for which accurate, site specific data are available, it will be very difficult to get a

proper representation of the regional variability of ecosystems in a country. Assigning generic model parameter values, as is the common approach up to now, has a strong disadvantage as it neglects the available information from monitoring programmes such as the intensive monitoring of ICP Forests. The challenge is to make use of forest monitoring data, while maintaining a sufficient number of computational units for regional-scale critical load calculations.

Objectives and methodology

The main objective of this thesis was to assess critical loads and target loads of nitrogen and sulphur for Europe, using forest monitoring data to calibrate a dynamic soil model and to quantify and reduce uncertainties. In this thesis the Very Simple Dynamic (VSD) soil acidification model (Posch and Reinds, 2009) was used to evaluate the impacts of air pollution. We assessed the uncertainty in the model parameters through a Bayesian calibration of VSD using data from European monitoring sites, and subsequently used this information to assess the uncertainty in the model results. Apart from this main objective, we also investigated the impact of the use of different chemical criteria on critical loads and the likely impact of climate change on the recovery from acidification, relative to the effects of reduced nitrogen and sulphur inputs. The various approaches used are described in more detail below.

Calibrate a simple acidification model and quantify the parameter uncertainty.
Although there is no way to directly calibrate critical load models because their result is a value for the infinite time scale, one can calibrate (part of) the processes contained in the model. We calibrated VSD using data from the Intensive Monitoring programme as input to the model. Some model parameters can be derived directly from the measurements at the site (e.g. soil parameters such as organic matter content and cation exchange capacity) while other parameters, such as the aluminium solubility constant and weathering rate, can be derived from measured soil solution and deposition data using calibration. The VSD model in its dynamic mode was calibrated using a method based on Bayes' Theorem. In this Bayesian calibration a set of input parameters was sampled from a priori assumed probability distributions of these parameters by stepping through this parameter space. The model was run for each visited point and the likelihood was computed by comparing model output with measurements. If, for a new point, the product of prior probability and likelihood exceeded that of the previous point, the new point was accepted. If the ratio of new and current products of the prior and likelihood

was between 0 and 1, the new point was accepted with a probability equal to that ratio. If the candidate point was not accepted, the previous point was duplicated in the chain of accepted points. In the end, the calibration procedure provided updated probability distribution functions of the input parameters based on the array of accepted input parameters.

Quantify the uncertainties in critical loads and target loads that stem from parameter uncertainty.
After Bayesian calibration of VSD, an uncertainty assessment was made using a Monte Carlo approach. The uncertainty in the model output was determined by sampling from the posterior parameter distributions, being the most realistic estimates of model parameters at the site, and running the model many times. Results of this analysis were compared to an application of the model using values for model parameters from literature and manuals. This reveals how essential the model calibration is to obtain accurate model results.

Quantify how the chemical criterion affects critical load magnitudes.
Apart from uncertainty in data, the uncertainty in critical loads is determined by model simplification, uncertainty in process descriptions and by the chemical criterion used. Most countries use a maximum allowable aluminium to base cation ratio in the soil solution as the basis for the critical loads of S and N. Some countries however, computed loads using different criteria such as zero depletion of the aluminium buffer pool, limits for the Acid Neutralizing Capacity or a maximum aluminium concentration in the soil solution. Use of different criteria may lead to very different critical loads, and add to the uncertainty. To quantify the uncertainty in critical loads that stems from the use of different criteria, an analysis with VSD in its static mode was made for entire Europe and Northern Asia. We analysed the effects of different criteria on the critical loads for the most sensitive ecosystems in a grid cell (normally the 5^{th} percentile critical load). Using these 5^{th} percentile critical loads is relevant as they are used in optimizations of air pollution control in the integrated assessment process.

Evaluate the effect of climate change on future recovery from acidification in European forests.
In the critical load and steady models, climate is assumed to be constant. Given the current state of knowledge about climate change, this is not a realistic assumption. To date, all studies that dynamically evaluate recovery from acidification on a European scale also assume a constant future climate. It is recognized however, that climate change may influence the effects of emission reductions on the soil

chemical status. For surface waters the influence of climate change on water chemistry has been studied in a number of countries (Wright et al., 2006; Posch et al., 2008), but for terrestrial ecosystem such an analysis is lacking. We have carried out a European-wide application of VSD for forests to determine the relative importance of deposition reductions and climate change on the recovery of the forests from their acidified state. We modelled soil solution chemistry for the period 1990-2050 for given deposition and climate scenarios (scenario analysis), investigated possibilities for forests to recover within a certain time-period using deposition targets (i.e. target loads) and determined the time-delay in recovery from an acidified state for given scenarios (recovery times).

Outline of this thesis

This thesis follows the objectives and methodologies described above. A schematic overview of the outline of the thesis and the relations between the chapters is provided in Figure 2.

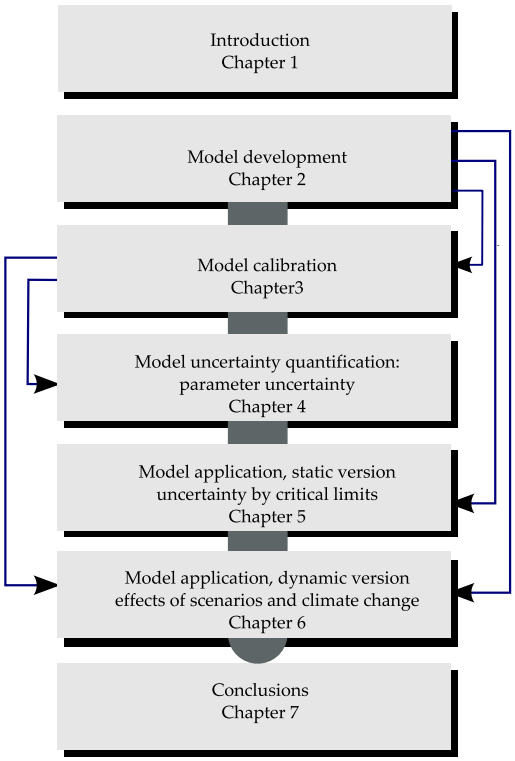

Figure 2 The structure of the thesis and the interactions between the different analyses

Chapter 2 provides a description of the Very Simple Dynamic model for soil acidification that is used throughout the chapters. It describes the process descriptions included in VSD and illustrates its functionality: not only scenario analysis, but also the computation of critical loads, target loads and delay times. Chapter 3 outlines an innovative Bayesian calibration of VSD on data from monitoring sites in Europe. The calibration method is described as well as the results. The results are illustrated using, for example, differences in model error before and after calibration and the differences between a priori assumed parameter distributions and posterior distributions. In chapter 4, results from the Bayesian calibration of VSD are used to quantify the uncertainty in critical loads and target loads, caused by uncertainties in model parameters. Chapter 5 describes an analysis for Europe and northern Asia on critical loads and their sensitivity to the assumptions on the chemical criterion. It also shows that chemical criteria are not independent but inter-linked. In chapter 6 an evaluation is provided of the recovery of European forest from acidification and the role of climate change therein. Assessments with VSD were made to evaluate the effectiveness of deposition-reduction scenarios and the relative importance of climate change on recovery. Illustrations are provided on areas where target loads could be a relevant policy tool and on the possible speed of recovery in strongly acidified areas. In chapter 7 conclusions are drawn and some recommendations for future research are given. This thesis describes the entire chain from model development, via calibration and uncertainty analysis to model application; here the procedure is applied for the VSD model but in principle it is applicable for any model.

Note: all figures in the text are printed in black and white; color versions of the maps and of some of the figures are provided at the end of the thesis.

A Very Simple Dynamic soil acidification model for scenario analyses and target load calculations

Posch, M. & Reinds, G.J. 2009. A very simple dynamic soil acidification model for scenario analyses and target load calculations, *Environmental Modelling & Software* **24,** 329–340.

Abstract

A very simple dynamic soil acidification model, VSD, is described, which has been developed as the simplest extension of steady-state models for critical load calculations and with an eye on regional applications. The model requires only a minimum set of inputs (compared to more detailed models) and execution time is minimised by reducing the set of model equations to a single non-linear equation. To facilitate the exploration of model behaviour at individual sites, the model is linked to a graphical user interface (GUI). This GUI allows easy (Bayesian) calibration, forward simulation (scenario analyses) and can also be used to compute target loads and delay times between deposition reductions and ecosystem recovery. VSD compares well to other widely-used more complex models and is currently used in several European countries in the support of effects-based emission reduction policies.

Keywords: Dynamic model; soil acidification; critical load; target load; delay times; Bayesian calibration, VSD

Software availability

Name of software: VSDStudio: Very Simple Dynamic (soil acidification) model, version 3.1, with graphical user interface
Hardware required: PC
Software required: Microsoft Windows
Program languages: VSD model: Fortran 95; graphical user interface: C++
Program size: 8 MB of disk space, 128 MB of memory required
Availability: free download from www.trentu.ca/ecosystems/i-like-it or www.mnp.nl/cce

1. Introduction

Numerous models for simulating the acidification of soils and surface waters have been developed during the past decades (see, e.g. Tiktak and Van Grinsven, 1995). These models cover a wide spectrum of applications and objectives. Many of them are 'research models' that have been developed for a certain project and/or sites for which detailed measurements are available. Examples of such models are ForSVA (Arp and Oja, 1997) and NUCSAM (Groenenberg et al., 1995). In general, they are

not intended or suitable for regional applications, as they require detailed input data not readily available on a regional scale. At the other end of the spectrum are models designed to be easily applicable at many sites: their developers try to minimise input requirements and pay attention to ease (and speed) of use. This is especially important if the model is to be used on a regional scale, where input data is sparse and fast model execution is important. Examples of such models currently in use are the soil models SMART (De Vries et al., 1989; Posch et al., 1993) and SAFE (Warfvinge et al., 1993) and the catchment model MAGIC(Cosby et al., 1985a; Cosby et al., 2001).

Here we describe the 'very simple dynamic' (VSD) model, which is designed for sites with few data available and applications on a large regional or continental scale. The VSD model has been developed as a minimal extension of steady-state mass balance models for calculating critical loads, which have been widely used during the past 15 years in European sulphur (S) and nitrogen (N) emission reduction negotiations under the UNECE Convention on Long-range Transboundary Air Pollution (LRTAP) (Hettelingh et al., 1995a; Hettelingh et al., 2001). Critical loads are steady-state quantities, which define upper limits for S and N deposition that do not cause 'harmful effects' on specified ecosystems. They are mostly calculated with a 'simple mass balance' (SMB) model, which assumes that soil processes are in equilibrium with depositions (UBA, 2004). Critical loads are based on a soil chemical criterion, such as an Al/Bc ratio in the soil solution. A deposition equal to a critical load will, in the long run, lead to the soil chemical state not 'harmful' to the ecosystem. Critical loads, however, do not give any information on the time when a certain soil chemical state is obtained for a given future deposition pathway. To this end dynamic models are required; and the VSD model is the simplest extension of the steady-state SMB model into a dynamic model by including cation exchange and time-dependent N immobilisation (accumulation). The simplicity of the model results in a short execution time that allows rapid scenario analyses and the calculation of target loads, i.e. deposition targets which result in a desired chemical condition in the soil (solution) in a specified year. Assessment of target loads requires the solution of an inverse problem, i.e. to find depositions which lead to a given chemical state at a given time in the future. They are determined by running the VSD model iteratively, and thus may require many model runs. Furthermore, delay times can be determined with VSD, i.e. the year when a certain soil chemical condition is met for a given deposition scenario. Despite its simplicity, the VSD model incorporates the main processes also present in more complicated models, and model comparisons have shown that results obtained are very similar for most soils (Kurz and Posch, 2002).

This gives confidence that the VSD model properly describes the average chemical development of the major ions in the soil and soil solution over long time periods.

The paper presents a description of the VSD model (listing all processes and equations) followed by a description of the model's functionality, i.e. how the software developed around the core VSD model – called VSDStudio – can be used to calibrate the model and to use it for different tasks, such as scenario analyses, critical load and target load calculations as well as delay time estimates. Finally, we discuss model evaluation and list some limitations of the model.

2. Model description

The VSD model is designed to simulate the acidification (and recovery) of non-calcareous (unmanaged) soils. It consists of a set of mass balance equations, describing the soil input-output relationships, and equations describing rate-limited and equilibrium soil processes. Simulated soil solution chemistry depends solely on the net element input from the atmosphere (deposition), net uptake, net immobilisation and denitrification and the geochemical interaction in the soil (CO_2 equilibria, mineral weathering, cation exchange and internal production or organic anions). Soil interactions are described by simple rate-limited (zero-order) reactions (e.g. uptake and weathering) or by equilibrium reactions (e.g. cation exchange). The exchange of aluminium (Al), protons (H) and sum of calcium (Ca), magnesium (Mg) and potassium (K), Bc=Ca+Mg+K, is modelled either with Gaines-Thomas or Gapon equations. All ions in soil solution are linked via a charge balance equation. Solute transport is described by assuming complete mixing of the element input within one homogeneous soil compartment with a constant density and a fixed depth. Since VSD is a single layer soil model neglecting vertical heterogeneity, it predicts the concentration of the soil water leaving this layer (normally defined as the rootzone). The annual water flux percolating from this layer is assumed equal to the annual precipitation excess. The time step of the model is annual, i.e. seasonal variations are not considered. The model was not designed for very wet ecosystems as it assumes that the soil is completely oxidized and does not account for upward transport of ions by seepage.

The VSD model resembles the model SMART(De Vries et al., 1989; Posch et al., 1993), but has been further simplified to make it fully compatible with the SMB model by (i) neglecting buffering by calcium carbonate and aluminium depletion

in highly acidified soils, (ii) ignoring sulphate adsorption and Al complexation, and (iii) assuming complete nitrification (no ammonium leaching).

Charge balance equation:
The charge balance links all ions considered in the VSD model:

$$(1)\ [H^+]+[Bc^{2+}]+[Na^+]+[Al^{3+}]=[SO_4^{2-}]+[NO_3^-]+[Cl^-]+[HCO_3^-]+[Org]$$

where we treat the sum of Ca, Mg and K as a single ion, $Bc=Ca+Mg+K$, and Na denotes sodium, SO_4 sulphate, NO_3 nitrate, Cl chloride and *Org* the sum of organic anions. All concentrations are expressed in moles of charge (equivalents), i.e. the ion molar concentration multiplied by its charge (thereafter we suppress the notation of charges). We assume complete nitrification and therefore $[NH_4]=0$. This simplification is justified by observations; for example, De Vries et al. (2003a) found that more than 90% of incoming ammonium at most of 120 forest sites across Europe was nitrified.

Equilibrium equations:
The equilibrium reactions considered in the VSD model are the dissolution of Al hydroxides, the dissociation of bicarbonate and organic acids, and cation exchange. The dissolution of Al hydroxides is calculated via:

$$(2)\qquad [Al]=K_{Alox}\cdot[H]^a$$

where K_{Alox} is the dissolution constant and a is the slope of the pH-pAl relationship ($a\leq 3$); $a=3$ being the well-known gibbsite equilibrium. The dissociation of HCO_3 is calculated as:

$$(3)\qquad [HCO_3]=\frac{K_1\cdot K_H\cdot p_{CO2}}{[H]}$$

where K_1 is the first dissociation constant, K_H Henry's constant and p_{CO2} is the partial pressure of CO_2 in the soil solution (in atm); p_{CO2} is a user input and the product $K_1 \cdot K_H$ is computed as a function of temperature. All organic anions are assumed monovalent in VSD, and they are produced by the dissociation of dissolved organic carbon:

(4) $$[Org^{-}] = \frac{m \cdot DOC \cdot K_{org}}{K_{org} + [H]}$$

where *DOC* is the concentration of dissolved organic carbon (in molC m^{-3}), m the concentration of functional groups (the "charge density", in mol $molC^{-1}$) and K_{org} the dissociation constant (see, e.g. Driscoll et al., 1989). Since a single value of K_{org} does not always model the dissociation of organic acids satisfactorily, three parameters for the following empirical relationship between K_{org} (in mol L^{-1}) and pH can be specified:

(5) $$-\log_{10} K_{org} = a + b \cdot pH - c \cdot (pH)^2$$

This relation was derived by Oliver et al. (1983), who found the values a=0.96, b=0.90 and c=0.039.

In the VSD model the exchange between the solid phase and the soil solution is considered for three ions: Al, H and Bc=Ca+Mg+K, where K is treated as divalent ion. The user has the choice between the Gaines-Thomas model and the Gapon model for cation exchange.

The Gaines-Thomas equations for these ions are:

(6) $$\frac{E_{Al}^2}{E_{Bc}^3} = K_{AlBc} \cdot \frac{[Al]^2}{[Bc]^3} \quad \text{and} \quad \frac{E_H^2}{E_{Bc}} = K_{HBc} \cdot \frac{[H]^2}{[Bc]}$$

where E_X is the equivalent fraction of ion X at the exchange complex, and K_{AlBc} and K_{HBc} are the selectivity constants for the Al-Bc and H-Bc exchange, respectively. These two equations are also used in the SMART model; with K not included in Bc.

The corresponding Gapon equations are given by:

(7) $$\frac{E_{Al}}{E_{Bc}} = k_{AlBc} \cdot \frac{[Al]^{1/3}}{[Bc]^{1/2}} \quad \text{and} \quad \frac{E_H}{E_{Bc}} = k_{HBc} \cdot \frac{[H]}{[Bc]^{1/2}}$$

with selectivity constants k_{AlBc} and k_{HBc}. The exclusion of Na exchange is clearly a simplification, but is also made in more complex models. For example, the SAFE model (Warfvinge et al., 1993; Alveteg, 1998) also uses Gapon exchange equations

for Al, H and Bc only. Since the exchange complex is assumed to comprise H, Al and Bc only, both models require that:

(8) $$E_{Bc} + E_{Al} + E_H = 1$$

Mass balance equations:
For each of the cations (Bc, Na) and anions (SO_4, NO_3, Cl) considered in the VSD model a mass balance equation is given by:

(9) $$\frac{d}{dt} X_{tot} = X_{in} - Q \cdot [X]$$

where X_{tot} (eq m^{-2}) is the total amount of ion X in the soil (per unit area), X_{in} (eq m^{-2} yr^{-1}) the sum of all inputs from deposition as well as interaction (uptake-release) fluxes in the soil due to rate-limited reactions, and Q is the runoff (precipitation surplus) (m yr^{-1}). For H, Al, CO_2 and organic acids no mass balance is considered; their supply is assumed to be unlimited. SO_4, NO_3, Na and Cl interactions with the soil are not modelled in VSD and therefore their total amount equals the amount in the soil water:

(10) $$Y_{tot} = \theta \cdot z \cdot [Y] \quad \text{with} \quad Y = SO_4, NO_3, Na, Cl$$

where θ is the volumetric water content of the soil (m^3 m^{-3}) and z the thickness of the soil compartment (m). The total amount of base cations is the sum of the amount in the soil solution and at the exchange complex:

(11) $$Bc_{tot} = \theta \cdot z \cdot [Bc] + \rho \cdot z \cdot CEC \cdot E_{Bc}$$

where E_{Bc} is the equivalent fraction of base cations at the adsorption complex, ρ the bulk density of the soil (g cm^{-3}) and CEC the cation exchange capacity (meq kg^{-1}).

Input fluxes:
The input fluxes for sulphate and chloride are given by deposition alone:

(12) $$SO_{4,in} = SO_{2,dep}$$

(13) $$Cl_{in} = Cl_{dep}$$

where the subscript *dep* denotes total deposition.

The input flux for each base cation is calculated as deposition plus weathering (subscript *we*; in eq m^{-3} yr^{-1}) minus net growth uptake (subscript *u*; in eq m^{-2} yr^{-1}), and it is not allowed to fall below a minimum concentration $[Y]_{min}$ (in eq m^{-3}) in the soil solution:

$$Y_{in} = \max\left\{ Y_{dep} + z \cdot Y_{we} - Y_u \,,\, Q \cdot [Y]_{min} \right\} \quad \text{with} \quad Y = Ca, Mg, K \tag{14}$$

Sodium uptake is neglected, and thus we get for the input fluxes:

$$Bc_{in} = Ca_{in} + Mg_{in} + K_{in} \quad \text{and} \quad Na_{in} = Na_{dep} + z \cdot Na_{we} \tag{15}$$

Since we assume complete nitrification, ammonium fluxes are zero. Net immobilisation of N is the sum of two terms: (i) a constant (acceptable, sustainable) long-term net immobilisation $N_{i,acc}$, which does not change the C:N ratio in the topsoil, i.e. a proportional amount of C is assumed to be immobilised as well; (ii) a time-dependent N immobilisation, calculated as a fraction of the net N input, linearly depending on the C:N ratio in the topsoil.

The N (=NO_3) flux available for time-dependent immobilisation, N_{av}, is computed as:

$$N_{av} = \max\left\{ N_{dep} - N_u - N_{i,acc} \,,\, Q \cdot [N]_{min} \right\} \tag{16}$$

where N_{dep}=$NO_{x,dep}$+$NH_{3,dep}$, and $[N]_{min}$ is a prescribed minimum N concentration in the soil solution. Between a maximum, CN_{max}, and a minimum C:N ratio, CN_{min}, the amount of N immobilised per time step is a linear function of the actual C:N ratio, CN_t:

$$N_{i,t} = \begin{cases} N_{av,t} & \text{for} \quad CN_t \geq CN_{max} \\ \dfrac{CN_t - CN_{min}}{CN_{max} - CN_{max}} \cdot N_{av,t} & \text{for} \quad CN_{min} < CN_t < CN_{max} \\ 0 & \text{for} \quad CN_t \leq CN_{min} \end{cases} \tag{17}$$

The above equation states that when the C:N ratio reaches CN_{min}, $N_{i,t}$ becomes zero, and the total amount of N immobilised per time step equals the constant value $N_{i,acc}$. The amount of N immobilised in every time step updates the amount of N in the topsoil, N_{pool} (in mol m^{-2} =eq m^{-2}):

(18) $$N_{pool,t} = N_{pool,t-1} + N_{i,acc} + N_{i,t}$$

The amount of C in the topsoil, C_{pool} (in g m^{-2}), is also updated by two contributions: one due to $N_{i,acc}$ to keep the C:N ratio constant, and another which is controlled by the C:N ratio of the material immobilised according to eq.17, CN_{seq} (the factor 14 converts from eq to g):

(19) $$C_{pool,t} = C_{pool,t-1} + 14 \cdot CN_{t-1} \cdot N_{i,acc} + 14 \cdot CN_{seq} \cdot N_{i,t}$$

The last term follows Evans et al. (2006), who investigated the enhanced C sequestration due to elevated N inputs for heathlands in the UK. The updated pools, in turn, are used to update the C:N ratio:

(20) $$CN_t = \frac{C_{pool,t}}{14 \cdot N_{pool,t}}$$

The initial C pool and N pool (or C:N ratio) are needed as inputs. In general, these are obtained from measured (or estimated) pools at a given point in time, and the initial pools (and thus C:N ratio) are then obtained by calibration (see below), using historical N deposition and uptake time series. The C pool is estimated from soil properties as:

(21) $$C_{pool} = 10^6 \cdot \rho_{top} \cdot z_{top} \cdot C_{om} \cdot OM$$

where z_{top} is the thickness (m) of the top soil layer in which N immobilisation is assumed to occur; ρ_{top} is the bulk density (g cm^{-3}), C_{om} the fraction of C in organic matter, and OM the organic matter content of that layer. The factor 10^6 is a conversion factor to obtain C_{pool} in g m^{-2}. The N pool is estimated analogously.

Denitrification is modelled as fraction of the remaining N input:

(22) $$N_{de} = f_{de} \cdot \left(N_{dep} - N_u - N_i\right)$$

where f_{de} is the denitrification fraction ($0 \le f_{de} \le 1$) and $N_i = N_{i,acc} + N_{i,t}$. Thus we get for N_{in}:

$$N_{in} = (1 - f_{de}) \cdot \left(N_{dep} - N_u - N_i \right) \quad (23)$$

In order to solve the model equations, i.e. to compute the concentrations and total amounts of the different ions, the differential equations are discretised, using an implicit first-order method. The set of equations can be reduced analytically to a single equation with one unknown, which is solved by simple bisection, rendering simulations with VSD very fast.
On a 1.7 GHz Pentium M processor a single site simulation for 10,000 years takes only about 0.6 seconds CPU time.

3. Functionality

Around the VSD core-model described in the previous chapter, a software package and graphical user interface (GUI) has been developed, called VSDStudio, which not only allows – for a single site at a time – simple forward simulations for given deposition scenarios, but also automatic (Bayesian) calibration, computation of steady-states (critical loads), target loads and damage/recovery delay times. In the following the functionalities of VSDStudio are described in detail.

3.1 User interface and data input

The GUI of VSDStudio provides easy access to the full functionality of VSD and includes extensive help functions. Site specific data can be input either as files (exact format described in the Help-file) or directly entered through the GUI (and stored for later use). The tab sheet 'Input data' displays the input parameters for running VSD (Figure 1). Help on a parameter can be obtained by clicking its name. If a parameter name is displayed in bold, the value can be a fixed number or a file (from which a time series is read). Values for parameters not specified in the input file and for which VSD can provide default values are displayed in yellow. For mandatory parameters for which no value is specified, the edit field has a red colour and the text 'Missing!' (see Figure 1). VSD can only be run if all mandatory parameters have a value assigned. The user can change the values of all parameters, except for the edit fields in blue, which are model options that can be specified on the tab sheet 'Model options' (not shown here).

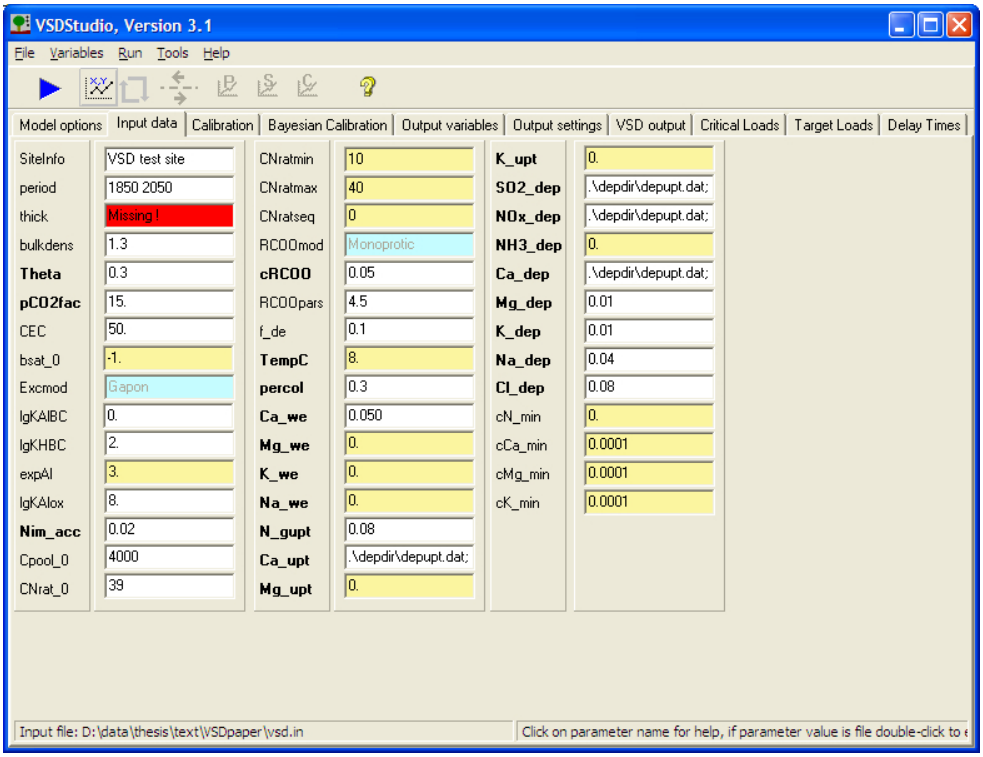

Figure 1 Input data screen of VSDStudio.

3.2 Model initialization and calibration

To run the VSD (or any other dynamic) model, all parameters as well as the initial conditions, i.e. the values of the time-dependent variables at the beginning of the simulation, have to be known. In the case of the VSD model the initial soil solution concentrations $[SO_4]_0$, $[NO_3]_0$, $[Bc]_0$, $[Na]_0$, $[Cl]_0$ and the initial values of the C pool, $C_{pool,0}$, the N pool, as CN_0, and of the base cation pool, given as initial base saturation EBc_0, are needed. However, due to the lack of such initial conditions in most practical cases and due to the fact that especially exchange constants are poorly known, the following procedure is adopted in VSDStudio (in line with analogous procedures in other models) to initialise a model run and calibrate the exchange constants:

a) Calibrating initial C pool and C:N ratio:
The initial C pool and C:N ratio are obtained from observed values (in a specified 'year of observation') by running the calculation steps outlined in eqs.17 and 18 backwards, starting from the year of observation going back to the starting year of

the simulation. In VSDStudio this is implemented on the tab sheet 'Calibration' (see Figure 2). Note, that the calibration of $C_{pool,0}$ and CN_0 is independent from the soil solution status (only N-related inputs are needed), but influences it, and thus their calibration has to precede the calibration of exchange constants. If time-dependent immobilisation is not to be simulated, the initial C pool has to be set to zero (and an initial C:N ratio need not be specified).

b) Initial concentrations and calibrating exchange constants:
In VSDStudio, the initial concentrations are derived internally by assuming that they are in equilibrium with the respective inputs at the beginning of the simulation period. Therefore, it is advised to start simulations before major anthropogenic emissions occurred. (The VSD model itself allows specification of any initial condition which does not violate charge balance, but this is not (yet) implemented in VSDStudio.) Using an observed base saturation for a given point in time, calibration of the exchange constants is then carried out in an iterative way until the observed value is reproduced by the model. The same calibration procedure is used in the SAFE model (Alveteg, 1998). The procedure does not guarantee the proper simulation of the individual exchangeable fractions E_{Al} and E_H, only of their sum. However, if data for one of them is available, the exchange constants can be adjusted to fit all three exchangeable fractions (see button 'Fine-tune exchange constants' in Figure 2).

To simulate with the calibrated parameters, results can be transferred to the input data sheet (Figure 1), by clicking the respective check-box (see Figure 2).

It is recognised that also other model parameters, such as Al-H relationship or N-related parameters are often uncertain; such (complex) calibrations of multiple parameters simultaneously can be accomplished with Bayesian techniques, which have been tested for the MAGIC model (Larssen et al., 2006), and have also been developed for the VSD model.

3.3 Bayesian calibration

To facilitate a more extensive calibration of VSD, including uncertainties in observed soil chemistry, a procedure for Bayesian calibration was developed and implemented in VSDStudio. Details on the implementation of Bayesian calibration for VSD can be found in Reinds et al. (2008b); the method strongly resembles that described in Van Oijen et al. (2005).

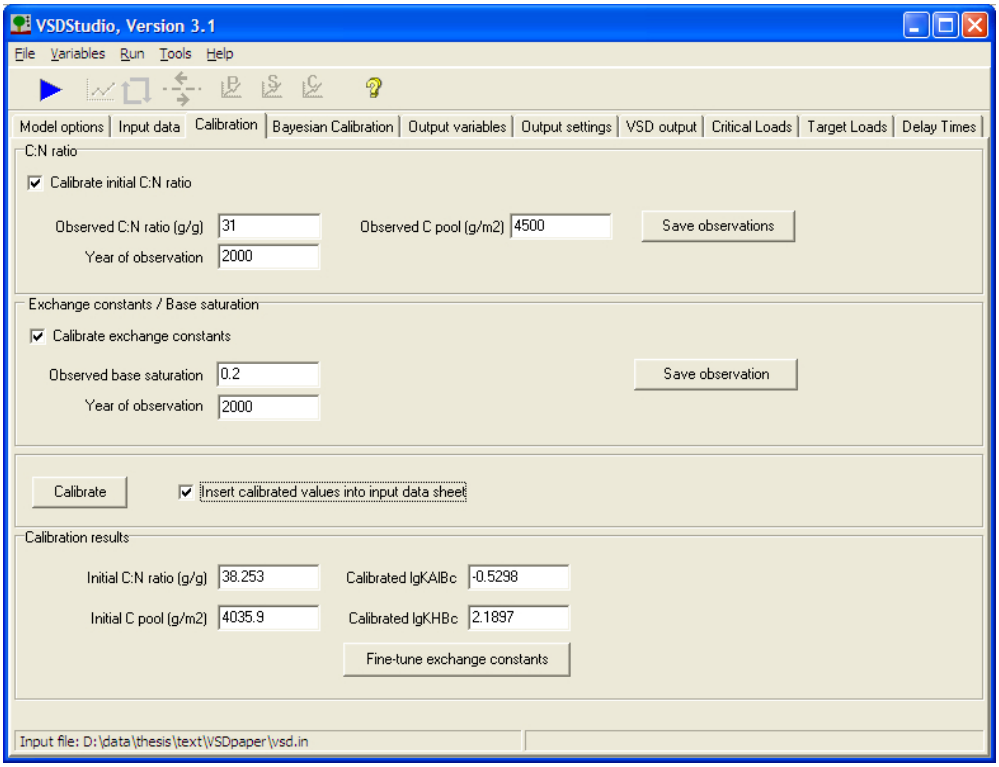

Figure 2. Calibration screen of VSDStudio.

Here only a brief summary is provided. In the Bayesian approach the prediction of uncertain parameters is taken to be conditional on data, and their conditional probability is given by:

$$p(\theta \mid D) = c \cdot p(D \mid \theta) \cdot p(\theta) \tag{24}$$

where $p(\theta \mid D)$ is the posterior (conditional) probability of the parameter (vector) θ given the data (observations) D, $p(D \mid \theta)$ is the likelihood-function for θ and $p(\theta)$ is the prior distribution of θ. The value of c (=1/$p(D)$) is fixed and usually does not need to be computed explicitly (Van Oijen et al., 2005).

In the Bayesian calibration of VSD the prior distributions, $p(\theta)$, for a number of VSD input parameters must be defined based on best available knowledge. Next, the posterior distribution of input parameters given data on model output, $p(\theta \mid D)$,

is computed based on comparison of the outcome of VSD with the set of measurements of soil (solution) chemistry, including their uncertainty (specified as standard deviation around the observed value). The posterior probability for θ increases with an increased prior probability and an increased likelihood (eq.24), i.e. when the selected set of parameter values have a larger prior probability and when the model is able to reproduce the measurements. The prior probability is directly computed from the probability of a candidate point of θ; for candidate points from normal distributions close to the mean the probability will be large, for points in the 'tail' of the distribution the probability will be small. The likelihood, $p(D|\theta)$, is computed from the comparison of model output with measurements. The better the model is able to reproduce the measurements, the greater the likelihood (Van Oijen et al., 2005). To calculate the posterior $p(\theta|D)$ a simple Markov Chain Monte Carlo algorithm is used, known as the Metropolis-Hastings random walk (Robert and Casella, 1999). In this method, the multi-dimensional parameter space (where the number of dimensions equals the number of uncertain model parameters) is explored by randomly stepping through this space and running the model for each visited point. Points visited are either accepted or rejected based on the computed likelihood.

VSDStudio offers options to adapt the calibration procedure by, for example, changing the length of the Markov chain and the step size used to compute the next point in the chain. Results are displayed as the optimal parameter values, in the form of posterior distributions and as correlation matrix. Running the model with this set of parameters and comparing simulated with observed soil (solution) chemistry shows whether the calibration was successful. The posterior distributions of the parameters could then be used in an uncertainty analysis of VSD.

As an example, Figure 3 shows (part of) the results of a calibration of VSD on a Forest Intensive Monitoring site in Belgium (for a description of the Intensive Monitoring plots see e.g. De Vries et al., 2003d). The graph on the left shows the posterior distribution function of the logarithm of the Gapon H-Bc exchange constant (*lgKHBc*) in the form of a bar graph as well as the prior distribution as a red line. The graph shows that calibration has strongly reduced the parameter uncertainty (and shifted the mean to the right). The graph on the right shows the relationship of *lgKHBc* with the logarithm of the other exchange constant (*lgKAlBc*) by displaying the pairs of values for each accepted point in the Markov chain. The graph shows the correlation between the two parameters which – after some

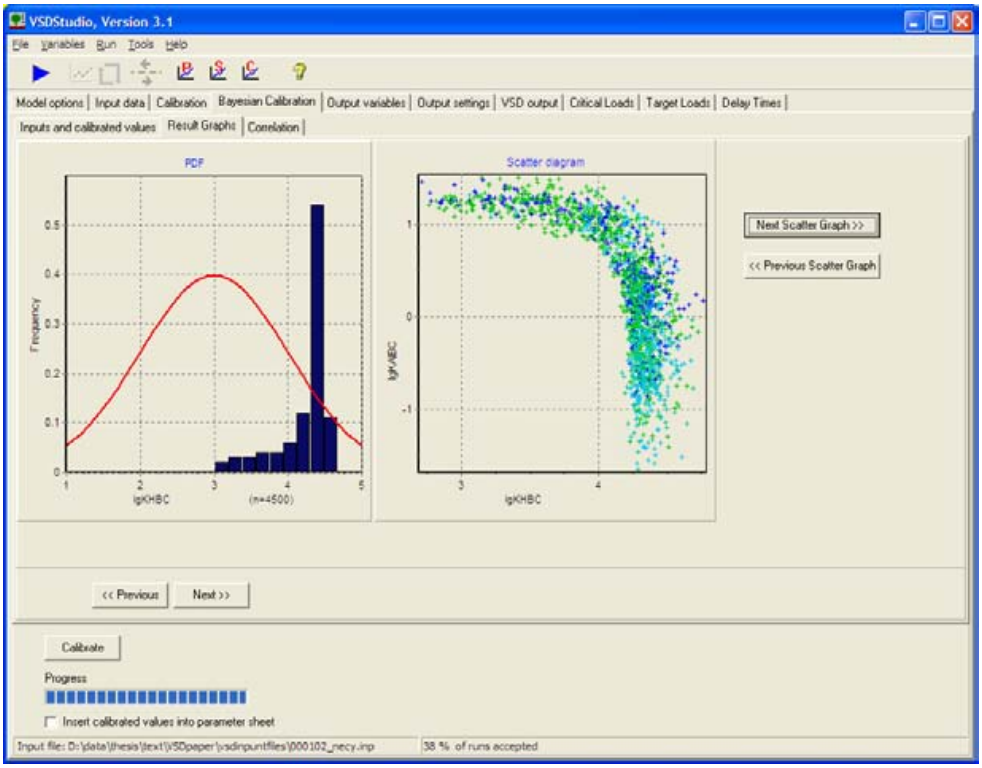

Figure 3. Bayesian calibration output screen of VSDStudio.

mathematical transformations – can be also derived from the exchange equations (eq.7) and the Al-H equilibrium (eq.2) for a=3.

3.4 Scenario analysis

After completing input data (and calibration) the VSD model can be run. Output is displayed on the tab sheet 'VSD output' as multiple time series graphs (see Figure 4) or as a sequence of X–Y-plots for all pairs of variables (not shown).
VSD simulations are shown as red line and green lines, and observations of C:N ratio, C pool and base saturation are displayed as red crosses with a vertical line indicating their uncertainty expressed by the standard deviation of the measurements. The green line shows results of a previous simulation for comparison. The numerical values of all displayed variables in any year can be queried by moving the trackbar at the bottom: the year is indicated by a black marker on the graph with the simulated value shown next to it.

Figure 4. Example model output of VSD.

The GUI allows the user to select which model variables are to be displayed on the tab sheet 'Output variables' (not shown). If results should also be stored as a PostScript file (showing the graphs) and/or an ASCII text file (containing the model output for the selected variables), this can be controlled on the tab sheet 'Output settings' (not shown), which also offers the possibility to change the display order of the graphs and the settings and look of the individual panes. To compare different model runs, for example. the influence of a particular parameter choice or an alternative deposition scenario, up to nine model previous runs can be displayed simultaneously with the current simulation.

3.5 Critical loads

VSDStudio can also be used to derive critical loads, which are widely used in effects-based integrated assessments of emission reductions (Hettelingh et al.,

1995a; Hettelingh et al., 2001), by running a steady-state version of the VSD model. Steady state in the mass balance equations (eq.9) means no change over time in the total amount (dX_{tot}/dt=0), and thus

(25) $$X_{le} = X_{in}$$

where X_{le} =Q·[X] is the leaching of ion X at the bottom of the soil compartment. Inserting the respective expressions for the input fluxes of sulphate, nitrate, base cations and chloride, the charge balance equation (eq.1) becomes (expressed in terms of leaching fluxes):

(26) $$S_{dep} + (1 - f_{de}) \cdot (N_{dep} - N_u - N_i) = BC_{dep} + BC_w - Bc_u - Cl_{dep} - ANC_{le}$$

where the uptake and immobilisation fluxes are those for $t \to \infty$, which means, for example, that no time-dependent N immobilisation (eqs.17 and 18) takes place, i.e. N_i=$N_{i,acc}$. In eq.26 we have also defined the leaching of acid neutralising capacity leaching (ANC):

(27) $$ANC_{le} = Q \cdot [ANC] = HCO_{3,le} + RCOO_{le} - H_{le} - Al_{le}$$

Equation 26 can be used to compute for a given input (deposition, uptake, …) the leaching of ANC at steady state. Conversely it can be used to compute the upper limits for the deposition inputs by setting limit values for the leaching. This is the idea behind deriving maximum permissible depositions – critical loads – by setting limits on soil chemical variables, derived from studies linking them to adverse impacts on, for example, vegetation. Inserting the chosen chemical criterion allows calculation of the critical leaching of ANC, $ANC_{le,crit}$. Inserting this into eq.26 (and assuming that BC_{dep} remains constant), critical loads of sulphur, $CL(S)$, and nitrogen, $CL(N)$, can be obtained:

(28)
$$CL(S) + (1 - f_{de}) \cdot CL(N) = (1 - f_{de}) \cdot (N_u + N_i) + BC_{dep} + BC_w - Bc_u - Cl_{dep} - ANC_{le,crit}$$

Equation 28 does not give a unique critical load for S or N. Nitrogen sinks cannot compensate incoming sulphur acidity, and therefore the maximum critical load for sulphur is given by:

(29) $$CL_{max}(S) = BC_{dep} - Cl_{dep} + BC_w - Bc_u - ANC_{le,crit}$$

as long as N deposition is lower than all the N sinks, termed the minimum critical load of N, $CL_{min}(N)=N_i+N_u$. Finally, the maximum critical load of nitrogen (in case of zero S deposition) is given by:

(30) $$CL_{max}(N) = CL_{min}(N) + \frac{CL_{max}(S)}{1 - f_{de}}$$

The three quantities $CLmax(S)$, $CL_{min}(N)$ and $CL_{max}(N)$ define the *critical load function* (see Figure 5): Every pair of deposition (N_{dep},S_{dep}) lying on that function are critical loads of acidifying S and N.

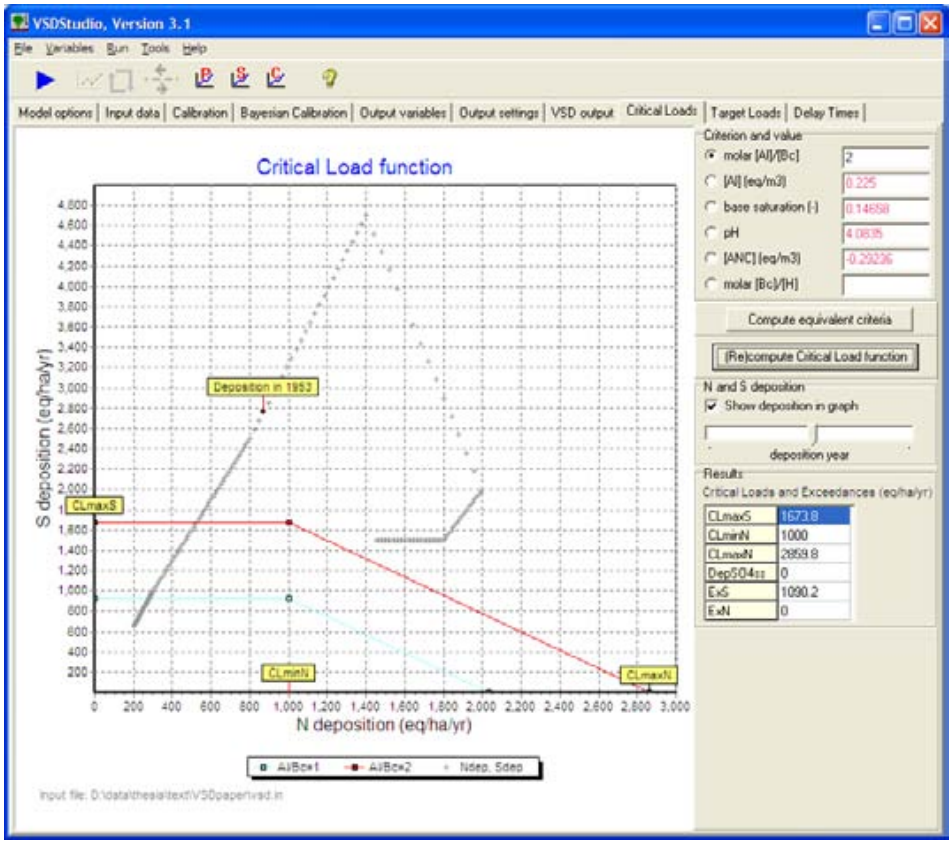

Figure 5. Critical Load screen of VSDStudio.

Originally critical loads were derived without recourse to dynamic models, starting from steady-state models (SMB) instead (see UBA, 2004).

The chemical criterion for the determination of the critical load function has to be selected by the user. For a given criterion, for example, molar [Al]/[Bc] = 1 in soil solution, the values for the other criteria leading to the same critical load function (called 'equivalent criteria') can be computed (see top-right in Figure 5). The N and S deposition can also be displayed in the graph, shown as a grey cross for every year. Depending on the position of the trackbar, the N and S deposition in the corresponding year within the time series is labelled. This illustrates for which years the deposition is above critical loads, i.e. when there is critical load exceedance. The influence of relevant inputs on the critical load function can be immediately seen by varying parameters and re-computing the critical load function.

3.6 Target loads

The simplest and most straightforward use of a dynamic model is scenario analysis (see above). Scenario analysis is, however, an *ex-post* process, i.e., the future deposition is determined first, and then the (chemical) consequences for the soil are evaluated. This process can be repeated until a suitable deposition reduction is found. To speed up this process, so-called target loads can be used. A target load is the deposition which ensures that the prescribed chemical criterion (e.g., the Al/Bc ratio) is achieved in a given year. Here we define a target load as a deposition path characterised by three numbers (years): (i) the protocol year, (ii) the implementation year, and (iii) the target year (see Figure 6).
The *protocol year* is the year up to which the deposition path is assumed to be known and cannot be changed any more. The *implementation year* is the year in which all reduction measures, needed to reach the final deposition (the target load), are to be implemented. Between the protocol year and the implementation year depositions are assumed to change linearly (see Figure 5). Finally, the *target year* is the year in which the chemical criterion (e.g., the Al/Bc ratio) is met (for the first time). The above three special years define a unique deposition path that is referred to as target load. The earlier the target year, the lower will be the target load (at sites where the chemical criterion is violated – for other sites a target load is hardly relevant), since higher deposition reductions are needed to achieve the desired status in a shorter time period.

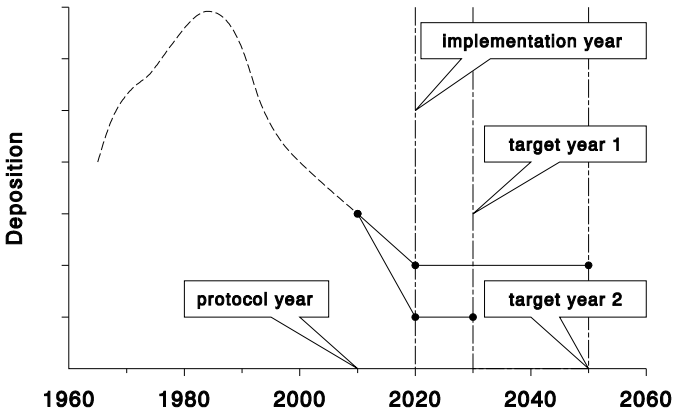

Figure 6. Schematic representation of deposition paths leading to target loads by dynamic modelling, characterised by three key years. (i) The year up to which the (historic) deposition is fixed (protocol year); (ii) the year in which the emission reductions leading to a target load are implemented (implementation year); and (iii) the year in which the chemical criterion is to be achieved (target years). Two examples of target years are shown.

In extreme cases, a target load might not exist at all, since even reduction to zero deposition will not result in the desired soil status within the prescribed time. For more information on target loads and related topics see Posch et al. (2003) or UBA (2004).

Dynamic models are in general not designed to compute target loads, i.e. they are not designed to derive the driving force (deposition) for a given soil chemical status. Thus trial and error has to be used to find the deposition (path) which produces a prescribed chemical status. VSDStudio, however, has a built-in functionality for computing target loads. As with critical loads, pairs of N and S deposition are be determined that result in the desired chemical status in the target year. All pairs define the *target load function* (TLF) in the (N_{dep},S_{dep}) plane, in the same way as critical loads define the critical load function (Figure 7).
Different TLFs are obtained for different target years, approaching the critical load function when the target year moves towards infinity.
As it is of interest how soil chemistry develops over time for a given pair of N and S deposition, in particular for a point on the TLF, the user can select such a pair by clicking anywhere in the displayed (N_{dep},S_{dep}) plane and then run VSD by clicking the 'Show time development' button. This displays the simulation for the selected deposition pair for nine relevant output variables (as in Figure 4).

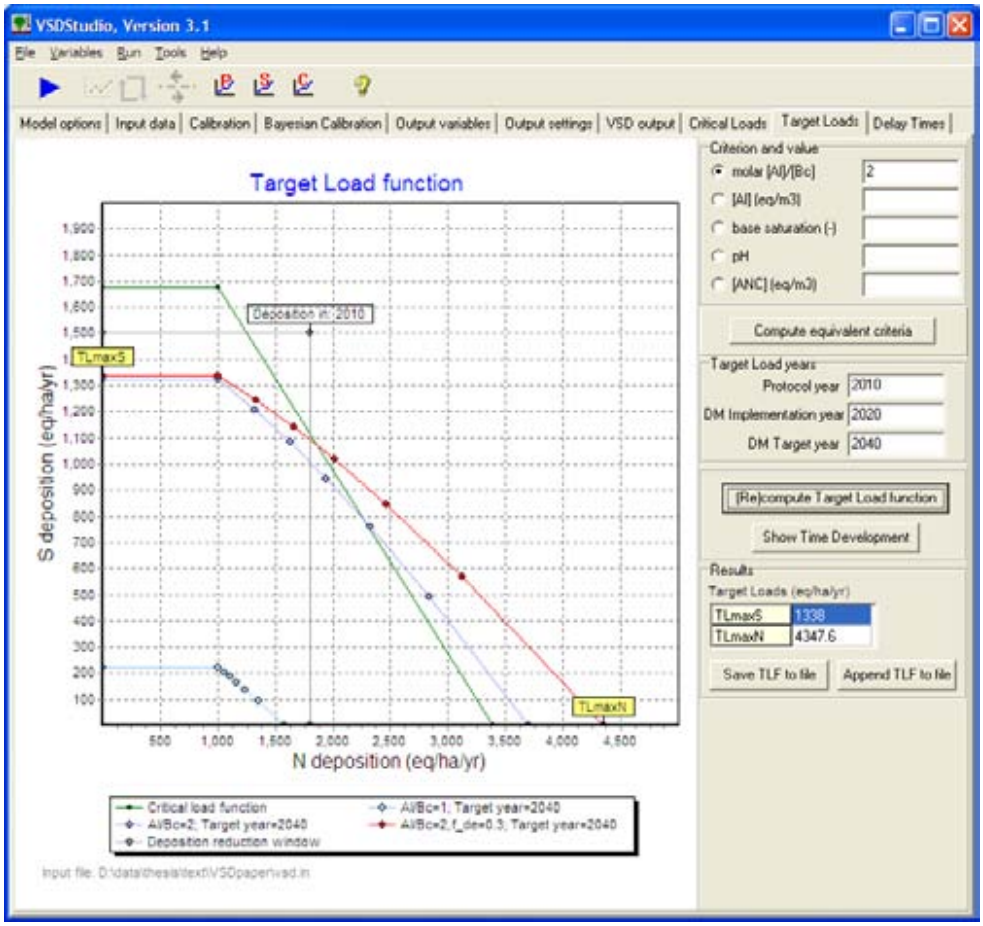

Figure 7. Target Load screen of VSDStudio.

3.7 Delay times

Only two cases can be distinguished when comparing critical loads to deposition: (1) the deposition is below critical load(s), and (2) the deposition is greater than critical load(s), i.e. there is critical load exceedance. In the latter case there is, by definition, an increased risk of damage to the ecosystem. Thus a critical load serves as a warning as long as there is exceedance, since it states that deposition should be reduced. However, it is often assumed that reducing deposition to (or below) critical loads immediately removes the risk of 'harmful effects', i.e. the chemical criterion (e.g. the Al/Bc ratio) immediately attains a non-critical ('safe') value. But the reaction of soils, especially their solid phase, to changes in deposition is

delayed by (finite) buffers, the most important being the cation exchange capacity (CEC). These buffer mechanisms delay the attainment of a critical chemical parameter, and it might take decades or even centuries, before steady state is reached. The times involved in attaining a certain chemical state in response to given deposition scenarios can be computed with a dynamic model.

The time between the first exceedance of the CL and the first violation of the criterion is termed the *damage delay time* (DDT) and the time between the first non-exceedance of the CL and the subsequent non-violation of the criterion is termed the *recovery delay time* (RDT) (see Posch et al., 2003, for a detailed discussion). With VSDStudio damage and recovery delay times – or rather the year in which damage or recovery occurs – can be computed for the special case of constant S and N deposition after a specified year (Figure 8). Note that (a) damage delay exists only if there is exceedance of critical loads, but the chemical criterion is not yet violated; and (b) recovery can only occur if there is non-exceedance of critical loads in the specified year, but the criterion is still violated. In the other two possible cases – (c) exceedance and violation of the criterion, and (d) non-exceedance and non-violation – the system remains 'damaged' or 'safe', respectively.

In addition to displaying the delay time (if it exists) the tab sheet also shows the net S+N input ($=S_{dep}+N_{dep}-N_u-N_i-N_{de}$) as green or red cross for every year versus the chosen chemical criterion (Figure 8). Moving the trackbar displays the corresponding deposition year and thus allows a quick assessment how far away the chemical parameter is at any point in time from its critical value (red horizontal line) or its steady-state value (brown horizontal line). The approach to equilibrium can also be investigated by specifying a year (far) in the future, for which VSD will compute the value of the criterion for constant future inputs and display it as a blue line (shown for the year 10,000 in Figure 8).

4. Model evaluation and outlook

VSD has been tested on 182 intensively monitored forest sites in Europe. These sites are part of the European Commission/UNECE Intensive Monitoring Programme, also known as the Level II programme of the ICP Forests (De Vries et al., 2003c). Using measured soil solution data, aggregated to annual averages, VSD was calibrated using a Bayesian calibration technique employing a Markov Chain Monte Carlo approach to sample the parameter space (see above and

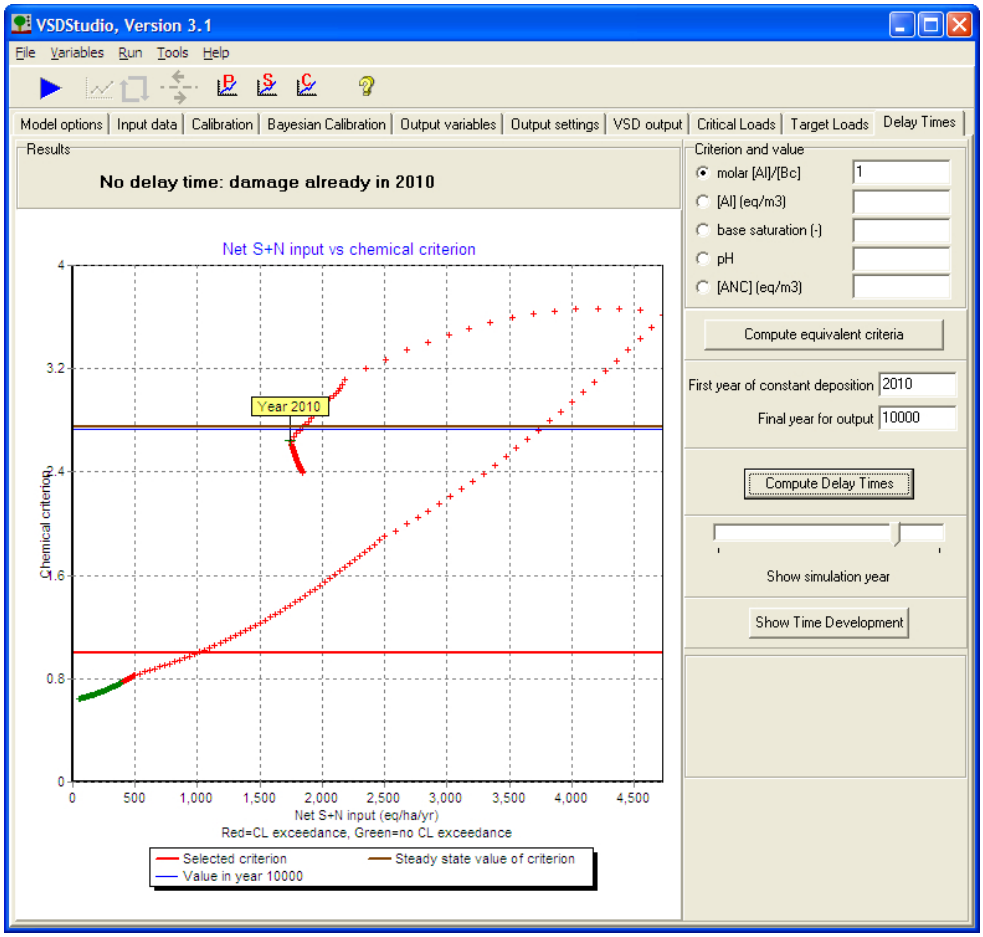

Figure 8. Delay Times screen of VSDStudio.

Reinds et al., 2008b). Results show that after calibration the median Normalized Root Mean Square Error (NRMSE) for 60 validation plots for pH is about 10%. For Al and base saturation the error is larger. In general, the calibration procedure was successful in reducing parameter uncertainty and increasing model performance (especially for pH and NO_3); only for a limited number of plots high simulation errors persisted after calibration, especially for N. Reinds et al. (2008b) also showed that it is not trivial to calibrate the nitrogen cycle with VSD, as many processes are involved (uptake, denitrification, immobilisation) and the individual contributions of these processes can (obviously) not be derived from the measurements of nitrate concentrations in the soil solution alone.

The VSD model has also been compared to other soil acidification models, most notably the SAFE model. In a detailed study for 176 sites in Switzerland, Kurz and Posch (2002) have shown that the VSD model, when fed with weathering rates calculated with the PROFILE model (a sub-module of the SAFE model by Warfvinge and Sverdrup (1992)), yields very similar results with the one-layer version of the more complex model SAFE. Also other model comparisons show that a simple model can perform equally well as (much) more complex models (see, e.g. Van der Salm et al., 1995). Several countries have adopted VSD for dynamic modelling on a regional scale performed under the Working Group on Effects of the LRTAP Convention (see Posch et al., 2005).

In this paper we have presented the basic equations of the VSD soil acidification model and its graphical user interface, VSDStudio, which allows easy application of it. In contrast to comparable models, VSDStudio allows not only 'traditional' scenario analyses, but also to compute critical loads, target loads and times to reach pre-specified soil chemical criteria. This makes the VSD model suitable – and widely used – in the context of European air pollution policy support. This paper focuses on the VSD model and the description of VSDStudio for single site applications, but the core-model VSD has also been linked (as Dynamic Link Library) to an MS Access database for regional applications; and VSD has been used to carry out scenario analyses and target load calculations on a European scale (Hettelingh et al., 2007).

Although simpler than other widely used models (such as MAGIC, SAFE and SMART), VSD contains the basic physical and chemical relationships common to all these models. Since the user can choose different 'model options', for example, the cation exchange model (Gapon or Gaines-Thomas; see above), VSD may be used to study the influence of 'model structure' on model performance. The ease of use and versatility of VSDStudio makes it also a practical tool for simple sensitivity analyses and demonstrations of a more 'didactic' nature. However, the model's simplicity also means that some processes have either been left out altogether (e.g. sulphate sorption) and others strongly simplified (e.g. N processes). As a consequence VSD will not be suited for sites where, for example, sulphate adsorption is important. Furthermore, the simple description of N processes does not allow simulating decreasing soil N pools (and increasing C:N ratios) under reduced N inputs.

As its name implies, the model was designed as 'very simple', but nevertheless some extensions are foreseen. This might include a simple N cycling description to

allow a better linking with (simple) vegetation models, in response to the current focus on nitrogen processes and their influence on biodiversity. Furthermore, the addition of a simple lake module is being investigated. However, any envisaged extension will be carefully vetted, so as not to jeopardise the simplicity and versatility of the tool.

Acknowledgements

Thanks to the users of earlier versions of VSDStudio who provided valuable suggestions for the improvement and extension of the interface. The preparation of this paper has been co-financed by the European Commission LIFE III programme within the framework of the European Consortium for Modelling Air Pollution and Climate Strategies (EC4MACS) and the trust fund for the partial funding of effect-oriented activities under the Convention on Long-range Transboundary Air Pollution.

Bayesian calibration of the VSD soil acidification model using European forest monitoring data

Reinds, G.J., van Oijen, M., Heuvelink, G.B.M. & Kros, H. 2008. Bayesian calibration of the VSD soil acidification model using European forest monitoring data, *Geoderma* **146**, 475-488.

Abstract

Over the past years, Bayesian calibration methods have been successfully applied to calibrate ecosystem models. Bayesian methods combine prior probability distributions of model parameters, based on assumptions about their magnitude and uncertainty, with estimates of the likelihood of the simulation results by comparison with observed values. Bayesian methods also quantify the uncertainty in the updated posterior parameters, which can be used to perform an analysis of model output uncertainty. In this paper, we applied Bayesian techniques to calibrate the VSD soil acidification model using data from 182 intensively monitored forest sites in Europe. Out of these 182 plots, 122 plots were used to calibrate VSD and the remaining 60 plots to validate the calibrated model. Prior distributions for the model parameters were based on available literature. Since the available literature shows a strong dependence of some VSD parameters on, for example, soil texture, prior distributions were allowed to depend on soil group (i.e. soils with similar texture or C/N ratio). The likelihood was computed by comparing modelled soil solution concentrations with observed concentrations for the period 1996-2001. Markov Chain Monte Carlo (MCMC) was used to sample the posterior parameter space. Two calibration approaches were applied. In the singe-site calibration, the plots were calibrated separately to obtain plot-specific posterior distributions. In the multi-site approach priors were assumed constant in space for each soil group, and all plots were calibrated simultaneously yielding one posterior probability distribution for each soil group. Results from the single-site calibrations show that the model performed much better after calibration compared to a run with standard input parameters when validated on the 60 validation plots. Posterior distributions for H-Al equilibrium constants narrowed down, thus decreasing parameter uncertainty. For base cation weathering of coarse textured soils the posterior distribution shifted to larger values, indicating an initial underestimation of the weathering rate for these soils. Results for the parameters related to nitrogen modelling showed that the nitrogen processes model formulations in VSD may have to be reconsidered as the relationship between nitrogen immobilization and the C/N ratio of the soil, as assumed in VSD, was not substantiated by the validation. The multi-site calibration also strongly decreases model error for most model output parameters, but model error was somewhat larger than the median model error from the singe-site calibration except for nitrate. Because the large number of plots calibrated at the same time provides very many observations, the Markov Chain converged to a very narrow parameter space, leaving little room for posterior parameter uncertainty. For an uncertainty analysis with VSD on the European scale, this study provides

promising results, but more work is needed to investigate how the results can be used on a European scale by looking at regional patterns in calibrated parameters from the site calibration or by calibrating for regions instead of all of Europe.

Keywords: Parameter Estimation, Markov Chain Monte Carlo, Soil Chemical Processes , Forest Soils

1. Introduction

Over the last decade, reductions of sulphur and, to a lesser extent, nitrogen emissions from industry, traffic and agriculture have led to a decrease in the deposition of acidifying compounds in Europe. Under the Convention of Long-range Transboundary Air Pollution (LRTAP) within the United Nations Economic Commission for Europe (UNECE), so-called critical loads for sulphur and nitrogen have been used as an indicator of the sensitivity of natural ecosystems to acidification and eutrophication. Critical loads provide the maximum deposition on an ecosystem that, on an infinite time-scale and according to current knowledge, will not lead to significant harmful effects (Nilsson and Grennfelt, 1988). Critical loads are mostly computed using simple steady state mass balance models (Sverdrup and De Vries, 1994; UBA, 2004). As shown by for example Hettelingh and co-workers (Hettelingh et al., 2001; 2007), exceedances of critical loads for sulphur and nitrogen have been reduced and will even be further reduced in the future if current emission reduction agreements come into force. In areas where the critical load was exceeded in the past and where the present or future deposition is smaller than the critical load, ecosystems are expected to recover from acidification. Critical loads, however, do not provide information about the (speed of) recovery of an ecosystem. Therefore, dynamic acidification models such as SMART (De Vries et al., 1989), MAGIC (Cosby et al., 1985b; Cosby et al., 2001) and SAFE (Warfvinge et al., 1993) have been used to evaluate the effects of future deposition scenarios on recovery. Ideally, the dynamic model should extend the critical load model so that dynamic processes are taken into account while all other process descriptions are compatible with those in the critical load model. To this end the Very Simple Dynamic model (VSD) has been developed (Posch et al., 2003) that extends the widely used Simple Mass Balance (SMB) critical load model (Sverdrup and De Vries, 1994) with dynamic soil processes, including cation exchange.

Because a critical load model provides the maximum allowable deposition for an ecosystem on an infinitely long time scale, the model cannot be calibrated or validated directly. Dynamic models, on the other hand, simulate soil solution concentrations as a function of atmospheric inputs and soil processes, and can thus be calibrated and/or validated on plots where such measurements are available. Until recently, calibration of most dynamic acidification models was performed by fitting the simulation results to (a series of) observations by 'trial and error' procedures: the model is re-run with different settings until the observation(s) are reproduced well. Sometimes a set of parameters is calibrated using various soil (solution) concentrations simultaneously (De Vries et al., 2003a), whereas in other studies only one parameter, such as the base saturation, is calibrated (Aherne et al., 1998; Belyazid et al., 2006). A more advanced model calibration was performed by Kros et al. (2002) who calibrated the SMART2 acidification model to soil observation data scaled up to 5×5 km blocks using the Gauss-Levenberg-Marquardt algorithm. The MAGIC model for soil and stream water chemistry is normally calibrated sequentially, by first calibrating deposition of S compounds using stream water chemistry, then calibrating N concentrations by adjusting uptake functions and finally calibrating base saturation using an optimization procedure (Jenkins et al., 1997). Most of these studies do not take into account the uncertainty in the observations and model input parameters: only the run that provides the best estimate of the observations defines calibrated parameter set. It is clear, however, that observations of soil solution concentrations are uncertain, mainly due to spatial variation within a plot. Furthermore, several combinations of input parameters may give the same model result, which hampers the identification of a unique set of input parameters. For example, base cation concentration in the soil is influenced by weathering, deposition and uptake of base cations. Adjusting growth rates, base cation contents in stem wood or weathering rates could all lead to the same simulation of base cation concentrations. Calibration methods that include these uncertainties and interactions are thus to be preferred over methods that use a simple fit through a (set of) observation(s) yielding one set of calibrated parameters without their uncertainty. In recent years, Bayesian calibration methods have been used for calibration of ecosystem models (e.g. Larssen et al., 2006; Van Oijen et al., 2005; Vrugt et al., 2006). Larssen et al. (2006) performed a Bayesian calibration of the hydrogeochemical model MAGIC. Using simulated and observed stream water concentrations from a catchment in southern Norway, they quantified uncertainties and examined the propagation of these uncertainties in forecast simulations for 3 different deposition scenarios. Van Oijen et al. (2005) presented a Bayesian calibration for process based forest models, illustrated by the calibration

of the BASFOR forest growth model using data from a site in Sweden. De Vrugt et al. (2006) presented the Shuffled Complex Evolution Metropolis (SCEM-UA) global optimization algorithm for environmental models. They provided examples of its effectiveness for 3 different case studies, among which an application for a watershed model.

Bayesian methods combine probability distributions of model parameters, based on prior assumptions about their magnitude and uncertainty, with estimates of the likelihood of the simulation results in view of the observed, uncertain values for model output variables. They use the combined information to quantify uncertainty in parameters and use the updated parameter uncertainty to perform an analysis of model output uncertainty. Bayesian calibration (BC) can be seen as a twofold extension of Maximum Likelihood estimation (ML). First, BC uses more information than just output data by including prior information about model parameters. Secondly, BC goes beyond identifying a single parameter vector with maximum probability to also estimate its uncertainty. In other words, BC provides a complete multi-variate probability distribution.

In this study, we applied Bayesian techniques to calibrate and validate the VSD model on 182 intensively monitored forest sites in Europe for which data on atmospheric inputs, soil solution chemistry and soil properties are available (De Vries et al. (2003c). Two calibrations of the VSD model were carried out on a subset of 122 plots: (i) each plot was calibrated individually, called 'single-site calibration' hereafter and (ii) the entire set of plots was calibrated simultaneously, called 'multi-site calibration'. The multi-site calibration is used to investigate effect of the grouping of model parameters for various soil types on calibrated parameters, since it is assumed that model parameters for a soil group are spatially constant. In this way we investigate the applicability of the calibration method on a large set of plots and analyse whether the available measurements allow a calibration of input parameters such that the model performance after calibration is significantly improved compared to that using parameter settings based on regional information alone. This validation is carried out on the remaining 60 plots. Eventually, results of this study could be helpful for parameterization of the VSD model when applied on a European scale.

2. Materials and methods

2.1 Location of the plots

The data for the calibration of VSD were derived from the set of EU/UNECE Intensive Monitoring plots (De Vries et al., 2003c), using those 182 plots where sufficient data on soil solution, soil solid phase, forest growth and deposition were available. Sixty validation locations were selected by k-means clustering of the 182 locations into 60 clusters, using the Cartesian x- and y-coordinates of the 182 locations as classification variables. Details on the selection method can be found in de Gruijter et al. (2006). The locations closest to the centroids of the clusters were selected as validation location. This selection procedure ensures that the validation locations cover the study area. The remaining 122 plots were used to calibrate VSD. Figure 1 shows the location of the calibration and validation plots, that mainly consist of pine- (43 plots), spruce- (80 plots), beech- (29 plots) and oak forest (21 plots). Most of the plots cover about 0.25 ha.

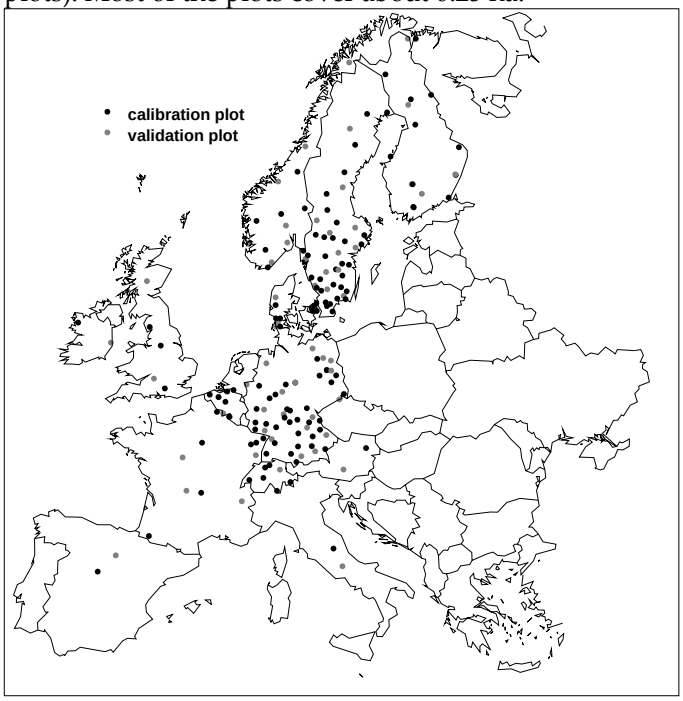

Figure 1. Location of the plots used for calibration and validation

Measurements from surveys on soil condition and forest growth were used to obtain variables such as soil cation exchange capacity (CEC), soil bulk density and

the average stem growth at the sites. Measured soil solution concentrations below the root zone from the period 1996 to 2001 were used to assess the VSD model performance by comparing these measurements with concentrations simulated by the model.

2.2 The VSD model

As its name implies, the VSD model (Posch et al., 2003) is a very simple dynamic model that simulates soil solution chemistry and soil nitrogen pools for natural or semi-natural ecosystems. The VSD model can be seen as the simplest extension of the simple mass balance (SMB) critical load model. The SMB model (Posch and De Vries, 1999; De Vries and Posch, 2003a) computes the maximum input of S and N to an ecosystem (i.e. critical load) that will not lead to harmful effects, using simple mass balance equations. VSD also consists of a set of mass balance equations, describing the soil input-output relationships of ions, and a set of equations describing the rate-limited and equilibrium soil processes. The soil solution chemistry in VSD depends solely on the net element input from the atmosphere (deposition minus net uptake minus net immobilisation) and the geochemical interactions in the soil (CO_2 equilibrium, base cation weathering, and cation exchange). Soil interactions are described by simple rate-limited reactions (e.g. nutrient uptake and weathering), first order processes (denitrification) and by equilibrium reactions (e.g. cation exchange). VSD models the exchange of Al, H and Ca+Mg+K with the Gaines-Thomas or Gapon equations. Solute transport is described by assuming complete mixing of the element input within one homogeneous soil compartment with a constant density and a fixed depth. VSD is a single layer soil model that neglects vertical heterogeneity. It predicts the concentration of the soil water leaving this layer (mostly the root zone). Validation of the model should thus be based on measurements from soil solution just below the root zone. The annual water flux percolating from this layer is taken equal to the annual precipitation excess. The model resembles the SMART model (De Vries et al., 1989) but leaves out some of the processes modelled by SMART such as aluminium mass balance and the soil solution chemistry in carbonate rich soils. The time-step of simulations is one year.

2.3 Model input data

Input to VSD consists of a set of 24 parameters, listed in Table 1. We have chosen to calibrate only model process parameters such as equilibrium constants and denitrification and immobilization fractions. These parameters are (highly)

uncertain because estimates are often based on small data sets and the most import VSD output parameters (pH, [Al], [Bc] and base saturation) are sensitive to these process parameters. Furthermore, these parameters cannot be measured directly and were therefore selected for calibration. Parameters for which measurements were available at the plot were not calibrated: the measurement was assumed to be the best estimate at the plot, even though it can be uncertain due to within-plot spatial variability and measurement error.

Table 1. VSD parameters

Parameter	Description	Calibration	Parameter	Description	Calibration
thick	Thickness of the rootzone	No	f_de	Denitrification fraction	Yes
bulkdens	Bulk density	No	percol	Precipitation surplus	No
Theta	Soil water content	No	Bcwe	Base cation weathering	Yes
pCO2fac	Partial pressure of CO_2 in soil	No	ctNst	N content in stems for N uptake	No
CEC	Cation exchange content	No	ctCast	Ca content in stems for Ca uptake	No
lgKAlox	Equilibrium constant H-Al	Yes	Ca_dep	Ca deposition	No
lgKAlBc	Exchange constant Al-BC	Yes	SO2_dep	SO_2 deposition	No
lgKHBc	Exchange constant H-BC	Yes	NOx_dep	NOx deposition	No
Nim_acc	N immobilization	Yes	Mg_dep	Mg deposition	No
Cpool_0	Initial C pool	No	K_dep	K deposition	No
CNrat_0	Intial CN ratio	No	Na_dep	Na deposition	No
cRCOO	Organic anion concentration	No	Cl_dep	Cl deposition	No

Calibrating such inputs may improve model performance but calibration results will be difficult to generalise because the results might become very site-specific.

2.3.1 Parameters not subject to calibration

The thickness of the root zone was set to 50 cm, except for a few plots where evidence exists that the soil is very shallow. Bulk density was obtained from plot

data unless it was not measured, in which case it was computed using a transfer function between bulk density and clay- and organic matter content (Reinds et al., 2001). The hydrological characteristics (soil water content and precipitation surplus) were derived from simulations with the hydrological model WATBAL (Starr, 1999). The validity of the hydrological model was tested using the chloride budgets at the plots and turned out to be quite satisfactory for the vast majority of plots (De Vries et al., 2003b).
Cation exchange capacity, organic anion concentrations and all deposition fluxes were obtained from measurements at the plots (De Vries et al., 2003b). Total deposition was computed from measured bulk and throughfall data, using an adapted version of the canopy budget model (Ulrich and Pankrath, 1983; Draaijers and Erisman, 1995; De Vries et al., 2001). Deposition of SO_x and total N outside the measurement period were computed by applying the trend in deposition modelled by EMEP (EMEP, 2001) for the 50 × 50 km EMEP grid cell that the plot is located in to the measured data; historical trends before 1960 were obtained from Schöpp et al. (2003). Base cation deposition was assumed constant in time and was set to the average measured value from the measurement period as neither historical nor future projections of base cation depositions were available.
C/N ratio and carbon pool at the beginning of the simulations (in the year 1880) were back-calculated from the measured C/N ratio and carbon pool and historical N inputs.

2.3.2 Calibration parameters

As the 182 Intensive Monitoring plots cover a wide range of soil and forest types, it is unlikely that one prior probability distribution function (pdf) for each parameter would be sufficient to arrive at a successful calibration. It is known that, for example, weathering rates and exchange constants vary strongly with soil texture (UBA,2004, De Vries and Posch, 2003b). Since we want to use the best available information, prior distributions were defined for each *soil group*. Such a soil group consists of soils with the same soil texture and C/N ratio in organic matter. For each plot, a prior distribution for the uncertain parameter was defined appropriate for the local soil type. For example, plots in the soil group consisting of sandy soils receive only values selected from the distributions of *lgKAlBc* and *BCwe* that are valid for sandy soils. Even if the priors are identically defined for all soil groups, the calibration can still yield different posterior distributions for soil groups. An overview of the prior distributions is provided in Table 2. It lists for each calibration parameter its VSD code, a description, the distribution assumed

Table 2. Prior distributions of VSD calibration parameters

Parameter	Description	Distribution	Mean	Stddev	Min	Max
lgKAlox_sand	Log10 of Equilibrium constant Al hydroxides sandy soils $(mol\ l^{-1})^{-2}$	normal	8	1		
lgKAlox_clay	Log10 of Equilibrium constant H-Al clay soils	normal	8	1		
lgKAlox_hclay	Log10 of Equilibrium constant H-Al heavy clay soils	normal	8	1		
lgKAlBc_sand	Log10 of Exchange constant Al-BC sandy soils	normal	0.5	0.6		
lgKAlBc_clay	Log10 of Exchange constant Al-BC clay soils	normal	-0.6	0.7		
lgKAlBc_hclay	Log10 of Exchange constant Al-BC heavy clay soils	normal	-0.6	0.7		
lgKHBc_sand	Log10 of Exchange constant H-BC sandy soils	normal	3.3	0.35		
lgKHBc_clay	Log10 of Exchange constant H-BC clay soils	normal	3.6	0.5		
lgKHBc_hclay	Log10 of Exchange constant H-BC heavy clay soils	normal	3.6	0.5		
fde_mod	Denitrification fraction moderately-well drained soils	truncated normal	0.4	0.1	0	1
fde_well	Denitrification fraction well drained soils	truncated normal	0.2	0.075	0	1
BCwe_iwr1	BC weathering acid sandy soils $(eq.m^{-2}\ yr^{-1})$	truncated normal	0.025	0.025	0	
BCwe_iwr2	BC weathering intermediate/basic sandy soils	truncated normal	0.075	0.0375	0	
BCwe_iwr3	BC weathering acid loamy/clayey soils	truncated normal	0.125	0.0625	0	
BCwe_iwr4	BC weathering intermediate loamy/clayey soils	truncated normal	0.175	0.0875	0	
BCwe_iwr5	BC weathering basic loamy/clayey soils	truncated normal	0.225	0.1125	0	
BCwe_iwr6	BC weathering heavy clay soils	truncated normal	0.275	0.1375	0	
bNim_cnh	Immobilisation fraction soils with high C/N (-)	uniform			0	1
bNim_cnm	Immobilisation fraction soils with intermediate C/N	uniform			0	1
bNim_cnl	Immobilisation fraction soils with low C/N	uniform			0	1

(uniform or (truncated) normal), the mean, the standard deviation (*Stddev*), the minimum (*Min*, if any) and maximum value (*Max*, if any).

Weathering rates were calibrated for six soil groups (i.e. weathering rate classes) that consist of a combination of soil texture and parent material. Initial distributions were obtained from De Vries et al. (1994b) and Reinds et al. (2001). Exchange constants and the H-Al equilibrium constant and exponent were defined as a function of the soil texture class. Initial values for exchange constants were obtained from De Vries and Posch (2003b) and are based on an analysis of hundreds of measurements from Dutch forest soils. The initial distributions of the log of the equilibrium constant *KAlox* was defined using the standard value of 8 as the average for all texture classes with a standard deviation of 1. Uptake of nutrients (Ca, Mg, K and N) was computed as forest growth rate multiplied with nutrient content (Jacobsen et al., 2002). Principally these nutrient contents are uncertain as well, but since measurements only provide the final base cation concentration, it is not possible to calibrate both uptake and weathering in a meaningful way. We therefore decided to calibrate only base cation weathering. For nitrogen, the various sinks (uptake, denitrification, immobilization) cannot be distinguished either. Nevertheless, we decided to calibrate both the denitrification fraction assuming a relatively small uncertainty and two parameters in an immobilization function.
Denitrification was calibrated for two different drainage classes: well-drained and moderately well-drained. Prior estimates of denitrification fraction were obtained from Reinds et al. (2001). Poorly or very poorly drained soils were not included in the set of 182 calibration plots as no hydrological data were available for such wet soils.
N immobilization can be substantial in the current environmental situation (Gundersen et al., 1998; De Vries et al., 2001) and was estimated as a function of the N deposition according to:

$$N_{imm} = a + b \cdot N_{dep} \quad (1)$$

where a was set to 1 kg N as an estimate of the long-term immobilization even at very low N input (UBA, 2004) and the parameter b was calibrated. Parameter b thus expresses the proportion of the N input that is immobilized additional to the long-term constant immobilization. Since some evidence exists that there is a (weak) relationship between C/N ratio in organic matter and immobilization rates of N (Gundersen et al., 1998; Gundersen et al., 2006), three prior distributions for b were defined: one for soils with low C/N ratio (< 25), one for soils with intermediate C/N ratios and one for soils with high C/N ratio (> 35). For each class a prior uniform distribution between 0 and 1 was assumed as there is also evidence that within C/N ratios classes, immobilization fractions can strongly vary (De Vries

et al., 2001). This is the reason that for the calibration the original VSD formulation of N immobilization as a function of C/N ratio was replaced by Equation 1.If no literature data were available, expert judgment was used to define the prior distributions of some parameters. Prior distributions for these parameters were taken such that the range was wide enough to cover all possible values. This limitation is to a large extent compensated by the calibration procedure that provides posterior distributions that are more strongly determined by the likelihood than by the prior distributions.

2.4 Observations

To assess the likelihood of the simulation results, comparisons were made between simulated and measured soil solution concentrations below the root zone. Measured concentrations of H, Ca + Mg + K, and NO_3 were used. Free Al was recomputed externally from the measurements of total Al, by modelling complexation of Al with organic anions, using measured DOC values and dissociation and Al complexation constants provided by Santore et al. (1995). Measurements were aggregated to average annual concentrations, yielding about 5-6 values per plot (1996-2001). Furthermore, a single measurement of the base saturation of the soil solid phase was used. The uncertainty in the measured soil solution concentrations cannot be obtained from the data directly as the samples collected from various samplers within the plot were pooled into a mixed sample before analysis. It is likely that the uncertainty in the measured concentrations is mostly determined by spatial variability within the plot. A study at some monitoring plots in the Netherlands showed that this variability varies between 20 and 60% depending on depth and ion (De Vries et al., 1999). An uncertainty of 30% was used as an uncertainty estimate for all plots in Europe as this was about the uncertainty for the major ions at 40-60 cm depth in the Dutch plots. For very low concentrations that often are observed for Al and NO_3 , 30% uncertainty is probably an underestimate. For measurements equal to or lower than the detection limit of the most widely used analysis equipment (Inductive Coupled Plasma spectrometry , ICP) the uncertainty was therefore set at two times the detection limit of the ICP.

2.5 Calibration method

2.5.1 Bayes' theorem

The VSD model was calibrated using Bayesian calibration. Our implementation of Bayesian calibration strongly resembles the method applied by Van Oijen et al. (2005).
In the Bayesian approach the prediction of uncertain parameters is taken to be conditional on data, and their conditional probability is given by:

$$p(\theta \mid D) = c \cdot p(D \mid \theta) \cdot p(\theta) \quad (2)$$

Where $p(\theta|D)$ is the posterior probability distribution for the parameter vector θ given the data D, $p(D|\theta)$ is the likelihood-function for θ and $p(\theta)$ is the prior distribution of θ. The value of c (=1/$p(D)$) is independent of the parameters and need not be computed explicitly (Van Oijen et al., 2005).
In our approach, the prior distribution for the parameter vector $p(\theta)$ is formed by multiplication of marginal distributions for individual parameters, so no correlations between parameters are assumed in the prior. The distributions of VSD input parameters are listed in Table 1. As Equation (2) shows, the posterior probability for θ increases with both increased prior probability and increased likelihood, i.e. when the selected set of parameter values has larger a-priori probability and when the model is able to reproduce the measurements more closely. The prior probability for any parameter vector is found by inspection of the prior distribution, whereas the likelihood associated with a parameter vector is derived from a comparison of model output (generated using those parameter values) with data. The likelihood $p(D|\theta)$, is computed assuming measurement errors are Gaussian and uncorrelated (Van Oijen et al., 2005):

$$\log p(D \mid \theta) = \sum_{i=1}^{n} \left(-0.5 \left(\frac{O_i - S_i}{M_i} \right)^2 - 0.5 \log(2\pi) - \log M_i \right) \quad (3)$$

Where the S_i are simulation results and O_i observations, n is the number of observations and M_i. is the standard deviation of the measurements. The observations we used are measurements of soil (solution) chemistry at the Intensive Monitoring plots.
When calibrating VSD we assume that the model is correct and thus ignore model error. Our estimates of model output uncertainty thus only show the contribution

from parameter uncertainty. After site specific calibration, the remaining error, here expressed in the normalized root mean square error (NRMSE), is a measure of model error but it also includes measurement error (Larssen et al., 2006).

2.5.2 Markov Chain Monte Carlo

In practice, Equation (2) has to be evaluated numerically when using dynamic models like VSD. In such cases, Bayesian techniques rely on carrying out a large number of simulations, often in the form of a Markov Chain Monte Carlo (MCMC) approach. To calculate the posterior $p(\theta|D)$, we used a simple MCMC algorithm, the Metropolis-Hastings random walk (Robert and Casella, 1999). In this method, the multi-dimensional parameter space (where the number of dimensions, N_p, equals the number of uncertain model parameters) is explored by randomly stepping through this space and running the model for each visited point. The combination of number of steps and step size should be chosen such that the parameter space is adequately sampled during the MCMC. In the first step, a candidate value for each parameter is chosen. The model is run for N plots (with N =1 for the single site-calibration or N equals a set of plots for the multi site-calibration) and the likelihood is determined. We started the Markov Chain by selecting for each parameter the midpoint of the prior distribution. To test the sensitivity of the method to the starting point of the Markov Chain, we have also calibrated the model using a starting point that consists of parameter values randomly chosen within the 95% confidence interval of the prior distribution. For subsequent runs a new candidate point (consisting of N_p parameter values) is computed by moving randomly away from the current point in the multi-dimensional parameter space. If, for the new point, the product of prior probability and likelihood exceeds that of the current point, the new point is accepted. On the other hand, if the ratio of new and current products of the prior and likelihood is between 0 and 1, the new point can still be accepted, but with a probability equal to that ratio. The algorithm is inherently stochastic since candidate points that perform (somewhat) worse than previous points can still be accepted. If the candidate point is not accepted, the previous candidate point is duplicated in the chain of accepted points. Eventually, this procedure yields a chain of points in the N_p-dimensional parameter space. To account for a 'burn-in' of the chain, i.e. to remove the effect of the choice of the starting point, the first 10% of the runs are removed from the chain. The remaining chain contains all accepted (or duplicated) parameter values. From this chain we derived the posterior distribution of each parameter. Furthermore, correlation and covariance matrices were computed from the chain using the standard statistical routine CORVC from the IMSL statistical

library (Visual Numerics, 1997). By running multiple chains with different starting points, we verified convergence of the calibration.

2.5.3 Practical implementation

In the single-site calibration every plot was calibrated separately so that the posterior distributions are computed on a plot by plot basis. In the multi-site calibration all plots within a soil group are calibrated simultaneously, thus obtaining posterior distributions for the entire soil group. In the single site calibration we assume that soil parameters vary in space, i.e. even within a soil group parameters values can be different for different sites. For each plot the calibration yields a plot-specific estimate of the posterior distribution of parameters. In the multi-site calibration we assume that parameters are constant in space. For each group of plots with uniform soil characteristics, one posterior distribution per parameter will be computed. Calibrating for each plot separately can provide insight in the variation and patterns in posterior distributions over Europe. Such patterns can provide means to extrapolate the results to an European scale. Calibrating all plots simultaneously yields posterior distributions that can be directly used on an European scale but only with the assumption that for a given soil group parameters are constant in space.

3. Results and discussion

3.1 Results for single-site calibrations

In the following, the success of the BC application to the VSD model is evaluated by checking whether (a) the goodness-of-fit of VSD has increased after calibration, (b) the posterior distribution is narrower than the prior, indicating reduced parameter uncertainty (c) running the calibrated model on the 60 validation plots. The calibration used a chain length of 50000 and the mean step length, i.e. the standard deviation of the proposal distribution, is set at 3% of the width of the prior.

3.1.1 Likelihood

To quantify the gain in model performance, a comparison was made between the goodness-of-fit using a run at every calibration plot with parameters set to the mean of their prior distributions and the average goodness of fit over those runs in

the Markov Chain that form the posterior distribution. Goodness-of-fit is expressed here as the Normalized Root Mean Square Error (NRMSE), defined as the root of the mean squared difference between measurements and simulations, divided by the mean of the measurements. Figure 2 shows the cumulative frequency distributions of NRMSE for pH, Al, NO_3 and base saturation (EBc) based on all 122 calibrated plots before and after calibration.

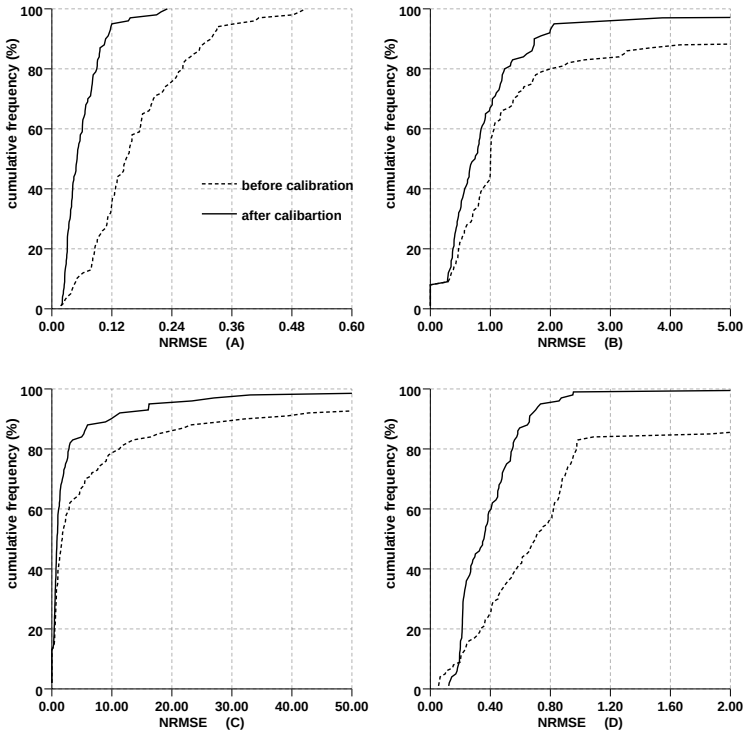

Figure 2. Cumulative frequency distributions of NRMSE for pH (a),Al (b), NO_3(c) and EBc (d) at the calibration plots before (dashed) and after calibration (solid).

Figure 2 shows, as expected, that for all VSD output parameters the average NRMSE computed from all runs from the MCMC is much smaller than the NRMSE of the run using the mean of the priors. Especially for pH and NO_3, the model prediction error decreases strongly: the median error after calibration is less than half the error prior to calibration.

For Al and NO_3 errors for about 10-20% of the plots are zero as both the measured as well as the simulated concentrations are zero. Figure 2 also shows that for a limited number of plots (about 10%), model prediction errors in especially NO_3 and base saturation remain large despite calibration. For EBc these are probably the plots where the combination of observed EBc and observed pH cannot be

reproduced by the VSD model. Since there is only one observation on EBc and mostly 5-6 observations for pH, it is likely that the calibration procedure will move towards a good fit on pH rather than on EBc. Large residual NRMSE can be due to model error, but could also be caused by measurement error, indicated by, for example, unlikely combinations of measured pH and base saturation.

Figure 3 shows the spatial pattern in the NRMSE before calibration minus the NRMSE after calibration, for pH and NO_3. The larger the value, the larger the gain in model performance. Figure 3a shows that for most plots a substantial gain in model performance is achieved for pH, but that in parts of Germany, the UK and the plots in southern Europe the NRMSE does not strongly decrease. Part of the explanation is given by Figure 3b that shows the gain in NRMSE for NO_3. This figure shows a strong increase in model performance for most of the plots for which pH did not strongly improve. Obviously, the calibration at these plots leads to much lower errors in the simulated nitrate concentrations but the parameterisation improves the simulation of total acidity to a lesser extent. Figure 3b also shows that for many plots in Southern Scandinavia, Eastern parts of Germany and southern Europe, the calibrated model performs much better for NO_3 with calibrated parameters than with the default mean parameter values.

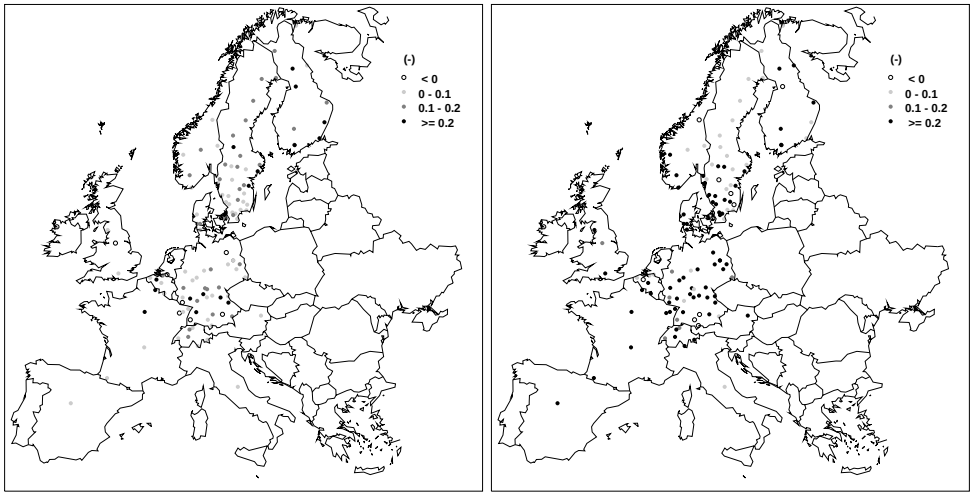

Figure 3. Gain in NRMSE for pH (left) and NO3(right) after calibration.

3.1.2 Posterior distributions of model parameters

The main result of the Bayesian calibration procedure is the joint posterior distribution for the model parameters. The posterior distribution also contains correlations between parameters. However, it is difficult to visualize a multi-dimensional distribution for many sites, so in the following we shall focus on the marginal distributions for individual parameters. If the measurements are conclusive enough, broad prior distributions will narrow down and thus demonstrate a reduction of parameter uncertainty. Posterior distributions may also lie in the high or low parts of the prior distributions, indicating that the data forced a small probability to parameter vectors that were considered plausible before. If the a priori assumed relationship between soil characteristics and parameter values is confirmed by the data, one may expect that the mean of the posterior probability distribution functions will not differ much from the mean of the prior pdf, but uncertainty could be significantly reduced.
Figure 4 shows the prior and combined posterior distribution of the base cation weathering rates for the low (1), intermediate (3) and high (6) weathering rate classes. For the other classes only a few plots (< 15) were available so the posterior distribution may be more strongly determined by the prior distribution.

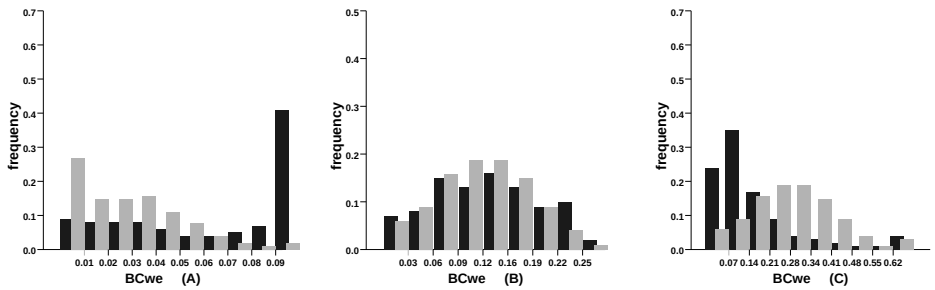

Figure 4 Prior (light grey) and posterior (dark grey) distribution functions for weathering rates classes 1 (A),3 (B) and 6 (C).

It shows, as expected, that weathering rates increase with increasing weathering rate class. It also shows that the prior for weathering rate class 1 was underestimated: after calibration the distribution is at much larger values than the prior, with the median weathering rate being about 2 times as large as initially assumed. Posterior weathering rates for class 6 (rich clay soils) tend to be skewed towards small values, whereas the posterior for weathering rate class 3 (clay soils) indicates that the observations do not significantly change the prior estimate, although the posterior distribution function is more uniform than the prior normal

distribution.In Figure 5, the distribution functions are displayed for the *lgKAlox* parameter, i.e. the logarithm of the equilibrium constant of amorphous Al hydroxide in equilibrium with H and Al in the soil solution.

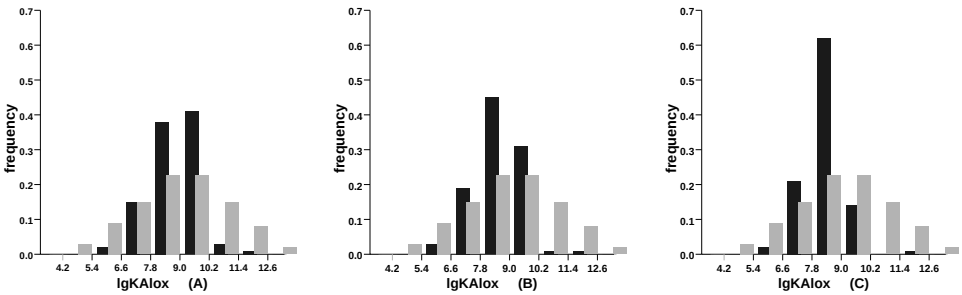

Figure 5. Prior (light grey) and posterior (dark grey) distributions of lgKAlox for sand (A), clay (B) and heavy clay (C)

It clearly shows that the data strongly narrow the prior distributions; uncertainties in the posterior parameter distributions are much smaller than the a priori assumed. Furthermore, the posterior distributions show that there is little difference between the three texture classes. As expected *lgKAlox* values decrease somewhat with increasing clay content.

Figure 6 shows the prior and posterior distributions for the exchange constants *KAlBc* and *KHBc* for sand and clay. It shows that the posterior distributions of *KAlBc* and *KHBc* for sand hardly differ from their priors, indicating that the data cannot improve the accuracy of the initial estimates of the exchange constants.For clay soils, the posterior distributions differ somewhat from the prior. For *KAlBc* there is a shift towards somewhat smaller values, for *KHBc* there is a shift to somewhat larger values.

Figure 7 indicates some differences in nitrogen retention between plots with low and intermediate C/N ratios: as expected low N retention fractions occur more frequently for low C/N ratios (indicating nitrogen saturation) than for large C/N ratios. In the majority of the plots with high C/N ratios more than 80% of the incoming N is retained. In Figure 7 the prior and posterior distribution of the fraction of nitrogen after N uptake and denitrification that is immobilized (parameter *b* in equation 1) is shown for the two C/N ratio classes, 'low' and 'intermediate'.

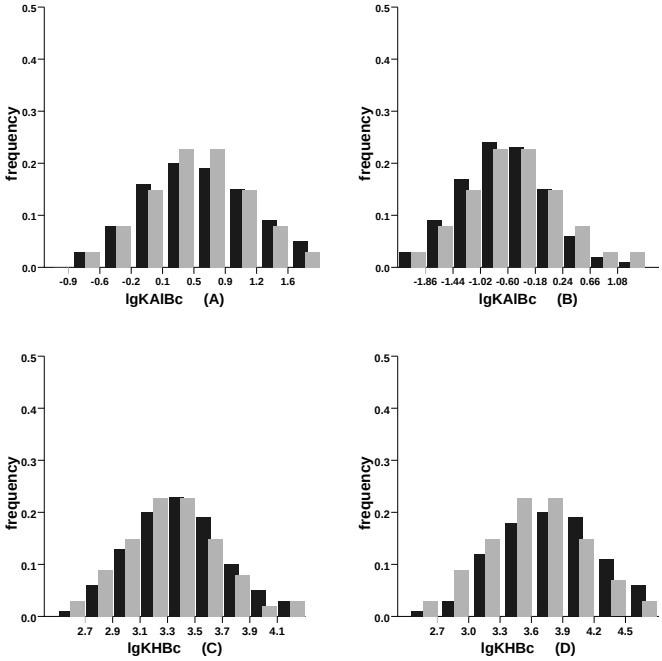

Figure 6 Prior (light grey) and posterior (dark grey) distributions for the exchange constants KAlBc for sand (A) and for clay (B) and KHBc for sand (C) and for clay (D).

The graphs clearly show that the calibration procedure confirms findings based on other datasets (e.g. Gundersen et al., 2006), namely that the immobilisation fraction varies widely even within different C/N ratio classes but that low retention occurs mainly at sites with low C/N ratios.

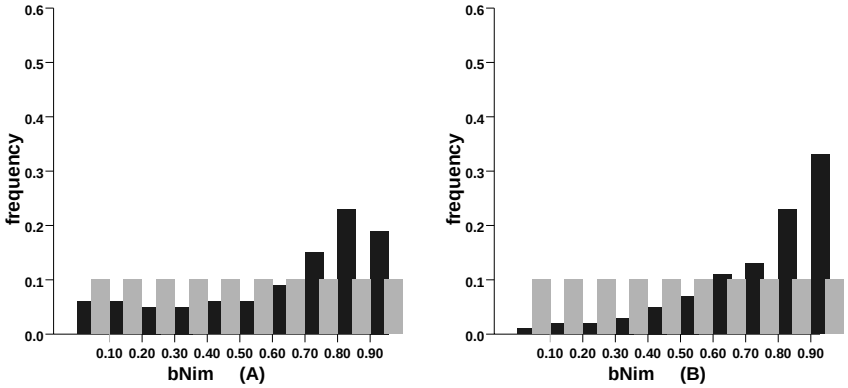

.

Figure 7. Prior (light grey) and posterior (dark grey) distributions of the N immobilization fraction b for soils with a low C/N ratio (A) and intermediate C/N ratio (B)

The majority of sites retain most of the incoming nitrogen (parameter values close to one)

3.1.3 Influence of the starting point of the Markov Chain

In the standard run, the Markov Chain is started at the mean of each prior parameter distribution. Ideally the starting point should have no influence on the posterior distributions. Different posterior distributions may be obtained from different starting points if the parameter space is not explored sufficiently. Figure 8 shows the posterior distributions for *lgKAlox* for sand and clay and for the *BCwe* for soils with texture class 1 for different starting points. The figure shows that the posteriors are very similar, indicating that the Markov Chain converged to the same part of the parameter space, independent of its starting point.

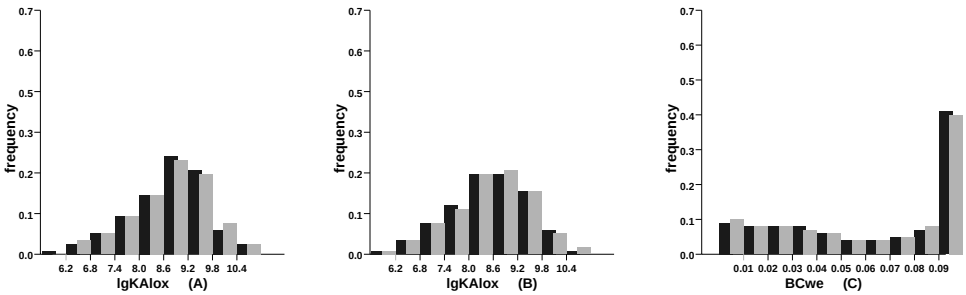

Figure 8. Posterior distributions of lgKAlox for sand (A) and clay (B) and of weathering rate for texture class 1 (C) as a function of the starting point of the Markov Chain (dark grey = mean, light grey = random).

3.1.4 Validation

For validation, the NRMSE for the VSD output parameters was computed for each of the 60 validation plots. One run was made using parameter values set equal to the mean of the priors (uncalibrated run) whereas in the second run input parameters were set to the median of the posterior parameter distributions obtained from the calibration. For each validation plot, the proper posterior distribution was selected based on soil texture, parent material and topsoil C/N ratio of the plot. The cumulative frequency distributions of the NRMSE for pH, Al, NO_3 and base saturation (EBc) before and after calibration show that NRMSE decreases for pH, NO_3 and to a lesser extent for EBc if the model is run at the validation plots using the results from the calibration (Figure 9).

Comparing Figures 9 and 2 shows that the gain in NRMSE for the validation plots is smaller than for the calibration plots. This is as expected. For the VSD application to the validation plots the median value from the posterior distributions obtained from the entire set of calibration plots was used, whereas the calibration plots were calibrated individually, thus obtaining the best fit for each plot. Nevertheless, the calibration has shown to be successful because the application of the calibrated model to the validation plots yields a (much) better fit to the observed soil solution concentrations (except for aluminium) than the application with parameter values at the mean of the prior distribution.

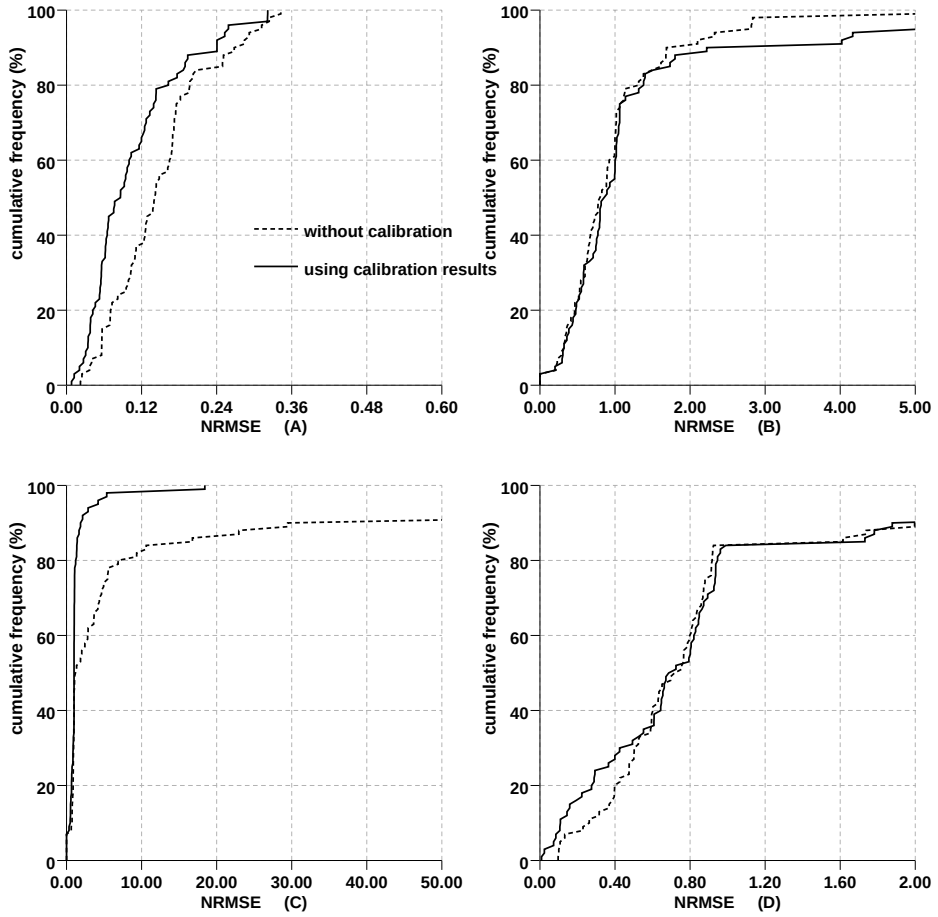

Figure 9. Cumulative frequency distributions of NRMSE for pH (a),Al (b), NO3(c) and EBc(d) at the validation plots, before (dashed) and after single-site calibration (solid).

3.2 Multi-site calibration

3.2.1 Calibration

In the multi-site calibration, for every soil group (i.e. a set of sites with the same soil characteristics), the vector of model parameters was selected from a single prior multivariate distribution and the overall prior probability was computed. We thus assumed that the parameter values per soil group are constant. For example, all plots with poor sandy soils were assigned the same *lgKAlox* value selected from the prior for poor sandy soils. Then, simulations were made for all plots and the overall likelihood, being the product of all the likelihoods over all plots was computed. It was thus assumed that observation and model errors are independent. Next a new candidate point was selected by taking a step in the multi-dimensional parameter space following the same procedure as for the single-site calibration.
This procedure thus calibrates all sites simultaneously and uses MCMC to obtain values of the N_P model parameters that give a good fit for all plots within a soil group simultaneously. In this case the Markov Chain converges to a very narrow posterior distribution due to the large number of observations, and the uncertainty about the model parameters becomes very small (Figure 10). The figure shows the prior and very narrow posterior distributions of *lgKAlox* for sand and clay and *BCwe* for weathering rate class 3. The large number of observations (120 plots and 3-5 years of soil solution measurements) causes this very small parameter uncertainty. Because we assume VSD to be correct, and thus ignore model error, the uncertainty shown here is parameter uncertainty only.

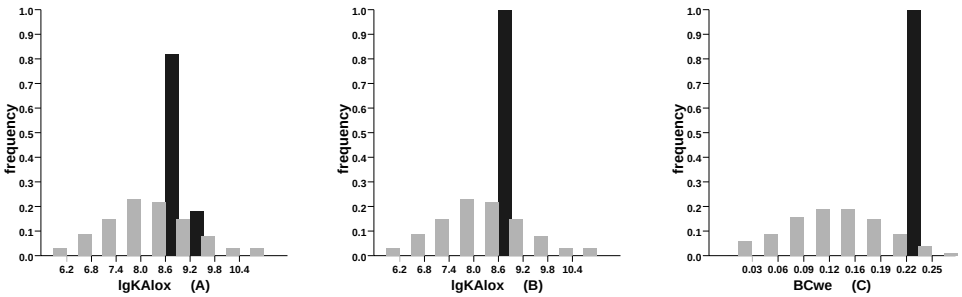

Figure 10. Prior (light grey) and posterior (dark grey) distributions for the parameter lgKAlox for sand (A) and clay(B) and for base cation weathering for weathering rate class 3 (C); multi site calibration.

Comparing the NRMSE from the multi-site calibration with the single-site calibration shows that the NRMSE at the calibration plots from the multi-site calibration exceeds the NRMSE from the single-site calibration for all parameters. Largest differences occur for pH where the median error over all 122 plots from the multi-site calibration is about twice that of the single-site calibration. For NO_3, Al and EBc differences are much smaller (20-25% in the median NRMSE). This shows that assuming constant parameter values for a soil group leads to a larger model prediction error than calibrating the parameters for each plot separately. Although parameter uncertainty after calibration is small, the model uncertainty is large, i.e. VSD parameterized with spatially constant parameters has a larger model error than VSD with local parameter settings.

3.2.2 Validation

The multi-site calibration was verified by running VSD for the 60 validation plots with parameter values sampled from the posterior distributions obtained from the multi-site calibration and comparing the NRMSE with the NRMSE obtained with parameters set to the mean from their prior distributions (see also section 3.1.4). Figure 11 shows that for pH and NO_3 the calibration leads to (much) smaller simulation errors, but for aluminium no improvement is achieved. The same was observed in the validation of the singe site calibration. For EBc the NRMSE decreases for part of the plots but increases for other plots, but the the largest errors disappear due to the calibration. Comparing Figure 11 with Figure 9 shows that the NRMSE at the validation plots using the multi-site calibration exceeds the NRMSE from the singe-site calibration for EBc. For pH and Al the errors are about equal. For a number of plots the error in NO_3 when using the results from the multi site calibration is substantially smaller than the error from the single-site calibration.
These are most likely the plots in the validation set where despite a high N input, all N is retained. In the multi site calibration the median f_{nim} is close to one and thus almost all incoming N is retained, but in the singe site calibration, also small f_{nim} values are present leading to a smaller median f_{nim}. Using the smaller value leads to large errors for some of the validation plots. Furthermore, because the NRMSE is defined as the square root of the mean squared difference between measurements and simulations divided by the mean of the measurements, NRMSE can become very large if simulated nitrate concentrations exceed observed concentrations and the observed nitrate concentrations are very small.

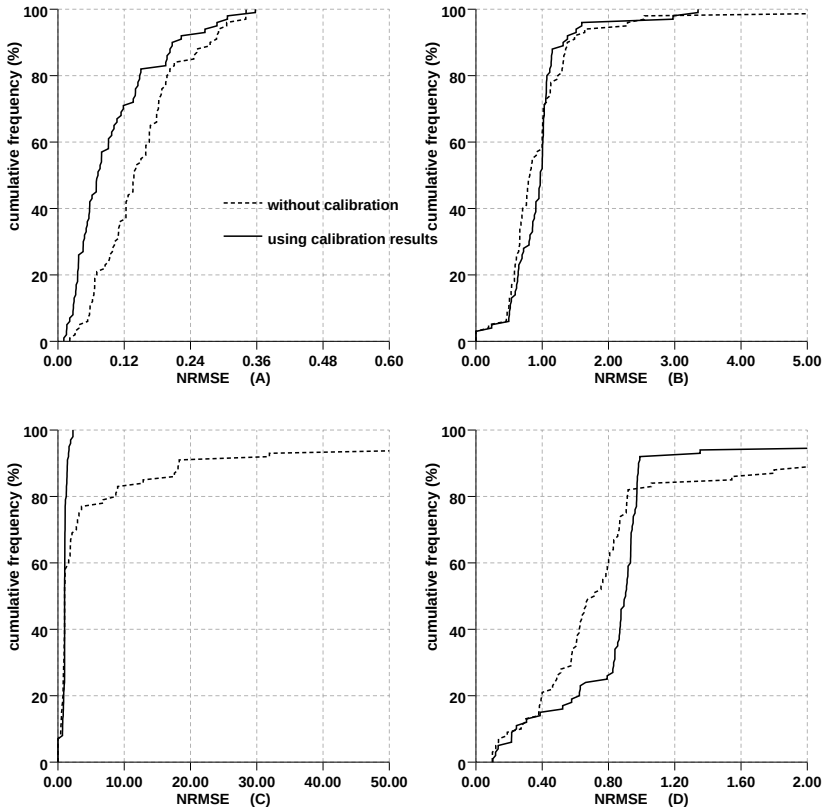

Figure 11. Cumulative frequency distributions of NRMSE for pH (a),Al (b), NO3(c) and EBc(d) at the validation plots, before (dashed) and after multi-site calibration (solid).

To check that the Markov Chain in the multi-site calibration converges to the area with the combination of highest prior probability and highest likelihood, the Markov Chain was run (a) with another, random, starting point and (b) by crudely assuming that all parameters have a uniform distribution (with lower and upper bounds set at the 5 and 95 percentile of the normal distribution, respectively). In case (b) we eliminated the effect of the form of the prior probability and gave the Markov Chain more liberty in exploring parameter space.

Results from the run with the uniform distribution and the run with a random starting point of the Markov Chain show also a very low acceptance (about 0.3-0.5%) and the posterior distributions only slightly differ from the ones of the standard run. This is illustrated in Figure 12, which shows the cumulative frequency diagrams for the three runs for *lgKAlox* for sand and clay and *BCwe* for weathering rate class 3.

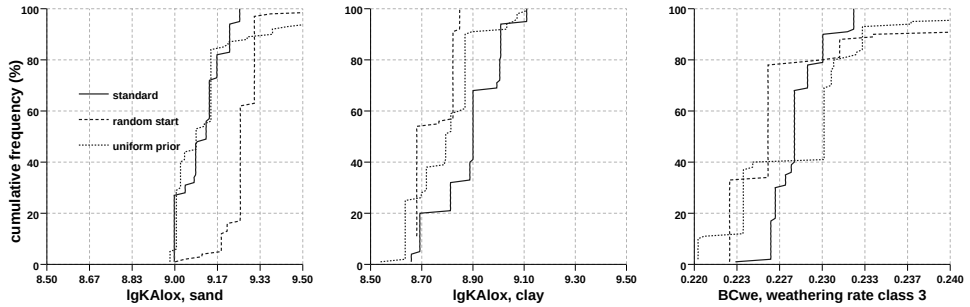

Figure 12. Cumulative frequency distributions of lgKAlox for sand (A) and clay (B) and BCwe for weathering rate class 3(C) for the standard run (solid), run with uniform prior (dot) and run with random start (dash)

In all cases the posterior distributions are very narrow and very similar. This shows that the Markov Chain of the multi site calibration converges to the same posterior pdf, irrespective of the starting point or assumptions about the distribution type of the prior, proving the robustness of the procedure.

4. Discussion and conclusions

The Bayesian calibration technique using MCMC applied in this study has proven a successful method to calibrate the VSD model at a large set of locations. By applying a single-site calibration and sampling from a set of prior distributions defined as a function of site characteristics such as soil texture, the fit of the model on the soil solution measurements strongly improved compared to model runs with standard values for the input parameters. At the same time the parameter uncertainty was quantified, and the posterior distributions can be used for uncertainty assessments with VSD at the plots. This gives a clear advantage over simple calibration techniques used for VSD previously. An application of the calibrated model (using the median parameter values from the posterior distributions obtained from the calibration) to the 60 validation plots showed that a (much) better fit to the observed soil solution concentrations is obtained than for an application with parameter values at the mean of the prior distribution. Only for the aluminium concentration no improvement in the fit was achieved.

Posterior distributions of base cation weathering rates show that for plots in the sandy texture class, often relatively high weathering rates compared to literature data, such as De Vries et al. (1994b), are required to simulate the observed base

cation concentrations. This can be explained by the fact that the prior base cation weathering for class 1 is mainly based on data from pure sandy soils. Texture class 1 though, is a texture class encompassing pure sandy soils as well as soils with clay contents up to 8 per cent. It seems that a substantial number of plots with weathering class 1 have a relatively rich mineralogy and/or high clay content, leading to higher weathering rates than initially assumed.

Comparison of posterior distributions with the prior distributions showed that the data are conclusive for the *lgKAlox* parameter, because the posterior distribution is much narrower than the prior. For the exchange constants, the calibration does not lead to narrower distributions, but some shifts do occur.

The simulation of the nitrogen cycle in VSD is very simple and may sometimes be too simple to adequately model the nitrogen fluxes observed in the field (Evans et al., 2006). In VSD, nitrogen immobilization is modelled as a function of C/N ratio in the soil. In this study we have modelled immobilization using a linear function, where immobilization is modelled irrespective of C/N ratios as a fraction of the remaining nitrogen after uptake and denitrification. By defining three identical prior distributions for different C/N ratios, we could judge by the posterior whether the data yielded a clear difference between the three classes. The posterior distribution of the immobilized fraction of nitrogen for soils with a low C/N ratio is similar to that of soils with a higher C/N ratio although low N retention fractions are clearly more frequent for low C/N ratios than for intermediate C/N ratios. Also other studies have shown that the fraction of N immobilized can strongly vary within C/N classes (Gundersen et al., 1998). Consequently, the way in which N removal is currently modelled in the standard VSD model needs to be reconsidered. However, the fact that many processes influence the N balance (uptake, denitrification, immobilization, leaching), makes it difficult to adequately model and calibrate the associated parameters.

The multi-site calibration in which all sites were modelled simultaneously aiming at the highest combination of prior probability and likelihood over all plots within a soil group also strongly improved the goodness of fit of the model results compared to a run with standard values for model parameters for the 60 validation plots. The median *NRMSE* for pH after calibration was about 2 times as high as the median *NRMSE* from the validation of the single-site calibration, but for Al, NO_3 and EBc a difference in NRMSE of only 20-25% was observed. Due to the large amount of data and the assumption that VSD is 'correct', the multi-site calibration leads to a very small parameter uncertainty with very narrow posterior

distributions. The NRMSE for the validation plots is higher than the NRMSE of the single-site calibration because we assumed that parameters are constant in space for a given soil group. This assumption limits the flexibility of the model to adapt to the local situation. A compromise could be to perform multi-site calibrations within environmental zones (Metzger, 2005) instead of entire Europe. This could reduce model error and still allow the use of the calibration results in European-wide applications of VSD.

Further study is required to make a full in-depth analysis of the multi-site calibration to confirm that the narrow posterior distributions are caused by the large amount of data only that makes parameter uncertainty small, and that the result is not strongly influenced by (sets of) plots with certain (deviating) characteristics or specific measurements. We have noticed in the singe-site calibration that a few measurements with small uncertainty can strongly limit the acceptance in the MCMC procedure. Such small uncertainty in data must be realistic to justify small uncertainty in the posterior distributions. Therefore we also feel that more data on the (spatial) variation of the soil solution measurements are needed to improve the uncertainty estimates as the current assumption of a fixed 30% standard deviation was a crude assumption based on a single data set.

In the multi-site calibration the parameter uncertainty becomes very small because we do not include a model error term in the computation of the likelihood. To assess the uncertainty in model structure, a Bayesian model comparison of VSD could be used in which VSD is compared with, for example, more detailed models . Another way to assess the error due to model structure would be to run VSD at plots with completely independent validation data using the posterior distributions of the calibrated parameters obtained in this study and then compare the model error with the model error at the calibration plots (Heuvelink and Pebesma, 1999; Kros et al., 2002), but this requires a.o. a correct quantification of the measurement error of the observations.

Acknowledgements
We thankfully acknowledge the European Commission, DG Agriculture and DG Environment, as well as the Dutch Ministry of Agriculture, Nature and Food Quality for their co-financing of the project.

Uncertainties in critical loads and target loads of sulphur and nitrogen for European forests: analysis and quantification

Reinds, G.J. & De Vries, W. 2009. Uncertainties in critical loads and target loads of sulphur and nitrogen for European forests: analysis and quantification. Submitted to *Science of the Total Environment*.

Abstract
An analysis of the uncertainties in critical loads and target loads of sulphur and nitrogen for 182 European forest soils was carried out using the Very Simple Dynamic (VSD) model. VSD was calibrated with a Bayesian approach using prior probability functions for all model parameters based on literature data, data from a Dutch study at 200 forets sites as well as simulated denitrification rates from a detailed ecosystem model. The calibration strongly improved the fit of the model to the observed soil and soil solution concentrations, especially for pH and base saturation. Calibration also narrowed down the ranges in input parameters. The uncertainty analysis showed which parameters contribute most to the uncertainty in the critical loads and target loads simulated by VSD. Base cation input by weathering and deposition, and the parameters describing the H-Al equilibrium in the soil solution determine the uncertainty in the maximum critical loads for S, $CL_{max}(S)$, when based on the widely used aluminium to base cation (Al/Bc) criterion. Uncertainty in $CL_{max}(S)$ based on an Acid Neutralizing Capacity (ANC) criterion is completely determined by base cation inputs alone. The denitrification fraction, f_{de}, is the most important source of uncertainty for the maximum critical loads of N, $CL_{max}(N)$. Nitrogen (N) uptake and N immobilisation determine the uncertainties in the critical load for N as a nutrient, $CL_{nut}(N)$. Calibration of VSD reduced the uncertainty in critical loads and target loads: the coefficient of variation (CV) was reduced for all critical loads and criteria. After calibration, the CV for $CL_{max}(S)$ was below 0.4 for almost all plots; however for $CL_{max}(N)$ high values occured for plots with a high denitrification rate. Model calibration improved the robustness of the need for target loads: after calibration, no target loads were needed in any of the simulations for 40% of the plots, with the uncalibrated model there was a positive probability for the need of a target load for almost all plots.

Keywords: Bayesian calibration, Forest Soils, Critical loads, Target Loads, Uncertainties

1. Introduction

Critical loads of nitrogen and sulphur play an important role in the political process targeted at the abatement of air pollution in Europe (Hettelingh et al., 1995a; Hettelingh et al., 2007). Critical loads, defined as "a quantitative estimate of an exposure to one or more pollutants below which significant harmful effects

on specified sensitive elements of the environment do not occur according to present knowledge" (Nilsson and Grennfelt, 1988) are used to for quantifying the sensitivity of ecosystems to acidification and eutrophication. Critical loads for nitrogen and sulphur in view of their acidifying effects are mostly computed with the Simple Mass Balance (SMB) model (Sverdrup and De Vries, 1994; UBA, 2004). Critical loads for nitrogen as a nutrient can also be modelled with SMB or be derived from N addition experiments in the field (empirical critical loads; (Bobbink et al., 2002).

Critical loads indicate the sensitivity of ecosystems to acidification and eutrophication, but do not provide any information on (the speed of) damage to these systems if deposition is above the critical load, nor about their recovery if the deposition is reduced below the critical load. For such assessments a dynamic approach is needed. The Very Simple Dynamic (VSD) model is a simple extension of the SMB model that includes finite buffer processes, such as cation exchange and time-dependent N immobilisation (Posch and Reinds, 2009). VSD evaluates the effects of deposition changes on soil and soil solution chemistry, and is thus suited to evaluate the temporal aspects of deposition reduction scenarios in view of the desired chemical status of the soil. It is also suited for computing target loads, i.e. the deposition of N and S that leads to a desired chemical state of the ecosystem in a given future year (Posch et al., 2003).

Modelled critical loads and target loads are uncertain (Skeffington, 2006) caused by uncertainty in (a) model structure and model assumptions, (b) input data and model parameters, and (c) the value of the chemical criterion used. Uncertainty in model structure is caused by, for example, model simplifications, such as assuming a homogenous soil layer. De Vries et al. (1994a) showed that critical loads are sensitive to the depth at which the chemical criterion is applied: critical loads at the bottom of the root zone are lower than at 10cm depth, mainly due to differences in water fluxes and the H-Al equilibrium. Uncertainties in critical loads due to in uncertainties in the chemical criterion can be substantial. Reinds et al. (2008a) showed in an analysis for Europe and northern Asia that the uncertainty in the criterion for nitrate lead to major differences in critical loads.

Uncertainties in critical loads due to parameter uncertainty have been studied for individual sites (Zak and Beven, 1999; Bosman et al., 2001; Li and McNulty, 2007; Skeffington et al., 2007) and countries (Barkman et al., 1995; Barkman et al., 1999; Barkman and Alveteg, 2001; Hall et al., 2001b). Some of these studies examine the effects of one uncertain input parameter only, whereas other studies include many or all model parameters and inputs. In most of these assessments, uncertainties in input data are obtained from measurements, whereas uncertainties in model parameters are mostly obtained from literature data.

Expert judgement is often needed to quantify the uncertainties in both input data and model parameters for which no other information is available.
In this study we quantified the uncertainties in critical loads and target loads of nitrogen and sulphur for 182 monitoring plots in Europe. For process parameters, such as chemical equilibrium constants, and input parameters, such as atmospheric deposition of nitrogen, sulphur and base cations, we defined prior distributions based on site measurements, literature data and on uncertainties derived from a Dutch data set with soil and soil solution measurements (De Vries and Leeters, 2001). In this paper we refer to input data and process parameters as model parameters. The uncertainty in the uncalibrated model was computed by sampling the prior distributions. We then applied a Bayesian calibration of VSD (Reinds et al., 2008b) from which we obtained posterior distributions of all model parameters. The uncertainty in critical loads and target loads from the calibrated model was assessed by performing a Monte Carlo analysis, sampling model parameters from the posterior parameter distributions.

2. Methods

2.1 Calculation of critical loads and target loads with the VSD model

VSD (Posch and Reinds, 2009) is a simple dynamic model that simulates soil solution chemistry and cation exchange pools. It consists of a set of mass balance equations, describing the soil input-output relationships of ions, and a set of equations describing the rate-limited and equilibrium soil processes. The soil solution chemistry in VSD depends solely on the net element input from the atmosphere (deposition minus net uptake minus net immobilisation) and the geochemical interactions in the soil (CO_2 equilibrium, bass weathering, and cation exchange). Soil interactions are described by simple rate-limited reactions (e.g. nutrient uptake and weathering), first order processes (denitrification) and by equilibrium reactions (e.g. cation exchange). VSD models the exchange of Al, H and Ca+Mg+K with Gaines-Thomas or Gapon equations. Solute transport is described by assuming complete mixing of the element input within one homogeneous soil compartment with a constant density and depth. VSD predicts the concentration of the soil solution leaving this layer (mostly the root zone). The time-step of simulations is one year.

In steady-state mode, VSD reduces to the simple mass balance (SMB) model for computing critical loads of sulphur (S) and nitrogen acidity (Sverdrup and De Vries, 1994; UBA, 2004):

(1)
$$CL(S) + (1 - f_{de}) \cdot CL(N) = (1 - f_{de}) \cdot (N_u + N_i) + BC_{dep} + BC_w - Bc_u - Cl_{dep} - ANC_{le,crit}$$

with:

$CL(S)$	critical load of sulphur (eq ha^{-1} yr^{-1})
$CL(N)$	critical load of nitrogen (eq ha^{-1} yr^{-1})
f_{de}	denitrification fraction (-)
N_u	nitrogen uptake (eq ha^{-1} yr^{-1})
N_i	nitrogen immobilized (eq ha^{-1} yr^{-1})
BC_{dep}	base cation (Ca+Mg+K+Na) deposition (eq ha^{-1} yr^{-1})
Cl_{dep}	chloride deposition (eq ha^{-1} yr^{-1})
BC_w	base cation weathering (eq ha^{-1} yr^{-1})
Bc_u	base cation (Ca+Mg+K) uptake (eq ha^{-1} yr^{-1})
$ANC_{le,crit}$	critical leaching of acid neutralizing capacity (eq ha^{-1} yr^{-1})

Equation 1 gives a critical load function (*CLF*) for S and N. Nitrogen sinks cannot compensate incoming sulphur acidity, and therefore the maximum critical load for sulphur is given by UBA (2004):

(2) $$CL_{max}(S) = BC_{dep} - Cl_{dep} + BC_w - Bc_u - ANC_{le,crit}$$

as long as N deposition is smaller than the sum of the N sinks, termed the minimum critical load of N. The minimum critical load for N equals the sum of N uptake and immobilization, $CL_{min}(N)=N_u+N_{im}$. The maximum critical load of nitrogen (in case of zero S deposition) is given by:

(3) $$CL_{max}(N) = CL_{min}(N) + \frac{CL_{max}(S)}{1 - f_{de}}$$

The critical leaching of acid neutralizing capacity (ANC) is computed as:

(4) $$ANC_{le} = HCO_{3,le} + Org_{le} - H_{le} - Al_{le}$$

with:

HCO_{3le} leaching of bi-carbonate (eq ha^{-1} yr^{-1})
Org_{le} leaching of organic anions (eq ha^{-1} yr^{-1})
H_{le} leaching of protons (eq ha^{-1} yr^{-1})
Al_{le} leaching of aluminium (eq ha^{-1} yr^{-1})

The chemical criterion used to compute the critical load determines the critical ANC leaching. If, for example the molar aluminium (Al) to base cation ratio is soil solution, Al/Bc=1, criterion is used, the critical Al concentration equals the Bc concentration, and [H] is computed assuming equilibrium with Al according to:

$$[Al^{3+}] = K_{Alox} \cdot [H]^{\alpha} \quad (5)$$

with K_{Alox} as the equilibrium constant. The exponent $\alpha \equiv expAl$ is often set to 3, so that eq. 5 describes the gibbsite equilibrium. The proton concentration is then used in the computation of bicarbonate and organic anion concentrations.
Finally, the critical load for nutrient N, $CL_{nut}(N)$, can be computed according to (UBA, 2004):

$$CL_{nut}(N) = N_{im} + N_u + Q \cdot [N]_{acc} / (1 - f_{de}) \quad (6)$$

with Q being the water flux leaving the rootzone (m yr^{-1}) and $[N]_{acc}$ the acceptable nitrate concentration in soil solution. Equation 6 implies that a critical nitrate concentration must be defined, related to for example the risk of changes in understory vegetation.
We calibrated the N immobilization by defining it as a fraction of net N input (N_{dep}-N_{up}) and calibrating the immobilisation fraction, f_{im}, according to:

$$N_{im} = f_{im} \cdot (N_{dep} - N_u) \quad (7)$$

Target loads are obtained by running VSD in an iterative mode to find the deposition (path) that produces a prescribed chemical status (e.g. Al/Bc=1 or ANC=0) in a specified target year (Posch et al., 2003; Posch and Reinds, 2009). As with critical loads, pairs of N and S deposition are determined that result in the desired chemical status in the target year. All pairs define the *target load function* (TLF) in the (N_{dep},S_{dep}) plane, in the same way as critical loads define the critical load function. Different TLFs are obtained for different target years; target loads increase with increasing target year and the target load approaches the critical load function when the target year moves towards infinity.Target loads are only required if neither the current deposition nor a reduction to the

critical load leads to the desired chemical soil state in the target year. Target loads must be lower than the critical loads; otherwise the desired chemical state *after* the target year will be violated. When computing target loads, three possible outcomes exist (Posch et al., 2003):

- no target load is required: the system is safe in the target year and thereafter with either current deposition or critical load (Case 1)
- there exists a target load lower than the critical load, i.e. a deposition below the critical load is required for attaining the desired chemical state in a specific year (Case 2)
- no target load exists, i.e. even at zero deposition the soil cannot recover in time (Case 3)

In this paper, target loads were computed using the year 2050 as the target year and 2020 as the year in which all measured to reduce acid deposition are implemented. As opposed to critical loads, target loads include the effect of finite buffer processes such as cation exchange. Hence, also the uncertainty in the parameters governing these buffer processes must be taken into account when assessing the uncertainties in target loads.

2.2 Input data

An overview of the parameters needed to run VSD can be found in Posch and Reinds (2009). In contrast to the study by Reinds et al. (2008b) who used a subset of these parameters for calibration, in this study all VSD parameters were subject to calibration, except for the thickness of the rooting zone, soil water content, CO_2 pressure in the soil and acid deposition. Acid deposition was not calibrated as it is only used to initialize VSD for target load computations. Thickness of the rooting zone was assumed constant as this is the depth at which we want the chemical criterion to be met and is thus not a real model parameter. Soil water content and CO_2 pressure were not calibrated as VSD is quite insensitive to changes in these parameters.

Part of the data used in the uncertainty analysis were derived from a set of 182 EU/UNECE Intensive Monitoring forest plots (De Vries et al., 2003c), for which sufficient data on soil solution, soil solid phase, forest growth and deposition were available. The plots mainly consist of pine (43 plots), spruce (80 plots), beech (29 plots) and oak forest (21 plots). Most of the plots cover about 0.25 ha. Measurements from surveys on soil condition and forest growth were used to obtain VSD model input data such as soil cation exchange capacity (CEC), soil bulk density and average stem growth. Annual mean measured soil solution concentrations from the period 1996 to 2001 sampled on a bi-weekly or monthly

basis below the root zone were used in the calibration procedure by comparing them with concentrations simulated by VSD.
Table 1 lists the parameters that were calibrated and their prior distributions. For parameters measured at the site (such as CEC and base cation deposition) the mean of the prior was set to the measured value and a standard deviation was set according to expert knowledge. For model parameters that cannot be measured directly (such as exchange constants), values for the prior distributions were derived from literature and from a data set with 150 Dutch forest plots (De Vries et al., 1995). For the latter input parameters and for the denitrification fraction that was obtained from simulations with a detailed model (DNDC; Li et al., 1992), details on the methods to derive the prior distributions are provided in subsequent sections. We did not assume any correlation between the parameters.

H-Al equilibrium
In the VSD model it is assumed that Al concentrations in the soil solution at the bottom of the root zone are in equilibrium with aluminium hydroxides such as gibbsite (Eq.5). However, undersaturation with respect to gibbsite has also been reported for a large number of sites, in particular in organic rich soils, at shallow depth or during episodes of high flow (Seip et al., 1989; Matzner, 1992; Mulder and Stein, 1994). Moreover, experiments show that Al concentrations in the soil solution are strongly influenced by reactions with organic pools and by the kinetically constrained dissolution of Al hydroxides and silicates (Dahlgren and Walker, 1993; Berggren and Mulder, 1995; Van der Salm and De Vries, 2001). To account for this non-gibbsite behaviour, both KAl_{ox} and the exponent α were calibrated. The prior distributions of the Al dissolution parameters were derived by using Al and H concentrations measured in bottom of the rootzone (30-100 cm depth) of 292 forested Dutch soils (227 sand, 32 loess and 34 clay soils).
A regression relationship between pAl (= -log[Al]) and pH assuming the relationship given in Eq. (5) was determined using measurements with pH < 5 (at higher pH, Al concentrations are too low to derive reliable relationships).
The measurements included only total Al concentrations. Free Al concentrations were calculated from the total concentration of Al and dissolved organic carbon (DOC) using a chemical speciation model. Details of the data used and the calculation procedure are given in De Vries and Leeters (2001).

Table 1. VSD parameter and their prior distributions

Parameter	Description	Distribution	Minimum	Maximum	Mean		Sigma	Source
ϱ	Bulk density (g cm^{-3})	Truncated normal	0		Measured at site		10%	1
CEC	Cation exchange capacity (meq kg^{-1})	Truncated normal	0		Measured at site		20%	1
Q	Precipitation surplus (m yr^{-1})	Truncated normal	0.05		Modelled from site data		15%	1
lgKAl_{ox}	Log10 of H-Al equilibrium constant (mol $l^{-1})^{1-expAl;}$ values in brackets for expAl=3	Normal			Sand	6.74 (7.33)	0.48 (0.55)	2
					Loam	7.52 (8.25)	1.62 (0.56)	
					Clay	7.52 (7.41)	1.62 (1.0)	
expAl	Exponent in H-Al equilibrium (-)	Normal			Sand	2.85	0.12	2
					Loam/Clay	2.82	0.38	
lg*KAlBc*	Log10 of Al-Bc exchange constant	Normal			Sand	0.408	0.63	3
					Loam	-0.6	0.7	
					Clay	0.3	0.675	
					Heavy clay	-0.92	0.38	
lg*KHBc*	Log10 of H-Bc exchange constant	Normal			Sand	3.3	0.34	3
					Loam	3.6	0.5	
					Clay	3.2	0.21	
					Heavy clay	3.6	0.65	
Ca_{dep}, Mg_{dep}, K_{dep}	Ca, Mg, K deposition (eq m^{-2})	Truncated normal	0.0025		Measured at site		40%	1
Na_{dep}–Cl_{dep}	Na minus Cl deposition (eq m^{-2})	Normal			Measured at site		40%	1
[*RCOO*]	Organic acid concentration	Truncated normal	0		Measured at site		40%	1

Table 1. Continued

ctN	N content in stems (%)	Truncated normal	0.005		Pine	1.09	0.3	4
					Spruce	1.22	0.49	
					Beech	1.54	0.25	
					Oak	2.1	0.46	
ctCa	Ca content in stems (%)	Truncated normal	0.005		Pine	1.08	0.3	4
					Spruce	1.41	0.4	
					Beech	1.8	1.12	
					Oak	2.47	1.42	
ctMg	Mg content in stems (%)	Truncated normal	0.005		Pine	0.24	0.09	4
					Spruce	0.18	0.06	
					Beech	0.26	0.09	
					Oak	0.18	0.07	
ctK	K content in stems (%)	Truncated normal	0.005		Pine	0.65	0.28	4
					Spruce	0.77	0.43	
					Beech	1.04	0.13	
					Oak	1.05	0.51	
f_{de}	Denitrification fraction (-)	Truncated normal	0	1	Sand	0.15	0.17	5
					Loam	0.24	0.23	
					Clay	0.24	0.19	
					Heavy clay	0.47	0.38	
BC_w	Base cation weathering (eq ha^{-1}) for a soil depth of 0.5 m; as a function of texture class and parent material	Truncated normal	50		Sand	125-375	75%	4
					Loam	625-1125	50%	
					Clay	625-1125	20%	
					Heavy clay	1375	10%	
f_{im}	Immobilisation fraction (-)	Truncated normal	0	1	0.64		0.24	2

Sources: [1]Site data, [2]Dutch data set,[3]De Vries et al (2003b),[4] UBA(2004),[5]Derived from DNDC results

Denitrification fractions

The uncertainty in the denitrification fraction was assessed from results of the DNDC model (Li et al., 1992), in which total denitrification or N emission from the soil is derived as the sum of N2O, NO and N2 emissions. The way in which N2O and NO emissions for European forest soils were calculated with DNDC is described in Kesik et al. (2005).

Using the result of DNDC for Europe, denitrification fractions were derived as a function of clay content while constraining the results to plots where N emission is less or equal than N deposition (Table 2). The results show increasing denitrification fractions as a function of clay content, illustrating the effect of increasing soil wetness. The denitrification fraction was derived as total N emission divided by N deposition, which is not equal to the denitrification fraction in VSD, which is related to the *net* N input. However, since net uptake was not calculated in DNDC, we used this approach to get an estimate of the denitrification fractions. The average denitrification fractions for various texture classes in Table 2 are in reasonable accordance with denitrification fractions given in UBA (2004), and were therefore used to define the prior distribution of the denitrification fraction.

Table 2. Denitrification fractions f_{de} as a function of soil texture derived from DNDC modelling results.

Texture	Clay content (%)	f_{de}			
		Average	St dev	min	Max
Sand	<10	0.15	0.17	0	1
Loam	10-18	0.24	0.19	0.0011	1
Clay	18-25	0.24	0.23	0.0013	1
Heavy clay	>25	0.47	0.38	0.033	1

Immobilisation fraction

A prior distribution for the immobilisation fraction f_{im} was obtained from the N budget at 150 Dutch forest plots (De Vries and Leeters, 2001). Results indicate that on average about 64% of the net N input is immobilized. Only a weak relationship of f_{im} with tree species and C/N ratio was observed. This is in accordance with results from other studies (Dise et al., 2009). It was therefore decided to use one single prior distribution for all plots, specified in Table 1.

Weathering rates

Average weathering rates were calculated as a function weathering rate class according to the standard approach given in UBA (2004). For a soil depth of 0.5 m

the initial weathering rates, $BC_{w,0}$, were assumed to range from 125 to 1325 eq ha^{-1} yr^{-1}, depending on the parent material and texture class (Table 3). Parent material class and soil texture at the plots were obtained from the monitoring data. The uncertainty (in % standard deviation) assigned to the five texture classes is also given in Table 3. The uncertainty is based on research by Van de Salm (2001) on the regional variation in weathering rates of sand, loess and clay soils. The uncertainties are mainly based on uncertainties in relationships between laboratory-derived weathering rates and soil mineralogy and soil texture, while correcting for pH differences in the field and laboratory.

Table 3. Annual average weathering rate at an average soil temperature and their uncertainties as a function of texture class.

Texture	Texture class	Definition	$BC_{w,0}$ eq $ha^{-1}yr^{-1}$	Standard deviation (%)
Sand	1 Coarse	Clay < 18%	125-375	75
Loam	2 Medium	Clay < 35% and Sand >15% or 18% <Clay < 35%	625-1125	50
Clay	3 Medium fine	Clay < 35% and Sand <15%	625-1125	20
Heavy clay	4 Fine and 5 Very fine	Clay > 30%	1375	10

The temperature dependence of weathering rates was modelled according to (UBA, 2004):

$$BC_w = BC_{w,0} \cdot \exp\left(\frac{A}{281} - \frac{A}{273 + T}\right) \quad (8)$$

with $BC_{w,0}$ being the annual average weathering rate at an average soil temperature of 8°C (281 K), T is temperature in Kelvin and A = 3600 K.

2.3 Model initialisation

To compute target loads with VSD, the model has to be initialized in the past and run until the present year. Target loads are then determined by iteratively running the model to the target year with varying depositions until the desired chemical state in the target year is obtained. We initialized VSD in 1880, assuming the soil to be in equilibrium with (atmospheric) inputs and ran it until 2010. Time patterns in uptake and deposition were derived using growth curves and scaling the deposition at the sites with historical trends in deposition according to the methods

described in Reinds et al. (2009). Uptake of N and base cations for the critical load and target load computations (after 2010) were computed by averaging the yearly product of growth and calibrated nutrient contents over a 100 year forest rotation period. The same procedure was used to estimate average N immobilisation, using Equation 7 and inserting the calibrated value of f_{im}.

2.4 Model calibration

VSD was calibrated using a Bayesian approach. Details of the procedure are given in Reinds et al (2008b) and Van Oijen et al. (2005). Here we only provide a brief summary. First a set of prior distributions of all VSD parameters was defined. Next VSD was run using a Monte Carlo approach by sampling from the prior distributions and computing likelihoods based on the comparison of model outputs with measurements of soil solution chemistry. The posterior probability for a parameter set increases with an increased prior probability and an increased likelihood, i.e. when the selected parameter set has a large prior probability and when the model is able to reproduce the measurements with these parameter settings. To calculate the posterior distribution, a Markov Chain Monte Carlo algorithm was used, known as the Metropolis-Hastings random walk (Robert and Casella, 1999). In this method, the multi-dimensional parameter space (where the number of dimensions equals the number of uncertain model parameters) is explored by stepping through that space and running the model for each visited point. If, for a new point, the product of prior probability and likelihood exceeds that of the previous point, the new point is accepted. The likelihood is computed by comparing model output with measurements. If the ratio of new and current products of the prior and likelihood is between 0 and 1, the new point can still be accepted, but with a probability equal to that ratio. The algorithm is inherently stochastic since candidate points that perform (somewhat) worse than previous points can still be accepted. If the candidate point is not accepted, the previous point is duplicated in the chain of accepted points. For the calibration, three separate Markov chains were run of 30,000 simulations each, of which the first 10% of the simulations was considered burn-in and discarded. Three chains were used to verify that a stable posterior distribution was reached that is unaffected by the arbitrary starting position. The first chain was started at the mean of each prior parameter distribution, the second and third chain used initial values that were randomly chosen within the 95% confidence interval of the parameters. Since this study aimed at quantifying the uncertainty at each of the plots, a calibration was performed for each plot separately, without validating on a subset of plots as done by Reinds et al. (2008b).

To compare the calibrated with the uncalibrated model, 27,000 simulations were made with VSD, for which the parameter values were obtained by random sampling from the prior distributions but with a fixed exponent $\alpha = 3$ in the H-Al equilibrium; results were compared with critical loads from the calibrated model using the same model settings.
The performance of the calibration was further evaluated by comparing the Normalized Root Mean Square Error (NRMSE) of the output of the calibrated model versus the uncalibrated model. NRMSE is the square root of the mean squared differences between measurements and simulations (using all observations at the plots), divided by the mean of the measurements (Janssen and Heuberger, 1995).

2.5 Uncertainty analysis

Uncertainties in critical loads were quantified by running a Monte Carlo analysis of VSD, sampling from the posterior distributions of the input parameters obtained from the model calibrations. For each plot, the mean and the 5th, 50th and 95th percentiles of $CL_{max}(S)$, $CL_{min}(N)$, $CL_{max}(N)$ and $CL_{nut}(N)$ were computed as well as the standard deviation and the coefficient of variation (CV), defined as the ratio between the standard deviation and the mean.
Because SMB (the steady state version of VSD) is almost linear, the contribution of each single parameter to the uncertainty can be analyzed using a standardized regression model relating the model parameters to the modelled critical loads using all 27,000 simulations, according to (see Kros et al., 1993):

$$\frac{y-\bar{y}}{S_y} = \beta_1 \cdot \frac{x_1-\bar{x}_1}{S_{x1}} + \cdots + \beta_p \cdot \frac{x_p-\bar{x}_p}{S_{xp}} \qquad (9)$$

with y being the model output (critical load or target load), $x_1 \ldots x_k$ are the model parameters, S_y and the S_x's are the standard deviations of y and x_k, and β_k ($k = 1,..,p$) are the estimated standardized regression coefficients for the parameters x_k. Average values for x and y over all 27000 simulations are denoted as $\bar{x}$ and $\bar{y}$. The standardized regression coefficients indicate the relative importance of a parameter x_k in explaining the variability of the model output y. Only when the regression model gives a good fit, equation (8) can be used to indicate the contribution of the model parameters to the output uncertainty: this contribution

was determined by ranking parameters on the basis of the regression coefficients from regression with an r^2 of at least 0.8.

3 Results and discussion

3.1 Results from the calibration

3.1.1 Posterior distributions

Calibration reduced the uncertainty in model parameters. For the denitrification and immobilisation fractions, f_{im} and f_{de}, the standard deviation of the calibrated values was smaller than a-priori assumed (Figure 1a). For f_{im} the standard deviation is below 0.20 for 90% of the plots whereas a-priori a standard deviation of 0.24 was assumed for all plots. The standard deviation of f_{de} reduced from values between 0.17 and 0.38 depending on soil texture class to average value of 0.16. Calibrated values for f_{im} varied between 0.20 and 1.0, but at most plots more than 65% of the net N input is immobilized (f_{im} > 0.65). For sandy and loamy/clayey soils, calibrated values for f_{de} lie in the upper part of the prior distribution (about 0.15-0.27 for sandy soils, and 0.15-0.40 for loamy soils). For heavy clay the posterior distribution resembles the prior.
For most plots the posterior base cation weathering, BC_w, is different from the prior (Figure 1, right).

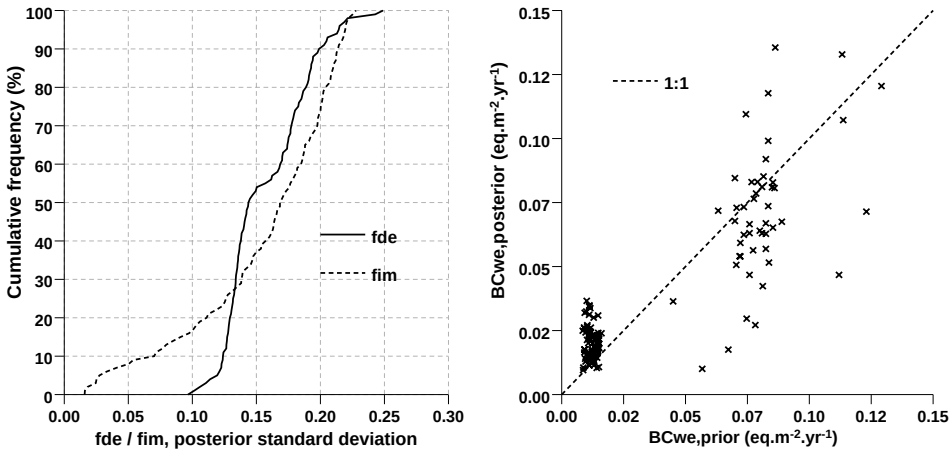

Figure 1. Cumulative frequency distribution of the standard deviation in calibrated f_{im} and f_{de} (left) and mean BC_w per plot before and after calibration (right).

For acid sandy soils, a-priori weathering rates derived from literature data are an underestimate for many of the plots, indicated by the higher mean BC_w from the posterior distributions. For plots with intermediate weathering rates (around 0.15 eq.m^{-2} yr^{-1}), both higher and lower average weathering rates followed from the calibration. Calibrated values for the logarithm of the H-Al equilibrium constant *lgKAlox*, vary between 6.5 and 7.6 with a median of 7.1 for sand and between 6.6 and 7.8 for clay with a median of 7.55 (Figure 2). The exponent *expAl* is strongly correlated with *lgKAlox* and varies between 2.6 and 2.8 for sandy soils and between 2.7 and 3.0 for clayey soils. A comparably strong correlation was found for this data set based on a regression of the [*H*] and [*Al*] observations at the plots (Reinds et al., 2009).

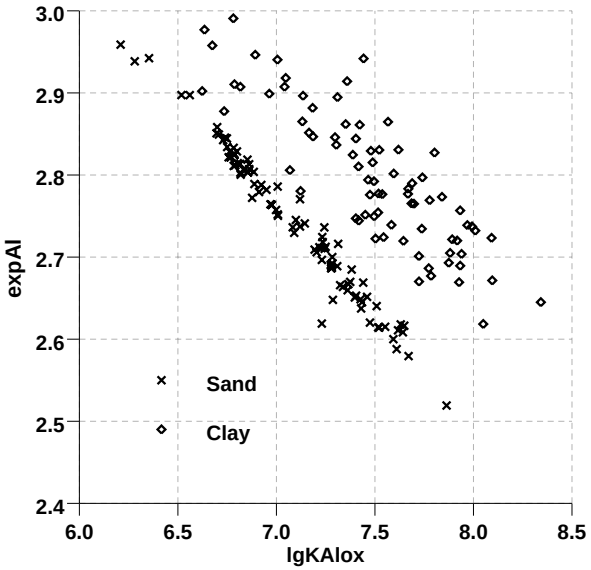

Figure 2. Relationship after calibration between lgKAlox and expAl for sandy soils (crosses) and clay soils (diamonds).

Calibration has reduced the a-priori assumed uncertainty for both parameters: for clay soils the average standard deviation of *lgKAlox* was 1.2 whereas the prior has a standard deviation of 1.6. The average standard deviation of *expAl* was 0.30 compared to 0.38 in the prior. For sand, posterior distributions resemble prior distributions, which may be explained by the fact that a narrow prior was assumed based on measurements in Dutch soils.

When the model was calibrated using a fixed value α =3 in the H-Al equlibrium, using a normal prior distribution for *lgKAlox* with a mean value of 8.13 and a standard deviation of 0.96, the mean *lgKAlox* over all plots becomes 8.70 with a standard deviation of 0.90.

3.1.2 Model outputs compared with measurements before and after calibration

Calibration of VSD reduced the differences between observed and simulated soil (solution) chemistry (Figure 3). The NRMSE strongly reduced for pH and base saturation (*Bsat*) and reduced for Al and nitrate concentrations.

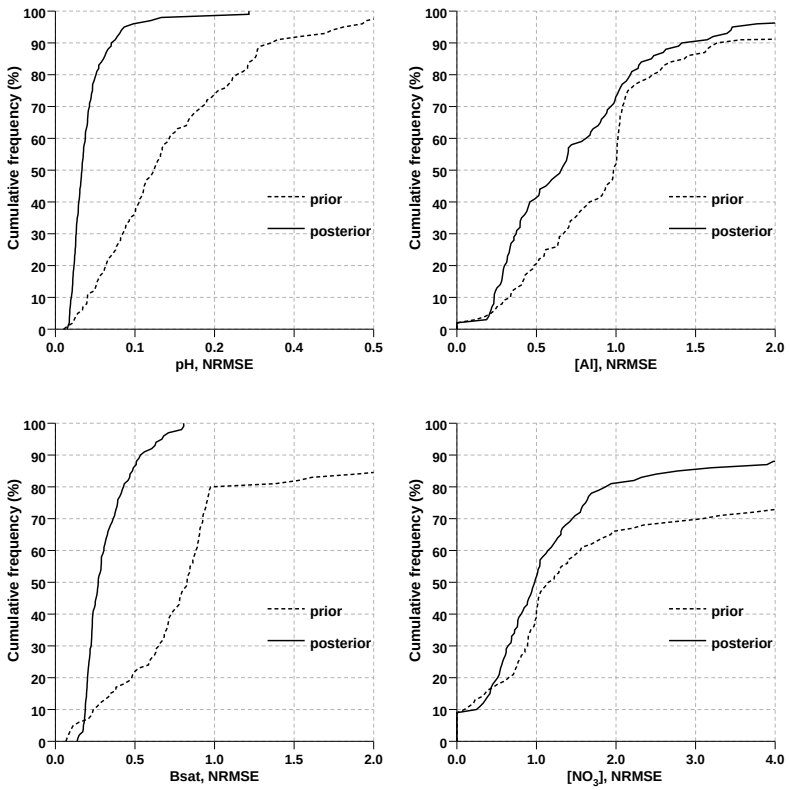

Figure 3 Cumulative frequency distributions of NRMSE for pH, [Al], Bsat and [NO3] before (prior) and after (posterior) calibration for 182 plots.

3.2 Variation in critical loads over Europe

Average critical loads (as an average over the 27,000 simulations per plot) based on the Al/Bc=1 and ANC=0 criterion vary strongly over the 182 plots (Table 4).

Average maximum critical loads for N and S using the ANC=0 criterion are smaller than those with Al/Bc=1. This is consistent with the results from Reinds et al. (2008a) who, in a regional assessment for Europe and northern Asia, also found mostly smaller critical loads for S when using the ANC=0 criterion.

Table 4: Percentiles of average critical loads (eq ha^{-1} yr^{-1}) for the Al/Bc and ANC criteria after model calibration.

Percentile	Al/Bc=1 criterion		ANC=0 criterion			
	$CL_{max}(S)$	$CL_{max}(N)$	$CL_{max}(S)$	$CL_{max}(N)$	$CL_{min}(N)$	$CL_{nut}(N)$
5	659	1393	4	502	181	246
10	794	1595	83	571	239	312
25	1156	2426	193	846	371	556
50	1636	4132	368	1530	792	970
75	3508	8411	671	2618	1165	1387
90	5339	19438	1375	4949	1485	1836
95	9670	31247	1815	8754	1606	2124

The relation between the two chemical criteria can be illustrated by computing the ANC at each plot equivalent to Al/Bc=1 and the value of Al/Bc equivalent to ANC=0. For almost all plots, a value of ANC=0 is equivalent to an Al/Bc value smaller than one (i.e. more stringent than Al/Bc=1) and Al/Bc=1 is equivalent to a negative ANC for almost all plots (i.e. less stringent than ANC=0), showing that ANC=0 is clearly the more stringent criterion (Figure 4).

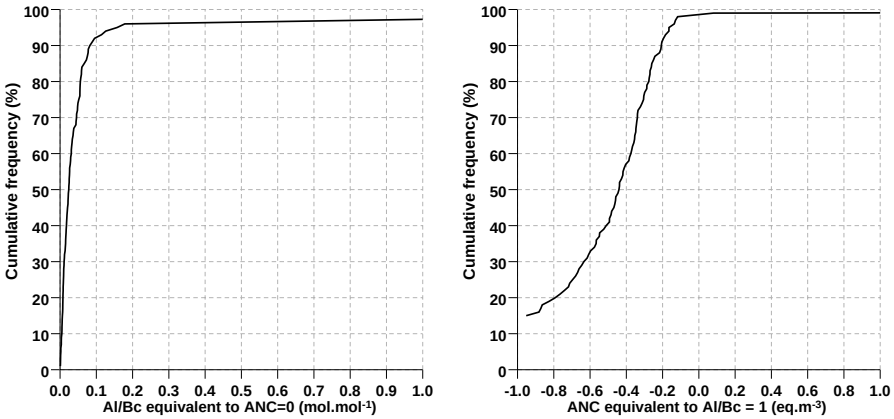

Figure 4. Cumulative frequency of the average Al/Bc (mol mol^{-1}; left) equivalent to ANC=0 and average ANC (eq m^{-3}; right) equivalent to Al/Bc=1 per plot.

Details on the procedure to compute equivalent criteria can be found in Reinds et al. (2008a).

The minimum critical load for nitrogen, $CL_{min}(N)$, ranges from about 200 eq ha^{-1} yr^{-1} for slow growing conifer forests with low N immobilisation to very large values in areas with high N immobilisation, and is obviously independent of the criterion (Table 4). Since we assumed a constant N immobilisation equal to the average amount of N immobilized per year following from the calibration (Eq. 7), these plots are mainly located in countries with a high N deposition. Critical loads of nutrient N, based on a critical nitrate concentration of 0.3 mg l^{-1}, range from 250 to about 2100 eq ha^{-1} yr^{-1} (3.5 – 30 kg N ha^{-1} yr^{-1}). Low values occur at dry plots with little leaching and low denitrification.
The maximum critical load for sulphur, $CL_{max}(S)$, for Al/Bc=1, ranges from approximately 700 eq ha^{-1} yr^{-1} for sensitive sandy soils with low weathering rates to > 5000 eq ha^{-1} yr^{-1} for rich clayey soils. Because the maximum critical load for N, $CL_{max}(N)$, is the sum of $CL_{min}(N)$ and of $CL_{max}(S)$ divided by $1–f_{de}$, values of $CL_{max}(N)$ are higher than the other two critical loads with a median of about 4000 eq ha^{-1} yr^{-1}. Very high values occur for plots with a clayey texture that have a high f_{de}: in some runs f_{de} approaches 1 and consequently values for $CL_{max}(N)$ become very high. In such cases, $CL_{max}(N)$ has little relevance as it will be much higher than N deposition.
For the ANC=0 criterion, $CL_{max}(S)$ values near 100 eq ha^{-1} yr^{-1} are calculated for sensitive sandy soils, while the insensitive (rich, clayey) soils have critical load values between 1000 and 1750 eq ha^{-1} yr^{-1}. At about 10% of the plots, median $CL_{max}(S)$ approaches zero, meaning that there are hardly enough base cations in the soil solution to buffer incoming acidity to an ANC level of zero.

3.3 Contribution of model parameters to the uncertainty in critical load

The contribution of uncertain parameters to the uncertainty of critical loads depends on the chemical criterion chosen (Al/Bc=1, ANC=0) and on the type of critical load ($CL_{max}(S)$, $CL_{min}(N)$, $CL_{max}(N)$). Because $CL_{min}(N)$ consists of N uptake and N immobilisation only, all uncertainty stems from these two parameters. N immobilisation contributes most to the uncertainty for 60% of the plots, at 40% of the plots N uptake is more important. Because $CL_{min}(N)$ is the sum of these two parameters, the r^2 of the regression is 100% for all plots.
The uncertainty in $CL_{nut}(N)$ is determined by the four parameters that influence the removal of N from the soils: N_i, N_u, f_{de} and because it determines the leaching of N, the water flux Q (Table 4).

$CL_{max}(S)$ and $CL_{max}(N)$ based on Al/Bc=1

The input fluxes of base cations (weathering, deposition) are important sources of uncertainty for $CL_{max}(S)$ based on Al/Bc=1 (Table 5), as well as the parameters that determine the relationship between [*Al*] and [*H*] (*lgKAlox* and *expAl*). The denitrification fraction is the most important source of uncertainty for $CL_{max}(N)$ at the majority (~60%) of the plots, which is obvious when looking at Equation 4.

Table 5. Percentage of plots for which a parameter is one of the five most important sources of uncertainty with Al/Bc=1 as the criterion.

	Rank				
Parameter	1	2	3	4	5
			$CL_{max}(S)$		
lgKAlox	20.6	21.3	22.1	5.1	15.4
expAl	9.6	20.6	15.4	20.6	11.0
Ca_{dep}	10.3	11.0	14.7	16.2	18.4
Mg_{dep}	0.0	11.8	3.7	7.4	13.2
K_{dep}	32.4	13.2	14.0	14.7	12.5
Ca_u	1.5	8.8	2.9	14.7	11.8
K_u	0.7	0.0	2.9	1.5	3.7
BC_w	25.0	13.2	24.3	19.1	9.6
Q	0.0	0.0	0.0	0.7	2.2
			CLmax(N)		
lgKAlox	3.7	17.8	19.6	17.8	8.4
expAl	1.9	10.3	15.9	15.9	16.8
Ni	0.0	0.0	1.9	2.8	6.5
f_{de}	59.8	22.4	10.3	5.6	0.0
Ca_{dep}	6.5	6.5	11.2	13.1	15.0
Mg_{dep}	0.0	4.7	8.4	1.9	7.5
K_{dep}	20.6	15.0	11.2	15.0	13.1
N_u	0.0	0.9	0.9	0.9	0.9
Ca_u	0.9	2.8	7.5	1.9	15.9
K_u	0.9	0.0	0.0	2.8	0.9
BC_w	5.6	19.6	13.1	22.4	14.0
			CLnut(N)		
N_i	58.2	37.7	2.5	1.6	-
f_{de}	1.6	9.8	83.6	4.9	-
N_u	40.2	52.5	3.3	4.1	-
Q	0.0	0.0	10.7	89.3	-

Apart from f_{de}, the same parameters that determine the uncertainty in $CL_{max}(S)$, are also important for $CL_{max}(N)$. For $CL_{max}(N)$ the regression (Eq. 8) has an $r^2 > 0.75$ for about 60% of the plots. Especially at plots with a large f_{de} , the uncertainty of the

SMB model becomes non-linear (see Equation 4). The input fluxes of base cations are the only sources of uncertainty for $CL_{max}(S)$ based on the ANC=0 criterion.

$CL_{max}(S)$ and $CL_{max}(N)$ based on ANC=0

Because the ANC value contains the *sum* of [*H*] and [*Al*] in the soil solution, the H-Al equilibrium parameters are unimportant as these determine only the split between H and Al. For $CL_{max}(N)$ based on ANC=0, f_{de} is the most important source of uncertainty followed by N_u, BC_w and N_i.

Target loads for S

Base cation deposition, N immobilisation, the H-Al equilibrium constants and N uptake mainly determine the uncertainties in $TL_{max}(S)$ based on Al/Bc=1. Because target loads are computed using the dynamic version of VSD, also the uncertainty in parameters such as CEC and the H-Bc exchange constant contributes to the uncertainty in $TL_{max}(S)$, but these additional parameters are only among the five most important parameters when the ANC=0 criterion is used.

3.4 Uncertainties in critical loads

In this section the uncertainty of the various types of critcal loads are quantified, based on the 30,000 simulations. Coefficients of variation (CV) for $CL_{max}(S)$ are similar for both criteria (Table 6).

Table 6 Percentiles of coefficients of variation (CV) for derived critical loads for the Al/Bc and ANC criterion after model calibration

	Al/Bc=1 criterion		ANC=0 criterion			
Percentile	CV of CLmax(S)	CV of CLmax(N)	CV of CLmax(S)	CV of CLmax(N)	CV of CLmin(N)	CV of CLnut(N)
5	0.11	0.18	0.12	0.10	0.02	0.02
10	0.13	0.20	0.13	0.12	0.05	0.05
25	0.18	0.24	0.16	0.16	0.08	0.08
50	0.25	0.31	0.23	0.20	0.13	0.15
75	0.40	1.31	0.45	0.71	0.20	0.37
90	0.71	9.36	1.18	7.94	0.27	2.16
95	0.79	12.09	2.11	10.06	0.33	4.89

The uncertainty in $CL_{min}(N)$ is only caused by uncertainty in the N content in stem wood; for most plots the CV is below 0.3. Uncertainties in $CL_{nut}(N)$ are in the same order of magnitude as those of $CL_{min}(N)$ for plots with low denitrification rates, but high at about 10% of the plots. Uncertainties in $CL_{max}(S)$ and $CL_{max}(N)$ are higher;

the coefficient of variation is highest for $CL_{max}(N)$ and varies between 0.1 and 1.5 for most of the plots with a median value of about 0.3; i.e. the standard deviation is about 30% of the mean value. Uncertainties in $CL_{max}(N)$ are mostly higher than those of $CL_{max}(S)$ because of the additional uncertainty in f_{de}. Standard deviations in the average maximum critical loads for N and S are much lower when using the ANC=0 criterion than when using the Al/Bc=1 criterion, but even for the ANC=0 criterion, the coefficients of variation of $CL_{max}(S)$ and $CL_{max}(N)$ are very high for 30% of the plots. The extremely high uncertainties up to 10, are related to the large impact of small changes in f_{de} when in approaches one. $CL_{max}(S)$ for sensitive ecosystems are mostly below 1500 eq ha^{-1} yr^{-1} (Slootweg et al., 2007). If we limit our analysis to plots with an average $CL_{max}(S)$ below 1500 eq ha^{-1} yr^{-1}, the uncertainty in $CL_{max}(S)$ and $CL_{max}(N)$ is comparable to the uncertainty in the entire set. There is thus no systematic difference between uncertainties at low critical loads and high critical loads for S and N.

The effect of calibration on the uncertainties

Although the uncertainties in critical loads are considerable, they have been reduced by calibration (Figure 5).

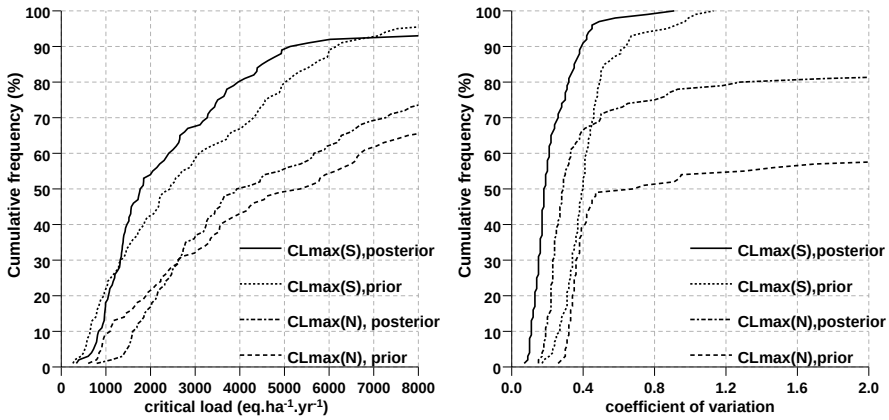

Figure 5. Cumulative frequencies of the maximum critical loads of S and N (left) and their coefficients of variation (right), before (prior) and after (posterior) calibration using Al/Bc=1 and a fixed exponent $\alpha = 3$.

Calibration caused some reduction in the magnitude of the critical loads. The median plot-average $CL_{max}(S)$ decreased from 2380 to 1800 eq^{-1} ha^{-1} yr^{-1}, whereas for $CL_{max}(N)$ it decreased from 4800 to 4300 eq^{-1} ha^{-1} yr^{-1}.

The median CV of $CL_{max}(S)$ and $CL_{max}(N)$ after calibration was about half of the median CV in results of the uncalibrated model. The CV for $CL_{max}(S)$ after

calibration was below 0.5 for almost all plots whereas CV values above 0.5 occurred at about 30% of the plots before calibration, and exceeded 1.5 at more than 20% of the plots. The gain in accuracy is most likely caused by the much narrower posterior distributions of the gibbsite equilibrium constant for clay soils and of base cation weathering. The uncertainty in calibrated $CL_{max}(N)$ was also lower, due to reduced uncertainty in for example f_{im}, but it remained high at 50% of the plots, mainly because the uncertainty in f_{de} is not much reduced. Because the measurements at the plots do not allow a targeted calibration of f_{de}, posterior distributions often resemble prior distributions. Uncertainties in critical loads using a fixed exponent (i.e. α = 3) were higher than when calibrating with a variable exponent (compare Figure 5 and Table 5).

3.5 Uncertainties in target loads

As for critical loads, target loads were computed with VSD using model parameters drawn from the posterior distributions. Uncertainties in target loads were computed only for those runs in which a target load lower than the critical load was obtained. Because we selected a different set of model parameters for each simulation, true target loads (Case 2; see section 2.1) may exist for only some of the 27,000 simulations. Comparing the number of Case 2 target loads with those of Case 1 and/or Case 3 provides insight in the robustness of the target load computations. Here, we limit ourselves to maximum target loads for sulphur, $TL_{max}(S)$.

Al/Bc=1 can be reached in 2050 for 70% of the plots with current deposition or with a deposition equal to the critical. At these plots a true target load is computed in less than 1% percent of the 27,000 simulations. At the remaining 30% of the plots he percentage of simulations with a target load is between 1% and 35%, but exceeds 10% only for a few plots. To reach ANC=0 in 2050, target loads are needed for 60% of the plots (a Case 2 $TL_{max}(S)$ exists in more than 1% of the runs). Plots with robust target load estimates (i.e. those plots were most of the runs lead to Case 2 $TL_{max}(S)$) are rare: only for 10% of the plots target loads are required in the majority of the runs. Plots were target loads are needed to arrive at ANC=0 in 2050 are mainly located in central Europe (Figure 6).

Comparing target loads with critical loads shows that for the ANC=0 criterion $TL_{max}(S)$ is much smaller than $CL_{max}(S)$, indicating that substantial additional deposition reductions would be required; on average the $TL_{max}(S)$ is half of $CL_{max}(S)$. For Al/Bc=1, $TL_{max}(S)$ is closer to $CL_{max}(S)$, about 70% of the critical load value. Due to the uncertainties in the additional parameters that VSD requires to compute target loads, such as exchange constants and CEC, the relative

uncertainty in target loads, expressed as the CV, exceeds that of critical loads (Figure 7, left). After calibration, the percentage of runs where target loads are required for ANC=0 in 2050 is considerably different than before calibration (Figure 7, right). Before calibration, target loads are required in at least some of the runs for all plots, but after calibration no target loads are required in any of the runs for 40% of the plots, due to the lower parameter uncertainty.

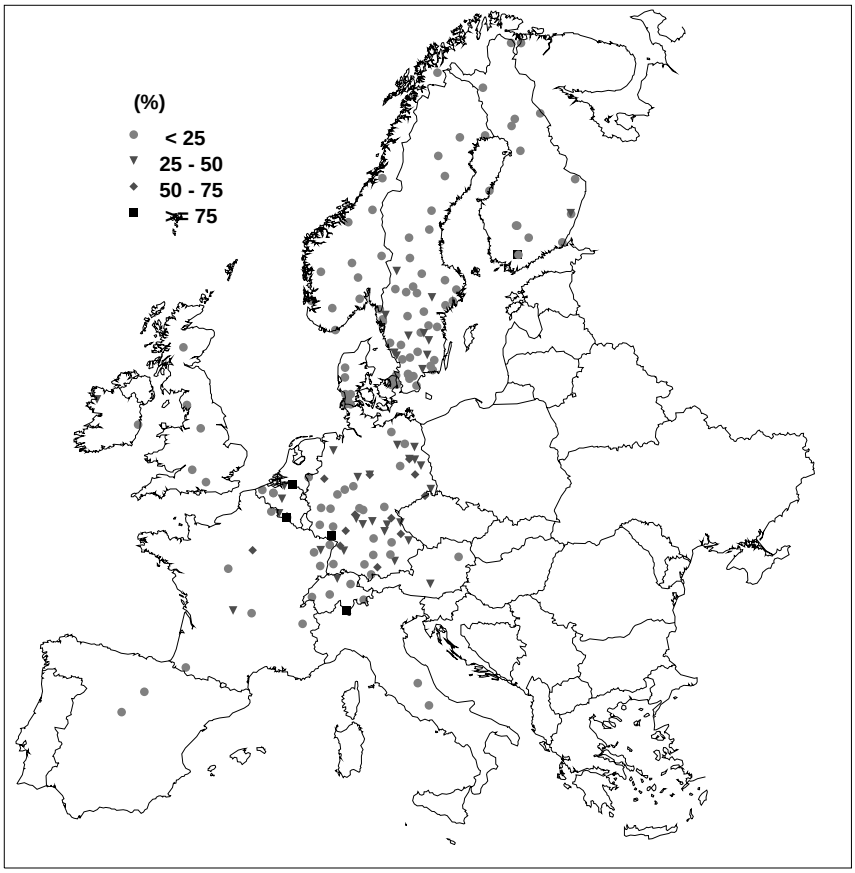

Figure 6. Geographical distribution of the percentage of runs where true target loads (Case 2) are required to reach ANC=0 in 2050.

Calibration thus improves the robustness of the assessment of ecosystem recovery: 40% of the plots will recover in 2050 under either current reduction plans or under a deposition equal to critical load. Because the percentage of runs with target loads is quite different between the uncalibrated and calibrated model runs, a sound comparison of the uncertainties is difficult.

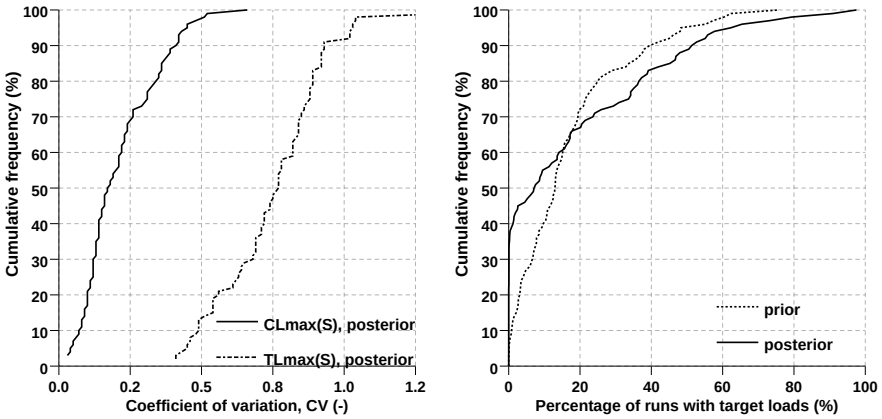

Figure 7. Coefficient of variation for CLmax(S) and TLmax(S) (left), and percentage of runs in which a target load was required to reach ANC=0 in 2050 (right).

4 Conclusions

Calibration of the VSD model significantly reduced the uncertainty in the maximum critical loads for S. For both chemical criteria (Al/Bc=1, ANC=0), the median CV was about compared to the uncalibrated model. A median CV of about 20 to 30% was obtained after model calibration, using an H-Al relationship with variable exponent. Relative uncertainties in low and high critical loads are about the same. Uncertainties in critical loads can be reduced by calibrating the model: data from monitoring programmes that allow such a calibration are thus very important and can contribute to more robust model estimates of critical loads. We have shown that from the results of the calibrated model more robust statements on the necessity of target loads can be made than prior to calibration.

Results are in agreement with the CV of 37% found for a sensitive site in the UK (Skeffington et al., 2006), with the CVs between 20-50% for 4 sites in the UK (Skeffington et al., 2007), with the uncertainty for four sites in China (Larssen et al., 2000) and with the CV of 40% found by Li and McNulty (2007) for critical loads of acidity in the US. In all these studies attempts were made to include the uncertainties in all relevant model parameters, which make them comparable to this study. Except for the study by Larssen et al. (2000), all other analyses were carried out without calibration of model parameters. Li and McNulty (2007) took the entire range of possible weathering rates for all soil and parent material types given in UBA (2004) to perform an uncertainty analysis of the SMB model, but it is unlikely that the weathering rate at a site would be that uncertain. Their conclusion that weathering rates contribute most to the uncertainty in SMB calculations thus

has a limited meaning. In our study we have shown that base cation weathering is an important source of uncertainty for critical loads based on Al/Bc=1, but that base cation deposition and the parameters in the H-Al equilibrium are also important at many plots.

There are some limitations in this study regarding model uncertainties that should be acknowledged:

- In the uncalibrated model runs, we assumed that all parameters are uncorrelated, but for the base cation deposition this is not realistic. The uncertainty quantification of the uncalibrated model could thus be improved by including correlations between some of the input parameters, such as the deposition of the various base cations.
- We assessed the uncertainty in critical loads and target loads due to parameter uncertainty and choice of chemical criterion. Other studies also showed that the choice and magnitude of the chemical criterion has a major effect on the magnitude of the critical load (Reinds et al., 2008a). Especially for critical loads of nutrient nitrogen, the uncertainty in the acceptable nitrate concentration is likely to be more important than the uncertainty in the model parameters.
- Most important for policy applications are the uncertainties in the exceedances of critical loads. In addition to the uncertainties in critical loads, this requires knowledge on the uncertainties in S and N deposition. The uncertainties in the exceedances are largest when the critical loads and deposition are of comparable magnitude, and further analyses can thus be restricted to regions where this applies (Syri et al., 2000; Suutari et al., 2001).
- The uncertainty assessments in this paper were carried out for 182 forest plots in Europe. The next step would be to investigate uncertainties at mapping units used to compute critical loads at a European scale. This will add additional uncertainty sources, such as spatial variability in soil characteristics (e.g. soil texture), and would also require an analysis of spatial patterns in the calibrated parameters and if these patterns can be related to environmental factors. If so, geostatistical methods such as regression kriging (Hengl et al., 2007) could be used to create maps of VSD input parameters for Europe, including their uncertainty. This would allow assessment of uncertainties in critical loads and target loads for the whole of Europe which would be of great importance for policies related to the protection of ecosystems against atmospheric pollution in Europe.

Acknowledgements.
We thankfully acknowledge the European Commission, DG Environment and the Dutch Ministry of Agriculture, Nature and Food Quality for co-financing this work. Many thanks are also due to the National Focal Centers of the various

countries who by the intensive monitoring of forests made this study possible. We thank Claus Butterbach-Bahl for supplying the DNDC results for Europe. The valuable comments by Gerard Heuvelink on a draft version of this paper are gratefully acknowledged.

Critical loads of sulphur and nitrogen for terrestrial ecosystems in Europe and Northern Asia using different soil chemical criteria

Reinds, G.J., Posch, M., De Vries, W., Slootweg, J. & Hettelingh, J.-P. 2008. Critical loads of sulphur and nitrogen for terrestrial ecosystems in Europe and Northern Asia using different soil chemical criteria, *Water, Air, and Soil Pollution* **193**, 269-287.

Abstract

A critical load data base was developed for Europe and Northern Asia using the latest data bases on soils, vegetation, climate and forest growth. Critical loads for acidity and nutrient nitrogen for terrestrial ecosystems were computed with the Simple Mass Balance model. The resulting critical loads are in accordance with critical loads from previous global empirical studies, but have a much higher spatial resolution. Critical loads of acidity are sensitive to both the chemical criterion and the critical limit chosen. Therefore a sensitivity analysis of critical loads was performed by employing different chemical criteria. A critical limit based on an acid neutralizing capacity (ANC) of zero resulted in critical loads that protect ecosystems against toxic concentrations of aluminium and unfavourable Al/Bc ratios, suggesting that ANC could be an alternative to the commonly used Al/Bc ratio. Critical loads of nutrient nitrogen are sensitive to the specified critical nitrate concentration, especially in areas with a high precipitation surplus. If limits of 3–6 mg N L^{-1} are used for Western Europe instead of the widely used 0.2 mg N L^{-1}, critical loads double on average. In low precipitation areas, the increase is less than 50%. The strong dependence on precipitation surplus is a consequence of the simple modelling approach. Future models should explore other nitrogen parameters (such as nitrogen availability) instead of leaching as the factor influencing vegetation changes in terrestrial ecosystems.

*Keywords***:** critical loads, acidification, Eurasia, soil and land cover, uncertainties, equivalent criteria

1. Introduction

During the past two decades, critical loads of sulphur (S) and nitrogen (N) have been used as an indicator of ecosystem sensitivity to acidification and eutrophication under the Convention of Long-range Transboundary Air Pollution (LRTAP) within the United Nations Economic Commission for Europe (UNECE). Starting with the Sulphur Protocol of 1994, critical loads, as part of integrated assessment modelling, were used in the negotiations on emission reductions (Bull et al., 2001; Gregor et al., 2001). More recently critical loads have also been used in the revision of the European Commission's National Emission Ceilings (NEC) directive (Amann et al., 2006). Critical load maps used for policy support in Europe consist of data submitted by National Focal Centres as well as of critical loads

based on models applied to a general, European-wide background database (Hettelingh et al., 1995a; Hettelingh et al., 2001; Hettelingh et al., 2007).

Several studies have determined critical loads for nitrogen and acidity for terrestrial ecosystems at the European (De Vries et al., 1994b; Kuylenstierna et al., 1998), SE-Asian (Hettelingh et al., 1995b), Northern Asian (Bashkin et al., 1995; Semenov et al., 2001) and global scale (Kuylenstierna et al., 2001; Bouwman et al., 2002). The global scale studies assigned low resolution critical loads based on literature data on ecosystem sensitivity, whereas the study by De Vries et al.(1994b) used the simple mass balance model. In recent years, high-resolution data bases have become available for soils (JRC, 2006), land cover (Bartholome et al., 2002), climate (New et al., 1999, 2000) and forest growth (Schelhaas et al., 1999). These data bases provide much more spatial detail for Europe and Northern Asia than those used in previous studies. A harmonized land cover map has been recently completed by combining CORINE land cover (Version 12/2000 extended coverage) with additional sources from the Stockholm Environment Institute (SEI) (Cinderby et al., 2007) to provide a Pan-European coverage on a 100×100 m grid. Furthermore, EUNIS ecosystem codes (Davies et al., 2004) have been assigned to all land cover classes (Slootweg et al., 2005).

In addition to the need to use more recent data, it has been suggested that chemical criteria other than the widely used Al/Bc ratio could be used for the computation of critical loads of acidity for soils (Holmberg et al., 2001; UBA, 2004). Several national studies have shown that the choice of the chemical criterion can have a strong influence on critical load values (e.g. Hall et al., (2001a); Aherne et al., (2001; 2001a), for the UK and Ireland), and on critical load exceedances (e.g. Holmberg et al. (2001) for Finland). Similarly a recent study has shown that the widely used nutrient nitrogen limit of 0.2 mg N L^{-1} related to vegetation changes in forests is applicable for Scandinavia but not for Western Europe (De Vries et al., 2007a). These authors suggested new limits for several forest and vegetation types. Finally, in recent years the (mostly) Asian part of the UNECE region – termed EECCA (Eastern Europe, Caucasian and Central Asian) countries – as well as Cyprus and Turkey have become more involved in the work under the LRTAP Convention, necessitating the extension of the European background data base to these countries.

In this study we describe the latest data bases and methodologies and use them to compute critical loads of S and N as well as of nutrient N for terrestrial ecosystems in Europe and Northern Asia, comprising the successor states of the former Soviet Union. In addition, uncertainties in the regional patterns of critical loads were explored using a range of chemical criteria. Furthermore, we show how various chemical criteria are interconnected introducing the concept of equivalent criteria.

2. Methods

2.1 The critical load model

Critical loads were computed with the so-called Simple Mass Balance (SMB) model, which links deposition to a chemical variable in the soil or soil solution, which can be associated with ecosystem effects; and the violation of specific values of such a variable (the 'critical limit') can be linked to ecosystem damage. In this way deposition(s) are linked to a 'harmful effects': a low critical load implies a high sensitivity of the ecosystem to deposition, and *vice versa*. The critical load of S and N acidity is not a single value, but a trapezoidal function in the N-S-deposition plane characterised by three quantities, $CL_{max}(S)$, $CL_{min}(N)$ and $CL_{max}(N)$. For the eutrophying effect of N, the critical load is given as a single number, $CL_{nut}(N)$. These quantities are derived in the Appendix and are illustrated in Figure 1. In this paper we specifically look at the distribution of $CL_{max}(S)$ – also called the critical load of acidity – and $CL_{nut}(N)$, the main quantities characterising ecosystem sensitivity to S and N deposition.

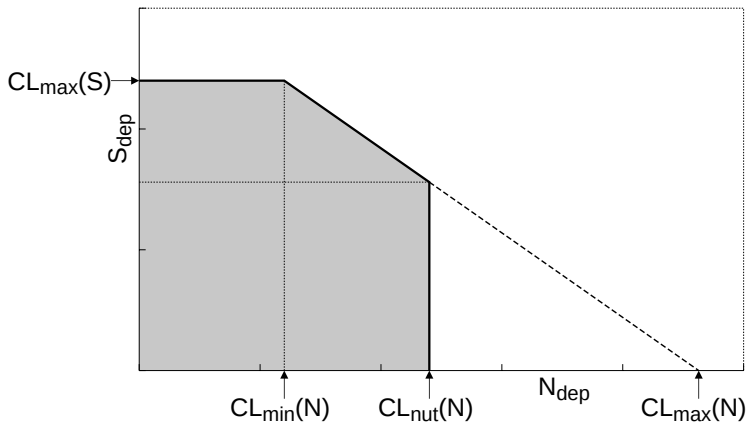

Figure 1. Critical load function of sulphur and nitrogen, defined by the three quantities $CL_{max}(S)$, $CL_{min}(N)$ and $CL_{max}(N)$ of the acidity critical loads and the critical load of nutrient N, $CL_{nut}(N)$. The grey area below the CL function denotes deposition pairs (N_{dep},S_{dep}) resulting in an ANC leaching smaller than $ANC_{le,crit}$ and a nitrate leaching less than $Q \cdot [N]_{acc}$, i.e. non-exceedance of critical loads.

2.2 Chemical criteria

Critical loads link deposition to ecosystem effects via soil chemical criteria (critical limits). These limits are based on dose-response relationships between chemical characteristics and ecosystem functioning. A critical load equals the deposition that

results in a steady state in an ecosystem compartment (e.g. soil, groundwater, plant) that does not exceed the selected critical limit, thus preventing 'significant harmful effects on specified sensitive elements of the environment' (Nilsson and Grennfelt, 1988). Consequently, the selection of the chemical criterion and its critical limit is a crucial step in deriving a critical load, and has to be guided by the negative effect(s) one wants to avoid.

To date mostly soil chemical criteria (e.g. nitrate and aluminium concentrations or aluminium to base cation ratios) have been used to derive critical loads with simple steady-state models. The relationship between these critical limits and the 'harmful effects' is one of the largest sources of uncertainty. For surface waters, there is a clear relationship between damage (fish dieback) and critical loads exceedance (Jensen and Snekvik, 1972; Dickson, 1978; Henriksen et al., 1989), but for terrestrial ecosystems the correlation is less convincing, although damage to tree crowns has been recorded in association with exceedance of critical loads (e.g. Nelleman and Frogner, 1994). One reason may be that effects are mainly invisible, such as effects of aluminium (Al) on fine root growth. Several authors have doubted the validity of the widely-used critical *Al*/*Bc* ratio as an indicator for harmful effects on forests, as no field evidence of such a relationship on mature trees has been demonstrated (Løkke et al., 1996; De Wit et al., 2001; Göransson and Eldhuset, 2001; Nyberg et al., 2001; Nygaard and De Wit, 2004). Some authors have therefore suggested to use other criteria such as a critical value for base saturation (*Bsat*) or Acid Neutralising Capacity (ANC) leaching (Holmberg et al., 2001) or to preserve stable pools of aluminium hydroxides (De Vries, 1993). There is more empirical evidence for relationships between atmospheric N deposition and effects on plant species diversity, and these form the basis for (empirical) critical loads of nutrient nitrogen (e.g. Bobbink et al., 1988; Nordin et al., 1998; Clark and Tilman, 2008). However, use of a single critical N concentration for Europe to derive critical N loads with the SMB model is not a valid option: De Vries et al. (2007) demonstrated that it is possible to define several associated 'critical' N concentration ranges for various ecosystems in Europe to protect for vegetation change, in contrast to the single values previously used. They also showed that effects are better related to other predictors such as the N mineralization flux (De Vries et al., 2007a). In this study several criteria were used to investigate the effect of the choice of the criterion on the (patterns in) critical loads (Table 1).

For a given site a fixed relationship exists between each of the acidification criteria, referred to hereafter as 'equivalent criteria' (see Appendix and Figure 2). The widely used criterion of *Al*/*Bc=1* leads to (strongly) negative ANC values in the soil solution, except for soils with a very low base cation (Bc) concentration (Figure 2).

Table 1. Chemical criteria for computing critical loads.

Criterion	Critical value
Al/Bc	1 mol mol^{-1}
[*Al*]	0.2 eq m^{-3}
Bsat	15%
ANC	0
Al&Al/Bc	*Al/Bc=1* only if [*Al*] > 0.2 eq m^{-3}
Al_{ox} depletion (ΔAl_{ox})	0
N concentration	Fixed: 0.2 mg l^{-1}
	Vegetation-dependent: 0.2 – 5 mg l^{-1}

The decrease in ANC equivalent to *Al/Bc=1* for increasing Bc concentrations is due to the fact that with increasing Bc concentration the Al concentration has to increase to keep the Al/Bc ratio constant, and the increasing Al concentration leads to a decreasing ANC.

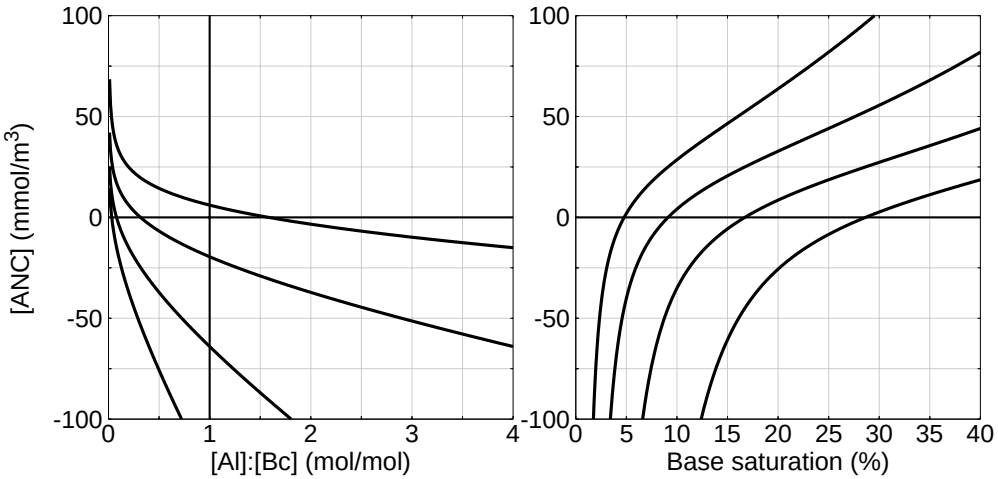

Figure 2. Functional relationship between ANC and molar Al/Bc ratio (left) and base saturation (right). The graphs on the left are for [Bc]=1 (top curve), 5, 20 and 50 meq.m^{-3}; the ones to the right for $K_{Gap}\sqrt{[Bc]}$=1 (top curve), 2, 4 and 8 meq.m^{-3}. All graphs are made with $K_{HCO3}\cdot p_{CO2}$=200 (mmol $m^{-3})^2$, $m\cdot DOC$=20 mmol m^{-3} and pK_1=4.5 (for notation see Appendix). The parameters used to compute these curves cover the majority of soils in Europe and Northern Asia.

A critical ANC of zero results in an equivalent base saturation between about 5% for soils poor in base cations (such as podzols) to about 30% for richer soils. Aiming at a base saturation for all soils of, for example, 15% requires an (unrealistically) high ANC especially in soils poor in base cations.

2.3 Geographical data bases

The required input data for critical load calculations consist of spatial information describing climatic variables, base cation deposition and weathering, nutrient uptake and N transformations and were derived combining maps of soils, land cover and forest growth regions. To cover the entire geographical area of interest, several thematic maps had to be combined:

(a) Land cover: The harmonised land cover map produced by the CCE and SEI was used for Europe (Slootweg et al., 2005; Slootweg et al., 2007). For the EECCA countries we used the Global Land Cover 2000 project map at 1 km resolution (Bartholome et al., 2002). Only forests (EUNIS code 'G') and (semi-)natural vegetation (codes 'D', 'E' and 'F') were considered in this study.
(b) Soils: The European Soil Database v2 polygon map (JRC, 2006) at a scale 1:1M was used for Europe including the entire Russian territory, Belarus and Ukraine. For the other CIS (Commonwealth of Independent States) countries, Turkey and Cyprus the less detailed FAO 1:5M soil map (FAO, 1988) was selected.
(c) Forest growth: Average forest growth was derived from an updated data base of the European Forest Institute (EFI), which contains growth data for a variety of species and age classes in about 250 regions in Europe (Schelhaas et al., 1999). This map was combined with a map of 74 administrative regions in Russia for which forest stock data are provided by Alexeyev et al. (2004). For other CIS States, Cyprus and Turkey a map was used that delineates the forest growth regions in these countries.
Overlaying these maps and merging polygons with common soil, vegetation and region characteristics within blocks of 10×10 km (a subdivision of the EMEP 50×50 km grid) resulted in about 3.8 million computational units with a total area of 16.6 M km^2. In the standard model runs, we used only computational units larger than 1 km^2 reducing their number to 1.3 M but occupying 96% of the total area. One simulation was performed with all units included to determine the effect of leaving out the very small units on the distribution of critical loads.
The soil maps are composed of so-called soil associations, each polygon on the map representing one soil association. Every association, in turn, consists of several soil typological units (soil types) that each occupy a known percentage of the soil association, but with unknown location within the association. The soil units on the maps are classified into more than 200 soil types (European Soil Bureau Network, 2004), with associated attribute data such as soil texture, parent material class and drainage class. Six texture classes are defined, based on clay and sand content (FAO-UNESCO, 2003). The drainage classes, which are used to estimate the

denitrification fraction, are derived from the dominant annual soil water regime (FAO-UNESCO, 2003; European Soil Bureau Network, 2004).
Combining soil- and land cover maps shows that podzols are most frequent (about 18%), especially in the north-western part of the area, followed by gleysols (17%), cambisols (about 13%) and regosols and podzoluvisols (Table 2). Whereas in Europe podzols are by far the most important soils (De Vries et al., 1994b; Posch and Reinds, 2005), large natural areas in the EECCA countries are occupied by wet soils such as gleysols. Soils in natural areas mainly occur on coarse (texture class 1, 41%) and medium soil textures (class 2, 48%). Natural vegetation on fine textures (classes 3-5) is rare and occupies only about 10% of the area. About 4% of the vegetation is located on peat soils.

Table 2. Area and share of the 10 most common vegetation-soil combinations.

Soil type	Area (km²)	Area (%)
Podzol (P)	2,963,052	17.9
Gleysol (G)	2,848,593	17.2
Cambisol (B)	2,170,137	13.1
Regosol (R)	1,653,685	10.0
Podzoluvisol (D)	1,624,314	9.8
Rendzina (E)	856,541	5.2
Fluvisol (J)	709,925	4.3
Lithosol (I)	698,571	4.2
Histosols (O)	616,632	3.7
Kastanozem (K)	559,267	3.4
SUM	14,700,717	88.8

There are inaccuracies in these estimates, because the soil map consists of soil associations. The map overlay thus gives an area for each association, not for each soil type. Vegetation has been assigned evenly to all soil types within the association, which in reality will not always be the case. Nevertheless, a previous study showed that an uneven allocation of forests, in which they are assigned to poor and steep soils first, yields an almost identical distribution of forest-soil combinations in Europe as an even distribution (De Vries et al., 1994c).

2.4 Meteorology and hydrology

The annual water flux through the soil at the bottom of the rooting zone is required to compute the concentration and leaching of compounds. The bottom of the root zone was set at 50 cm, except for lithosols which have a soil depth of 10 cm only. The leaching rate was estimated from meteorological data and soil properties. Long-term (1961-1990) average monthly temperature, precipitation and cloudiness

were derived from a high resolution European data base (New et al., 1999) that contains monthly values for the years 1901-2001 for land-based grid-cells of 10′×10′ (approx. 15×18 km in central Europe). For sites east of 32°, a coarser 0.5°×0.5° global database from the same authors was used (New et al., 2000).
Evapotranspiration was calculated with a sub-model used in the IMAGE global change model (Leemans and Van den Born, 1994) following the approach by Prentice et al. (1992,1993). Potential evapotranspiration was computed from temperature, sunshine and latitude. The effect of snow cover on evapotranspiration was included by simulating accumulation and melting of a snow layer at each site using the temperature and precipitation data. Actual evapotranspiration was then computed using a reduction function for potential evapotranspiration based on the available water content in the soil described by Federer (1982). Soil water content is in turn estimated using a simple bucket-like model that uses water holding capacity and precipitation data. The available water content (AWC) and the water content at wilting point were estimated as a function of soil type and texture class according to Batjes (1996). Batjes (1996) provides texture class dependent AWC values for FAO soil types based on an extensive literature review and developed a transfer function to compute wilting point from soil texture and soil organic carbon content. A complete description of the hydrological model (without the snow module) can be found in Reinds et al. (2001).
The critical load models implicitly assume free draining soils. Large areas of Northern Russia, however, have shallow permafrost where the critical load model in its present form cannot be applied. Therefore, soils in areas with an average monthly temperature below zero for at least eight months of the year have been excluded from the simulations. This area corresponds well with the areas with shallow permafrost reported in (FAO-UNESCO, 2003).

2.5 Base cation deposition and weathering

Base cation deposition for Europe was taken from simulations with an atmospheric dispersion model for base cations (Van Loon et al., 2005). For northern Asia calcium (Ca) deposition was taken from a global map computed with a model of Tegen and Fung (1995) using estimates of soil Ca content (Bouwman et al., 2002). Comparing the spatial patterns of Ca deposition of the European map and the global map, it is clear that the global Ca map underestimates the deposition in Europe by at least a factor of two. This underestimation was also recognized by Lee et al. (1999) who attribute the difference mainly to the fact that they did not include all important, local, sources of Ca in their modelling. Using both maps

would thus lead to a non-smooth transition in BC deposition in eastern Europe. Since the European map does include all sources (natural and anthropogenic) it was taken as the reference and the Ca from the global were multiplied by two to generate a consistent deposition pattern over the entire modelling area in the combined map.

Magnesium (Mg) and potassium (K) deposition are also needed in the EECCA countries; relationships between Ca deposition and Mg and K deposition were derived on the basis of measurements at 95 EMEP/CCC monitoring stations in Europe (Hjellbrekke et al., 1997). Because of the different origin of base cations, the spatial patterns in these ratios are far from constant. In southern areas Bc input is dominated by Ca from Saharan dust, whereas in Northern Europe Mg and K become more important with Mg dominating the Bc input in coastal regions. Mg deposition was modelled as a function of Ca deposition, Ca_{dep} (eq ha^{-1} yr^{-1}), and the distance to coast:

$$(1) \qquad Mg_{dep} = a \cdot Ca_{dep} + b \cdot f(DistToCoast)$$

Regression (r^2=0.375) yields a=0.4748 and b=239.6, 171.6, 104.9, –18.2 and –39.4 for distance-to-coast classes <10, 10–20, 20–50, 50–100 and >100 km, respectively. Mg deposition thus increases with increasing Ca deposition and strongly decreases with distance from the coast. K deposition was estimated as a function of Ca deposition, Ca_{dep} (in eq ha^{-1} yr^{-1}), and latitude, $Ylat$ (in degrees):

$$(2) \qquad K_{dep} = a + b \cdot Ca_{dep} + c \cdot Ylat$$

Regression yields a=–95.1, b=0.2419 and c=1.731 with r^2 = 0.552; K deposition increases with increasing Ca deposition and with latitude.

Weathering of base cations was computed as a function of parent material class and texture class and corrected for temperature, as described in (UBA, 2004). For Europe and all of Russia parent material was obtained from the 1:1M soil map and for the rest of the territory as a function of soil type as described by De Vries (1991). The texture class attribute is common to both soil maps. From the total BC weathering, the weathering rates of Ca, Mg, K and Na were estimated as a function of clay and silt content for texture classes 2 to 5 (following Van der Salm, 1999) and as fixed fractions of total weathering for texture class 1 (De Vries, 1994).

2.6 Nutrient uptake, nitrogen immobilization and denitrification

The net growth uptake of Bc and N by forests was computed by multiplying the estimated annual average growth of stems and branches with the element contents of base cations and N in these compartments based on an extensive literature review by Jacobsen et al. (2002). The average nutrient contents of spruce and pine were assigned to conifers and the average of oak and beech to deciduous forests. An average of these two values was used for mixed forests. Wood densities of 450 $kg.m^{-3}$ and 650 $kg.m^{-3}$ as well as branch-to-stem ratios of 0.15 and 0.20 for coniferous and deciduous trees, respectively, have been used (Kimmins et al., 1985). For mixed forests the averages of these values were applied. For other (semi-) natural vegetations, *net* uptake was set to zero assuming that no net removal of N and Bc occurs.

Forest growth for Europe was derived from the EFI database (Schelhaas et al., 1999) that provides measured growth data for about 250 regions in Europe for various species and age classes. Growth was assessed by computing the area-weighted average growth over all age classes for each combination of region and tree species group. Forest growth for Russia was estimated from data by Alexeyev et al. (2004) who compiled statistical data on growing stock and areas of stocked land from available data sources, tabulated for 74 administrative regions within Russia. Alexeyev et al. (2004) provide areas per region of conifers forest, deciduous hardwood and deciduous softwood forests for the age classes young, middle-aged, maturing and mature/over mature forests as well as the standing biomass per region for these species and age classes. Net growth was estimated by computing the standing volume per hectare (using total volumes and stocked areas) per age class, assuming ages of 30, 60, 90 and 140 years and fitting a logistic growth curve to the volume-age data. Finally the average growth was obtained from this growth curve. For the other CIS states, growth rates were obtained from Prins and Korotkov (1994), who provide the growing stock per hectare. Assuming an average stand age of 60 years gives an approximation of average forest growth in these regions.

For Turkey, growth rates were kindly supplied by the Turkish ICP Forest National Focal Centre as growth rates for thirty species and two forest states (degraded and non-degraded). Furthermore, for a few tree species, growth rates were supplied for coppice and high forest separately. These data were combined with a map showing the distribution of species over Turkey to arrive at growth rates per region per species group (conifers, broadleaves). For Cyprus a crude approximation of an average growth rate of 0.8 m^3 ha^{-1} was made based on the average standing

biomass of 43 m^3 ha^{-1} given by FAO (2000) and assuming an average stand age of 60 years.
The denitrification fraction, f_{de}, was computed as a function of the soils' drainage status (Reinds et al., 2001) and varies between 0.1 for well drained soils to 0.8 for peaty soils. The long-term net N immobilization was set at 1 kg N $ha^{-1}a^{-1}$, which is at the upper end of the estimated annual accumulation rates for the build-up of stable C-N compounds in soils (UBA, 2004).

2.7 Al-H relationship and organic acids

The Al concentration is computed from a gibbsite equilibrium and the equilibrium constant K_{gibb} is estimated as a function of soil texture class based on simultaneous measurements of Al concentration and pH at about 150 European forest monitoring plots (De Vries et al., 2003a). The dependence of K_{gibb} on the (soil) temperature T (°C) is modelled according to the Van't Hoff equation:

$$K_{gibb}(T) = K_{gibb}(T_0) \cdot \exp\left[\frac{\Delta H}{R} \cdot \left(\frac{1}{273+T_0} - \frac{1}{273+T}\right)\right] \quad (3)$$

where ΔH is the reaction enthalpy (=–95490 $J.mol^{-1}$), R the gas constant (=8.314 $J.mol^{-1}.K^{-1}$) and T_0 (=10°C) is a reference temperature. The same database was used to derive a relationship between DOC concentration and soil pH and texture. In turn, estimates of soil pH were obtained from an extensive soil data base with about 6000 soil profiles in Europe (Van Mechelen et al., 1997) and a data base for the Russian territory (Stolbovoi and Savin, 2002). The same datasets were used to estimate soil organic carbon contents needed for estimating soil water holding capacity (see section 2.4).

3. Results

The input data have been derived for each of the 1.3 M receptors. In the following sections results are presented as maps showing the median values within each 50 × 50 km EMEP grid cell for input data. For critical loads, however, 5th percentiles are shown to indicate the most sensitive ecosystems. The area in Northern Russia with no data shown is the area excluded from modelling because of shallow permafrost.

3.1 Input data

Leaching fluxes vary from less than 100 mm yr^{-1} in arid regions such as central Spain, central Turkey and large parts of the southern CIS states to >300 mm yr^{-1} in areas with high precipitation such as along the west coast of Europe and along many mountain ranges (Figure 3a). The uncertainty in the leaching flux is linked to the reliability of the climate data: values in western Europe are more certain than those in the EECCA area, as the density of rainfall stations used to estimate the grid rainfall is much higher in Europe than in the EECCA area (New et al., 1999). Median base cation deposition shows a strong north-south gradient with values >600 eq ha^{-1} yr^{-1} in southern Europe and the southern parts of the CIS states, caused by high dust input from nearby desert areas, and very low values of <200 eq ha^{-1} yr^{-1} in the northern part of the modelled area (Figure 3b). The map also shows that a reasonably consistent spatial pattern is achieved even though two data sources were used.

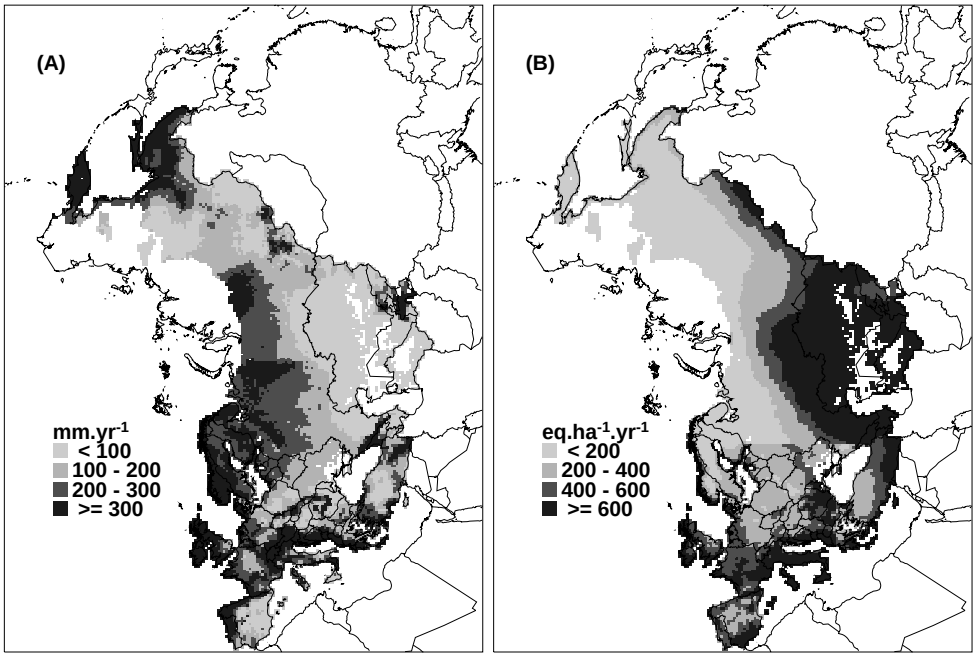

Figure 3. A: grid-median leaching flux from root zone (mm yr^{-1}); B: base cation deposition (eq ha^{-1} yr^{-1}).

Very low weathering rates (< 150 eq ha^{-1} yr^{-1}) are found in most of Scandinavia where poor soils prevail and temperatures are low (Figure 4a). The same holds for large parts of Northern Russia. Very low weathering rates also occur in central and

western Spain in areas dominated by acid dystric regosols developed on granites. High weathering rates (>1000 eq ha^{-1} yr^{-1}) are confined to regions with soils developed on volcanic materials and especially in areas dominated by calcareous soils that occupy parts of Spain, France, Hungary, large parts of Turkey and most of the areas with forests and/or natural vegetation of, for example, Kazakhstan, Uzbekistan and Turkmenistan.

The high weathering rates in eastern Russia occur in areas dominated by rendzic leptosols, soils with an organic rich topsoil overlying parent material with at least 40% calcium carbonate equivalent (FAO, 1988). This is also reflected in the forest growth rates in this region in eastern Russia which are somewhat higher than in the surrounding areas (see Figure 4b), showing the influence of site quality on growth.

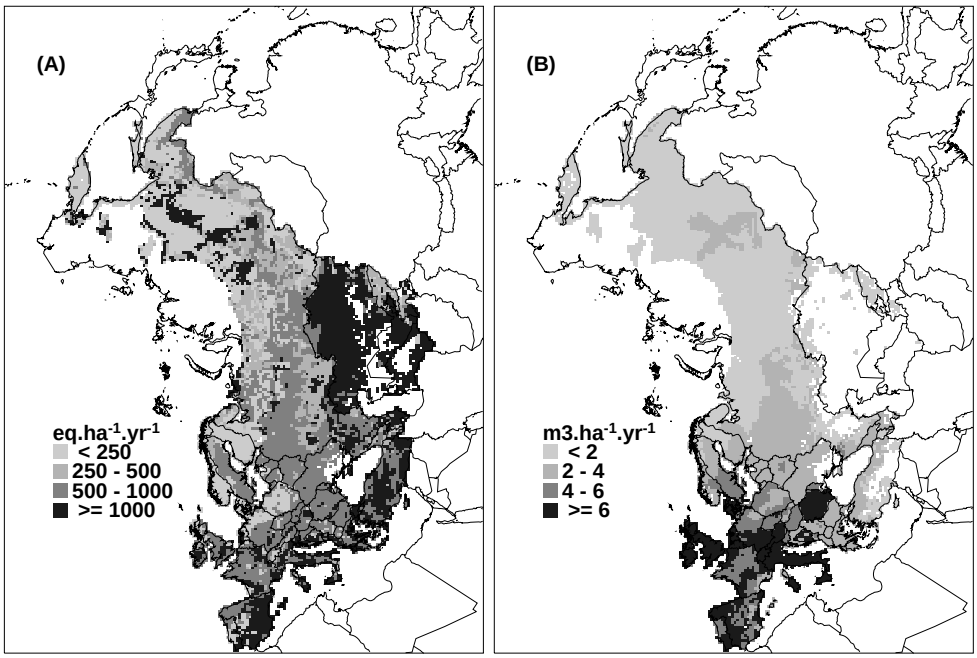

Figure 4. A: grid-median base cation weathering (eq ha^{-1} yr^{-1}); B: grid-median forest growth rate (m^3 ha^{-1} yr^{-1}).

Net uptake of nitrogen and base cations in forest ecosystems is determined by nutrient contents and growth rate. Median growth rates of forests show the well-known pattern in Europe were high growth rates are found in central Europe were climate, site quality and intensive management allow highly productive forests (Figure 4b). Low growth rates in Europe are confined to arid regions such as central Spain, parts of France and Turkey and to areas with low temperature and

poor site quality (shallow, poor soils) such as northern Scandinavia. In the EECCA territory growth rates are generally low (1–3 m^3 ha^{-1} yr^{-1}), although relative high forest productivity can be found in the areas west of the Ural mountains and in Georgia.
Very low growth rates (<0.5 m^3 ha^{-1} yr^{-1}) occur in arid regions such as Tajikistan, Turkmenistan and Uzbekistan. Growth rates for Russia are somewhat uncertain as they were derived indirectly from growing stock data. For the other CIS states and Cyprus, where only one growth rate per country could be assigned, the growth data do not represent the spatial variability in growth rates. Although the European data are based on a large data set, it is clear that some border effects occur, probably due to the fact that for some countries (e.g. Ukraine and Romania) the area-representation of the supplied data is relatively poor.

3.2 Critical loads of acidity (sulphur)

The critical load of acidity, $CL_{max}(S)$, based on Al/Bc=1, is computed as the sum of base cation input through weathering and deposition minus the removal of base cations by uptake minus ANC leaching (see Appendix). Highest critical loads are thus found in areas with high base cation weathering and/or base cation deposition such as along the Mediterranean coast, parts of eastern Europe and the southern parts of the CIS states (Figure 5a). For calcareous soils $CL_{max}(S)$ has been set to 10,000 eq ha^{-1} yr^{-1}, representing the very high weathering rates in such soils. Furthermore, high critical loads are found in areas with high acidity leaching (areas with a high precipitation surplus) such as along the coast of north-western Europe. Such high acidity leaching due to high base cation (especially Mg) input from sea salts is considered inappropriate by some authors, who have used alternative criteria, for example, pH in Ireland (Aherne et al., 2001) and Ca/Al ratio in the UK (Hall et al., 2001a). Lowest critical loads are found in areas with low weathering rates associated with coarse soils on acid parent material such as central Spain and/or low temperatures (Scandinavia and northern Russia).
The cumulative frequency distributions of $CL_{max}(S)$ for the three vegetation groups: forests, grasslands and heath-lands/tundra show that the critical load distribution for forests and heath land/tundra are very similar (Figure 5b). For the heath-lands/tundra a larger fraction is located on calcareous soils, illustrated by the larger fraction of $CL_{max}(S)$ of 10,000 eq ha^{-1} yr^{-1}. Grasslands generally have higher critical loads because they occur on richer soils than forests and heath-lands/tundra: average computed weathering rates for grassland soils are about twice as high as those for forest and heath land soils. About 35% of the grasslands are located on calcareous soils.

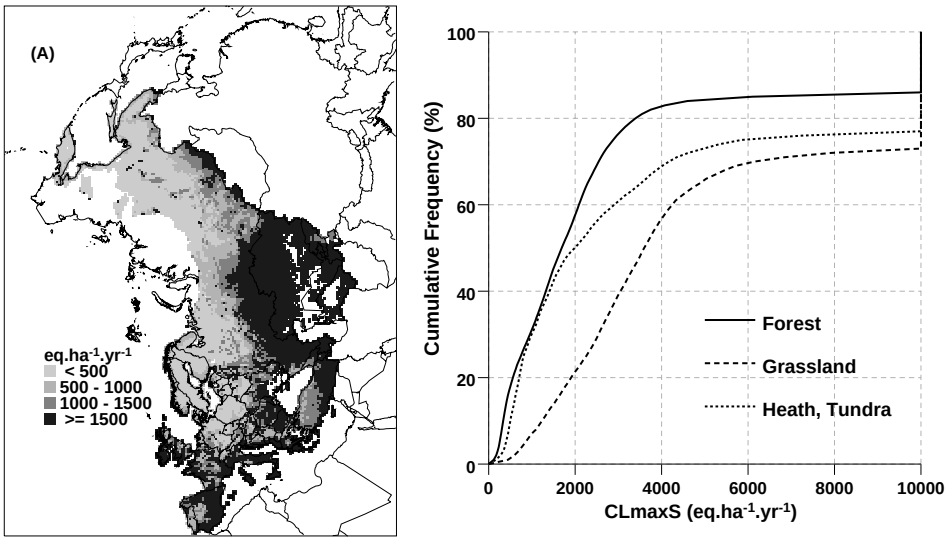

Figure 5. A: 5th percentile critical load $CL_{max}(S)$ (eq ha^{-1} yr^{-1}); B: cumulative frequency distribution of $CL_{max}(S)$ for three vegetation classes (eq ha^{-1} yr^{-1}).

3.3 Critical loads of N

The minimum critical load of N (see Figure 1) consists of the long-term immobilization and net uptake. Because we assumed no removal of growing material from natural vegetations such as grasslands and heath lands, the minimum critical N load consists of the fixed N immobilisation of 1 kg N per year (=71 eq ha^{-1} yr^{-1}) only. For forests, net N uptake is accounted for and $CL_{min}(N)$ ranges between 150 eq ha^{-1} yr^{-1} in low productive areas to about 600 eq ha^{-1} yr^{-1} in regions with high forest growth.

The critical load of nutrient N, $CL_{nut}(N)$, is computed from $CL_{min}(N)$ by adding a critical N leaching and denitrification. Average critical nitrogen concentrations were set to 0.2–0.4 mg N L^{-1} for forests, 3 mg N L^{-1} for natural grassland (UBA, 2004) and 4 mg N L^{-1} for heath land (De Vries et al., 2007a). Figure 6a show the spatial patterns in $CL_{nut}(N)$. Highest critical loads are confined to regions dominated by grass and heath lands with a high precipitation surplus, leading to high N leaching rates. Such regions are Ireland, the western parts of the UK and Norway, northern Spain and the region along the Adriatic coast. Low critical loads are found in arid regions were N leaching is low such as in the southern part of the CIS states, most of Turkey and parts of Central Europe. As expected, there is a marked difference in distribution of $CL_{nut}(N)$ between various ecosystems (Figure

6b). Because the critical N concentration for forests is much lower than for the other ecosystems, also the critical leaching rate is much lower.

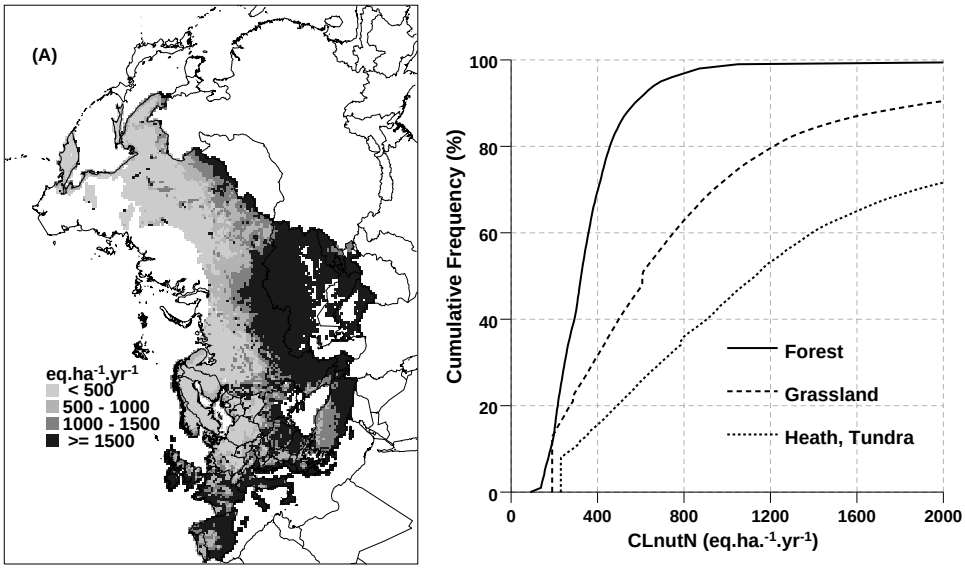

Figure 6. A: 5th percentile critical load $CL_{nut}(N)$ (eq ha^{-1} yr^{-1}); B: cumulative frequency distribution of $CL_{nut}(N)$ for three vegetation classes (eq ha^{-1} yr^{-1}).

In low precipitation areas, critical loads for all ecosystems are about equal as the sum of the low leaching rate in forest and the N uptake in forests is about equal to the higher leaching rate for grasslands and heath lands. In high precipitation areas, leaching becomes the dominant process and the $CL_{nut}(N)$ for grasslands and heath land is much higher than that for forest.

3.4 Sensitivity of critical loads

3.4.1 Sensitivity to the selection of receptors

To reduce computing time and to eliminate spurious polygons from the map overlay that may be due to map inaccuracies, only receptors of at least 1km^2 were included in the modelling. To determine the effect of this cut-off, one simulation was made with all 3.8 million receptors. Results show that only in about 4–5% of the EMEP grid cells the 5th percentiles of $CL_{max}(S)$ and $CL_{nut}(N)$ differ by more than 5% from the 5th percentile values based on all 3.2 million data points and that in

more than 90% of the cells the difference is less than 1%, thus justifying the limitation to receptors larger than 1km^2.

3.4.2 Sensitivity to criteria

Critical load of acidity: $CL_{max}(S)$

To test the sensitivity of the model to the chemical criterion used, a number of simulations were made with the criteria listed in Table 1. Results are shown in Table 3 that lists the 5th percentiles and median values of $CL_{max}(S)$ per region for non-calcareous soils.

Table 3. 5th percentile and median values for $CL_{max}(S)$ for non-calcareous soils in six regions for various criteria (Central Europe consists of Austria, Belarus, Bulgaria, Czech Republic, Hungary, Moldavia, Poland, Rumania, Slovakia, Switzerland and Ukraine; the CIS except Russia, Ukraine and Belarus comprises Armenia, Azerbaijan, Georgia, Kazakhstan, Kyrgyzstan, Tajikistan, Turkmenistan and Uzbekistan; Scandinavia is defined as Norway, Sweden, Finland and the Baltic states; western Europe consists of Belgium, Germany, Denmark, France, Ireland, Luxemburg, the Netherlands and the United Kingdom; Southern Europe comprises the remaining European countries).

Region	5th percentile						median						Nr
	Al/Bc	*Al*	*Bsat*	*ANC*	*Al & Al/Bc*	*ΔAlox*	*Al/Bc*	*Al*	*Bsat*	*ANC*	*Al & Al/Bc*	*ΔAlox*	receptors
Central Europe	373	394	93	157	444	571	2208	1292	1028	893	2272	2898	113497
Other CIS states	1529	953	698	610	1572	1692	2944	1561	1599	1184	2948	2617	34124
Russia	242	278	70	137	351	613	1199	925	634	505	1231	1501	527848
Scandinavia	244	583	16	69	587	326	879	1080	248	357	1233	1177	142760
Western Europe	619	628	91	231	741	616	2913	1892	1131	1075	3050	3229	111328
Southern Europe	977	745	310	392	1063	979	2805	1665	1213	1115	2824	3094	130214

For most regions the Al/Bc and combined Al&Al/Bc criteria yield about the same critical loads. Exceptions are the 5th percentile critical loads in Russia and Scandinavia which have a low base cation input, and therefore an *Al/Bc* based critical load can be very low because of low base cation concentrations, even though the associated Al concentration is (far) below the critical value of 0.2 eq.m^{-3}. In such cases the critical load is determined by the Al concentration alone, resulting in a higher critical load than the *Al/Bc*-based critical load.

Using a critical Al concentration alone instead of Al/Bc to compute critical loads gives mostly lower critical loads. The only exception is Scandinavia were the 5th

percentile is higher than the *Al*/*Bc*-based CL because of the very poor soils in these regions: the low Bc input causes very low *Al*/*Bc*-based critical loads.
Using *Al*/*Bc*=1 to compute the critical load for these sensitive ecosystems will lead in steady state to Al concentrations (far) above 0.2 eq.m^{-3} for more than half of the ecosystems, base saturations below 15% and to negative ANC concentrations for almost all grid cells (Figure 7): an *Al*/*Bc* ratio of 1 is mostly equivalent to negative ANC concentrations and low base saturation values (see also Figure 2).

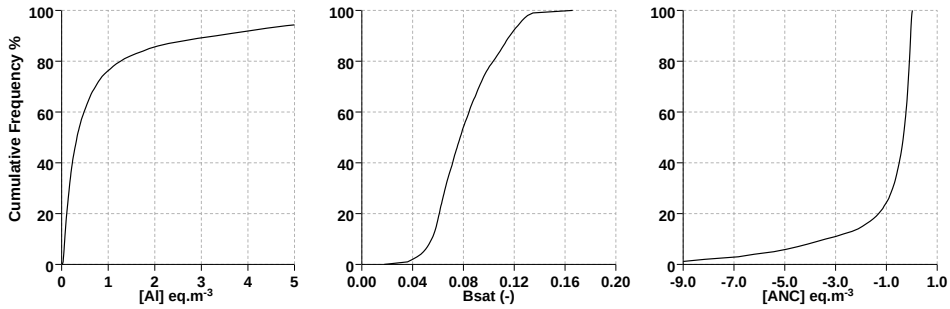

Figure 7. Cumulative frequency distributions of grid-average Al/BC=1 equivalent values of [Al], Bsat and ANC for sensitive receptors in an EMEP grid cell defined as having a $CL_{max}(S)$ within 50% of the 5th percentile $CL_{max}(S)$ of that cell (based on Al/Bc=1)

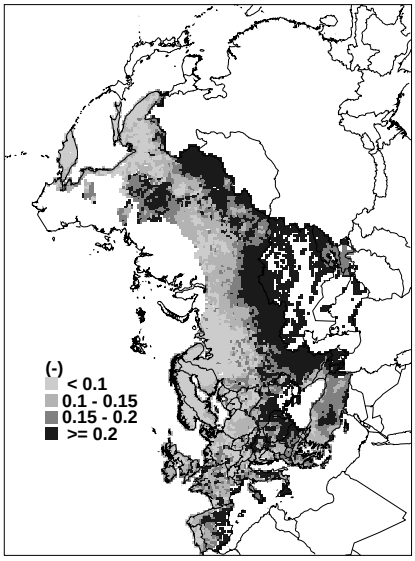

Figure 8. Average base saturation (-) per grid cell equivalent to ANC=0 for sensitive ecosystems.

Critical loads based on a base saturation of 15% as critical limit are even lower than those computed from a critical Al concentration (Table 3). Especially in Scandinavia the base saturation criterion leads to very low critical loads due to the very low base cation input: in these poor, sandy soils the equilibrium base saturation with no acid input at all would be less than 15%. The average base saturation for the sensitive receptors per EMEP cell equivalent to an ANC concentration of zero is shown in Figure 8. For Scandinavia and Northern Russia the equivalent base saturation at ANC_{le}=0 would be about 10% or lower, due to natural soil acidification processes: aiming at 15% base saturation in such poor acid soils leads to negative critical loads.

Critical loads for ANC_{le}=0 show strong similarities with those based on the [*Al*] and *Bsat* criteria, but as with the *Bsat*-based CLs, *ANC*-based CLs can be very low for the most sensitive ecosystems in Russia, Scandinavia and Western Europe. The highest critical loads are computed when aiming at a stable Al_{ox} pool. This shows that all other criteria protect the soils from loosing their Al buffering capacity.

Critical load for eutrophication: $CL_{nut}(N)$

If the denitrification rate is low, the critical load of nutrient N mainly consists of N removal through leaching, net growth and immobilization.

In the past $CL_{nut}(N)$ was mostly computed with a critical limit of 0.2-0.4 mg N L^{-1} which was considered to be representative for forests. This limit was recommended as the concentration in soil solution above which vegetation changes in the under story of forests could occur (UBA, 2004). A recent study on critical limits for critical loads of nitrogen (De Vries et al., 2007a) revealed that such low limits are mostly related to vegetation changes in Scandinavia, but effects elsewhere in Western Europe probably occur at higher values.

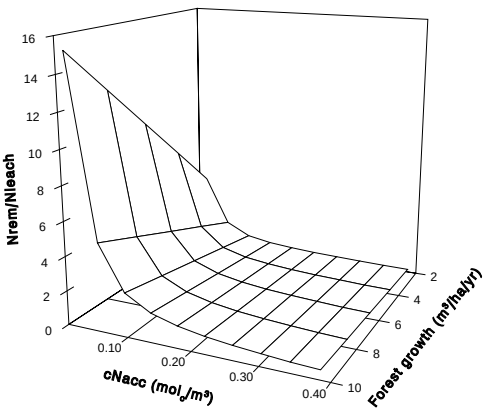

Figure 9. Ratio $(N_u+N_i)/N_{le}$ as a function of forest growth rate and critical N concentration.

Based on literature data and on model results from the Netherlands, the authors therefore suggest that higher limits of about 3-6 mg N L^{-1} for Western Europe may be used. The choice of the critical concentration strongly determines the relative importance of N removal and N leaching in the critical load. The ratio $(N_u+N_i)/N_{le}$ as a function of forest growth rate and critical N concentration, $[N]_{acc}$, is shown in Figure 9. In this example Q=300 mm yr^{-1}, f_{de} = 0, N_i=1 kg N ha^{-1} and the N content in stem wood is set at 1.15 $g.kg^{-1}$ representing conifers forest. At $[N]_{acc}$=0.0143 $eq.m^{-3}$ (=0.2 mg N L^{-1}) the ratio between removal and leaching steeply increases from 3 at a growth rate of 2 m^3 ha^{-1} yr^{-1} to 12 at a growth rate of 10 m^3 ha^{-1} yr^{-1}. This illustrates that in areas with high growth rates such as central Europe, N leaching is unimportant compared to N uptake at such low critical N concentrations. For $[N]_{acc}$=0.3 $eq.m^{-3}$ (= 4.2 mg N L^{-1}) leaching and removal are

almost equal at a growth rate of 10 m^3 ha^{-1} yr^{-1}, but leaching dominates at lower growth rates. At a growth rate of 2 m^3 ha^{-1} yr^{-1}, N leaching is five times higher than N removal.

Comparing the cumulative frequency distributions of $CL_{nut}(N)$ for forests in western Europe, using the critical limits of 0.2 mg N L^{-1} for conifers forest and 0.3 mg N L^{-1} for deciduous forests, with $CL_{nut}(N)$ using the limit of 3 mg N L^{-1} (specifically suggested for non-Nordic forests) shows an obvious increase in $CL_{nut}(N)$ with higher concentrations (Figure 10): the median value over Europe is 930 eq ha^{-1} yr^{-1} which is about twice as high as the median value computed with the lower critical concentrations. The ratio between the 5th percentile $CL_{nut}(N)$ for each EMEP grid cell computed with a critical concentration of 3 mg N L^{-1} and the 5th percentile $CL_{nut}(N)$ computed with 0.2–0.3 mg N L^{-1} is shown in Figure 10b.

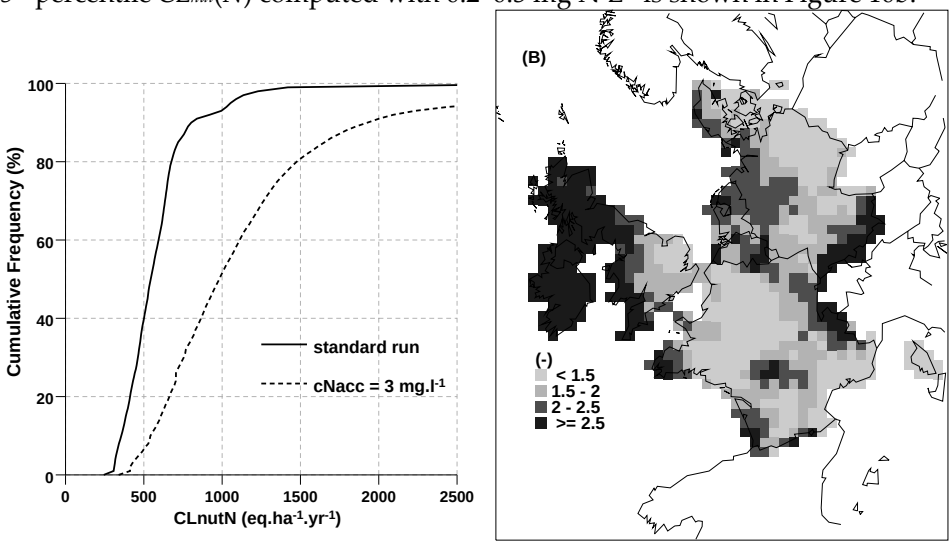

Figure 10. A: cumulative frequency distributions of $CL_{nut}(N)$ for forests in western Europe; B: ratio between the 5th percentile $CL_{nut}(N)$ with different values for $[N]_{acc}$.

Large differences are found in regions with a high precipitation surplus such as Ireland, UK and the northern part of the Alps. In areas with a low leaching rate such as the eastern part of Germany, and southern and central France, the increase in the 5th percentile critical load is less than 50%. This shows that increasing the critical N concentration by a factor of 10 does not always mean a commensurate increase in critical N load.

4. Discussion and conclusions

Combining the latest data bases on soil, land cover, climate and forest growth provided a detailed map with almost 4 million receptors for Europe and Northern Asia suitable for spatially highly disaggregated critical load calculations. The patterns in critical loads show a similarity with those shown in (Kuylenstierna et al., 2001), but since their empirical critical loads for acidity are based on soil sensitivity alone (determined by weathering rate), they do not show the influence of the removal of nitrogen or precipitation excess on critical load patterns.

Critical loads are sensitive to the criterion chosen. This study shows that for the most sensitive ecosystems critical loads based on an *Al*/*Bc*=1 or [*Al*]=0.2 eq.m^{-3} are comparable but that critical loads based on an ANC=0 are substantially lower. These conclusions can also be drawn by looking at the concept of equivalent criteria: *Al*/*Bc*=1 leads to positive ANC in soils with a very low base cation concentration only. Very low critical loads are also computed when using a critical base saturation of 15%. The same result was found by Holmberg et al. (2001) who computed much higher exceedances of *Bsat*-based critical loads than of *Al*/*Bc*-based critical loads.
Computing *Bsat* from *Al*/*Bc* shows that in the most sensitive ecosystems *Al*/*Bc*=1 will be equivalent to base saturations (far) below 15%. To obtain 15% base saturation in poor sandy soils requires an ANC far above zero which is not very realistic for soils that undergo natural acidification due to leaching of bicarbonates and organic acids (e.g. De Vries and Breeuwsma, 1986).

Using *ANC*=0 yields critical loads lower than with *Al*/*Bc*=1 but higher than with *Bsat*=15%. This seems to contradict the results of Holmberg et al. (2001) who found lowest critical loads when using *ANC*=0. However, they included neither bicarbonate leaching nor organic acids in the computation of ANC, leading to an underestimation of actual ANC and very low critical loads. Bicarbonate leaching is important at higher pH values and organic acid leaching is important in soils rich in organic matter (Holmberg et al., 2001); both terms have been added to the ANC calculation (UBA, 2004).

This study shows that as an alternative to *Al*/*Bc=1*, using *ANC*=0 with bicarbonate and organic acid leaching included is a more realistic option than using a *Bsat* criterion, as the latter criterion forces naturally acid soils to unrealistically high base saturations and ANC concentrations in the soil solution, thus leading to extremely low critical loads. An advantage of using ANC instead of Al/Bc is that it

provides a more general protection against acidification, not based on a weak relationship with forest health alone. However, studies providing limits for ANC leaching related to concrete effects on terrestrial ecosystems are lacking.

Critical loads for nutrient N computed for Western Europe using limits of 3–6 mg N L^{-1} for the N concentration in soil solution, as suggested in De Vries et al. (2007a) for forests in this region, are much higher than the critical loads based on the generally applied limits of 0.2–0.4 mg N L^{-1}, that may be reasonable values for Northern Europe. This sensitivity to the N criterion was already reported by De Vries et al. (1994b). Over the whole of western Europe, the median critical load for nutrient N with the revised N limits is about 1000 eq ha^{-1} yr^{-1} (=14 kg N yr^{-1}). This is in better accordance with the empirical critical loads of 10–15 kg provided by Bobbink et al. (2002) related to vegetation changes in forests than the 500 eq ha^{-1} yr^{-1} obtained with the limit of 0.2 mg N .L^{-1}. The strong dependence of the critical load on leaching rate does however show the limitations of the SMB model for the assessment of nutrient N critical loads, as it assumes a relationship between nitrate concentration and plant species sensitivity, whereas N availability may be more important (De Vries et al., 2007a). Moving to more elaborate models that compute critical N loads based on limits for, for example, pH and N availability related to occurrence of plant species (see e.g. Van Dobben et al., 2006) may improve estimates of nutrient N critical loads.

In this study we have only investigated the uncertainty in critical loads due to the use of different soil chemical criteria. It is clear that the overall uncertainty of the critical loads is also determined by model uncertainty and parameter uncertainty (see, e.g. Zak and Beven, 1999; Skeffington et al., 2007). Parameter uncertainty can be substantial and strongly contribute to uncertainty in critical loads as shown by, for example, De Vries et al. (1994b). A study for a forested catchment in Belgium showed that using various local and general estimates for nutrient removal by the forest lead to a wide range in critical N loads (Bosman et al., 2001). Others have shown that different methods of estimating weathering rates can yield strongly varying results (Hodson and Langan, 1999). Model structure is another important source of uncertainty. The SMB model by definition is a very simple model of reality. The way denitrification is modelled and the fact that we assume a homogenous soil layer contributes to uncertainty. Earlier studies showed that there is a strong effect of the depth at which the chemical criterion should be met especially when using the Al/Bc criterion (De Vries et al., 1994b).

Acknowledgements

We thank Ina Tegen (Leibniz Institute for Tropospheric Research,Leipzig, Germany) for providing the calcium deposition data for Asia and our colleague Lex Bouwman for pointing out this data source. The Dutch Ministry of Housing, Spatial Planning and the Environment (VROM) and the Trust Fund of the LRTAP Convention are acknowledged for financial support. We also thank the Turkish NFC of the ICP Forest for kindly supplying growth rates for forests in Turkey.

Appendix: Simple Mass Balance (SMB) models

In this Appendix we summarise the critical load models used in this paper. The basic reference is the Mapping Manual (UBA, 2004), where also original references are given, but see also (Posch and De Vries, 1999) and (De Vries and Posch, 2003a).

Critical load of nutrient nitrogen:
Critical loads of N for terrestrial ecosystems can be derived from the N mass balance. Neglecting adsorption, volatilisation and fixation this reads (in eq ha^{-1} yr^{-1}):

(A1) $$N_{dep} = N_i + N_u + N_{de} + N_{le}$$

The subscript *dep* refers to total deposition, *i* to net immobilisation, *u* to net growth uptake, *de* to denitrification, and *le* to leaching. Denitrification is modelled as a fraction of the net input of N (De Vries et al., 1994b):

(A2) $$N_{de} = f_{de} \cdot \left(N_{dep} - N_i - N_u\right)$$

where f_{de} ($0 \le f_{de} < 1$) is the denitrification fraction. From Eq.A1 a critical load is obtained by defining a critical (acceptable) limit to the leaching of N being the product of a critical concentration $[N]_{acc}$ and the water flux Q (m yr^{-1}). Combining Eqs.A1 and A2 we thus obtain the critical load of nutrient N, $CL_{nut}(N)$:

(A3) $$CL_{nut}(N) = N_i + N_u + Q \cdot [N]_{acc} / (1 - f_{de})$$

In this equation N_i stands for a long-term acceptable N immobilisation and N_u for the long-term average net growth uptake.

Critical loads of acidity:
Critical loads of acidity, induced by deposition of N and S, can be derived from the steady-state charge balance for the ions in the soil leachate (in eq ha^{-1} yr^{-1}) leaving the root zone (modelled as a single homogeneous layer):

$$(A4) \quad H_{le} + Al_{le} + BC_{le} + NH_{4,le} = SO_{4,le} + NO_{3,le} + Cl_{le} + HCO_{3,le} + Org_{le}$$

where Org_{le} is the leaching flux of the sum of organic anions. Neglecting OH^- and CO_3^{2-} (a reasonable assumption even for calcareous soils), the (leaching of) alkalinity or ANC (Acid Neutralizing Capacity) can be defined as:

$$(A5) \quad ANC_{le} = HCO_{3,le} + Org_{le} - H_{le} - Al_{le}$$

A steady-state situation with respect to acidification implies a constant pool of exchangeable base cations. Consequently the following mass balance holds for base cations:

$$(A6) \quad BC_{le} = BC_{dep} + BC_w - Bc_u$$

Note, that BC_{dep} and BC_w include all four base cations (BC=Ca+Mg+K+Na), whereas sodium is not taken up by vegetation (Bc=BC–Na). Since sulphur is regarded a tracer one has:

$$(A7) \quad SO_{4,le} = S_{dep}$$

Combining Eqs.A5-A7 and the N balance derived in Eq.A1 ($NO_{3,le}=N_{le}$) yields for the charge balance (Eq.A4):

$$(A8) \quad S_{dep} + N_{dep} = BC_{dep} - Cl_{dep} + BC_w - Bc_u + N_i + N_u + N_{de} - ANC_{le}$$

It is assumed that there are no sources or sinks of chloride in the soil compartment, and therefore leaching equals deposition. Knowledge of the deposition terms, weathering and net uptake of base cations as well as nitrogen uptake, immobilisation and denitrification allows to calculate the ANC leaching, and thus to assess the acidification status of the soil. Conversely, critical loads of S and N can be computed by defining a critical (or acceptable) ANC leaching, $ANC_{le,crit}$, which is set to avoid "harmful effects" on a "sensitive element of the environment"

(e.g. damage to fine roots). Using also the equation for the deposition-dependent denitrification (Eq.A2), one obtains for the critical loads of sulphur, *CL*(*S*), and acidifying nitrogen, *CL*(*N*):

(A9)
$$CL(S) + (1 - f_{de}) \cdot CL(N) = BC_{dep} - Cl_{dep} + BC_w - Bc_u + (1 - f_{de}) \cdot (N_i + N_u) - ANC_{le,crit}$$

Note, that these critical loads of S and N are not unique; every pair of deposition (N_{dep},S_{dep}) which fulfils Eq.A9 are critical loads of acidity. However, when comparing S and N deposition to critical loads one has to bear in mind that the N sinks cannot compensate incoming S acidity, i.e. the maximum critical load of sulphur is given by:

(A10) $$CL_{max}(S) = BC_{dep} - Cl_{dep} + BC_w - Bc_u - ANC_{le,crit}$$

Furthermore, if

(A11) $$N_{dep} \le N_i + N_u = CL_{min}(N)$$

all deposited N is consumed by uptake and immobilisation, and S can be considered alone. The maximum amount of allowable N deposition (in case of zero S deposition) is given by:

(A12) $$CL_{max}(N) = CL_{min}(N) + CL_{max}(S)/(1 - f_{de})$$

Derivation of the critical ANC leaching:
To compute acidity critical loads, the critical leaching of ANC has to be specified. With the aid of equilibrium reactions the concentration of Al, bicarbonate and organic acids can be expressed as function of [*H*] and thus ANC becomes a function of [*H*] alone. The concentration of Al is modelled by a gibbsite equilibrium:

(A13) $$[Al] = K_{gibb} \cdot [H]^3$$

where K_{gibb} is the gibbsite equilibrium constant. The concentration of HCO_3 is derived from the dissociation of CO_2 according to:

(A14) $$[HCO_3]\cdot[H] = K_{HCO3}\cdot p_{CO2}$$

where K_{HCO3} is the temperature-dependent dissociation constant and p_{CO2} the partial pressure of CO_2. The dissociation of organic acids is modelled assuming that only monoprotic organic anions are produced:

(A15) $$[Org] = \frac{m\cdot DOC\cdot K_1}{K_1 + [H]}$$

where *DOC* is the concentration of dissolved organic carbon (molC.m^{-3}), *m* is the charge density and K_1 the dissociation constant. A charge density of *m*=0.023 mol molC^{-1} and pK_1=4.5 was used throughout. The leaching of ANC (eq.A5) is computed as $Q\cdot[ANC]$.

Eqs.A13-A15 allow to compute the critical ANC leaching for any critical limit defined in terms of [*H*] (or [*Al*]). If a critical molar Al/Bc ratio is defined, the corresponding critical Al concentration is obtained as:

(A16) $$[Al]_{crit} = 1.5\cdot(Al/Bc)_{crit}\cdot[Bc]$$

with $[Bc]=Bc_{le}/Q$; and the factor 1.5 arises from the conversion of moles to equivalents (assuming K as divalent). In addition to soil solution variables, also base saturation has been suggested as a criterion. To link base saturation to soil solution chemistry, we use the Gapon model with simulating the exchange between Al, protons and base cations (Bc), as used in the dynamic soil model SAFE (Warfvinge et al., 1993). Then the following relationship between [*H*] and base saturation E_{Bc} can be derived:

(A17) $$[H] = K_{Gap}\cdot\sqrt{[Bc]}\cdot\left(\frac{1}{E_{Bc}} - 1\right)$$

with

(A18) $$K_{Gap} = \frac{1}{k_{HBc} + k_{AlBc}\cdot K_{gibb}^{1/3}}$$

where k_{HBc} and k_{AlBc} are the two selectivity coefficients describing cation exchange.

Modelling recovery from soil acidification in European forests under climate change

Reinds, G.J., Posch, M. & Leemans, R., 2009. Modelling recovery from soil acidification in European forests under climate change. Science of the Total Environment 407, 5663–5673

Abstract

A simple soil acidification model was applied to evaluate the effects of sulphur and nitrogen emission reductions on the recovery of acidified European forest soils. In addition we included the effects of climate change on soil solution chemistry, by modelling temperature effects on soil chemical processes and including temperature and precipitation effects on nitrogen uptake and on leaching. Model results showed a strong effect of the emission reduction scenarios on soil solution chemistry. Using the Current Legislation (CLE) scenario, the forest area in Europe with soil solution Al/Bc > 1 mol mol^{-1} (a widely used critical limit) decreased from about 4% in 1990 to about 1.7% in 2050. Under Maximum Feasible Reductions (MFR), the exceeded area will be < 1% in 2050. In addition, the area where limits for the nitrate concentration in soils are violated are predicted to be smaller under MFR than under CLE. Using the most stringent criterion for nitrate ($[NO_3] < 0.3$ mg l^{-1}), the area with nitrate concentrations in excess of the critical limit is about 33% in 2050 under CLE, but only 12% under MFR. Recovery, i.e. attaining non-violation of the criterion, is also much faster under MFR than under CLE. Climate change leads to higher weathering rates and nitrogen uptake in the model, but positive effects on recovery from acidification are limited compared to current climate, and differences between the A1 and B2 climate change scenarios were small. Target loads for 2050 exist for 4% of the area for Al/Bc=1 and for 12% of the area when using a criterion of ANC=0 for the soil solution. In about 30% of the area where meaningful target loads exists, the computed target load is lower than the deposition under MFR, and thus cannot be attained with current emission abatement technologies.

Keywords: acidification, climate change, target loads, recovery times, VSD

1. Introduction

The impacts of acidifying deposition on terrestrial ecosystems have been of concern since the 1970's (Gorham, 1976; Odén, 1976; Ulrich et al., 1980). In the early 1980s, models were used to study these impacts on a European scale in the context of the integrated assessment of long-range air pollution (Alcamo et al., 1985); this assessment included a simple regional-scale soil acidification model (Kauppi et al., 1986). Several studies have been carried out since the early 1990's to analyse the impacts of reductions of sulphur (S) and nitrogen (N) emissions in Europe on soil chemistry (e.g. De Vries et al., 1994d). After 2000, dynamic modelling of soil and

surface water acidification and recovery entered the agenda of the Convention on Long-range Transboundary Air Pollution (LRTAP), leading to guidelines for dynamic modelling (Posch and Hettelingh, 2001; Posch et al., 2003; UBA, 2004). In addition to national efforts (Alveteg et al., 1998; Kurz et al., 1998; Sverdrup et al., 2005), dynamic modelling in support of the LRTAP Convention was carried out on a European scale (Posch and Reinds, 2005; Slootweg et al., 2007).

Although it is now well established that climate is changing and will continue to change in the future (IPCC, 2007) and recent studies have shown that observed climate change over the last decades accelerates and is consistent with the higher climate change projections (Rahmstorf et al., 2007), all above mentioned studies have assumed a constant climate. Climate change, however, may influence the effects of emission reductions on the soil chemical status (Posch, 2002). The impacts of climate change on terrestrial ecosystems and its relation with air pollution is an important issue, both on the scientific and the policy level (Leemans and Eickhout, 2004; Grennfelt et al., 2007). Since European forest ecosystems have many functions, related to biodiversity, forest products, ground water protection and carbon sequestration (Metzger et al., 2005), it is crucial to know to what extent the current legislation on air pollution control protects them against acidification and eutrophication under climate change.

Climate change could increase as well as decrease the levels of acidity and N in forest soils. For example, higher temperatures lead to higher base cation weathering rates that buffer acidity. On the other hand, increased drought stress leads to higher concentrations in soil solution and may lead to lower tree growth rates causing lower N removal from the soil. This increases acidification and eutrophication. To gain insight in the combined effects of climate change (temperature, precipitation and radiation) and deposition reductions of N and S, we applied the Very Simple Dynamic (VSD) model (Posch and Reinds, 2009) to a large number of forest receptors across Europe (excluding Belarus, Iceland, Moldova and Russia). We evaluated the resulting simulated soil solution chemistry relative to widely used critical limits (molar Al/Bc=1 and ANC=0 in soil solution). The relative importance of deposition reductions and climate change on modelled soil solution chemistry for the period 1990-2050 was assessed for combinations of two deposition and two climate scenarios (scenario analysis). Furthermore, the potential to recover within a specified time-period (target loads) and the time-delay in recovery from an acidified state (recovery times) were evaluated for these scenario combinations.

2. Modelling

2.1 The VSD model

The Very Simple Dynamic model (Posch and Reinds, 2009) was used to simulate the combined effects of acidification and climate change. This model has been widely used on a national and European level to simulate the acidification of soils in support of European air pollution control policies (Hettelingh et al., 2007). The VSD model simulates soil solution chemistry and soil nitrogen pools for (semi-) natural ecosystems. The model consists of a set of mass balance equations that describe the soil input-output relationships of ions, and a set of equations that describe the rate-limited and equilibrium soil processes. The soil solution chemistry in VSD depends solely on the net element input from the atmosphere (deposition minus net uptake minus net immobilisation) and the major geochemical interactions in the soil (bicarbonate equilibrium, base cation weathering, aluminium (Al) dissolution and cation exchange). Soil interactions are described by simple rate-limited processes (e.g. nutrient uptake and weathering), first order processes (denitrification) and by equilibrium reactions (e.g. bicarbonate equilibrium, cation exchange and Al-H equilibrium). VSD does not model the nutrient cycling explicitly (assumed to be a closed cycle) and nitrification is assumed to be complete (no ammonium leaching). VSD models the exchange of Al, protons (H) and the sum of Ca+Mg+K with the Gaines-Thomas or Gapon equations, with Gapon exchange used in this study. It is a single layer model that predicts the concentration of the soil water leaving this layer (mostly defined as the root zone) with the annual water flux taken equal to the annual precipitation excess. The simulation time-step is one year.
For this study, VSD was adapted to incorporate effects of climate change by making model inputs and chemical processes temperature-dependent. Temperature-dependence was modelled for the bicarbonate equilibrium, H-Al equilibrium, base cation weathering, nutrient uptake and precipitation surplus.

Bicabonate equilibrium
Bicarbonate is modelled according to

(1) $$[HCO_3]\cdot[H] = K_{HCO3}\cdot p_{CO2}$$

where the dissociation constant K_{HCO3} is now temperature dependent according to (Harned and Davis, 1943):

(2) $$\log_{10} K_{HCO3} = -\frac{1018}{T} - 0.0175T + 0.826$$

where T is the temperature (K). The partial pressure of CO_2 in the soil, p_{CO2} , is an input to the model implemented as a multiple of the CO_2 pressure in air (atm). Since climate change increases the CO_2 pressure in air, the effect on the soils CO_2 pressure is modelled by updating p_{CO2} at every time step.

H-Al equilibrium
The effect of temperature on the H-Al equilibrium constant was modelled with an Arrhenius equation according to (Mol-Dijkstra and Kros, 2001):

(3) $$K_{Alox}(T) = K_{Alox}(T_1) \cdot \exp\left(-\frac{95490}{R}\left(\frac{1}{T_1} - \frac{1}{T}\right)\right), \quad T_1 = 283\,\mathrm{K}$$

where R = 8.314 J.mol^{-1}.K^{-1} is the universal gas constant.

Base cation weathering
Analogous to the *H-Al* equilibrium, the effect of temperature on base cation weathering was modelled according to (UBA, 2004):

(4) $$BC_w(T) = BC_w(T_2) \cdot \exp\left(-3600\left(\frac{1}{T_2} - \frac{1}{T}\right)\right), \quad T_2 = 281\mathrm{K}$$

Forest growth and nutrient uptake
In VSD, net nutrient uptake is modelled as net growth multiplied by a (fixed) nutrient content. We assumed that nutrient contents are not influenced by climate change. Effects of climate change on forest growth, however, were considered to act through effects of increased temperature and possibly elevated CO_2 (Hyvönen et al., 2007), drought stress and respiration. To model the effect of climate change on forest growth, we followed most of the concepts of the C-Fix model (Veroustraete et al., 2002) that models Net Primary Production (NPP) as a function of temperature, CO_2, incoming radiation, radiation use efficiency, fraction of adsorbed radiation and respiratory losses. Current forest growth was derived from an updated EFISCEN data base, which contains growth data for a variety of species and age classes for about 250 regions in Europe (Schelhaas et al., 1999). The

growth data in this database represent the period 1970-1990; to include the effect of climate change, growth for a specific year was obtained by scaling the reference growth (from the data base) according to:

$$NPP = NPP_{ref} \cdot f_{temp} \cdot f_{CO_2} \cdot f_{resp} \cdot f_{drought} \cdot f_{Ndep} \quad (5)$$

where *NPP* is the Net Primary Production, for a given temperature, CO_2 concentration and N deposition, NPP_{ref} is the reference production (current growth), f_{temp} is the temperature function, f_{CO2} is the fertilizing effect of CO_2, f_{resp} is the respiration factor, $f_{drought}$ is a factor for the effect of drought stress, and f_{Ndep} represents the influence of N deposition. The temperature effect on growth was modelled according to:

$$f_{temp} = \frac{g(T)}{g(T_{ref})} \quad (6)$$

where T_{ref} is the reference temperature (K) and $g(T)$ is the temperature-dependence factor modelled and parameterized according to Veroustraete et al. (2002) who used a bell-shaped function based on Wang (1996):

$$g(T) = \frac{\exp\left(C_1 - \frac{\Delta H_a}{RT}\right)}{1 + \exp\left(\frac{\Delta ST - \Delta H_d}{RT}\right)} \quad (7)$$

with ΔH_a as the activation energy (52750 $J.mol^{-1}$), ΔH_d is the deactivation energy (211000 $J.mol^{-1}$), ΔS is the entropy of the denaturation equilibrium of CO_2 (704.98 $J.K^{-1}.mol^{-1}$) and C_1=21.77; values given are those used in the C-Fix model. A temperature increase at low current temperatures increases growth by about 10-50%, but at temperatures above 15°C a further temperature rise will hardly increase growth (Figure 1). If current temperatures of more than 20°C increase by 4-6 degrees, growth will decrease by about 5-10%.

In the C-fix model, NPP is a function of the CO_2 concentration. An increase in CO_2 concentration will enhance NPP, although an accompanying increase in temperature reduces the CO_2 effect. It is, however, disputed whether increased atmospheric CO_2 concentration will enhance NPP: some authors claim substantial effects (Hyvönen et al., 2007), while others strongly doubt whether there is any effect at all, especially on mature trees (Tognetti et al., 2000; Körner et al., 2005; Körner, 2006).

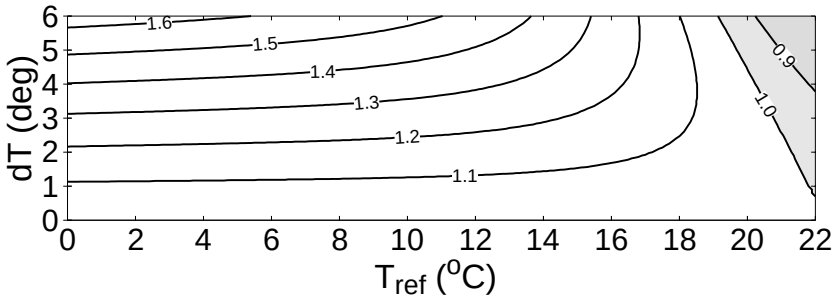

Figure 1. Isolines of f_{temp} as a function of current temperature and a temperature increase dT. White areas indicated parameter combinations leading to increased growth.

We therefore decided not to include a CO_2 fertilization effect on forest production (i.e. $fCO_2 = 1$ in eq. 5) in this study.

The respiration factor, f_{resp}, was modelled according to the ratio of autotrophic respiration (Ar) for current and reference temperatures (in °C) according to:

$$f_{\text{resp}} = \frac{1 - Ar(T)}{1 - Ar(T_{ref})} \quad \text{with} \quad Ar(T) = (7.825 - 1.145T)/100 \tag{8}$$

The autotrophic respiration is modelled as a linear function of T according to Veroustraete et al. (2002). Increased temperature thus leads to higher respiration indicated by lower values for f_{resp}.

Precipitation surplus was computed as precipitation minus actual evapotranspiration. The latter was simulated using a sub-model of the IMAGE global change model (Leemans and Van den Born, 1994) following the approach by Prentice et al. (1993). This model was also used in the computation of critical loads for Europe and Northern Asia (Reinds et al., 2008a); details can be found in Reinds et al. (2001). Model inputs include historical and future time-series of monthly values of temperature, precipitation and cloudiness.

The effect of drought stress on growth was incorporated by assuming a linear relation with the ratio of current and reference (mean of 1961-1990) evapotranspiration such that a decrease in evapotranspiration decreases growth:

$$f_{drought} = \frac{AET}{AET_{ref}} \tag{9}$$

Nitrogen availability, and thus N deposition, influence forest production (Tamm et al., 1995; Spiecker et al., 1996; Kahle et al., 2007; Solberg et al., 2009). In this study, we have modelled the effect of N deposition according to:

$$f_{Ndep} = 1 + (N_{dep,act} - N_{dep,ref}) \cdot 0.01 \quad (10)$$

Equation 10 is based on Solberg et al. (2009) who, through a statistical analysis of growth data from 363 Intensive Forest Monitoring plots, concluded that 1 kg of extra N deposition leads on average to about 1% of growth increase, with only minor variation between tree species. The effect of N was modelled in this study using the difference in N deposition in a simulation year and 1980, which represented most of the growth data from the EFISCEN database. Decreasing N deposition in our model will lead to decreased growth, as we did not include a hysteresis effect. For systems that have received large amounts of N in the past and thus have a large N pool, this is a simplification, as on the short or even medium term mineralisation of organic matter may still supply enough N to maintain an elevated growth rate.

In VSD a closed nutrient cycle is assumed. Changes in climate may also effect the nutrient cycling in forests through changes in litterfall and/or litter composition (Körner, 2006; Hyvönen et al., 2007); these effects have not been modelled in this study. Wright et al. (2006) simulated a 50% increase in DOC between 2000 and 2030 due to increased temperature. To test the sensitivity of our results to possible changes in soil DOC, one simulation for Europe was made assuming an increase in DOC of 50% between 1990 and 2050.

Target loads

In addition to the evaluation of various deposition and climate scenarios on future soil solution chemistry, which requires simple forward running of VSD, target loads were computed. A target load is the deposition which ensures that a prescribed value of a chemical variable (e.g., the Al concentration in soil solution) is attained in a given (future) year (Posch et al., 2003). A target load is defined here as a deposition path characterised by three years: (i) the branching year, (ii) the implementation year, and (iii) the target year. The branching year is the year up to which the deposition path is assumed to be known and cannot be changed. The implementation year is the year in which all reduction measures needed to reach the final deposition (the target load) are implemented. Between the branching year and the implementation year, depositions are assumed to change linearly. Finally, the target year is the year in which the chemical criterion is met for the first time. In general, the earlier the target year, the lower the target load will be since more

deposition reductions are needed to achieve the desired status in a shorter time period. In extreme cases a target load might not exist at all, since even reduction to zero deposition will not result in the desired soil status within the prescribed time.

When computing target loads, three possible outcomes exist (Posch et al., 2003):
- the target load is higher than the critical load. This indicates that current deposition or reducing deposition to critical load ensures the criterion is met in the target year *and maintained thereafter* (Case 1).
- there exists a target load lower than the critical load, i.e. a deposition below the critical load is required for attaining the prescribed criterion in a specific year (Case 2)
- no target load exists, i.e. even at zero deposition the soil cannot recover by the target year (Case 3).

Systematic trial and error (i.e. repeated iterative runs of VSD) is needed for computing target loads. When computing a target load, pairs of N and S deposition have to be determined which result in the desired soil status in the target year. All such pairs define the so-called target load function (TLF) in the (N_{dep},S_{dep}) plane. If the target year approaches infinity, the model reaches a steady state and the resulting target load function becomes the critical load function (CLF). Critical loads are widely used indicators of ecosystem sensitivity, defining the maximum allowable S and N deposition not causing harmful effects in the long-run (Nilsson and Grennfelt, 1988; Hettelingh et al., 2007). Due to finite buffer processes, such as time-dependent N immobilisation, the TLF can intersect the CLF; one obtains target loads that exceed the critical load. In this case, the minimum of both functions is taken to ensure that the chemical criterion is never violated after the target year.

Recovery delay
It is often assumed that reducing deposition to (or below) critical loads immediately removes the risk of 'harmful effects', i.e. the chemical criterion (e.g. the Al/Bc-ratio) immediately attains a non-critical (or 'safe') value. However, the reaction of soils, especially their solid phase, to changes in deposition is delayed by (finite) buffers, the most important being the cation exchange capacity, and it may take decades or even centuries, before steady state is reached. It is therefore of interest to compute the future year in which the criterion is met for the first time after a deposition reduction below critical load, since this is more relevant for recovery then attaining critical load *per se*.

3 Data

3.1 Geographical input data

Input data for the VSD simulations consist of spatial information describing climatic variables, deposition of base cations, S and N, weathering of base cations, nutrient uptake, N transformations and soil properties such as carbon pool and cation exchange capacity. These data were derived combining maps and databases of soils, land cover and forest growth regions. A map with computational units (receptors) was created by overlaying maps on land cover, soils and forest growth (Reinds et al., 2008a). The resulting map with forest/soil combinations for Europe contains about 1 million receptors, 414,000 of which cover at least 1 km^2 and these were used in this study. Reinds et al. (2008a) showed that the effect on leaving out the very small units (< 1 km^2) had little effect on the distribution of critical loads.
Time series of temperature, precipitation and cloudiness were obtained from a high resolution European data base (Mitchell et al., 2004) containing monthly values for the years 1901-2100 for land-based grid-cells of 10'×10' (approx. 15×18 km in central Europe). Projections for 2001-2100 stem from the HADCM3 GCM model. Two sets of climate change scenarios based on the IPCC SRES A1 and B2 scenarios (Nakícenovíc et al., 2001), were used. The A1 scenario is based on a future world with globalization and rapid economic growth, low population growth, and the rapid introduction of new and more efficient technologies everywhere. The B2 scenario mimics a world in which the emphasis is on local solutions to economic, social, and environmental sustainability (Strengers et al., 2005). A reference climate set was created by computing the mean monthly temperature, precipitation and cloudiness of the period 1961-1990. Future scenarios for the same climatic variables were obtained for the three reference years 2005, 2030 and 2050 by averaging values for the periods 1991-2020, 2021-2040 and 2041-2060, respectively. Values between these periods were obtained by linear interpolation. This procedure provides a smoothed trend, which allows for better comparisons with the reference period 1960-1990, but ignores strong inter-annual variability in future climate. Future CO_2 air concentrations consistent with the above mentioned scenarios were obtained from Carter (2007).
Climate change under the A1 scenario is much more pronounced than under the B2 scenario (Figure 2).

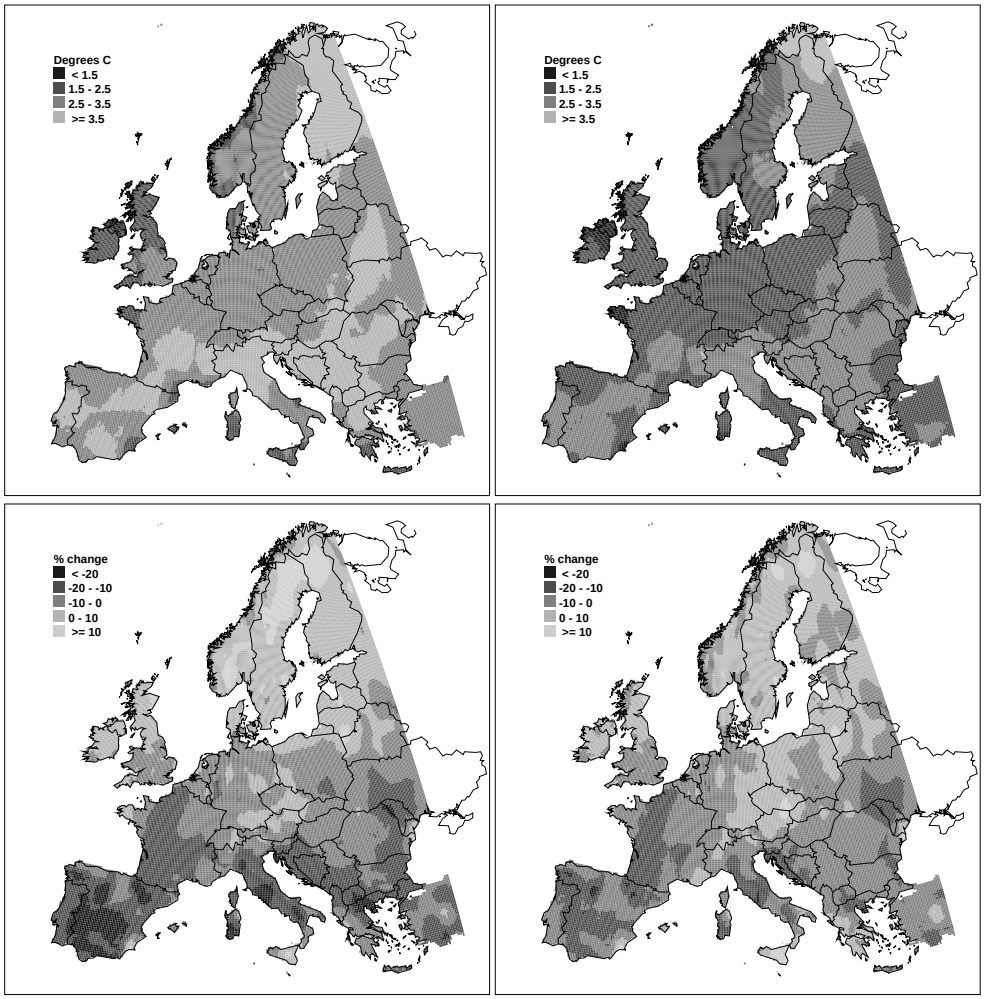

Figure 2. Absolute change in mean annual temperature (K) for IPCC SRES scenarios A1 (top left) and B2 (top right) and relative change in precipitation (in percent) for scenarios A1 (lower left) and B2 (lower right) between 1950 (2041-2060) and the reference period (1961-1990)

For the period 2041-2060, the increase in temperature under the A1 scenario is about 1.5-2.0 times that of the B2 scenario and is highest for Spain, the eastern part of Europe and northern Finland. Also the relative change in precipitation is higher under the A1 scenario, especially in the southern- and northernmost parts of Europe.

Base cation deposition for Europe was taken from simulations with an atmospheric dispersion model for base cations (Van Loon et al., 2005). Historic N and S

deposition data were taken from Schöpp et al. (2003). Scenarios of N and S deposition were obtained from the Eulerian atmospheric transport model of EMEP/MSC-W (Tarrasón et al., 2007). For 2020 two emission scenarios were used reflecting current legislation (CLE) and maximum (technically) feasible reductions (MFR), developed for the Thematic Strategy on Air Pollution of the EU (Amann et al., 2007). From 2020 onwards, deposition was assumed constant. Median S deposition in 2020 over Europe for the MFR scenario is 111 eq ha^{-1} yr^{-1} (compared to 268 eq ha^{-1} yr^{-1} for CLE) and 562 eq ha^{-1} yr^{-1} for N (684 eq ha^{-1} yr^{-1} for CLE).

3.2 Model parameterisation

Values for weathering rates, cation exchange constants, the H-Al equilibrium constant, N-immobilisation fractions and denitrification fractions were obtained from a calibration of VSD on 180 intensively monitored sites in Europe (Reinds et al., 2008b). The median values of the plot-wise calibrated parameters were used. Results for cation exchange constants and the H-Al equilibrium constant were categorized by soil texture (Table 1).

Table 1. Median values of $log_{10}KAl_{ox}$, $log_{10}KHBc$ and $log_{10}KAlBc$ for soils with texture classes sand, clay and heavy clay based on a calibration of VSD on 180 intensively monitored forest plots (Reinds et al., 2008b).

	$log_{10}KAl_{ox}$	$log_{10}KHBc$	$log_{10}KAlBc$
Sand	8.87	3.39	0.528
Clay	8.58	3.79	–0.65
Heavy clay	8.41	3.54	–0.67

Weathering rates of the root zone were calibrated for six weathering rate classes (Table 2). These classes were derived from soil texture and parent material (UBA, 2004).

Table 2. Median values of base cation weathering for 6 weathering rate classes based on a calibration of VSD on 180 intensive monitored forest plots. Each weathering rate class is a combination of soil texture (5 classes) and parent material type (acid, intermediate, basic).

Weathering rate class	1	2	3	4	5	6
BCwe (eq $ha^{-1}m^{-1}$ yr^{-1})	730	1050[1]	1360	3100[2]	3100	1100

[1] *No plots with weathering rate class 2 were in the set of calibration plot; the value is the average of classes 1 and 3.*

[2] *Values for weathering rate class 4 were set equal to those obtained for class 5.*

It should be noted that the calibrated weathering rate of class 1 (sandy soils on acidic materials) is substantially higher than the default value given in UBA (2004). Probably, the value in UBA (2004) is valid for very acid pure sandy soils, whereas most plots with texture class 1 in the set of calibration plots had a richer parent material. The median calibrated value is based on more than sixty plots in Europe; as such, we have used this value in the current study.
In VSD, N immobilisation is modelled as a function of the actual C/N ratio plus a constant immobilisation (Posch and Reinds, 2009). Because a meaningful simultaneous calibration of both processes was not feasible, we modelled N immobilization according to Reinds et al. (2008b):

$$N_{im} = a \cdot \left(N_{dep} - N_{upt} \right) \quad (11)$$

Where N_{im} is the nitrogen immobilized and N_{upt} is the net growth uptake and a is an empirical constant. Parameter a was calibrated as a function of the measured C/N ratio in the top soil. Calibration showed that most of the incoming N is immobilized: median calibrated values for a were 0.83 for high C/N ratios (> 30), 0.76 for intermediate C/N ratios (20-30) and 0.71 for low C/N ratios (< 20). These fractions are the current immobilisation fractions. Some studies have shown that soils may become nitrogen saturated and subsequently N immobilisation will diminish (Aber et al., 1989; Aber et al., 2003). In this study we may thus overestimate future N immobilisation in high N deposition areas. On the other hand, some climate change studies have shown that elevated CO_2 leads to litter with higher C/N ratios (see e.g. Hyvönen et al., 2007) which could increase the capacity to immobilize N. Reinds et al. (2008b) also calibrated the denitrification fraction; a median value of 0.2 was found for well drained soils and a value of 0.4 for soils with gleyic features. Very poorly drained soils (peat soils) were not present in the set of calibration plots; for these soils a denitrification fraction of 0.8 was used following UBA (2004). Data per soil type for bulk density, CEC, DOC and organic carbon were obtained from soil transfer functions as described in Reinds et al. (2001).
The VSD model was initialized using the calibrated model parameters. The model was run from 1990 to 2050 to assess the effects of changes in deposition and climate on soil solution chemistry in Europe for two deposition scenarios (CLE and MFR) and three climate scenarios (A1, B2 and a run in which the reference data from 1961-1990 (His) were also used for the period 1990-2050).

4 Results and discussion

4.1 Climate change effects on soil chemistry

To gain insight on the importance of climate change on soil solution chemistry, simulations with VSD were carried out for a single site, varying one-by-one the relevant model parameters (see equations 2-4) influenced by climate variables (Figure 3).

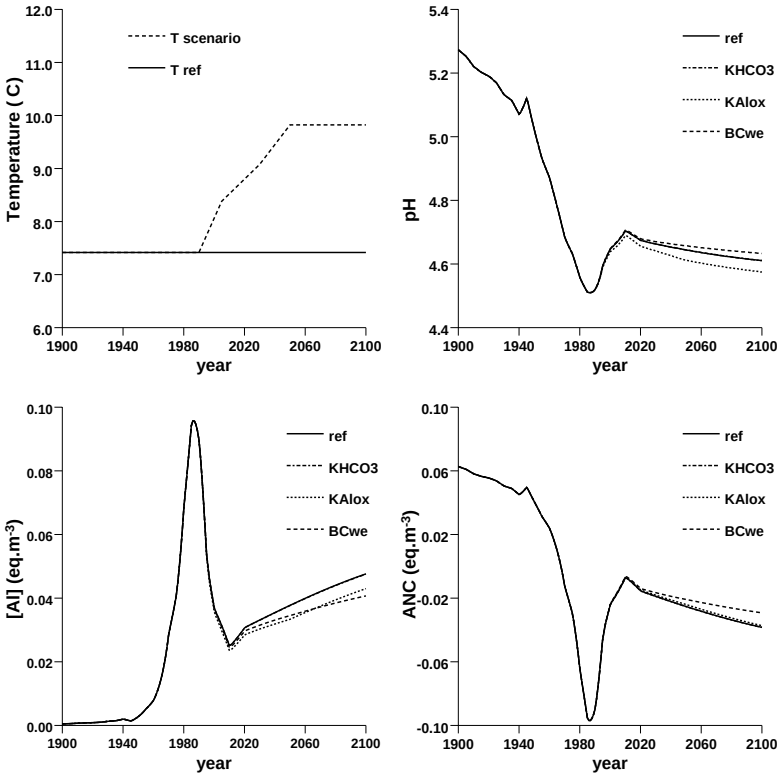

Figure 3. Influence of temperature change (upper left figure) from the A1 scenario on soil solution chemistry for a selected plot using the CLE deposition.effects are shown for pH (upper right), [Al] (lower left) and ANC (lower right).

Effects of temperature change are limited; and effects of climate on the bicarbonate constant K_{HCO3} show no effect due to the low pH at the site. Largest effects are due to the increase in weathering, accelerating recovery. ANC is not influenced by changes in the equilibrium constant for gibbsite.

4.2 Climate change effects on growth and uptake

To obtain insight in the effects of future climate on forest production, the combined effect of temperature, respiration and drought was computed for 2050 for both future climate scenarios using the CLE scenario for N deposition. Under the A1 scenario, growth decreases for about 5% of the forested area compared to the reference period (especially in southern Europe), mainly caused by increased drought stress (Figure 4 left).

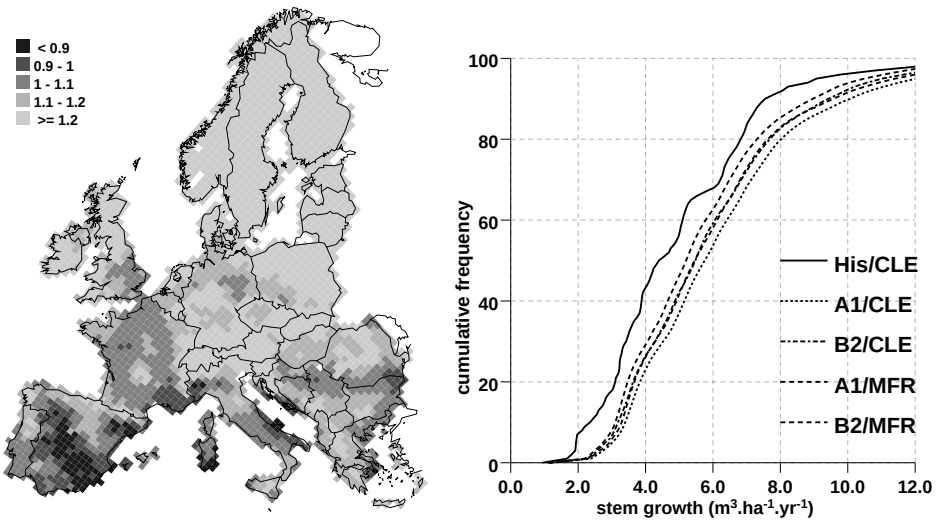

Figure 4. Growth under the A1 scenario in 2050 divided by the reference growth 1961-1990 (left) and cumulative frequency of modelled stem growth for two deposition (CLE, MFR) and three climate scenarios (His, A1,B2).

In central and western Europe growth is expected to increase by 10-20% and in Fennoscandia by more than 20%. The difference between the A1 and B2 scenario is small (Figure 4, right). The higher temperatures
in the A1 scenario lead to an on average 6% higher growth than the B2 scenario. The decrease in N deposition under MFR somewhat reduces growth compared to CLE: the mean difference over all plots is limited to 10%.
The higher growth in the A1 scenario mostly leads to a somewhat higher uptake of nutrients (Figure 5), and may thus cause lower nitrate concentrations in the soil, both for the CLE and the MFR deposition scenarios.
The actual nitrate concentration, however, also depends on precipitation surplus, which is affected by climate change. Since decreasing N deposition may lead to N shortage in the ecosystem, the N uptake in the MFR scenario is somewhat lower than for the CLE scenario (Figure 5).

4.3 Scenario analyses: impact on soil solution chemistry

Future soil chemistry strongly depends on the scenario used (Table 3). For both Al/Bc and ANC, the area where critical limits are exceeded is smaller under the MFR scenario. Under CLE, the area where ANC < 0 will decrease until the year 2020 but remains almost constant at about 5% of the European forested area afterwards.

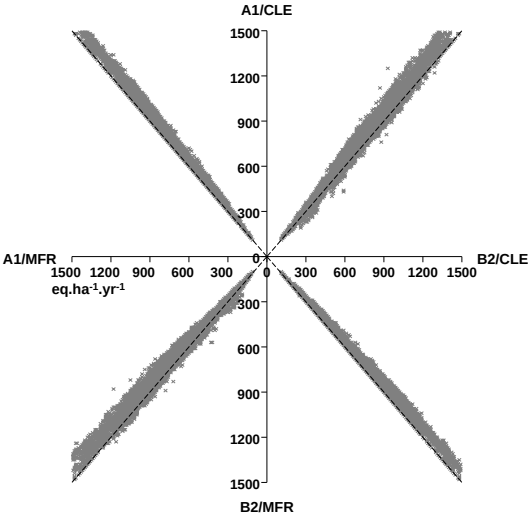

Figure 5. Net nitrogen uptake (eq ha^{-1} yr^{-1}) for the combined climate (A1 and B2) and deposition (CLE and MFR) scenarios. Each quadrant shows the relationship between two combined scenarios, and is an individual x-y graph.

The area with Al/BC > 1 will continue to decrease in time and will be < 1% in 2050 under the MFR scenario. Differences in future climate had little effect on the simulated trends in soil acidity. Only the trend in the area with Al/Bc > 1 is somewhat affected by climate: under the A1 scenario this area becomes smaller than when using the B2 scenario because of higher weathering rates (as a result of higher temperatures, see eq. 4) and thus higher Bc concentrations. The mitigating effect on soil acidity of higher N uptake is largely compensated by the higher uptake of base cations. Both climate scenarios lead to lower exceedances compared to current climate (His), most likely because weathering increases due to higher temperatures. The ANC criterion is more stringent then the Al/Bc criterion (Table 3). This is consistent with a study on critical loads in Eurasia that also showed the ANC=0 criterion to be more stringent (Reinds et al., 2008a). The vast majority of the soils have a (highly) negative ANC for Al/Bc=1; conversely for ANC=0 most sites have an Al/Bc ratio considerably smaller than one (Figure 6).

Table 3. The forested area (in %) where Al/Bc > 1 mol mol^{-1}, ANC < 0 and [NO_3] > 0.3 and 3 mg N L^{-1} for two emission scenarios (CLE and MFR) and two climate scenarios (A1, B2) as well as reference climate 1961-1990 (His) for different years.

Al/Bc	His,CLE	A1,CLE	B2,CLE	A1,MFR	B2,MFR
1990	4.17	4.17	4.17	4.17	4.17
2010	3.34	3.26	3.27	3.26	3.27
2030	2.60	2.37	2.40	1.25	1.27
2050	1.95	1.64	1.71	0.68	0.76
ANC					
1990	6.76	6.76	6.76	6.76	6.76
2010	5.31	5.25	5.25	5.25	5.25
2030	5.14	5.07	5.05	4.01	4.00
2050	5.14	4.97	4.97	3.53	3.56
NO_3 (0.3 mg N L^{-1})					
1990	54.85	54.85	54.85	54.85	54.85
2010	43.69	40.00	39.73	40.00	39.73
2030	40.32	35.08	34.60	15.20	14.65
2050	40.86	33.31	33.06	12.39	12.20
NO_3 (3 mg N L^{-1})					
1990	11.42	11.42	11.42	11.42	11.42
2010	2.29	1.86	1.80	1.86	1.80
2030	0.89	0.46	0.44	0.00	0.00
2050	1.01	0.22	0.21	0.00	0.00

For nitrogen concentrations in soil solution, the critical limit for vegetation varies within Europe. According to De Vries et al. (2007a), values vary between 0.3 mg N L^{-1} for regions with sensitive vegetations (Scandinavia) to about 3 mg N L^{-1} for western Europe; we have applied both these limits to the whole of Europe to assess the range of potential N effects.

Results show that the area where N limits are exceeded diminishes in the future under climate change through enhanced uptake of N and as a result of lower N deposition, especially under the MFR scenario.

The exceeded area strongly depends on the criterion chosen: the higher criterion leads to non-exceedance in 2030 under all scenarios, but when the strict N criterion is used, the area exceeded is still about 12% even under the most favourable scenarios (Table 3). If we combine both criteria and use a limit of 0.3 mg l^{-1} for Norway, Sweden and Finland as well as for the Alpine countries (Austria and Switzerland) because alpine vegetations are also sensitive for nitrogen (Bobbink et al., 2002) and 3 mg l^{-1} elsewhere, the forested area with exceedances decreases from about 16% in 1990 to 1% under CLE and to non-exceedance under MFR.The effect

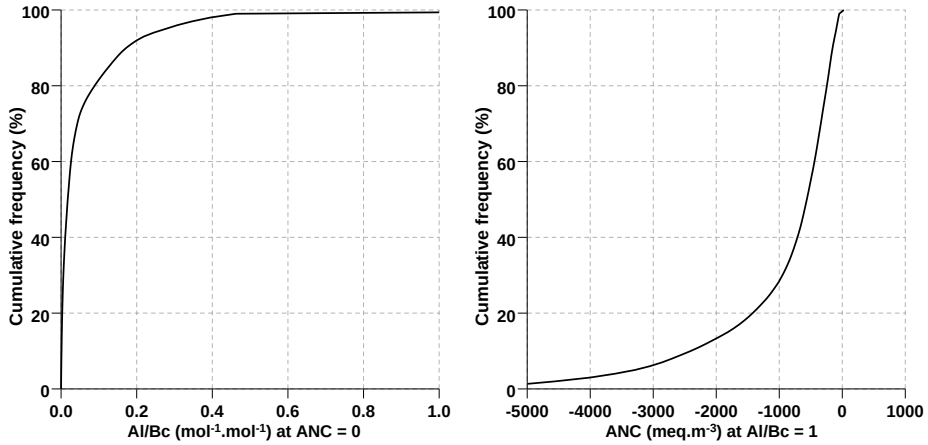

Figure 6. Cumulative frequency distribution of Al/Bc (mol mol^{-1}) equivalent to ANC=0 (left), and ANC (meq m^{-3}) equivalent to Al/Bc=1 (right) for all simulated receptors.

of the climate scenarios on nitrate concentrations and pH is limited, future deposition reductions are more important.

The MFR scenario is much more effective in reducing nitrate concentrations than the CLE scenario, as could be expected from the stronger reductions in NO_x and NH_3 deposition (Figure 7). Under MFR concentrations of N exceeding 3 mg N L^{-1} do not occur in 2050 whereas they persist under CLE.

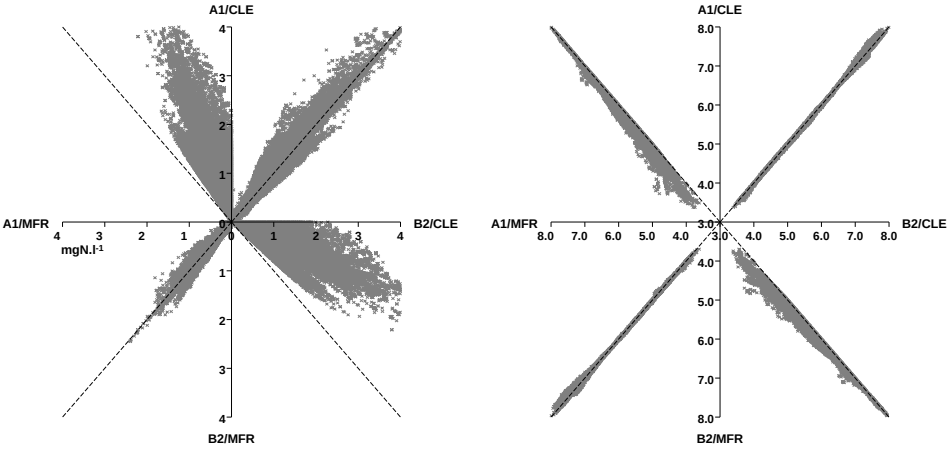

Figure 7. Simulated nitrate concentration (mg N L^{-1}left) and pH (right) for the climate (A1 and B2) and deposition (CLE and MFR) scenarios in 2050.

In the evaluation of the scenarios, we have assumed no influence of climate change on DOC concentrations. To test the implications of this assumption, we evaluated the B2/CLE scenario assuming an increase in DOC of 50% between 1990 and 2050. This has little effect on computed exceedances for Al/Bc: exceedances changed by less than 0.1% of the forested areas. For ANC the difference was limited to at most 0.15% in 2050.

4.4 Target loads

Target loads were computed for both the Al/Bc=1 and the ANC=0 criterion, using the target years of 2030 and 2050. Under both climate scenarios, most (89-96%) of the European forested area is protected by maintaining current deposition or reducing it to critical loads (Table 4).

Table 4. Percentage of forest area for the three target load cases for two criteria (Al/Bc=1, ANC=0) and two target years (2030, 2050).

Cases	Al/Bc=1		ANC=0	
	2030	2050	2030	2050
1: TL=CL	96.00	96.73	88.65	88.72
2: TL < CL	3.95	3.27	11.35	11.28
3: TL infeasible	0.05	0	0	0

For the remaining area, target loads exist almost everywhere; only for Al/Bc=1 in 0.05% of the area (about 54,000 ha) even zero deposition is not sufficient to attain the criterion in 2030.

The ANC=0 critical criterion is stricter than Al/Bc=1; for more than 11% of the forested area a target load smaller than the critical load is required as opposed to 3-4% for Al/Bc=1. Target loads (Case 2) can be found in strongly acidified areas such as Poland, the Czech Republic and the Netherlands (Figure 8).

Using ANC=0, this area also includes large parts of Germany, Eastern UK and Central Europe. In the rest of Europe, a reduction in deposition to the critical load is sufficient to attain the desired soil chemical state in (or before) the target year.

Target loads may exist, but they are only policy-relevant if it is feasible to reduce the deposition to or below it, and comparing the target loads with the deposition under the MFR scenario provides this insight. For 30% of the receptors with true target loads (Case 2), the target load for S is lower than the corresponding MFR deposition and can thus not be attained with current abatement technologies.

For nitrogen this occurs for less than 5% of the receptors because target loads for N, TL(N), always contain the removal of N from the system (N immobilisation and N uptake).

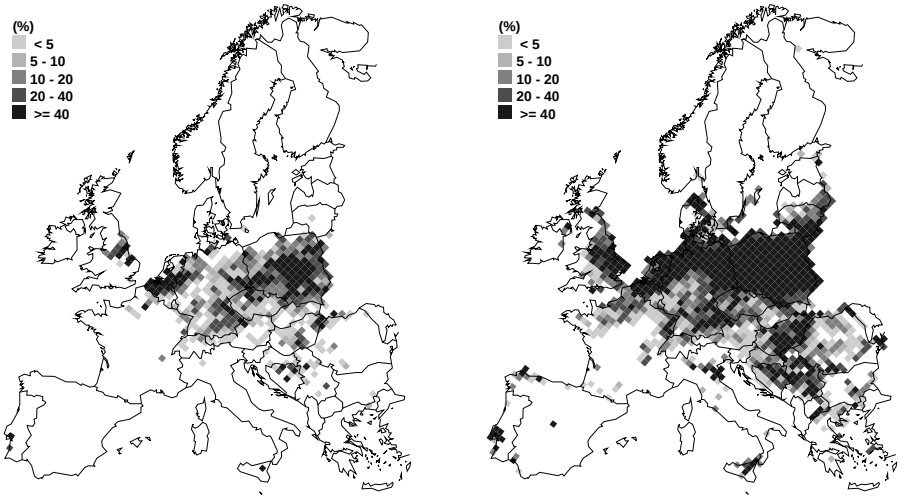

Figure 8. Percentage of forested area per EMEP grid cell with target loads < critical load (Case 2) for 2050 for Al/Bc=1 (left) and ANC=0 (right).

Target loads are sensitive to the criterion used but not very sensitive to differences in future climate (Figure 9).

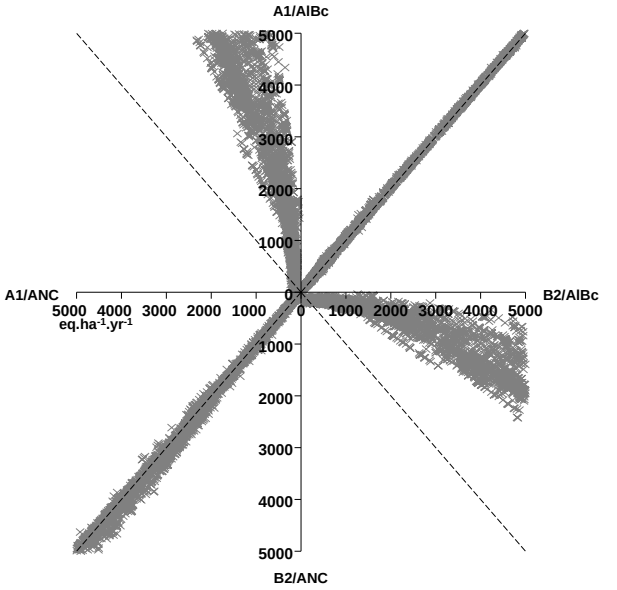

Figure 9. Target loads of S in 2050 (eq ha^{-1} yr^{-1}) for the combined climate scenarios (A1 and B2) and two criteria (ANC=0 and Al/Bc=1).

Target loads for ANC=0 are much lower than for Al/Bc=1, which is consistent with the results from the scenario analysis (Figure 6). There is little difference in TL(S) between the A1 and B2 climate scenario. Comparing TL(S) (Case 1) for Al/Bc=1 reveals that for 97 % of the receptors TL(S) for the A1 scenario is higher than that for the B2 scenario due to higher weathering rates. The differences in TL(S) are however small: on average the values for the A1 scenario exceed those of the B2 scenario by only about 30 eq ha^{-1} yr^{-1} (see first quadrant in Figure 9). For ANC=0, TL(S) for the A1 scenario are nearly equal to those for the B2 scenario (on average 15 eq ha^{-1} yr^{-1} difference; third quadrant in Figure 9). The 2050 TL(N) is higher for the A1 than for the B2 scenario due to higher uptake of N under the A1 scenario (not shown); for Al/Bc=1 the median difference is about 50 eq ha^{-1} yr^{-1} for ANC=0 about 25 eq ha^{-1} yr^{-1}.

4.5 Recovery delay

Recovery times (RT) were computed for the CLE and MFR scenario, setting the year after which deposition is held constant to 2020. Using Al/Bc=1, more than 95% of European forests are safe (i.e. the criterion is not violated) by 2030 even under CLE (see Table 4). In central Europe, a substantial percentage of forests have an Al/Bc > 1 in 2020 and a RT exists. In some areas, particularly in the Netherlands, Poland, the north of the Czech Republic and south-eastern Germany, no recovery occurs under CLE because the critical load is still exceeded; in these areas no RT exists. Recovery under MFR is much more rapid than under CLE (Figure 10). While under CLE it often takes 40-50 years for ecosystems to recover, most systems recover within 20 years under the MFR scenario.

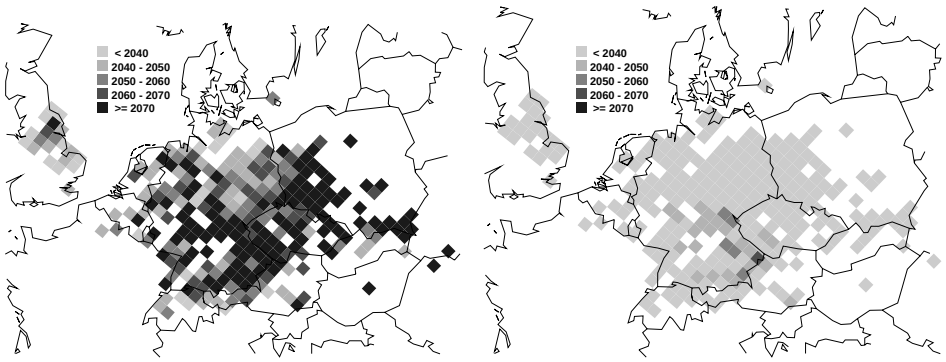

Figure 10. Average Recovery Times in central Europe for Al/Bc=1 per EMEP grid cell for the CLE scenario (left) and the MFR scenario (right) for those receptors for which a recovery time exists.

5 Conclusions

Recovery of most acidified forest soils in Europe can be achieved for both soil chemical criteria when depositions are reduced using current available technologies. Under this MFR scenario, the forest area exceeding the Al/Bc=1 criterion declined in our simulations from 4% in 1990 to about 0.7% in 2050. The area where ANC < 0 decreased from 7% to 3.5% in 2050. Under current-legislation deposition, we simulated a limited decrease in the area violating the ANC=0 criterion, but the area with Al/Bc > 1 reduces to 1.6% in 2050. Climate change reduces the area where chemical indicators were exceeded because of higher weathering rates owing to higher temperatures and because of higher uptake of nitrogen. However, differences between the A1 and B2 scenario were small. Areas where critical nitrogen concentrations are exceeded can be reduced by implementing MFR. Changes in future climate further reduce this area, due to higher N uptake through enhanced growth. In principal, recovery of most acidified soils in Europe is possible by 2050. Moreover, for the most acidified areas in central Europe, target loads can be found that return the soils to the desired chemical state by 2050. For about 30% of the receptors where TL<CL, however, the target load is lower than the deposition at MFR, indicating that no recovery in 2050 can be achieved with current emission reduction techniques. The speed of recovery under MFR is much more rapid than under CLE where recovery delay for Al/Bc takes 20 to >50 years, whereas under MFR recovery is mostly achieved within 20 years. Results are consistent with a study in Sweden where a detailed multi-layer model was applied at about 600 forest sites (Sverdrup et al., 2005); the study concluded that the Gothenburg Protocol (CLE scenario) would lead to significant improvement in the acidification of forest soils in Sweden. Similarly, measurements and simulations at a highly acidified forest site in the Czech Republic showed that a fast recovery of pH and Al/Bc in the topsoil can be achieved with current emission reductions (Navrátil et al., 2007).

We modified VSD such that formerly fixed processes became climate-dependent, however, the model was not explicitly developed to include (all) climate-sensitive processes and therefore final conclusions on the impact of climate change on soil acidification cannot be drawn from this study. For example, since the model assumes a closed nutrient cycling, we could not include effects of climate change on litter composition and organic matter mineralisation nor on future N immobilisation. To account for such effects, VSD is currently extended to simulate also dynamics in carbon and nitrogen pools as a function of these processes. Furthermore, possible interactions which may become important under climate

change such as the interaction between climate change and DOC (Freeman et al., 2001; Freeman et al., 2004) were not included.
All model results indicated that emission reductions are more important for the recovery of forest ecosystems than potential effects of climate change; moreover, climate change has only limited effects on soil chemistry. There was a small but positive synergistic effect of climate change, which is consistent with earlier studies (Wright and Jenkins, 2001). Changes in climate will also affect tree species distribution over Europe (Leemans and Eickhout, 2004); this effect was not taken into account. Such land cover changes may influence the recovery of soils, if the change is to species with very different growth rates than current species. Earlier studies found a strong synergy in simultaneously mitigating air pollution and climate change. This is because many of the traditional air pollutants and greenhouse gases have common sources, offering a cost-effective potential for concurrent improvements for both problems (Syri et al., 2001; Swart et al., 2004; Van Vuuren et al., 2006). This synergy does not carry on towards impacts.
This study demonstrated that climate change only negligibly changes the impacts of acidification and N deposition. This is because the impacts of climate change act mainly on the ecological, phenological and physiological processes in forests and other ecosystems (Metzger et al., 2008), while acidification and N deposition strongly alter the chemistry. Although this study applied a model with only a simple parameterization of the climatic factors, we think that it indicated the appropriate directions and magnitude of the interactive effects.
The model simulations in this study showed that most of the European forest soils could recover from their acidified state within a few decades under the current emission reduction plans, even under climate change. This reduces the risks of harmful effects in forest ecosystems caused by acidified conditions, and supports their functions related to biodiversity, forest production, ground water protection and carbon sequestration.

Acknowledgements

The preparation of this paper has been partially supported by the European Commission LIFE III programme within the framework of the European Consortium for Modelling Air Pollution and Climate Strategies (EC4MACS) and the trust fund for the partial funding of effect-oriented activities under the Convention on Long-range Transboundary Air Pollution.

Discussion and conclusions

Objectives

The main objective of this thesis was to assess critical loads and target loads of nitrogen and sulphur for European forest soils, using a newly developed simple soil acidification model. We used a large forest monitoring data set to calibrate the model and to quantify and reduce uncertainties. Next the impact of the use of different chemical criteria on critical loads was investigated as well as the likely impact of climate change on recovery from acidification in Europe, relative to the effects of reduced sulphur and nitrogen inputs.

The VSD model: a simple acidification model for European scale assessments

To evaluate the effects of the reductions in the emissions of sulphur and nitrogen on European forest soils, a simple dynamic soil model (VSD) was developed, calibrated and applied on a plot scale and on the European scale. The VSD model was developed as an extension of the steady-state Simple Mass Balance (SMB) model that has been widely used to compute critical loads for Europe for sulphur (S) and nitrogen (N), i.e. depositions that do not cause harmful effects on ecosystems in the long-term. The VSD model has proven to perform as well as a more complex model. In a detailed study for 176 sites in Switzerland it was shown that VSD, when fed with weathering rates calculated with the PROFILE model (a sub-module of the SAFE model), yields results that are very similar to those obtained with the one-layer version of the more complex model SAFE. An advantage of VSD over other models is its compatibility with the widely used critical load model SMB; in steady-state mode VSD reduces to SMB. The VSD model is thus very suited to dynamically evaluate deposition reduction scenarios based on critical loads: if the deposition is reduced to critical load, the soil solution concentrations simulated by VSD will in the long-run equal those on which the critical load was based. Although the model is simple, it has extended functionality: it can compute the time to reach the desired soil chemical status if deposition is reduced to or below critical load, or the time before a criterion is violated if deposition remains above critical load: recovery and damage delay times. Furthermore it can be used to compute target loads.

The graphical user interface of VSD (VSD-Studio) has proven to be of added value. The behaviour of single plots in the European application of VSD can easily be examined in detail using VSD-Studio by extracting the input data for the model from the European data bases. This can help understanding the behaviour of ecosystems or be used for illustration. This is especially true for the rather complex target load assessments.

VSD and its graphical interface provide relevant information for policy makers. For example, in some parts of Europe the proposed emission reductions are

insufficient to attain critical loads in the near future. For such areas model assessments can show what the consequences are in terms of prolonged elevated risks for forest health. For areas that have been severely acidified, VSD can compute the deposition reduction needed to attain recovery within a specified time-period.

Calibration of a simple acidification model and quantification of the parameter uncertainty

An innovative application of the Bayesian calibration method of VSD improved its parameterization. The calibration of the model on 122 forest monitoring sites from various European countries showed that initial estimates of, for example, weathering rates for sandy soils (based on literature data) were too low. When the calibrated model was applied on 60 additional sites, simulated pH and nitrate concentrations were much more accurate (when compared with measurements) than before calibration, due to the improved model parameter estimates. For aluminium concentrations and base saturation, no gain in accuracy was achieved. Bayesian calibration is a well-suited method for VSD. For complex models, the method has the disadvantage that it relies on a large number of simulations (10^3 – 10^4) leading to time-consuming calibrations, but due to the simplicity and efficiency of VSD, a Bayesian calibration using 30,000 simulations only takes 2-3 minutes of CPU time on a standard PC. Bayesian calibration has proven to be of added value compared to the simple methods used to calibrate acidification model in the past, as it does not only provide calibrated parameters but also their uncertainty. This information can be used for subsequent uncertainty analysis.

Apart from a calibration at individual sites, a multi-site calibration was also carried out in which all 122 plots were calibrated simultaneously, yielding one joint posterior distribution for model parameters per soil group. Results showed that this calibration also improved the model's accuracy, but when evaluated on the 60 test sites, the gain in model accuracy was somewhat less than when using the single-site calibration. This is not surprising: the multi-site calibration assumes parameters to be spatially constant, whereas in the single-site calibration parameters are allowed to vary from plot to plot. A disadvantage of the multi-site calibration was the low acceptance rate (1-2 %) in the calibration. This is most likely caused by the large amount of observations (122 plots with 4-6 years of soil solution measurements) and the fact that we did not account for a model error in the comparison of simulated and measured concentrations. As a result, the multi-site calibration left little room for uncertainty in the posterior parameter distributions, making them unfit for uncertainty analysis. Future research is needed to investigate how model error can be included in the calibration, as this

type of calibration would be very suited for parameterisation and uncertainty analysis of VSD applied on the European scale.

Quantification of uncertainties in critical loads and target loads due to parameter uncertainty

Since Bayesian calibration provides posterior distributions of model parameters rather than single values, the results can also be used for subsequent uncertainty analyses. We calibrated VSD on the 182 forest monitoring plots and assessed the uncertainty in critical loads and target loads that stems from the uncertainty in model parameters by running the model with sets of parameters obtained from the posterior distributions. Uncertainty analysis on such a large set of plots in Europe is quite unique and provides very valuable information, as many soil types, forest types and climatic conditions are included. The uncertainty in maximum critical load for sulphur, $CL_{max}(S)$, based on a critical value for Al/BC in soil solution is determined by the parameters that describe the equilibrium between Al and H in the soil solution and by parameters that determine the input of base cations. For the maximum critical load for nitrogen, the denitrification fraction is very important, as well as the parameters that determine $CL_{max}(S)$. The median uncertainty in critical loads over all 182 plots is about 15-30% after calibration, depending on the type of critical load and the soil chemical criterion used. Comparing the uncertainty in the calibrated model with the uncertainty in the uncalibrated model (i.e. running the model with parameters sampled from the prior parameter distributions), showed that calibration substantially reduced the uncertainty in critical loads. The same is true for target load computations: after calibration target load estimates are more robust than before calibration. The uncertainty assessments were carried out for 182 plots in Europe. The next step would be to investigate the uncertainties at a European scale. This will add additional uncertainty sources, including spatial variability in soil characteristics such as soil texture. Such an approach would also require an analysis of spatial patterns in the calibrated parameters and if these patterns can be correlated to environmental factors. If so, geostatistical methods such as regression kriging could be used to create maps of VSD input parameters for Europe, including their uncertainty.

Quantification of the effect of the chemical criterion on critical loads: model application for Europe and northern Asia

Different soil chemical criteria lead to different critical loads. We applied the SMB model (steady-state VSD model) to assess critical loads for Europe and northern Asia using very detailed and up-to-date maps and data on soil, vegetation and

climate. We showed that for the most sensitive ecosystems critical loads based on *Al*/*Bc*=1 mol mol^{-1} or [*Al*]=0.2 eq.m^{-3} are comparable but that critical loads based on an ANC=0 (with bicarbonate and organic acid leaching included) are substantially lower. These conclusions can also be drawn by looking at the concept of equivalent criteria (the value of a alternative criterion that leads to the same critical load function): for almost all soils *Al*/*Bc*=1 implies a negative ANC values. Very low critical loads are computed if a critical base saturation (*Bsat*) of 15% is used. Computing *Bsat* from *Al*/*Bc* shows that in the most sensitive ecosystems *Al*/*Bc*=1 will be equivalent to base saturations (far) below 15%. To obtain 15% base saturation in poor sandy soils requires an ANC far above zero which is not very realistic for soils that undergo natural acidification due to leaching of bicarbonates and organic acids; using a single *Bsat* criterion for Europe as suggested by some authors is thus not recommended. Our study showed that as an alternative to *Al*/*Bc*=1, using *ANC*=0 is a more realistic option than using a *Bsat* criterion. An advantage of using ANC instead of *Al*/*Bc* is that it provides a more general protection against acidification, not based on a weak relationship with forest health alone. Although studies providing limits for ANC leaching related to concrete biological effects on terrestrial ecosystems are lacking, *ANC*=0 avoids a depletion of base cations from the soil and is likely to protect surface waters.

Critical loads for nutrient N computed for Western Europe using limits of 3–6 mg N L^{-1} for the N concentration in soil solution, as suggested in De Vries et al. (2007a) for forests in this region, are much higher than the critical loads based on the generally applied limits of 0.2–0.4 mg N L^{-1}. The median critical load for nutrient N over western Europe with the revised N limits (about 1000 eq ha^{-1} yr^{-1} or 14 kg N yr^{-1}) is in better accordance with the empirical critical loads of 10–15 kg provided by Bobbink et al. (2002) related to observed vegetation changes in forests in western Europe than the 500 eq ha^{-1} yr^{-1} obtained with the limit of 0.2 mg N L^{-1}. For northern Scandinavia and other areas with sensitive ecosystems such as Alpine regions, the lower critical limit may still be applicable. The strong dependence of the critical load on leaching rate does however show the limitations of the SMB model for the assessment of nutrient N critical loads, as it assumes a relationship between nitrate concentration and plant species sensitivity, whereas N availability may be more important (De Vries et al., 2007a).

Recovery of acidified forest soils under climate change: model application for Europe

Recovery of most acidified forest soils in Europe can be achieved when emissions are reduced using all currently available technologies. Under the MFR scenario, the forest area exceeding the *Al*/*Bc*=1 criterion declined in our simulations from 4% in

1990 to about 0.7% in 2050. The area with negative ANC values decreased from 7% to 3.5% in 2050. Under current-legislation deposition, we simulated a limited decrease in the area violating the $ANC=0$ criterion, but the area with $Al/Bc>1$ reduces to 1.6% in 2050. Areas where critical nitrogen concentrations are exceeded can be reduced by implementing MFR; current legislation is probably not sufficient to eliminate the risks of vegetation changes in forest in at least some parts of Europe. In principle, recovery of most acidified soils in Europe is possible by 2050. Moreover, for the most acidified areas in central Europe, target loads can be found that return the soils to the desired chemical state by 2050. For about 30% of the receptors where TL<CL, however, the target load is lower than the deposition at MFR, indicating that no recovery in 2050 can be achieved with current emission reduction techniques.

Until now, climate change was not included in European assessments of recovery from soil acidification, but because climate change may affect recovery, VSD was adapted to incorporate effects of changes in temperature and precipitation. Simulations for Europe show that climate change reduces the area where chemical indicators were exceeded because of higher weathering rates owing to higher temperatures and because of the higher uptake of nitrogen. However, differences with current climate and differences between the A1 and B2 scenario were small. This shows that there is no need to adapt legislation on emission reductions because climate is changing: the effects are too limited to cause substantial changes in ecosystem sensitivity to acidification. It should be noted however, that this conclusion is based on the application of a simple model in which not all effects of climate change on forest ecosystems could be incorporated. Most important, the impact of temperature and water availability on N cycling processes was not included. Application of more elaborate models should substantiate our findings before final conclusions can be drawn.

Concluding remarks

The data from the combined EU/UNECE Forest Intensive Monitoring programme (De Vries et al., 2003c; De Vries et al., 2003d) have proven to be very valuable for model calibration. Available data on soils' solid phase such as CEC and soil texture were used to parameterize the model. Soil solution measurements were used to determine how well the model was able to reproduce the situation in the field. The analysis of the data from the large amount of plots, that have a reasonable spatial coverage over Europe, has proven that these data support the parameterisation and use of a model designed for regional assessments. Nevertheless, more plots with soil solution measurements in the southern and eastern parts of Europe would be welcome. Because more observations reduce the uncertainty in model

parameters estimates, monitoring should be continued and data should be made available to the modellers. Longer time-series also allow a verification of the modelled soil recovery of forest ecosystems.
Even though VSD is a simple model, the monitoring data do not allow full calibration of all the N processes involved. The nitrogen budget in VSD consists of uptake, immobilisation, denitrification and leaching, but the monitoring data only provide measurements of nitrogen leaching and a single assessment of the N pool in the soil: this is not sufficient to individually calibrate the nitrogen processes in VSD. Full calibration of the N processes would require at least some measurements on N contents in trees (to compute N uptake), repeated measurements of N pools in the soil (to compute N immobilisation) and measurements on N emissions from the soil (to compute denitrification). Such measurements would be very valuable, not only for VSD but also for other soil acidification models and models that estimate greenhouse gas emissions. A prerequisite would be that measurements are carried out with standard methods to avoid problems with incomparability of data due to differences in measurement and/or analysis techniques.

A definite statement on the risks of N induced risks in forests is hampered by the fact that in the current approach effects are related to nitrate concentrations which may not be the most appropriate indicator. Furthermore, critical values seem to vary widely over Europe making it difficult to assign the proper limits. As an alternative, more elaborate models may be applied that use other N related criteria to indicate risks, such as the soils C/N ratio or N availability. To accommodate such assessments, VSD is currently being extended with a module describing C and N interactions in the soils to allow simulations of changes in for example C/N ratios, N availability and pH as a function of N deposition. Linking it to models that compute the occurrence probability of plant species as a function of such a-biotic indicators could make it a powerful tool for computing critical loads for nutrient N. Even though VSD may thus become more suited for evaluations related to the eutrophying effect of N, the problem of defining proper limits remains. To compute critical loads, one would have to define targets related to plant species occurrence based on biodiversity criteria or the need to protect typical or red-list species. Only if international agreement on such limits and harmonization between countries is achieved, new assessments for nitrogen induced risks to forest ecosystems in Europe can be made.

Finally we can conclude that the emission reduction policies for acidifying compounds in Europe have been very successful. Not only have major emission reductions been achieved, but the use of ecosystem sensitivity expressed by critical

loads has lead to deposition reductions in those areas where the most vulnerable ecosystems occur. Our model simulations showed that if sufficient emission abatement technologies are applied, recovery from acidification in Europe can be achieved by 2050. Maybe this successful approach could serve as an example for policies dealing with other environmental issues such as biodiversity loss and greenhouse gas emissions.

Literature

Aber, J.D., Nadelhoffer, K.J., Steudler, P. & Melillo, J.M. 1989. Nitrogen saturation in northern forest ecosystems, *Bioscience* **39**, 378-386.

Aber, J.D., Goodale, C.I., Ollinger, S., M.-L., S., Magill, A.H., Martin, M.E., Hallett, R.A. & Stoddard, J.I. 2003. Is nitrogen deposition altering the nitrogen status of northeastern forests?, *Bioscience* **53**, 375–389.

Aherne, J., Sverdrup, H., Farrell, E.P. & Cummins, T. 1998. Application of the SAFE model to a Norway spruce stand at Ballyhooly, Ireland, *Forest Ecology and Management* **101**, 331-338.

Aherne, J., Farrell, E.P., Hall, J., Reynolds, B. & Hornung, M. 2001. Using multiple chemical criteria for critical loads of acidity in maritime regions, *Water Air and Soil Pollution: Focus* **1**, 75-90.

Alcamo, J., Hordijk, L., Kämäri, J., Kauppi, P., Posch, M. & Runca, E. 1985. Integrated analysis of acidification in Europe, *Journal of Environmental Management* **21**, 47-61.

Alexeyev, V.A., Markov, M.V. & Birdsey, R.A. 2004. Statistical data on forest fund of russia and chaning of forest productivity in the second half of the XX century, Ministry of Natural Resources of Russian Federation, St. Petersburg Research Institute of Forestry and St. Petersburg Forest Ecological Center, St. Peterburg, 272 pp.

Alveteg, M. 1998. Dynamics of forest soil chemistry, Thesis, Reports in Ecology and Environmental Engineering 3:1998, Department of Chemical Engineering II, Lund University, Lund, Sweden, 81 pp.

Alveteg, M., Sverdrup, H. & Kurz, D. 1998. Integrated assessment of soil chemical status. 1. Integration of existing models and derivation of a regional database for Switzerland, *Water Air and Soil Pollution* **105** (1), 1-9.

Amann, M., Asman, W.A.H., Bertok, I., Cofala, J., Heyes, C., Klimont, Z., Posch, M., Schöpp, W. & F., W. 2006. Emission control scenarios that meet the environmental objectives of the Thematic Strategy on Air Pollution IIASA, Laxenburg, 116 pp.

Amann, M., Asman, W., Bertok, I., Cofala, J., Heyes, C., Klimont, Z., Schöpp, W. & Wagner, F. 2007. Cost-effective emission reductions to meet the environmental

targets of the Thematic Strategy on Air Pollution under different greenhouse gas constraints, NEC Scenario Analysis Report Nr. 5, IIASA, Laxenburg, Austria.

Arp, P.A. & Oja, T. 1997. A forest soil vegetation atmosphere model (ForSVA), I: Concepts, *Ecological Modelling* **95**, 211-224.

Barkman, A., Warfvinge, P. & Sverdrup, H. 1995. Regionalization of critical loads under uncertainty, *Water Air and Soil Pollution* **85**, 2515-2520.

Barkman, A., Schlyter, P., Lejonklev, M., Alveteg, M., Warfinge, P., Arnström, T. & Sverdrup, H. 1999. Uncertainties in high resolution critical load assessment for forest soils: Possibilities and constraints of combining distributed soil modelling and geographic information systems, *Geographical & Environmental Modelling* **3** (2), 125-143.

Barkman, A. & Alveteg, M. 2001. Effects of data uncertainty in the Swedish critical load assessment for forest soils, *Water Air and Soil Pollution* **125**, 133-156.

Bartholome, E., Belward, A.S., Achard, F., Bartalev, S., Carmona-Moreno, C., Eva, H., Fritz, S., Gegoure, J.-M., Mayaux, P. & Stibig, H.-J. 2002. GLC 2000. Global Land Cover mapping for the year 2000. Project status November 2002, EUR 20524 EN, European Commission, Joint Research Centre, Ispra, Italy.

Bashkin, V.N., Kozlov, M.Y., Prepotina, I.V., Abramychev, A.Y. & Dedkova, I.S. 1995. Calculation and mapping of critical loads of S, N and acidity on ecosystems of the Northern Asia, *Water Air and Soil Pollution* **85**, 2395-2400.

Batjes, N.H. 1996. Development of a world data set of soil water retention properties using pedotransfer rules, *Geoderma* **71**, 31-52.

Belyazid, S., Westling, O. & Sverdrup, H. 2006. Modelling changes in forest soil chemistry at 16 Swedish coniferous forest sites following deposition reduction, *Environmental Pollution* **144** (2), 596-609.

Berg, B. & Matzner, E. 1997. Effect of N deposition on decomposition of plant litter and soil organic matter in forest systems, *Environmental Reviews* **5**, 1-25.

Berggren, D. & Mulder, J. 1995. The role of organic matter in controlling aluminum solubility in acidic mineral soils, *Geochimica et Cosmochimica Acta* **59**, 4167-4180.

Bergström, A.-K. & Jansson, M. 2006. 'Atmospheric nitrogen deposition has caused nitrogen enrichment and eutrophication of lakes in the northern hemisphere', in *Global Change Biology*, Vol. 12, pp. 635-643.

Bobbink, R., Bik, L. & Willems, J.H. 1988. Effects of nitrogen fertilization on vegetation structure and dominance of Brachypodium pinnatum (L.) Beauv. in chalk grassland, *Acta Botanica Neerlandica* **37** (2), 231-242.

Bobbink, R., Ashmore, M., Braun, S., Flückiger, W. & Van den Wyngaert, I.J.J. 2002. Empirical nitrogen critical loads for natural and semi-natural ecosystems: 2002 update, in Achermann, B. and Bobbink, R. (Eds.), Empirical Critical Loads for Nitrogen, Swiss Agency for Environment, Forests and Landscape, Berne,

Bosman, B., Remacle, J. & Carnol, M. 2001. Element removal in harvested tree biomass: scenarios for critical loads in Wallonia, South Belgium, *Water Air and Soil Pollution: Focus* **1** (1), 153-167.

Bouwman, A., Van Vuuren, D., Derwent, R. & Posch, M. 2002. A Global Analysis of Acidification and Eutrophication of Terrestrial Ecosystems, *Water Air and Soil Pollution* **141** (1), 349-382.

Boxman, A.W., Sinke, R.J. & Roelofs, J.G. 1986. Effects of NH_4^+ on the growth and K^+ (^{86}Rb) uptake of various ectomycorrhizal fungi in pure culture, *Water Air and Soil Pollution* **31**, 517-522.

Bull, K.R., Achermann, B., Bashkin, V., Chrast, R., Fenech, G., Forsius, M., Gregor, H.D., Guardans, R., Haussmann, T., Hayes, F., Hettelingh, J.P., Johannessen, T., Krzyzanowski, M., Kucera, V., Kvaeven, B., Lorenz, M., Lundin, L., Mills, G., Posch, M., Skjelkvåle, B.L. & Ulstein, M.J. 2001. Coordinated effects monitoring and modelling for developing and supporting international air pollution control agreements, *Water Air and Soil Pollution* **130** (1-4), 119-130.

Carter, T.R. 2007. General guidelines on the use of scenario data for climate impact and adaption assessment. Version 2. Task Group on Data and Scenario Support for Impact and Climate Assessment (TGICA), Intergovernmental Panel on Climate Change.

Cinderby, S., Emberson, L., Owen, A. & Ashmore, M. 2007. LRTAP Land Cover Map of Europe, in Slootweg, J., Posch, M. and Hettelingh, J.-P. (Eds.), *European Critical Loads of Nitrogen and Dynamic Modelling: CCE Progress Report 2007* Bilthoven, pp. 59-70.

Clark, C.M. & Tilman, D. 2008. Loss of plant species after chronic low-level nitrogen deposition to prairie grasslands, *Nature* **451** (7179), 712-715.

Cosby, B.J., Hornberger, G.M., Galloway, J.N. & Wright, R.F. 1985a. Modeling the effects of acid deposition: Assessment of a lumped parameter model of soil water and streamwater chemistry, *Water Resources Research* **21**, 51-63.

Cosby, B.J., Ferrier, R.C., Jenkins, A. & Wright, R.F. 2001. Modelling the effects of acid deposition: refinements, adjustments and inclusion of nitrogen dynamics in the MAGIC model, *Hydrology and Earth System Sciences* **5** (3), 499-517.

Cronan, C.S., April, R., Bartlett, R.J., Bloom, P.R., Driscoll, C.T., Gherini, S.A., Henderson, G.S., Joslin, J.D., Kelly, J.M., Newton, R.M., Parnell, R.A., Patterson, H.H., Raynall, D.J., Schaedle, M., Schofield, C.T., Sucoff, E.I., Tepper, H.B. & Thornton, F.C. 1989. Aluminium toxicity in forests exposed to acidic deposition: The ALBIOS results, *Water Air and Soil Pollution* **48**, 181-192.

Dahlgren, R.A. & Walker, W.J. 1993. Aluminium release rates from selected spodosol Bs horizons: Effects of pH and solid-phase aluminium pools, *Geochimica et Cosmochimica Acta* **57**, 57-66.

Davies, C.E., Moss, D. & Hill, M.O. 2004. EUNIS Habitat Classification Revised 2004, European Topic Centre on Nature Protection and Biodiversity, 310 pp.

De Vries, W. & Breeuwsma, A. 1986. Relative importance of natural and anthropogenic proton sources in soils in the Netherlands, *Water Air and Soil Pollution* **28** (1), 173-184.

De Vries, W. & Breeuwsma, A. 1987. The relation between soil acidification and element cycling, *Water Air and Soil Pollution* **35**, 293-310.

De Vries, W., Posch, M. & Kämäri, J. 1989. Simulation of the long-term soil response to acid deposition in various buffer ranges, *Water Air and Soil Pollution* **48** (3), 349-390.

De Vries, W. 1991. Methodologies for the assessment and mapping of critical loads and the impact of abatement strategies on forest soils, Staring Centre Report 46, Wageningen, 109 pp.

De Vries, W. 1993. Average critical loads for nitrogen and sulfur and its use in acidification abatement policy in the Netherlands, *Water Air and Soil Pollution* **68** (3-4), 399-434.

De Vries, W. 1994. Soil response to acid deposition at different regional scales; Field and laboratory data, critical loads and model predictions, Thesis, Wageningen University, Wageningen, 487 pp.

De Vries, W., Kros, J. & Voogd, J.C.H. 1994a. Assessment of critical loads and their exceedance on Dutch forests using a multi-layer steady-state model, *Water Air and Soil Pollution* **76**, 407-448.

De Vries, W., Reinds, G.J. & Posch, M. 1994b. Assessment of critical loads and their exceedance on European forests using a one-layer steady-state model, *Water Air and Soil Pollution* **72**, 357-394.

De Vries, W., Reinds, G.J. & Posch, M. 1994c. Assessment of critical loads and their exceedance on European forests using a one-layer steady-state model, *Water, Air, & Soil Pollution* **72**, 357-394.

De Vries, W., Reinds, G.J., Posch, M. & Kämäri, J. 1994d. Simulation of soil response to acidic deposition scenarios in Europe, *Water, Air, and Soil Pollution* **78**, 215-246.

De Vries, W., Van Grinsven, J.J.M., Van Breemen, N., Leeters, E.E.J.M. & Jansen, P.C. 1995. Impacts of acid deposition on concentrations and fluxes of solutes in acid sandy forest soils in the Netherlands, *Geoderma* **67** (1-2), 17-43.

De Vries, W., Reinds, G.J., Deelstra, H.D., Klap, J.M. & Vel, E.M. 1999. Intensive Monitoring of Forest Ecosystems in Europe. Technical Report 1999, UN/ECE, EC, Forest Intensive Monitoring Coordinating Institute, 173 pp.

De Vries, W. & Leeters, E.E.J.M. 2001. Chemical composition of the humus layer, mineral soil and soil solution of 150 forest stands in the Netherlands in 1990, Report 424.1., Alterra, Wageningen (Netherlands), 113 pp.

De Vries, W., Reinds, G.J., Van der Salm, C., Draaijers, G.P.J., Bleeker, A., Erisman, J.W., Auee, J., Gundersen, P., Kristensen, H.L., Van Dobben, H., De Zwart, D., Derome, J., Voogd, J.C.H. & Vel, E.M. 2001. Intensive Monitoring of Forest Ecosystems in Europe. Technical Report 2001, UN/ECE, EC, Forest Intensive Monitoring Coordinating Institute, Geneva and Brussels, 177 pp.

De Vries, W. & Posch, M. 2003a. Critical evels and critical loads as a tool for air quality management, in Hewitt, C.N. and Jackson, A.V. (Eds.), *Handbook of Atmospheric Science. Principles and Applications*, Blackwell Science, Oxford, UK, pp. 562-602.

De Vries, W. & Posch, M. 2003b. Derivation of cation exchange constants for sand, loess, clay and peat soils on the basis of field measurements in the Netherlands, Alterra Report 701, Wageningen, 50 pp pp.

De Vries, W., Reinds, G.J., Posch, M., Sanz, M.J., Krause, G.H.M., Calatayud, V., Renaud, J.P., Dupouey, J.L., Sterba, H., Gundersen, P., Voogd, J.C.H. & Vel, E.M. 2003a. Intensive Monitoring of Forest Ecosystems in Europe. Technical Report 2003, UN/ECE and EC, Forest Intensive Monitoring Coordinating Institute, Geneva and Brussels, 170 pp.

De Vries, W., Reinds, G.J. & Vel, E. 2003c. Intensive monitoring of forest ecosystems in Europe: 2. Atmospheric deposition and its impacts on soil solution chemistry, *Forest Ecology and Management* **174** (1-3), 97-115.

De Vries, W., Vel, E., Reinds, G.J., Deelstra, H., Klap, J.M., Leeters, E.E.J.M., Hendriks, C.M.A., Kerkvoorden, M., Landmann, G. & Herkendell, J. 2003d. Intensive monitoring of forest ecosystems in Europe: 1. Objectives, set-up and evaluation strategy, *Forest Ecology and Management* **174** (1-3), 77-95.

De Vries, W., Reinds, G.J., Gundersen, P. & Sterba, H. 2006. The impact of nitrogen deposition on carbon sequestration in European forests and forest soils, *Global Change Biology* **12**, 1151-1173.

De Vries, W., Kros, J., Reinds, G.J., Wamelink, W., Van Dobben, H., Bobbink, R., Emmett, B., Smart, S., Evans, C., Schlutow, A., Kraft, P., Belyazid , S., Sverdrup, H., Van Hinsberg, A., Posch, M. & Hettelingh, J.-P. 2007a. Developments in modelling critical nitrogen loads for terrestrial ecosystems in Europe., Alterra Report 1382, Wageningen, The Netherlands, 206 pp.

De Vries, W., Van der Salm, C., Reinds, G.J. & Erisman, J.W. 2007b. Element fluxes through European forest ecosystems and their relationships with stand and site characteristics, *Environmental Pollution* **148** (2), 501-513.

De Vries, W., Solberg, S., Dobbertin, M., Sterba, H., Laubhahn, D., Reinds, G.J., Nabuurs, G.-J., Gundersen, P. & Sutton, M.A. 2008. Ecologically implausible carbon response?, *Nature* **451** (7180), E1-E3.

De Vries, W., Kros, H. & Erisman, J.W. 2009. Adverse impacts of increased nitrogen use on terrestrial and aquatic ecosystems, air quality, climate and human health in Europe: an overview, *Environmental Pollution* **Submitted.**

De Wit, H.A., Mulder, J., Nygaard, P.H., Aamlid, D., Huse, M., Kortnes, E., Wollebæk, G. & Brean, R. 2001. Aluminium: the need for a re-evaluation of its toxicity and solubility in mature forest stands, *Water Air and Soil Pollution: Focus* **1** (1 - 2), 103-118.

Dickson, W. 1978. Some effects of acidification on Swedish lakes, *Verh. Internat. Verein. Limnol.* **20**, 851-856.

Dirkse, G.M. & Van Dobben, H. 1989. Het effect van bemesting op de samenstelling van de kruidlaag van dennenbossen., *Natura* **9**, 208-212.

Dise, N.B., Rothwell, J.J., Gauci, V., Van der Salm, C. & De Vries, W. 2009. Predicting dissolved inorganic nitrogen leaching in European forests using two independent databases, *Science of the Total Environment* **407** (5), 1798-1808.

Draaijers, G.P.J. & Erisman, J.W. 1995. A canopy budget model to assess atmospheric deposition from throughfall measurements, *Water Air and Soil Pollution* **85** (4), 2253-2258.

Driscoll, C.T., Fuller, R.D. & Schecher, W.D. 1989. The role of organic acids in the acidification of surface waters in the Eastern U.S., *Water Air and Soil Pollution* **43**, 21-40.

EMEP 2001. '*Transboundary acidification and eutrophication and ground level ozone in Europe.*' in EMEP Summary Report 2001 EMEP Report 1/01, July 2001. Joint CIAM & CCC & MSC-W report Norwegian Meteorological Institute.

EMEP 2004. European perspective. In: Lövblad, G., Tarrason, L., Tørseth, K. and Dutchak, S. (eds), EMEP Assessment. Norwegian Meteorological Institute, Oslo.

European Soil Bureau Network 2004. European Soil Database (v 2.0), EUR 19945 EN, European Soil Bureau Network and European Commission.

Evans, C.D., Caporn, S.J.M., Carroll, J.A., Pilkington, M.G., Wilson, D.B., Ray, N. & Cresswell, N. 2006. Modelling nitrogen saturation and carbon accumulation in heathland soils under elevated nitrogen deposition, *Environmental Pollution* **143** (3), 468-478.

Falkengren-Grerup, U. 1986. Soil acidification and vegetation chenges in deciduous forest in Southern Sweden, *Oecologia* **70**, 339-347.

FAO-UNESCO 2003. 'Digital soil map of the world and derived soil properties, CD-ROM', FAO, Rome.

FAO 1988. Soil map of the World, revised legend. World soil resources report 60, FAO, Rome, 138 pp.

FAO 2000. Global Forest Resources Assessment 2000, Main Report, FAO Forestry Paper 140, Rome, 479 pp.

Federer, C.A. 1982. Transpirational supply and demand: plant, soil and atmospheric effects evaluated by simulation, *Water Resources Research* **18**, 355-362.

Freeman, C., Evans, C.D., Monteith, D.T., Reynolds, B. & Fenner, N. 2001. Export of organic carbon from peat soils, *Nature* **412** (6849), 785-785.

Freeman, C., Fenner, N., Ostle, N.J., Kang, H., Dowrick, D.J., Reynolds, B., Lock, M.A., Sleep, D., Hughes, S. & Hudson, J. 2004. Export of dissolved organic carbon from peatlands under elevated carbon dioxide levels, *Nature* **430** (6996), 195-198.

Göransson, A. & Eldhuset, T.D. 2001. Is the (Ca+K+Mg)/Al ratio in the soil solution a predictive tool for estimating forest damage?, *Water Air and Soil Pollution: Focus* **1** (1 - 2), 57-74.

Gorham, E. 1976. Acid precipitation and its influence upon aquatic ecosystems — An overview, *Water, Air, & Soil Pollution* **6** (2), 457-481.

Gregor, H.-D., Nagel, H.-D. & Posch, M. 2001. The UN/ECE International Programme on Mapping Critical Loads and Levels, *Water Air and Soil Pollution: Focus* **1** (1 - 2), 5-19.

Grennfelt, P., Moldan, F., Alveteg, M., Warfvinge, P. & Sverdrup, H. 2001. Critical loads: is there a need for a new concept?, *Water Air and Soil Pollution: Focus* **1** (1 - 2), 21-27.

Grennfelt, P., Lindau, L. & Arnell, J. 2007. Air pollution and its relationship to climate change and sustainable development. Linking immediate needs with long term challenges "Saltsjöbaden 3", Gothenburg 12-14 March 2007, Main conclusions, Swedish Environmental Research Institute, Stockholm, Sweden.

Groenenberg, J.E., Kros, J., Van der Salm, C. & De Vries, W. 1995. Application of the model NUCSAM to the Solling spruce site, *Ecological Modelling* **83**, 97-107.

Gundersen, P., Callesen, I. & De Vries, W. 1998. Nitrate leaching in forest ecosystems is related to forest floor C/N ratios, *Environmental Pollution* **102** (1), 403-407.

Gundersen, P., Berg, B., Currie, W.S., Dise, N.B., Emmett, B.A., Gauci, V., Holmberg, M., Kjønaas, O.J., Mol-Dijkstra, J., van der Salm, C., Schmidt, I.K., Tietema, A., Wessel, W.W., Vestgarden, L.S., Akselsson, C., De Vries, W., Forsius, M., Kros, H., Matzner, E., Moldan, F., Nadelhoffer, K.J., Nilsson, L.-O., Reinds, G.J., Rosengren, U., Stuanes, A.O. & Wright, R.F. 2006. 'Carbon - nitrogen interactions in forest ecosystems', in *Forest & Landscape Working Papers.* Copenhagen, pp. 62.

Hall, J., Reynolds, B., Aherne, J. & Hornung, M. 2001a. The importance of selecting appropriate criteria for calculating acidity critical loads for terrestrial ecosystems using the Simple Mass Balance equation, *Water Air and Soil Pollution: Focus* **1** (1 - 2), 29-41.

Hall, J., Reynolds, B., Langan, S., Hornung, M., Kennedy, F. & Aherne, J. 2001b. Investigating the uncertainties in the Simple Mass Balance equation for acidity critical loads for terrestrial ecosystems in the United Kingdom, *Water Air and Soil Pollution: Focus* **1** (1 - 2), 43-56.

Harned, H.S. & Davis, R.J. 1943. The ionization constant of carbonic acid in water and the solubility of carbon dioxide in water and aqueous salt solutions from 0 to 50 °, *J. Am. Chem. Soc.* **65**, 2030-2037.

Hengl, T., Heuvelink, G.B.M. & Rossiter, D.G. 2007. About regression-kriging: From equations to case studies, *Computers & Geosciences* **33** (10), 1301-1315.

Henriksen, A., Lien, L., Rosseland, B.O., Traaen, T.S. & Sevalud, I.S. 1989. Lake acidification in Norway - Present and predicted fish status., *Ambio* **18**, 314-321.

Hetteling, J.-P., Posch, M. & Slootweg, J. (Eds.): 2008. Critical load, dynamic modelling and impact assessment in Europe: CCE Status Report 2008. PBL Report 50009003, Bilthoven, Netherlnads, 231 pp.

Hettelingh, J.-P., Posch, M., De Smet, P.A.M. & Downing, R.J. 1995a. The use of critical loads in emission reduction agreements in Europe, *Water Air and Soil Pollution* **85**, 2381-2388.

Hettelingh, J.-P., Sverdrup, H. & Zhao, D. 1995b. Deriving critical loads for Asia, *Water Air and Soil Pollution* **85** (4), 2565-2570.

Hettelingh, J.-P., Posch, M. & De Smet, P.A.M. 2001. Multi-effect critical loads used in multi-pollutant reduction agreements in Europe, *Water Air and Soil Pollution* **130**, 1133-1138.

Hettelingh, J.-P., Posch, M., Slootweg, J., Reinds, G.J., Spranger, T. & Tarrason, L. 2007. Critical loads and dynamic modelling to assess European areas at risk of acidification and eutrophication, *Water Air and Soil Pollution: Focus* **7**, 379-384.

Heuvelink, G.B.M. & Pebesma, E.J. 1999. Spatial aggregation and soil process modelling, *Geoderma* **89**, 47-65.

Hjellbrekke, A.G., Schaug, J., Hanssen, J.E. & Skjelmoen, J.E. 1997. Data Report 1995. Part 1: Annual summaries. NILU CCC Report 4/97., Norwegian Institute for Air Reseach, Kjeller, Norway.

Hodson, M.E. & Langan, S.J. 1999. Considerations of uncertainty in setting critical loads of acidity of soils: the role of weathering rate determination, *Environmental Pollution* **106**, 73-81.

Högberg, P., Fan, H., Quist, M., Binkley , D. & Tamm, C.O. 2006. Tree growth and soil acidification in response to 30 years of experimental nitrogen loading on boreal forest, *Global Change Biology* **12** (3), 489-499.

Holmberg, M., Mulder, J., Posch, M., Starr, M., Forsius, M., Johansson, M., Bak, J., Ilvesniemi, H. & Sverdrup, H. 2001. Critical loads of acidity for forest soils: tentative modifications, *Water Air and Soil Pollution: Focus* **1** (1 - 2), 91-101.

Hutchinson, T.C., Bozic, L. & Munoz-Vega, G. 1986. Responses to five species of conifer seedlings to aluminum stress, *Water Air and Soil Pollution* **31**, 283-294.

Hyvönen, R., Ågren, G.I., Linder, S., Persson, T., Cotrufo, M.F., Ekblad, A., Freeman, M., Grelle, A., Janssens, I.A., Jarvis, P.G., Kellomäki, S., Lindroth, A., Loustau, D., Lundmark, T., Norby, R.J., Oren, R., Pilegaard, K., Ryan, M.G., Sigurdsson, B.D., Strömgren, M., Van Oijen, M. & Wallin, G. 2007. The likely impact of elevated [CO_2], nitrogen deposition, increased temperature and management on carbon sequestration in temperate and boreal forest ecosystems: a literature review, *New Phytologist* **173** (3), 463-480.

IPCC 2007. Climate Change 2007: Synthesis Report., Cambridge University Press, Cambridge., 73 pp.

Jacobsen, C., Rademacher, P., Meesenburg, H. & Meiwes, K.J. 2002. Gehalte chemischer Elemente in Baumkompartimenten, Niedersächsische Forstliche Versuchsanstalt Göttingen; im Auftrag des Bundesministeriums für Verbraucherschutz, Ernährung and Landwirtschaft (BMVEL). Bonn, 80 pp.

Janssen, P.H.M. & Heuberger, P.S.C. 1995. Calibration of process-oriented models, *Ecological Modelling* **83**, 55-66.

Jenkins, A., Renshaw, M., Helliwell, R., Sefton, C., Ferrier, R. & Swingewood, P. 1997. Modelling surface water acidification in the UK. , Institute of Hydrology, Wallingford, 54 pp.

Jensen, K.W. & Snekvik, E. 1972. Low pH levels wipe out salmon and trout populations in southernmost Norway, *Ambio* **1**, 223-225.

JRC 2006. 'The European Soil Data Base, Distribution version v2.0', Joint Research Centre, European Commission, Ispra, Italy.

Kahle, H.-P., Karjalainen, T., Schuck, A., Ågren, G.I., Kellomäki, S., Mellert, K.H., Prietzel, J., Rehfuess, K.E. & Spiecker, H. 2007. Causes and Consequences of Forest Growth Trends in Europe, EFI Research report 21, Brill, Leiden- Boston, 261 pp.

Kauppi, P., Kämäri, J., Posch, M., Kauppi, L. & Matzner, E. 1986. Acidification of forest soils: Model development and application for analyzing impacts of acidic deposition in Europe, *Ecological Modelling* **33**, 231-253.

Kesik, M., Ambus, P., Baritz, R., Brüggemann, N., Butterbach-Bahl, K., Damm, M., Duyzer, J., Horvath, L., R. Kiese, Kitzler, B., Leip, A., Li, C., Pihlatie, M., Pilegaard, K., Seufert, G., Simpson, D., Skiba, U., Smiatek, G., Vesala, T. & Zechmeister-Boltenstern, S. 2005. Inventories of N_2O and NO emissions from European forest soils, *Biogeosciences* **2**, 353-375.

Kimmins, J.P., Binkley, D., Chatarpaul, L. & De Catanzaro, J. 1985. Biogeochemistry of temperate forest ecosystems: Literature on inventories and dynamics of biomass and nutrients, PI-X-47E/F, Petawawa National Forestry Institute, Canada, 227 pp.

Körner, C., Asshoff, R., Bignucolo, O., Hättenschwiler, S., Keel, S.G., Pelaez-Riedl, S., Pepin, S., Siegwolf, R.T.W. & Zotz, G. 2005. Carbon flux and growth in mature deciduous forest trees exposed to elevated CO_2, *Science* **309**, 1360-1362.

Körner, C. 2006. Plant CO_2 responses: an issue of definition, time and resource supply, *New Phytologist* **172** (3), 393-411.

Kraft, M., Reif, A., Schreiner, M. & Aldinger, E. 2003. Veränderungen der Bodenvegetation und der Humusauflage im Nordschwarzwald in den letzten 40 Jahren., *Forstarchiv* **74**, 3-15.

Kros, J., De Vries, W., Janssen, P.H.M. & Bak, C.I. 1993. The uncertainty in forecasting trends of forest soil acidification, *Water Air and Soil Pollution* **66** (1-2), 29-58.

Kros, J., Mol Dijkstra, J.P. & Pebesma, E.J. 2002. Assessment of the prediction error in a large-scale application of a dynamic soil acidification model, *Stochastic Environmental Research and Risk Assessment* **16** (4), 279-306.

Kuhn, N., R., A. & Hufsmidt, N. 1987. Veränderungen in der Waldvegetation der Schweiz infolge Nährstoffanreicherungen aus der Atmosphäre, *Allg. Forst Z.* **158** (5/6), 77-84.

Kukkola, E., Huttunen, S., Bäck, J. & Rautio, P. 1997. Scots pine needle injuries at subarctic industrial sites, *Trees - Structure and Function* **11** (6), 378-387.

Kurz, D., Alveteg, M. & Sverdrup, H. 1998. Integrated Assessment of Soil Chemical Status. 2. Application of a Regionalized Model to 622 Forested Sites in Switzerland, *Water Air and Soil Pollution* **105** (1), 11-20.

Kurz, D. & Posch, M. 2002. A comparison of the SAFE and VSD soil dynamic models using Swiss data, Report by EKG Geo-Science and CCE, Bern and Bilthoven, 32 pp.

Kuylenstierna, J.C.I., Hicks, W.K., Cinderby, S., Cambridge, H., Van der Hoek, K.W., Erisman, J.W., Smeulders, S. & Wisniewski, J.R. 1998. Critical loads for nitrogen deposition and their exceedance at European scale, *Environmental Pollution* **102** (Supp 1), 591-598.

Kuylenstierna, J.C.I., Rodhe, H., Cinderby, S. & Hicks, K. 2001. Acidification in developing countries: ecosystem sensitivity and the critical load approach on a global scale, *Ambio* **30** (1), 20-28.

Lameire, S., Hermy, M. & Honnay, O. 2000. Two decades of change in the ground vegetation of a mixed deciduous forest in an agricultural landscape, *Journal of Vegetation Science* **11**, 695-704.

Lamppu, J. & Huttunen, S. 2001. Scots pine needle longevity and gradation of needle shedding along pollution gradients, *Canadian Journal of Forest Research* **31** (2), 261-267(7).

Landmann, G. 1995. Forest decline and air pollution effects in the French mountains: a synthesis, in Landmann, G. and Bonneau, M. (Eds.), *Forest decline and atmospheric deposition effects in the French mountains*, Berlin, Springer, pp.

Larssen, T., Schnoor, J.L., Seip, H.M. & Dawei, Z. 2000. Evaluation of different approaches for modeling effects of acid rain on soils in China, *Science of the Total Environment* **246** (2-3), 175-193.

Larssen, T., Huseby, R.B., Cosby, B.J., Høst, G., Høgåsen, T. & Aldrin, M. 2006. Forecasting acidification effects using a Bayesian calibration and uncertainty propagation approach, *Environmental Science & Technology* **40** (24), 7841-7847.

Lee, D.S., Kingdon, R.D., Pacyna, J.M., Bouwman, A.F. & Tegen, I. 1999. Modelling base cations in Europe – sources, transport and deposition of calcium, *Atmospheric Environment* **33** (14), 2241-2256.

Leemans, R. & Van den Born, G.J. 1994. Determining the potential distribution of vegetation, crops and agricultural productivity, *Water Air and Soil Pollution* **76**, 133-161.

Leemans, R. & Eickhout, B. 2004. Another reason for concern: regional and global impacts on ecosystems for different levels of climate change, *Global Environmental Change Part A* **14** (3), 219-228.

Li, C., Frolking, S. & Frolking, T.A. 1992. A model of nitrous oxide evolution from soil driven by rainfall events: 1. Model structure and sensitivity, *Journal of Geophysical Research* **97**, 9759-9776.

Li, H. & McNulty, S.G. 2007. Uncertainty analysis on simple mass balance model to calculate critical loads for soil acidity, *Environmental Pollution* **149** (3), 315-326.

Løkke, H., Bak, J., Falkengren-Grerup, U., Finlay, R.D., Ilvesniemi, H., Nygaard, P.H. & Starr, M. 1996. Critical loads of acidic deposition for forest soils: Is the current approach adequate?, *Ambio* **25**, 510-516.

Lorenz, K., C.M. Preston, S. Krumrei & K-H. Feger 2004. Decomposition of needle/leaf litter from Scots pine, black cherry, common oak and European beech at a conurbation forest site, *Eur. J. Forest Res* **123**, 177-188.

Lorenz, M., Fischer, R., Becher, G., Granke, O., Seidling, W., Ferretti, M., Schaub, M., Calatayud, V., Bacaro, G., Gerosa, G., Rocchini, D., Sanz, M. & von Fischer, A. 2008. Forest Condition in Europe 2008 Technical Report of ICP Forests, von Thünen-Institute, Institute for World Forestry Hamburg, Germany, 107 pp.

Magill, A.H., Aber, J.D., Currie, W.S., Nadelhoffer, K.J., Martin, M.E., McDowell, W.H., Melillo, J.M. & Steudler, P. 2004. Ecosystem response to 15 years of chronic nitrogen additions at the Harvard Forest LTER, Massachusetts, USA, *Forest Ecology and Management* **196** (1), 7-28.

Magnani, F., Mencuccini, M., Borghetti, M., Berbigier, P., Berninger, F., Delzon, S., Grelle, A., Hari, P., Jarvis, P.G., Kolari, P., Kowalski, A.S., Lankreijer, H., Law, B.E., Lindroth, A., Loustau, D., Manca, G., Moncrieff, J.B., Rayment, M., Tedeschi, V., Valentini, R. & Grace, J. 2007. The human footprint in the carbon cycle of temperate and boreal forests, *Nature* **447** (7146), 849-851.

Matzner, E. 1992. Factors controlling Al-activity in soil solutions in an acid forest soil of the German Solling area, *Zeitschritf für Pflanzenernährung und Bodenkunde* **155**, 331-338.

Melillo, J.M., Aber, J.D. & Muratore, J.F. 1982. Nitrogen and lignine control of hardwood leaf litter decomposition, *Ecology* **63**, 621-626.

Metzger, M.J. 2005. European vulnerability to global change, Thesis, Wageningen University, Wageningen, 192 pp.

Metzger, M.J., Leemans, R. & Schröter, D. 2005. A multidisciplinary multi-scale framework for assessing vulnerabilities to global change, *International Journal of Applied Earth Observation and Geoinformation* **7** (4), 253-267.

Metzger, M.J., Bunce, R.G.H., Leemans, R. & Viner, D. 2008. Projected environmental shifts under climate change: European trends and regional impacts, *Environmental Conservation* **35** (01), 64-75.

Mitchell, T.D., Carter, T.R., Jones, P.D., Hulme, M. & New, M. 2004. A comprehensive set of high-resoluton grids of monthly climate for Europe and the globe: the observed record (1901-2000) and 16 scenarios (2010-2100), Tyndall Centre for Climate Change Research. Working paper 55., 19 pp.

Mol-Dijkstra, J.P. & Kros, H. 2001. Modelling effects of acid deposition and climate change on soil and run-off chemistry at Risdalsheia, Norway, *Hydrology and Earth System Sciences* **5** (3), 487-498.

Mulder, J., Van Grinsven, J.J.M. & Van Breemen, N. 1987. Impact of acid atmospheric deposition on woodland soils in the Netherlands. III: Aluminium chemistry, *Soil Science Society of America Journal* **51**, 1640-1646.

Mulder, J. & Stein, A. 1994. The solubility of aluminum in acidic forest soils: Long-term changes due to acid deposition, *Geochimica et Cosmochimica Acta* **58**, 85-94.

Müller-Edzards, C., De Vries, W. & Erisman, J.W. 1997. Ten Years of Monitoring Forest Condition in Europe - Studies on Temporal Development, Spatial Distribution and Impacts of Natural and Anthropogenic Stress Factors. Technical Background Report., EC-UN/ECE, Geneva, Brussels, 386 pp.

Murphy, K.L., Klopatek, J.M. & Coe Klopatek, C. 1998. The effects of litter quality and climate on decomposition along an elevational gradient., *Ecological Applications* **8**, 1061-1071.

Nadelhoffer, K.J., Emmett, B.A., Gundersen, P., Kjønaas, O.J., Koopmans, C.J., Schleppi, P., Tietema, A. & Wright, R.F. 1999. Nitrogen deposition makes a minor contribution to carbon sequestration in temperate forests, *Nature* **398**, 145 -148.

Nakícenovíc, N., Alcamo, J., Davis, G., de Vries, B., Fenhann, J., Gaffin, S., Gregory, K., Grübler, A., Jung, T.Y., Kram, T., Emilio la Rovere, E., Michaelis, L., Mori, S., Morita, T., Pepper, W., Pitcher, H., Price, L., Riahi, K., Roehrl, A., Rogner, H.-H., Sankovski, A., Schlesinger, M.E., Shukla, P.R., Smith, S., Swart, R.J., van Rooyen, S., Victor, N. & Dadi, Z. 2001. Special Report on Emission Scenarios: Intergovernmental Panel on Climate Change, Cambridge University Press, Cambridge, 599 pp.

Navrátil, T., Kurz, D., Krám, P., Hofmeister, J. & Hruska, J. 2007. Acidification and recovery of soil at a heavily impacted forest catchment (Lysina, Czech Republic)--SAFE modeling and field results, *Ecological Modelling* **205** (3-4), 464-474.

Nelleman, C. & Frogner, T. 1994. Spatial patterns of spruce defoliation seen in relation to acid deposition, critical loads and natural growth conditions in Norway, *Ambio* **23**, 255-259.

New, M., Hulme, M. & Jones, P.D. 1999. Representing twentieth century space-time climate variability. Part 1: development of a 1961-90 mean monthly terrestrial climatology, *Journal of Climate* **12**, 829-856.

New, M., Hulme, M. & Jones, P.D. 2000. Representing twentieth century space-time climate variability. Part 2: development of 1901-96 monthly grids of terrestrial surface climate, *Journal of Climate* **13**, 2218-2238.

Nilsson, J. & Grennfelt, P. 1988. Critical loads for sulphur and nitrogen, Miljø rapport 1988: 15. Nordic Council of Ministers, Copenhagen, Denmark, 418 pp.

Nordin, A., Nasholm, T. & Ericson, L. 1998. Effects of simulated N deposition on understorey vegetation of a boreal coniferous forest, *Functional Ecology* **12** (4), 691-699.

Nyberg, L., Lundström, U., Söderberg, U., Danielsson, R. & Van Hees, P. 2001. Does soil acidification affect spruce needle chemical composition and tree growth, *Water Air and Soil Pollution: Focus* **1**, 241-263.

Nygaard, P.H. & De Wit, H.A. 2004. Effects of elevated soil solution Al concentrations on fine roots in a middle-aged Norway spruce (Picea abies (L.) Karst.) stand, *Plant and Soil* **265** (1), 131-140.

Odén, S. 1976. The acidity problem — An outline of concepts, *Water, Air, & Soil Pollution* **6** (2), 137-166.

Oliver, B.G., Thurman, E.M. & Malcolm, R.L. 1983. The contribution of humic substances to acidity of colored nature waters, *Geochimica et Cosmochimica Acta* **47**, 2031-2035.

Overrein, L.N., Seip, H.M. & Tollan, A. 1980. Acid precipitation - Effects on Forest and Fish. Final report of the SNSF-Project 1972-1980, Norwegian Forest Research Institute, Aas, 175 pp.

Posch, M., Reinds, G.J. & De Vries, W. 1993. SMART: A Simulation Model for Acidification's Regional Trends. Model Description and User Manual, Mimeograph Series of the National Board of Waters and the Environment 477, Helsinki, Finland, 43 pp.

Posch, M., De Smet, P.A.M., Hettelingh, J.-P. & Downing, R.J. (Eds.): 1995. *Calculation and mapping of critical thresholds in Europe: CCE Status Report 1995.* RIVM Report 259101004, Coordination Centre for Effects, RIVM, Bilthoven, the Netherlands, 198 pp.

Posch, M. & De Vries, W. 1999. Derivation of critical loads by steady-state and dynamic soil models, in Langan, S.J. (Ed.), *The impact of nitrogen deposition on natural and semi-natural ecosystems*, Kluwer, Dordrecht, The Netherlands, pp. 213-234.

Posch, M. & Hettelingh, J.-P. 2001. From critical loads to dynamic modelling, in Posch, M., De Smet, P.A.M., Hettelingh, J.-P. and Dowing, R.J. (Eds.), *Modelling and mapping of critical thresholds in Europe, Status report 2001.* RIVM Report 259010101, Coordination Centre for Effects, RIVM, Bilthoven, Netherlands, pp. 33-39.

Posch, M. 2002. Impacts of climate change on critical loads and their exceedances in Europe, *Environmental Science & Policy* **5** (4), 307-317.

Posch, M., Hettelingh, J.-P. & Slootweg, J. 2003. Manual for dynamic modelling of soil response to atmospheric deposition. RIVM Report 259101012, Bilthoven, The Netherlands, 71 pp.

Posch, M. & Reinds, G.J. 2005. The European Background Database, in Posch, M., Slootweg, J. and Hettelingh, J.P. (Eds.), *European critical loads and dynamic modelling, CCE Status Report 2005,* Coordination Centre for Effects. RIVM Report No. 259101016, Bilthoven, Netherlands, pp. 63-69.

Posch, M., Slootweg, J. & Hettelingh, J.-P. (Eds.): 2005. *European critical loads and dynamic modelling, CCE Status report 2005,* Coordinating Centre for Effects, RIVM Report No. 259101016/2005, Bilthoven, Netherlands, 171 pp.

Posch, M., Aherne, J., Forsius, M., Fronzek, S. & Veijalainen, N. 2008. Modelling the impacts of European emission and climate change scenarios on acid-sensitive catchments in Finland, *Hydrol. Earth Syst. Sci.* **12**, 449-463.

Posch, M. & Reinds, G.J. 2009. A very simple dynamic soil acidification model for scenario analyses and target load calculations, *Environmental Modelling & Software* **24**, 329–340.

Prentice, I.C., W. P. Cramer, S. P. Harrison, R. Leemans, R. A. Monserud, and A. M. Solomon. 1992. A global biome model based on plant physiology and dominance, soil properties and climate. *Journal of Biogeography*, **19,** 117-134.

Prentice, I.C., Sykes, M.T. & Cramer, W. 1993. A simulation model for the transient effects of climate change on forest landscapes, *Ecological Modelling* **65**, 51-70.

Prins, K. & Korotkov, A. 1994. The forest sector of economies in transition in Central and Eastern Europe., *Unasylva* **179**, 3-10.

Rahmstorf, S., Cazenave, A., Church, J.A., Hansen, J.E., Keeling, R.F., Parker, D.E. & Somerville, R.C.J. 2007. Recent Climate Observations Compared to Projections, *Science* **316**, 709-709.

Rehfuess, K.-E., Ågren, G.I., Andersson, F., Cannell, M.G.R., Friend, A., Hunter, I., Kahle, H.-P., Prietzel, J. & Spiecker, H. 1999. Relationships between recent changes of growth and nutrition of Norway spruce, Scots pine and European beech forests in Europe-RECOGNITION, Working Paper 19, European Forest Institute, 94 pp.

Reinds, G.J., Posch, M. & De Vries, W. 2001. A semi-empirical dynamic soil acidification model for use in spatially explicit integrated assessment models for Europe, Alterra rapport 084, Wageningen, Netherlands, 55 pp.

Reinds, G.J., Posch, M., De Vries, W., Slootweg, J. & Hettelingh, J.-P. 2008a. Critical loads of sulphur and nitrogen for terrestrial ecosystems in Europe and northern Asia using different soil chemical criteria, *Water Air and Soil Pollution* **193** (1), 269-287.

Reinds, G.J., Van Oijen, M., Heuvelink, G.B.M. & Kros, H. 2008b. Bayesian calibration of the VSD soil acidification model using European forest monitoring data, *Geoderma* **146** (3-4), 475-488.

Reinds, G.J., Posch, M. & de Vries, W. 2009. Modelling the long-term soil response to atmospheric deposition at intensively monitored forest plots in Europe, *Environmental Pollution* **157** (4), 1258-1269.

Robert, C.P. & Casella, G. 1999. Monte Carlo statistical methods, New York, 507 pp.

Roberts, T.M., Skeffington, R.A. & Blank, L.W. 1989. Causes of type 1 spruce decline, *Forestry* **62** (3), 179-222.

Roelofs, J.G.M., Kempers, A.J., Houdijk, A.L.F.M. & Jansen, J. 1985. The effect of airborne ammonium sulphate on Pinus nigra var. maritima in the Netherlands, *Plant and Soil* **84**, 45-56.

Rost-Siebert, K. 1983. Aluminium-Toxizitat und -Toleranz an Keimpflanzen von Fichte (Picea abies Karst.) und Buche (Fagus silvatica L.), *Allgem. Forstz.* **26/27**, 686-689.

Santore, R.C., Driscoll, C.T. & Aloi, M. 1995. A model of soil organic matter and its function in temperate forest soil development, in McFee, W.W. and Kelly, J.M. (Eds.), *Carbon forms and functions in forest soils*, Soil Sci. Soc. of America, Madison, Wisconsin, pp. 275-298.

Schelhaas, M.J., Varis, S., Schuck, A. & Nabuurs, G.J. 1999. EFISCEN's European Forest Resource Database, EFI, European Forest Institute, Joensuu, Finland.

Schöpp, W., Posch, M., Mylona, S. & Johansson, M. 2003. Long-term development of acid deposition (1880–2030) in sensitive freshwater regions in Europe, *Hydrology and Earth System Sciences* **7** (4), 436-446.

Schulze, E.D. 1990. Die Wirkungen von Luftverunreinigungen auf Waldökosysteme, *Chemie in unserer Zeit* **24**, 117-130.

Seip, H.M., Andersen, D.O., Christophersen, N., Sullivan, T.J. & Vogt, R.D. 1989. Variations in concentrations of aqueous aluminium and other chemical species

during hydrological episodes at Birkenes, southernmost Norway, *Journal of Hydrology* **108**, 387-405.

Semenov, M., Bashkin, V. & Sverdrup, H. 2001. Critical loads of acidity for forest ecosystems of North Asia, *Water Air and Soil Pollution* **130**, 1193-1198.

Skeffington, R.A. 2006. Quantifying uncertainty in critical loads: (A) Literature review, *Water Air and Soil Pollution* **169**, 3-24.

Skeffington, R.A., Whitehead, P.G. & Abbott, J. 2006. Quantifying uncertainty in critical loads: (B) Acidity mass balance critical loads on a sensitive site, *Water Air and Soil Pollution* **169**, 25-46.

Skeffington, R.A., Whitehead, P.G., Heywood, E., Hall, J.R., R.A., W. & Reynolds, B. 2007. Estimating uncertainty in terrestrial critical loads and their exceedances at four sites in the UK, *Science of the Total Environment* **382**, 199-213.

Slootweg, J., Hettelingh, J.-P., Tamis, W. & 't Zelfde, M. 2005. Harmonizing European land cover maps, in Posch, M., Slootweg, J. and Hettelingh, J.-P. (Eds.), *European Critical Loads and Dynamic Modelling: CCE Report 2005*, Bilthoven, pp. 171.

Slootweg, J., Posch, M. & Hettelingh, J.-P. 2007. *Critical loads of nitrogen and dynamic modelling: CCE Progress Report 2007*. MNP Report 500090001, Bilthoven, Netherlands. pp 201.

Smith, W.H. 1981. Air Pollution and Forests. Interactions between Air Contaminants and Forest Ecosystems, New York, Heidelberg, Berlin.

Solberg, S., Dobbertin, M., Reinds, G.J., Lange, H., Andreassen, K., Fernandez, P.G., A., H. & De Vries, W. 2009. Analyses of the impact of changes in atmospheric deposition and climate on forest growth in European monitoring plots: A stand growth approach, *Forest Ecology and Management* **258**, 1735–1750.

Spiecker, H., Mielikäinen, K., Köhl, M. & Skovsgaard, J.P. 1996. Growth trends in European forests, Springer-Verlag, Berlin, Heidelberg, 372 pp.

Starr, M. 1999. WATBAL: a model for estimating monthly water balance components, including soil water fluxes, in Kleemola, S. and Forsius, M. (Eds.), *8th*

Annual report 1999. UN ECE ICP Integrated Monitoring., The Finnish Environment 325. Finnish Environment Institute, Helsinki, Finland, pp. 31-35.

Stefan, K., Fürst, A., Hacker, R. & Bartels, U. 1997. Forest Foliar Condition in Europe. Results of large-scale foliar chemistry surveys (survey 1995 and data from previous years). EC-UN/ECE, Brussels, Geneva, 207 pp.

Stolbovoi, V. & Savin, I. 2002. Maps of soil characteristics, in Stolbovoi, V. and McCallum, I. (Eds.), *Land resources of Russia.*, Laxenburg, Austria: Institute for Applied Systems Analysis and the Russian Academy of Science ;CD-ROM. Distributed by the National Snow and Ice Data Center/World Data Center for Glaciology, Boulder.

Strengers, B., Leemans, R., Eickhout, B., De Vries, B. & Bouwman, A. 2005. The land-use projections and resulting emissions in the IPCC SRES scenarios scenarios as simulated by the IMAGE 2.2 model *GeoJournal* **61**, 381-393.

Suutari, R., Amann, M., Cofala, J., Klimont, Z., Posch, M. & Schöpp, W. 2001. From economic activities to ecosystem protection in Europe. CIAM/CCE Report 1/2001, IIASA, Laxenburg, Austria., 57 pp.

Sverdrup, H. & De Vries, W. 1994. Calculating critical loads for acidity with the simple mass balance method, *Water Air and Soil Pollution* **72** (1/4), 143-162.

Sverdrup, H., Martinson, L., Alveteg, M., Moldan, F., Kronnäs, V. & Munthe, J. 2005. Modeling recovery of Swedish ecosystems from acidification, *Ambio* **34** (1), 25-31.

Swart, R., Amann, M., Raes, F. & Tuinstra, W. 2004. A Good Climate for Clean Air: Linkages between Climate Change and Air Pollution. An Editorial Essay, *Climatic Change* **66** (3), 263-269.

Syri, S., Suutari, R. & Posch, M. 2000. From emissions in Europe to critical load exceedances in Finland -- uncertainty analysis of acidification integrated assessment, *Environmental Science & Policy* **3** (5), 263-276.

Syri, S., Amann, M., Capros, P., Mantzos, L., Cofala, J. & Klimont, Z. 2001. Low-CO2 energy pathways and regional air pollution in Europe, *Energy Policy* **29** (11), 871-884.

Tamm, C.O., Aronsson, A. & Popovic, B. 1995. Nitrogen saturation in a long-term forest experiment with annual additions of nitrogen, *Water Air and Soil Pollution* **85**, 1683-1688.

Tarrasón, L., Fagerli, H., Jonson, J.E., Simpson, D., Benedictow, A., Klein, H., Vestreng, V., Aas, W. & Hjellbrekke, A.-G. 2007. Transboundary acidification, eutrophication and ground level ozone in Europe in 2005. EMEP Report 1/2007, Norwegian Meteorological Institute, Oslo, Norway.

Tegen, I. & Fung, I. 1995. Contribution to the atmospheric mineral load from land surface modification, *Journal of Geophysical Research* **100**, 18707-18726.

Thimonier, A., Dupouey, J.L. & Timbal, J. 1992. Floristic changes in the herb-layer vegetation of a deciduous forest in the Lorraine plain under the influence of atmospheric deposition, *Forest Ecology and Management* **55**, 149-167.

Tiktak, A. & Van Grinsven, J.J.M. 1995. Review of sixteen forest-soil-atmosphere models, *Ecological Modelling* **83**, 35-54.

Tognetti, R., Cherubini, P. & Innes, J.L. 2000. Comparative stem-growth rates of Mediterranean trees under background and naturally enhanced ambient CO2 concentrations, *New Phytologist* **146** (1), 59-74.

UBA 2004. Manual on methodologies and criteria for modelling and mapping critical loads & levels and air pollution effects, risks and trends, UNECE Convention on Long-range Transboundary Air Pollution, Federal Environmental Agency (Umweltbundesamt), Berlin.

Ulrich, B., Mayer, R. & Khanna, P.K. 1979. Die Deposition von Luftverunreinigungen und ihre Auswirkungen in Waldökosystemen im Solling, Schriften aus der Forstl. Fak. d. Univ. Göttingen und der Nieders. Vers. Anst. Bd. 58, 291 pp.

Ulrich, B., Mayer, R. & Khanna, P.K. 1980. Chemical changes due to acid precipitation in a loess-derived soil in Central Europe, *Soil Science* **130**, 193-199.

Ulrich, B. 1983. Soil acidity and its relations to acid deposition, in Ulrich, B. and Pankrath, J. (Eds.), *Effects of Accumulation of Air Pollutants in Forest Ecosystems*, Reidel Publ. Co., Dordrecht, the Netherlands, pp. 127-146.

Ulrich, B. & Pankrath, J. 1983. Effects of Accumulation of Air Pollutants on Forest Ecosystems, D. Reidel Publ. Co., Dordrecht, The Netherlands, 389 pp.

Van Breemen, N., Mulder, J. & Driscoll, C.T. 1983. Acidification and alkalinization of soils, *Plant and Soil* **75**, 283-308.

Van Breemen, N., Driscoll, C.T. & Mulder, J. 1984. Acidic deposition and internal proton sources in acidification of soils and waters, *Nature* **307**, 599-604.

Van der Salm, C., Kros, J., Groenenberg, J.E., De Vries, W. & Reinds, G.J. 1995. Application of soil acidification models with different degrees of process aggregation on an intensively monitored spruce site, in Trudgill, S.T. (Ed.), *Solute modelling in catchment systems*, John Wiley, Chichester, UK, pp. 327-346.

Van der Salm, C. 1999. Weathering of forest soils, Thesis, University of Amsterdam, Amsterdam, 287 pp.

Van der Salm, C. 2001. Assessment of the regional variation in weathering rates of loess and clay soils in the Netherlands, *Water Air and Soil Pollution* **131** (1/4), 217-243.

Van der Salm, C. & De Vries, W. 2001. A review of the calculation procedure for critical acid loads for terrestrial ecosystems, *Science of the Total Environment* **271** (1-3), 11-25.

Van Dobben, H.F., Van Hinsberg, A., Schouwenberg, E.P.A.G., Jansen, M., Mol-Dijkstra, J.P., Wieggers, H.J.J., Kros, J. & De Vries, W. 2006. Simulation of Critical Loads for Nitrogen for Terrestrial Plant Communities in The Netherlands, *Ecosystems* **9** (1), 32-45.

Van Loon, M., Tarrason, L. & Posch, M. 2005. Modelling base cations in Europe. EMEP Technical Report MSC-W 2/2005, Oslo, 47 pp.

Van Mechelen, L., Groenemans, R. & Van Ranst, E. 1997. Forest soil condition in Europe: Results of a Large-Scale Soil Survey, EC-UN/ECE, Brussels, Geneva, 261 pp.

Van Oijen, M., Rougier, J. & Smith, R. 2005. Bayesian calibration of process-based forest models: bridging the gap between models and data, *Tree Physiology* **25** (7), 915-927.

Van Scholl, L., Keltjens, W.G., Hoffland, E. & Van Breemen, N. 2004. Aluminium concentration versus the base cation to aluminium ratio as predictors for aluminium toxicity in Pinus sylvestris and Picea abies seedlings, *Forest Ecology and Management* **195** (3), 301-309.

Van Vuuren, D.P., Cofala, J., Eerens, H.E., Oostenrijk, R., Heyes, C., Klimont, Z., den Elzen, M.G.J. & Amann, M. 2006. Exploring the ancillary benefits of the Kyoto Protocol for air pollution in Europe, *Energy Policy* **34** (4), 444-460.

Veroustraete, F., Sabbe, H. & Eerens, H. 2002. Estimation of carbon mass fluxes over Europe using the C-Fix model and Euroflux data, *Remote Sensing of Environment* **83** (3), 376-399.

Vesterdal, L. 1999. Influence of soil type on mass loss and nutrient release from decomposing litter of beech and Norway spruce, *Canadian Journal of Forest Research* **29**, 95-105.

Visual Numerics 1997. 'IMSL Stat/Library, Volume 1', Houston.

Vrugt, J.A., O Nuallain, B., Robinson, B.A., Bouten, W., Dekker, S.C. & Sloot, P.M.A. 2006. Application of parallel computing to stochastic parameter estimation in environmental models, *Computers & Geosciences* **32** (8), 1139-1155.

Wang, K.Y. 1996. Canopy CO_2 exchange of Scots pine and its seasonal variation after four-year exposure to elevetaed CO_2 and temperature, *Agricultural and Forest Meteorology* **82**, 1-27.

Warfvinge, P. & Sverdrup, H. 1992. Calculating critical loads of acid deposition with PROFILE – a steady-state soil chemistry model, *Water Air and Soil Pollution* **63**, 119-143.

Warfvinge, P., Falkengren-Grerup, U., Sverdrup, H. & Andersen, B. 1993. Modelling long-term cation supply in acidified forest stands, *Environmental Pollution* **80**, 209-221.

Wright, R.F. & Jenkins, A. 2001. Climate change as a confounding factor in reversibility of acidification: RAIN and CLIMEX projects, *Hydrology and Earth System Sciences* **5**, 477-486.

Wright, R.F., Aherne, J., Bishop, K., Camarero, L., Cosby, B.J., Erlandsson, M., Evans, C.D., Forsius, M., Hardekopf, D.W., Helliwell, R., Hruska, J., Jenkins, A., Kopácek, J., Moldan, F., Posch, M. & Rogora, M. 2006. Modelling the effect of climate change on recovery of acidified freshwaters: Relative sensitivity of individual processes in the MAGIC model, *Science of the Total Environment* **365** (1-3), 154-166.

Zak, S.K. & Beven, K.J. 1999. Equifinality, sensitivity and predictive uncertainty in the estimation of critical loads, *Science of the Total Environment* **236**, 191-214.

Summary

Background

The deposition of acidifying compounds has led to acidification of soils and surface waters in Europe. The large amounts of sulphur (S) and nitrogen (N) that entered the ecosystems caused a depletion of base cations and a release of toxic aluminium in poorly buffered soils. Clear harmful effects were observed in surface waters, were sensitive fish species were lost in the 1970s and 1980s. In forest soils, buffer capacity declined and the forests became more vulnerable to stresses due to, for example, acid and nitrogen induced nutrient imbalances. Excessive nitrogen inputs have led to changes in vegetation in many European countries, and to eutrophication of surface waters.

As a result of the observed relationship between air pollution and acidification of soils and waters, a number of international emission reduction protocols were signed over the last decades. These protocols have been successful: compared to 1960, the European emissions of SO_x have been reduced by more than 60%, emissions of NO_x by about 40% and those of ammonia by 17%. The protocols are, amongst others, based on a comparison of data on ecosystem vulnerability to acidification and eutrophication under current deposition. Ecosystem vulnerability is expressed using critical loads, i.e. the deposition that according to present knowledge and on an infinite time-scale does not lead to significant harmful effects on the ecosystem; where critical loads are exceeded, the ecosystem is at risk and deposition should be reduced. Numerous soil acidification models have been developed in the past, but most of them have been applied to plots or regions only. Calibration on large regional data sets was often lacking. In this thesis a simple soil acidification model is described that was developed, calibrated and tested on 182 forest monitoring sites and applied to Europe and Northern Asia.

Development of the simple dynamic acidification model VSD

Although critical loads characterise the vulnerability of ecosystems, they do not provide any information on the time-path of their recovery if deposition is reduced to or below critical load. For such evaluations, dynamic soil models are required. In chapter 2 of this thesis we describe such a model. The Very Simple Dynamic (VSD) model is the simplest extension of the steady-state Simple Mass Balance (SMB) model into a dynamic model by including cation exchange and time-dependent N immobilisation; in steady-state mode, VSD equals SMB. SMB has been widely used to compute critical loads for Europe. The VSD model can be used to evaluate time paths of deposition, which follow from international agreements, with respect to their effects on the dynamics in soil acidity and nutrient status. It can thus be used to compute the time needed before a ecosystem is 'safe', by computing the time-trend in soil chemical criteria such as the ratio between

aluminium and base cations (Al/Bc) in the soil solution, the Acid Neutralizing Capacity (ANC) or the nitrate concentration. The VSD model can also be used to compute target loads. A target load is the deposition which ensures that a prescribed chemical criterion (e.g., the Al/Bc ratio) is achieved in a given year; it is only required if neither the current deposition nor the critical load will lead to timely recovery. Target loads are stricter than critical loads because a time-limit is set for recovery: the target year. VSD also comes with an extended graphical user interface that facilitates the use of all the above-mentioned functionalities and includes procedures for calibration of the model. Chapter 2 outlines the design principles and basic equations of VSD and shows examples of its functionality and user interface.

Calibration of VSD and quantification of parameter uncertainty

The calibration of VSD is described in chapter 3. Because VSD simulates soil solution concentrations as a function of atmospheric inputs and soil processes, it can be calibrated and/or validated on plots where such measurements are available. Until recently, calibration of most dynamic acidification models was performed by fitting the simulation results to (a series of) observations by 'trial and error' procedures: the model is re-run with different settings until the observation(s) are reproduced well. Sometimes a set of parameters is calibrated using various soil (solution) concentrations simultaneously, whereas in other studies only one parameter, such as the base saturation, was calibrated. Most studies did not consider the uncertainty in the observations and model input parameters: only the run that provided the best estimate of the observations defined the calibrated parameter set. It is clear, however, that observations of soil solution concentrations are uncertain, mainly due to spatial variation within a plot. Calibration methods that include these uncertainties and interactions are thus preferred over methods that use a simple fit through a (set of) observation(s) yielding one set of calibrated parameters without their uncertainty. In recent years, Bayesian calibration methods have been used for calibration of ecosystem models. They combine probability distributions of model parameters, based on prior assumptions about their magnitude and uncertainty, with estimates of the likelihood of the simulation results in view of the observed, uncertain values for model output variables. They use the combined information to quantify uncertainty in parameters and the updated parameter uncertainty can be used to perform an analysis of model output uncertainty. The most important VSD model parameters were calibrated with such a Bayesian approach, using data from 182 intensively monitored forest sites in Europe. Out of these 182 plots, 122 plots were used to calibrate VSD and the remaining 60 plots to validate the calibrated model.

Prior distributions for the model parameters were based on available literature. Since this literature shows a strong dependence of some VSD parameters on, for example, soil texture, prior distributions were allowed to depend on soil group (i.e. soils with similar texture or C/N ratio). The likelihood was computed by comparing modelled soil solution concentrations with observed concentrations for the period 1996-2001. Markov Chain Monte Carlo (MCMC) was used to sample the posterior parameter space. Two calibration approaches were applied. In the singe-site calibration, the plots were calibrated separately to obtain plot-specific posterior distributions. In the multi-site approach priors were assumed spatially constant for each soil group, and all plots in a soil group were calibrated simultaneously yielding one posterior probability distribution. Results from the single-site calibrations showed that the model performed much better after calibration compared to a run with standard input parameters when validated on the 60 validation plots. Posterior distributions for H-Al equilibrium constants narrowed down, thus decreasing parameter uncertainty. For base cation weathering of coarse textured soils the posterior distribution shifted to larger values, indicating an initial underestimation of the weathering rate for these soils. Results for the parameters related to nitrogen modelling showed that the relationship between nitrogen immobilization and the C/N ratio of the soil, as assumed in VSD, was not substantiated by the validation. The multi-site calibration also strongly decreased model error for most model output parameters, but it was somewhat larger than the median model error from the singe-site calibration except for nitrate. Because the large number of plots calibrated at the same time provided very many observations and we do not include a model error term in the computation of the likelihood, the Markov Chain converged to a very narrow parameter space, leaving little room for posterior parameter uncertainty.

Uncertainties in critical loads and target loads that stem from parameter uncertainty

Modelled critical loads and target loads are uncertain, caused by uncertainty in (a) model structure and model assumptions (b) input data and model parameters and (c) the value of the chemical criterion used. To asses the uncertainty caused by uncertainty in input data and model parameters, VSD was calibrated with the Bayesian approach described in chapter 3 using prior probability functions of all model parameters. By sampling the posterior distributions obtained from the calibration, uncertainty analyses were carried out. Chapter 4 shows which parameters contribute most to the uncertainty in the model output; and this varies with the type of critical load and chemical criterion used. Base cation input by weathering and deposition, and the parameters describing the H-Al equilibrium in

the soil solution mainly determine the uncertainty in the maximum critical loads for S, $CL_{max}(S)$, when based on the widely used aluminium to base cation (Al/Bc) criterion. Uncertainty in $CL_{max}(S)$ based on an ANC criterion is completely determined by base cation inputs alone. The denitrification fraction is the most important source of uncertainty for the maximum critical loads of N, $CL_{max}(N)$. N uptake and N immobilisation determine the uncertainties in the critical load for N as a nutrient, $CL_{nut}(N)$. Calibration of VSD reduced the uncertainty in critical loads and target loads: the coefficient of variation (CV) was reduced for all critical loads and criteria. After calibration, the CV for $CL_{max}(S)$ was below 0.4 for almost all plots; however for $CL_{max}(N)$ high values occurred for plots with a high denitrification rate. Model calibration improved the robustness of the need for target loads: after calibration, no target loads were needed in any of the simulations for 40% of the plots, with the uncalibrated model there was a positive probability for the need of a target load for almost all plots. The uncertainty assessments were carried out for the 182 plots in Europe. The next step would be to investigate the uncertainties at a European scale.

Quantification of the effect of the chemical criterion on critical loads: model application for Europe and northern Asia

In recent years, high-resolution data bases have become available for soils, land cover, climate and forest growth. These data bases provide much more spatial detail for Europe and Northern Asia than those used in previous studies. In addition to the need to use more recent data, it has been suggested that chemical criteria other than the widely used Al/Bc ratio could be used for the computation of critical loads of acidity for soils. Several national studies have shown that the choice of the chemical criterion can have a strong influence on critical load values and on critical load exceedances. Similarly a recent study showed that the widely used nutrient nitrogen limit of 0.2-0.3 mg N L^{-1} related to vegetation changes in forests is applicable for Scandinavia but not for Western Europe. Finally, in recent years the (mostly) Asian part of the UNECE region – termed EECCA (Eastern Europe, Caucasian and Central Asian) countries – as well as Cyprus and Turkey have become more involved in the work under the LRTAP Convention, necessitating the extension of critical load computations to these countries. Critical loads for acidity and nutrient nitrogen for terrestrial ecosystems were computed using detailed data bases for Europe and Northern Asia with VSD in steady-state (SMB), while investigating the sensitivity of the results to the chemical criterion used; the results are described in chapter 5.

A sensitivity analysis of critical loads was performed by employing different chemical criteria. The computed critical loads were in accordance with critical

loads from previous global empirical studies, but have a much higher spatial resolution. In this chapter we also introduce the concept of equivalent criteria: the values for the various criteria leading to the same critical load function. A critical limit based on an ANC of zero resulted in critical loads that protect ecosystems against toxic concentrations of aluminium and unfavourable Al/Bc ratios, suggesting that ANC could be an alternative to the commonly used Al/Bc ratio. Critical loads of nutrient nitrogen are sensitive to the specified critical nitrate concentration, especially in areas with a high precipitation surplus. If limits of 3–6 mg N L^{-1} are used for Western Europe instead of the widely used 0.2 mg N L^{-1}, critical loads double on average. In low precipitation areas, the increase is less than 50%. The strong dependence on precipitation surplus is a consequence of the simple modelling approach. We therefore suggest that future models should explore other nitrogen parameters (such as nitrogen availability) instead of leaching as the factor influencing vegetation changes in terrestrial ecosystems.

Recovery from soil acidification in Europe under climate change

Although it is now well established that the climate is changing and will continue to change in the future and recent studies have shown that observed climate change over the last decades accelerates and is consistent with the highest climate change projections, all European-wide simulations of recovery from soil acidification so far have assumed a constant climate. Since European forest ecosystems have many functions, related to biodiversity, forest products, ground water protection and carbon sequestration, it is crucial to know to what extent the current legislation on air pollution control protects them against acidification and eutrophication under climate change. In chapter 6 we evaluated the effects of sulphur and nitrogen emission reductions on the recovery of acidified European forest soils, and also included the effects of climate change on soil solution chemistry, by modelling temperature effects on soil chemical processes and including temperature and precipitation effects on nitrogen uptake and on leaching. It should be noted that although we modified VSD such that formerly fixed processes became climate-dependent, the model was not explicitly developed to include (all) climate-sensitive processes and therefore final conclusions on the impact of climate change on soil acidification cannot be drawn from this study.

The VSD model was parameterized using the results from the Bayesian calibration described in chapter 3. Model results show a strong effect of the emission reduction scenarios on soil solution chemistry. Using the Current Legislation (CLE) scenario, the forest area in Europe with soil solution Al/Bc>1 mol mol^{-1} (a widely used critical limit) decreased from about 4% in 1990 to about 1.7% in 2050. Under Maximum Feasible Reductions (MFR), the exceeded area was < 1% in 2050. In

addition, the area where limits for the nitrate concentration in soils are violated was predicted to be smaller under MFR than under CLE. Using the most stringent criterion for nitrate ($[NO_3]<0.3$ mg L^{-1}), the area with nitrate concentrations in excess of the critical limit was about 33% in 2050 under CLE, but only 12% under MFR. Recovery, i.e. attaining non-violation of the criterion, was also much faster under MFR than under CLE. Climate change leads to higher weathering rates and nitrogen uptake in the model, but positive effects on recovery from acidification are limited compared to current climate, and differences between the A1 and B2 climate change scenarios were small. Target loads for 2050 exist for 4% of the area for Al/Bc=1 and for 12% of the area when using a criterion of ANC=0 for the soil solution. In about 30% of the area where a meaningful target loads exists, the computed target load was lower than the deposition under MFR, and thus cannot be attained with current emission abatement technologies.

Synthesis

The data from the combined EU/UNECE Forest Intensive Monitoring programme have proven to be very valuable for calibration of the VSB model. Soil solution measurements were used to determine how well the model was able to reproduce the situation in the field. The analysis of the data from the large amount of plots, that have a reasonable spatial coverage over Europe, has proven that these data support the parameterisation and use of a model designed for regional assessments. More observations and longer time-series will improve these applications, as such monitoring with standardized methods should be continued, and data should be made available to the modellers.

Finally, the emission reduction policies for acidifying compounds in Europe have been very successful. Not only have major emission reductions been achieved, but the use of ecosystem sensitivity expressed by critical loads has lead to deposition reductions in those areas where the most vulnerable ecosystems occur. Our model simulations show that if sufficient emission abatement technologies are applied, recovery from acidification in Europe can be achieved in 2050. Maybe this successful approach could serve as an example for dealing with other environmental issues such as biodiversity loss and greenhouse gas emissions.

Samenvatting

Achtergrond

Zure regen heeft in Europa geleid tot verzuring van bodems en oppervlaktewater. De grote hoeveelheden zwavel (S) en stikstof (N) die via de lucht in de ecosystemen terecht kwamen hebben in verzuringsgevoelige gronden een uitloging van basische kationen (Bc) zoals calcium (Ca), magenesium (Mg) en kalium (K) en het vrijkomen van toxisch aluminium (Al) veroorzaakt. In bosbodems nam de buffercapaciteit af en de bossen werden gevoeliger voor stress als gevolg van, bijvoorbeeld, verstoorde nutriëntenbalansen veroorzaakt door een teveel aan stikstof in de bodem. Deze overmaat aan stikstof veroorzaakte ook veranderingen in natuurlijke vegetaties (meer stikstofminnende soorten). In oppervlaktewater zijn duidelijke schadelijke effecten waargenomen als gevolg van verzuring: in de jaren 70 en 80 trad, vooral in Scandinavië, grote sterfte op onder gevoelige vissoorten. Overmaat aan stiktof leidde lokaal tot eutrofiëring van oppervlaktewater

Om de verzuring van bossen en oppervlaktewater terug te dringen, is er de afgelopen decennia een aantal internationale overeenkomsten gesloten om de uitstoot van verzurende stoffen te verminderen. Met succes: in vergelijking met 1960 is de totale uitstoot van SO_x in Europa met meer dan 60% afgenomen, de uitstoot van NO_x met ongeveer 40% en die van NH_3 (ammoniak) met 17%. De internationale overeenkomsten zijn, onder andere, gebaseerd op een vergelijking van de gevoeligheid van ecosystemen voor verzuring en eutrofiëring met de huidige depositie van S en N. De gevoeligheid van ecosystemen wordt uitgedrukt door middel van het kritisch depositieniveau: de hoeveelheid depositie die volgens de huidige kennis en op een oneindige tijdschaal niet leidt tot significant schadelijke effecten. Daar waar de huidige depositie het kritische depositieniveaus overschrijdt, wordt het ecosysteem bedreigd en moet de depositie worden verminderd. Kritische depositieniveaus worden meestal berekend met een computermodel dat de bodemverzuring simuleert. Aan elk kritisch depositieniveau ligt een kritische waarde voor een chemisch criterium ten grondslag: er wordt verondersteld dat er geen schadelijke effecten optreden als bijvoorbeeld de verhouding tussen Al en Bc (Al/Bc) in het bodemvocht kleiner of gelijk is aan 1 mol mol^{-1}, of wanneer het zuurbufferend vermogen (ANC) groter of gelijk is aan 0 eq l^{-1}. Bij een depositie gelijk aan het kritisch depositieniveau zal de waarde van het chemische criterium in een uiteindelijke evenwichtssituatie in de bodem precies gelijk zijn aan de kritische waarde en zullen er dus geen schadelijke effecten optreden.

Er zijn vele bodemverzuringsmodellen ontwikkeld, maar de meeste daarvan zijn alleen toegepast op puntlocaties en/of regio's en bovendien zijn de modellen zelden gecalibreerd op grote, regionale datasets. Het doel van dit proefschrift was

om (a) na te gaan of beschikbare gegevens uit Europese bosmonitorings-programma's kunnen worden gebruikt om een eenvoudig bodemverzuringsmodel te calibreren (b) op basis van de calibratie na te gaan hoe onzeker de modeluitmosten zijn en of deze onzekerheid door modelcalibratie afneemt (c) het model toe te passen op Europa en Noord Azië en (d) vast te stellen of de afname van zure depositie leidt to herstel van bodemverzuring in Europa en na te gaan of klimaatverandering daar een invloed op heeft.

Ontwikkeling van het eenvoudige dynamisch verzuringsmodel VSD
Kritische depositieniveaus zijn een maat voor de verzuringsgevoeligheid van ecosystemen maar zeggen niets over het verloop van het herstel van ecosystemen als de depositie wordt verminderd tot een niveau dat gelijk is aan, of lager dan, het kritisch depositieniveau. Hiervoor is een dynamisch model nodig. In hoofdstuk 2 van dit proefschrift wordt een dergelijk model beschreven. Dit VSD (Very Simple Dynamic) model is de eenvoudigst denkbare dynamische versie van het veel gebruikte model voor de berekening van kritische depositieniveaus, SMB (Steady State Mass Balance model). Door toevoeging van kationuitwisseling en tijdsafhankelijke stikstofvastlegging in de bodem kunnen met VSD dynamische berekeningen worden uitgevoerd. Het VSD model kan de effecten van verminderde depositie op de bodem uitrekenen, door simulatie van zuurgraad en stikstofconcentraties in het verloop van de tijd. Het kan ook worden gebruikt om uit te rekenen hoelang het duurt voordat een ecosysteem 'veilig' is, door simulatie van tijdreeksen van Al/Bc, ANC en de nitraatconcentratie. Voor al deze chemische criteria zijn kritische waardes vastgesteld: wanneer de waarde van het criterium beneden deze kritische waarde komt (en blijft), is het systeem 'veilig'. Daarnaast kan VSD zogenaamde streefwaardes berekenen. Een streefwaarde is die depositie die leidt tot het halen van een bepaald chemisch criterium in de bodem, zoals Al/Bc=1, in een vooraf gedefinieerd jaar. Streefwaardes zijn alleen nodig als noch de huidige depositie noch het kritisch depositieniveau leiden tot tijdig (chemisch) herstel van het ecosysteem. Streefwaardes zijn stringenter dan kritisch depositieniveaus omdat er een tijdslimiet voor het herstel wordt gedefinieerd: het streefjaar. Het VSD model heeft een uitgebreide gebruikersinterface die het gebruik van alle bovengenoemde functionaliteit sterk vereenvoudigt, en bevat mogelijkheden om het model te calibreren op metingen uit het veld.
In hoofdstuk 2 wordt een inhoudelijke beschrijving van het VSD model gegeven, tevens zijn er voorbeelden opgenomen van de modelfunctionaliteit en de gebruikersinterface.

Calibratie van VSD en kwantificering van parameteronzekerheid

De calibratie van het VSD model wordt beschreven in hoofdstuk 3. Doel van de calibratie is om een zo goed mogelijke schatting te maken van modelparameters die niet of moeilijk te meten zijn, zoals de verweringssnelheid van basische kationen in de bodem en de constanten die de uitwisseling van protonen (H) en Al met basische kationen bepalen. Door het model met verschillende waardes voor deze parameters toe te passen, en de modelresultaten te vergelijken met metingen, kan worden vastgesteld met welke parameterwaardes acceptabele simulaties worden bereikt. VSD simuleert de bodemvochtsamenstelling als functie van de aan- en afvoer van verschillende ionen, en kan dus worden gecalibreerd en gevalideerd op locaties waar dergelijke metingen aanwezig zijn. Tot voor kort werden de meeste bodemverzuringsmodellen gecalibreerd door de simulaties te fitten op een (reeks) waarnemingen via een 'trial-and-error' procedure: het model werd een groot aantal keren toegepast met steeds wisselende parameterwaardes totdat de meting(en) goed gereproduceerd werden. Soms werd een set parameters gelijktijdig gecalibreerd op verschillende bodemvochtconcentraties, terwijl in andere studies alleen de basenverzadiging werd gecalibreerd. In de meeste studies is de onzekerheid in de metingen buiten beschouwing gelaten: de parameterwaardes worden afgeleid uit die éne modeltoepassing die het beste overeenkomt met de waarnemingen. Metingen van bodemvochtconcentraties zijn echter onzeker, door bijvoorbeeld ruimtelijke variatie binnen een locatie. Calibratiemethodes die rekening houden met deze onzekerheid zijn dus te verkiezen boven methodes die bestaan uit het eenvoudigweg fitten van een modelsimulatie door een (set van) waarneming(en), en die daarbij slechts één set van modelparameters zonder de bijbehorende onzekerheid leveren.

Recentelijk zijn Bayesiaanse calibratiemethodes gebruikt om ecosysteemmodellen te calibreren. Deze methodes combineren kansverdelingen van modelparameters, gebaseerd op a-priori schattingen van hun gemiddelde en onzekerheid, met schattingen van de aannemelijkheid van de modeluitkomsten op basis van een vergelijking met (onzekere) metingen. De methode gebruikt deze gecombineerde informatie om een uiteindelijke a-posteriori verdeling te maken van de modelparameters inclusief de bijbehorende onzekerheid en correlaties.

In deze studie zijn de belangrijkste modelparameters van VSD gecalibreerd en gevalideerd met een Bayesiaanse methode op basis van gegevens van 182 intensief gemonitorde boslocaties in Europa (het EU/UNECE Forest Intensive Monitoring programma). Uit deze set van 182 locaties, zijn 122 locaties gebruikt om het model te calibreren en de overige 60 locaties om het gecalibreerde model te valideren. A-priori verdelingen van modelparameters werden vastgesteld op basis van literatuurgegevens. Omdat uit de literatuur blijkt dat er een sterke samenhang

bestaat tussen een aantal van deze VSD modelparameters en bijvoorbeeld bodemtextuur, zijn de a-priori verdelingen gedefinieerd als functie van bodemgroep (zijnde bodems met een gelijke textuur of koolstof/stiktof (C/N) verhouding). De aannemelijkheid van de modeluitkomsten is berekend door deze te vergelijken met gemeten bodemvochtconcentraties uit de periode 1996-2001. Trekkingen van parameterwaardes uit de meerdimensionale parameterruimte verliep via een 'Markov Chain Monte Carlo' (MCMC) methode. Er werden twee verschillende calibratiemethodes gebruikt. In de 'single-site' calibratie werd elke plot afzonderlijk gecalibreerd en plotspecifieke sets met modelparameters vastgesteld. In de 'multi-site' calibratie werd verondersteld dat de modelparameters ruimtelijk constant zijn binnen een bodemgroep. Dit levert één set met a-posteriori parameterschattingen per bodemgroep. Het via de 'single-site' methode gecalibreerde model is vervolgens toegepast op de 60 validatie plot. De resultaten laten zien dat het gecalibreerde model pH en de nitraatconcentratie betere simuleert dan het ongecalibreerde model. De uiteindelijke kansverdelingen voor de H-Al evenwichtsconstante waren na calibratie aanzienlijk smaller dan ervoor: de onzekerheid is afgenomen. De kansverdeling van de verwerings-snelheid van basische kationen voor zandgronden is opgeschoven naar hogere waardes, dit betekent dat de a-priori aangenomen parameterwaarde een onderschatting was. De resultaten van de calibratie gaven geen bevestiging van de in het oorspronkelijke VSD model aangenomen relatie tussen C/N ratio in de bodem en de vastlegging van N in organische stof. Ook het via de 'multi-site' methode gecalibreerde model gaf betere resultaten op de validatielocaties, maar de fout in de simulaties was wel iets groter dan bij de 'single-site' methode. Omdat er gelijktijdig gecalibreerd is op een groot aantal plots met vele metingen, en er geen modelfout is meegenomen in de berekening van de aannemelijkheid van het model, leidt de 'multi-site' calibratie tot zeer nauwe kansverdelingen voor de modelparameters met weinig ruimte voor onzekerheid.

Onzekerheden in kritische depositieniveaus en streefwaardes, veroorzaakt door onzekerheid in modelparameters.

Kritische depositieniveaus zijn onzeker, vanwege onzekerheid in (a) model-structuur en modelaannames (b) invoergegevens en modelparameters en (c) de waarde van het chemische criterium dat wordt gebruikt (onzekerheid in b.v de kritische Al/Bc ratio). De onzekerheid in kritische depositieniveaus en streefwaardes als gevolg van de onzekerheid in modelparameters is vastgesteld door het VSD model te calibreren met een Bayesiaanse methode zoals beschreven in hoofdstuk 3 en vervolgens het model toe te passen met parameterwaardes die werden getrokken uit de a-posteriori kansverdeling. In totaal werden per plot

30000 berekeningen uitgevoerd van kritische depositieniveaus en streefwaardes, waaruit de onzekerheid in de uitkomsten werd afgeleid.
Hoofdstuk 4 laat zien welke modelparameters het meest bijdragen aan de onzekerheid in de uitkomsten; dit varieert per type kritisch depositieniveau en per chemisch criterium dat is gebruikt. De aanvoer van basische kationen via verwering en depositie, en de parameters die het evenwicht tussen H en Al in de bodem bepalen zijn de grootste bron van onzekerheid voor het maximale kritische depositieniveau voor zwavel, $CL_{max}(S)$, wanneer deze is gebaseerd op een kritische Al/Bc ratio in de bodem. Wanneer $CL_{max}(S)$ wordt gebaseerd op het ANC=0 criterium, dan wordt de onzekerheid vrijwel volledig bepaald door de onzekerheid in de aanvoer van basische kationen. De denitrificatiefractie bepaalt voor een groot gedeelte de onzekerheid in het maximale kritische depositieniveau voor stikstof, $CL_{max}(N)$. Opname en de immobilisatie van stikstof zijn verantwoordelijk voor de onzekerheid in het kritische depositieniveau voor stikstof gerelateerd aan eutrofiëring, $CL_{nut}(N)$. Modelcalibratie verkleint de onzekerheid in kritische depositieniveaus en streefwaardes: de variatiecoëfficiënt voor alle typen kritische depositieniveaus en streefwaardes na calibratie was lager dan ervoor. De variatiecoëfficiënt voor $CL_{max}(S)$ was minder dan 40% voor bijna alle locaties, behalve daar waar een hoge denitrificatie optreedt. Modelcalibratie leidt ook tot robuustere schattingen van streefwaardes. Na calibratie bleek er voor 40% van de plots in geen enkele van de 30000 simulaties een streefwaarde nodig te zijn om het chemische criterium in 2050 te halen, terwijl dit vóór calibratie maar voor enkele locaties het geval was. De onzekerheidsanalyse in hoofdstuk 4 is uitgevoerd voor 182 locaties in Europa. De volgende stap is het uitvoeren van een onzekerheidsanalyse op Europese schaal.

Kwantificering van het effect van het chemische criterium op de kritische depositieniveaus: modeltoepassing voor Europa en Noord Azië.
In de afgelopen jaren zijn gedetailleerde databestanden beschikbaar gekomen van bodem, landgebruik, klimaat en bosgroei. Deze bestanden geven veel meer detailinformatie dan de bestanden die eerder zijn gebruikt in studies waarin kritische depositieniveaus voor Europese bossen werden berekend. Daarnaast is gesuggereerd om andere dan het veelgebruikte Al/Bc criterium te gebruiken voor het berekenen van kritische depositieniveaus voor verzuring. Nationale studies hebben aangetoond dat de keuze van het criterium een grote invloed kan hebben op de hoogte van het berekende kritische depositieniveau en de overschrijding daarvan. Verder is een recente studie aangetoond dat de veelgebruikte kritische waarde van 0.2-0.3 mg L^{-1} N in het bodemvocht die ervoor moet zorgen dat er geen vegetatieverandering in de ondergroei van bossen optreedt, toepasbaar is voor

Scandinavië, maar niet voor Centraal en West Europa. Ten slotte zijn de landen uit het Aziatische deel van de UNECE regio – de EECCA (Eastern Europe, Caucasian and Central Asian) landen - samen met Turkije en Cyprus actief geworden binnen de conventie voor Long-range Transboundary Air Pollution (LRTAP), zodat een uitbreiding van het gebied waarvoor kritische depositieniveaus worden berekend nodig was. Kritische depositieniveaus voor Europa en Noord Azië voor verzuring en eutrofiëring en de invloed daarop van het chemische criterium zijn berekend met de statische variant van VSD, het SMB model; de resultaten worden beschreven in hoofdstuk 5. In hoofdstuk 5 introduceren we ook het concept van equivalente criteria: die waardes van verschillende chemische criteria die tot dezelfde kritische depositiefunctie leiden.
De berekende kritische depositieniveaus komen qua grootteorde overeen met waardes gevonden in eerdere studies, maar hebben een veel groter ruimtelijk detailniveau. Het gebruik van het ANC=0 criterium beschermt de ecosystemen tegen te hoge aluminiumconcentraties en te hoge Al/Bc ratio's: het ANC criterium kan dus een alternatief zijn voor de veel gebruikte maar ook bekritiseerde Al/Bc ratio.
Kritische depositieniveaus voor het eutrofiërend effect van stikstof bleken gevoelig voor gebruikte kritische nitraatconcentratie, vooral in gebieden met een hoog neerslagoverschot. Wanneer in West Europa een realistische kritische waarde van 3–6 mg N L^{-1} wordt gebruikt in plaats van de veelgebruikte limiet van 0.2 mg N L^{-1}, worden de kritische depositieniveaus gemiddeld twee keer zo hoog. In gebieden met een laag neerslagoverschot is de toename minder dan 50%. Die sterke maar weinig realistische afhankelijkheid van het neerslagoverschot is een consequentie van de eenvoud van het gebruikte model. Voor toekomstige berekeningen moet worden nagegaan of gebruik kan worden gemaakt van andere stikstofparameters (zoals stikstofbeschikbaarheid) die een betere relatie hebben met vegetatie-veranderingen in terrestrische ecosystemen dan de nitraatconcentratie in het bodemvocht.

Herstel van bodemverzuring in Europa bij klimaatverandering.
Hoewel het inmiddels duidelijk is dat het klimaat verandert en zal blijven veranderen in de toekomst, en recente studies laten zien dat de waargenomen klimaatverandering de laatste tientallen jaren versnelt en consistent is met het meeste extreme scenario, zijn alle tot nu toe uitgevoerde Europese studies naar herstel van bodemverzuring uitgegaan van een constant klimaat. Omdat Europese bossen vele functies hebben, gerelateerd aan biodiversiteit, houtproductie, grondwaterbescherming en koolstofvastlegging, is het cruciaal om te weten of de huidige wetgeving op het gebied van luchtkwaliteit deze bossen ook beschermt

tegen verzuring en eutrofiëring bij klimaatverandering. In hoofdstuk 6 worden de effecten van emissiereductiescenario's voor S en N op het herstel van verzuurde bosbodems in Europa geëvalueerd, en het effect van klimaatverandering hierop bepaald door het inbrengen van temperatuurseffecten op bodemchemische processen en effecten van temperatuur en neerslagveranderingen op de uitspoeling en opname van stikstof. Hierbij moet worden opgemerkt dat hoewel VSD is aangepast zodat processen nu klimaatafhankelijk zijn, het model niet expliciet ontwikkeld was om alle klimaateffecten op de bodemchemie en nutriëntenkringloop te simuleren. Zo is het effect van klimaatverandering op de stikstofkringloop niet ingebracht. Daarom kunnen uit deze studie geen definitieve conclusies over het effect van klimaatverandering op herstel van bodemverzuring worden getrokken.
Het VSD model is geparameteriseerd op basis van de resultaten van de Bayesiaanse calibratie beschreven in hoofdstuk 3, en vervolgens toegepast op Europa. Modelresultaten laten een sterk effect zien van het emissiereductiescenario op de bodemvochtsamenstelling. Onder de huidige wetgeving (CLE, Current Legislation), zal het bosareaal in Europa waar de Al/Bc ratio de waarde van 1 mol mol^{-1} overschrijdt, afnemen van 4% in 1990 tot ongeveer 1.7% in 2050. Als alle beschikbare technologie wordt ingezet (MFR, Maximum Feasible Reductions), neemt het areaal met overschrijdingen af tot minder dan 1% in 2050. Daarnaast is het areaal met overschrijding van de kritische nitraatconcentratie onder MFR kleiner dan onder CLE. Als we het meest strikte criterium gebruiken ($[NO_3]$<0.3 mg L^{-1}), dan is het areaal waar deze waarde in 2050 nog wordt overschreden ongeveer 33% onder CLE en nog maar 12% onder MFR. Het herstel van ecosystemen, gedefinieerd als het moment waarop het chemische criterium beneden de kritische waarde komt, gaat ook veel sneller onder MFR dan onder CLE.
Klimaatverandering leidt in het model tot hogere verweringssnelheden en hogere N opname en dus tot sneller herstel, maar de positieve effecten zijn beperkt en de verschillen tussen de twee klimaatscenario's (A1 en B2) zijn gering. Streefwaardes lager dan kritische depositieniveaus zijn nodig in 4% van het bosareaal om in 2050 Al/Bc = 1 te bereiken en in 12% van areaal voor het bereiken van ANC =0. In ongeveer 30% van dit areaal is deze waarde lager dan de depositie onder het MFR scenario. Dit betekent dat deze depositie niet gehaald kan worden met de huidige emissiereductietechnieken.

Synthese
De gegevens uit het gecombineerde EU/UNECE Forest Intensive Monitoring programma zijn zeer waardevol gebleken bij het calibreren van het VSD model. Metingen van de bodemvochtsamenstelling zijn gebruikt om na te gaan hoe goed

het model in staat was om waarnemingen in het veld te reproduceren. De resultaten laten zien dat na calibratie de modelparameters een nauwere bandbreedte hebben, en de voorspellingen een grotere betrouwbaarheid, dan voor calibratie. De analyse van de gegevens van een groot aantal bosmonitoringlokaties laten zien dat deze gegevens zeer bruikbaar zijn voor de calibratie en toepassing van het VSD model, ontwikkeld voor het uitvoeren van regionale beleidsevaluaties. Omdat meer waarnemingen en langere tijdreeksen deze evaluaties verder zullen versterken, zou het monitorings-programma moeten worden voortgezet met uniforme methodes, en zouden de gegevens eenvoudig toegankelijk moeten zijn voor modelleurs.
Ten slotte: de emissiereductiemaatregelen voor verzurende stoffen in Europa zijn zeer succesvol gebleken. Niet alleen zijn er substantiële reducties behaald, maar het gebruik van kritische depositieniveaus heeft ertoe geleid dat deze reducties plaatsvonden daar waar de gevoeligste ecosystemen voorkomen. Onze modelberekeningen laten zien dat wanneer voldoende emissiereductietechnieken worden ingezet, herstel van bodemverzuring in Europa in 2050 bereikt kan worden. Deze succesvolle benadering kan als voorbeeld dienen voor andere milieuthema's zoals het behoud van biodiversiteit en het terugdringen van broeikasgasemissies.

Color figures

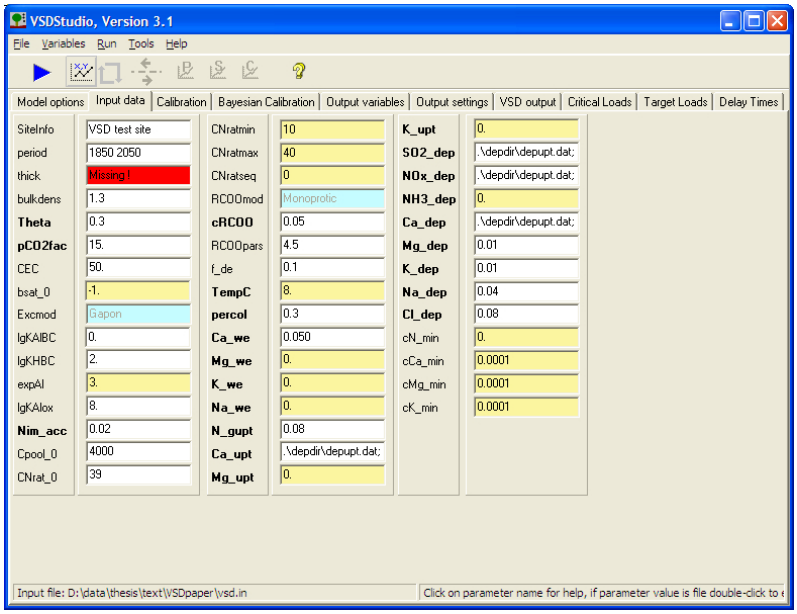

Figure 2.1. Input data screen of VSDStudio.

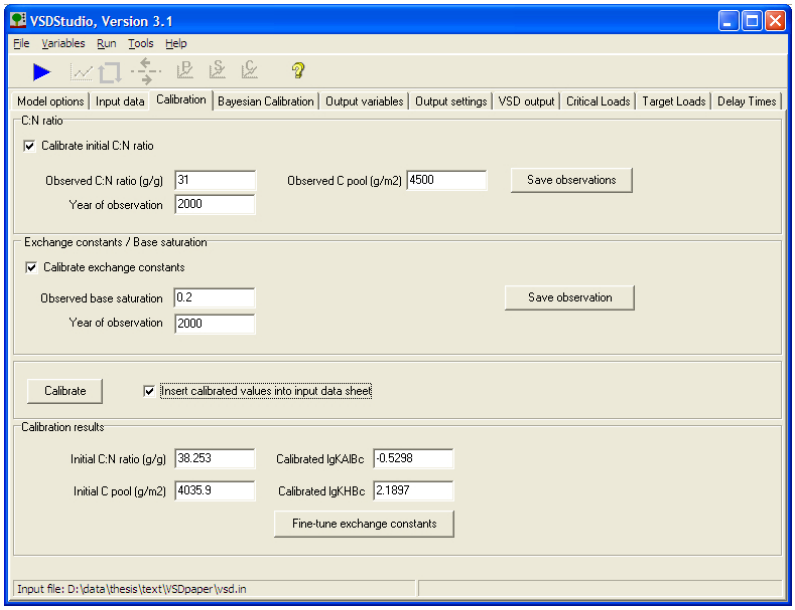

Figure 2.2. Calibration screen of VSDStudio.

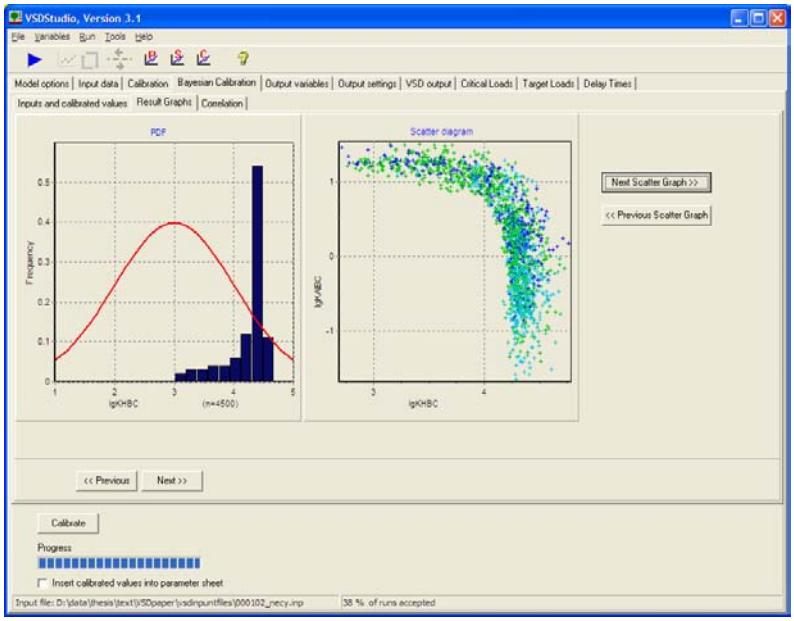

Figure 2.3. Bayesian calibration output screen of VSDStudio.

Figure 2.4. Example model output of VSD.

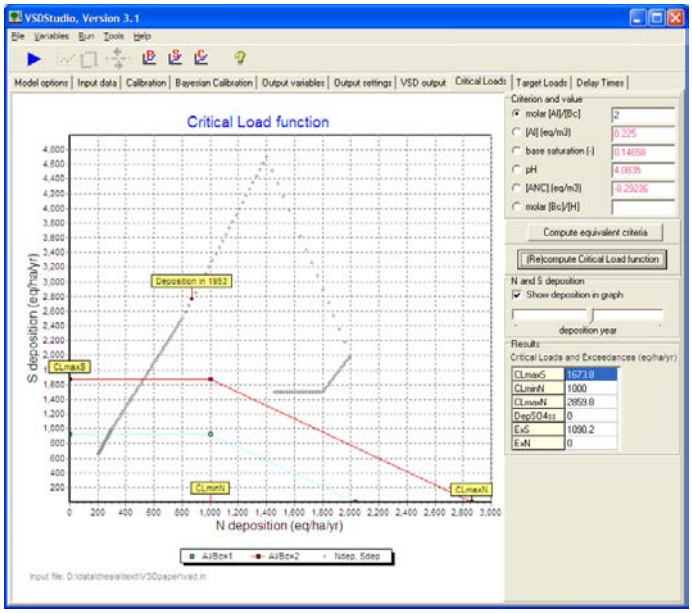

Figure 2.5. Critical Load screen of VSDStudio.

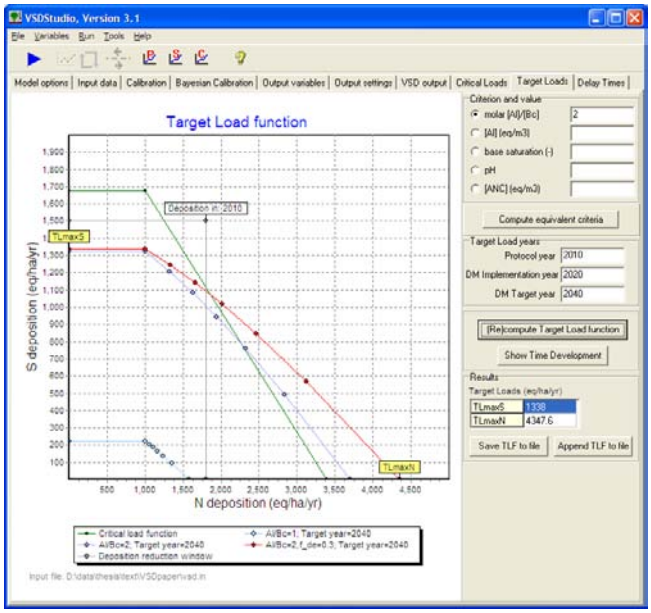

Figure 2.7. Target Load screen of VSDStudio.

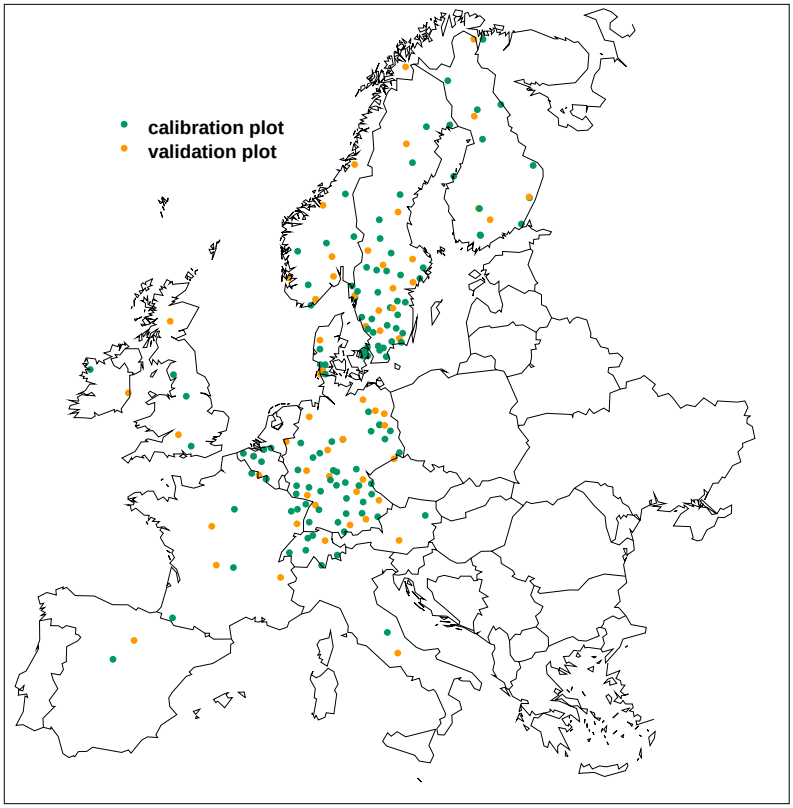

Figure 3.1. Location of the plots used for calibration and validation

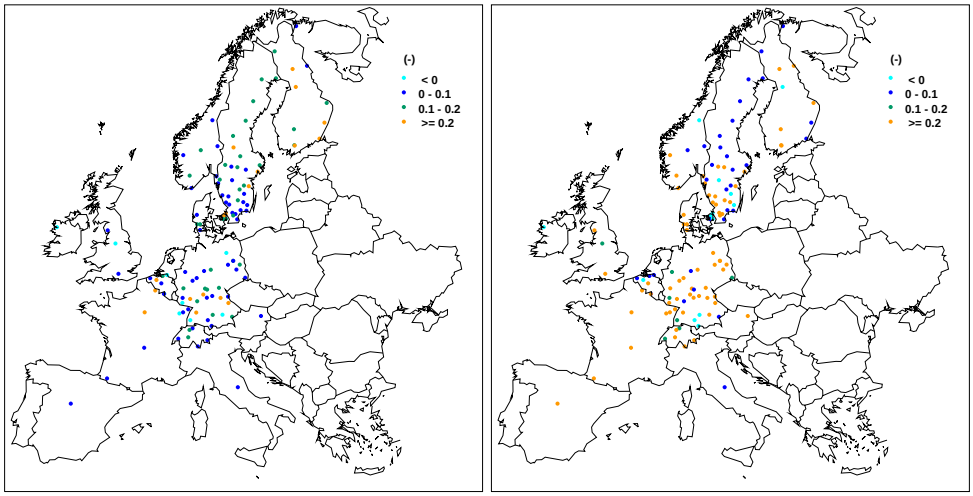

Figure 3.3. Gain in NRMSE for pH (left) and NO3(right) after calibration.

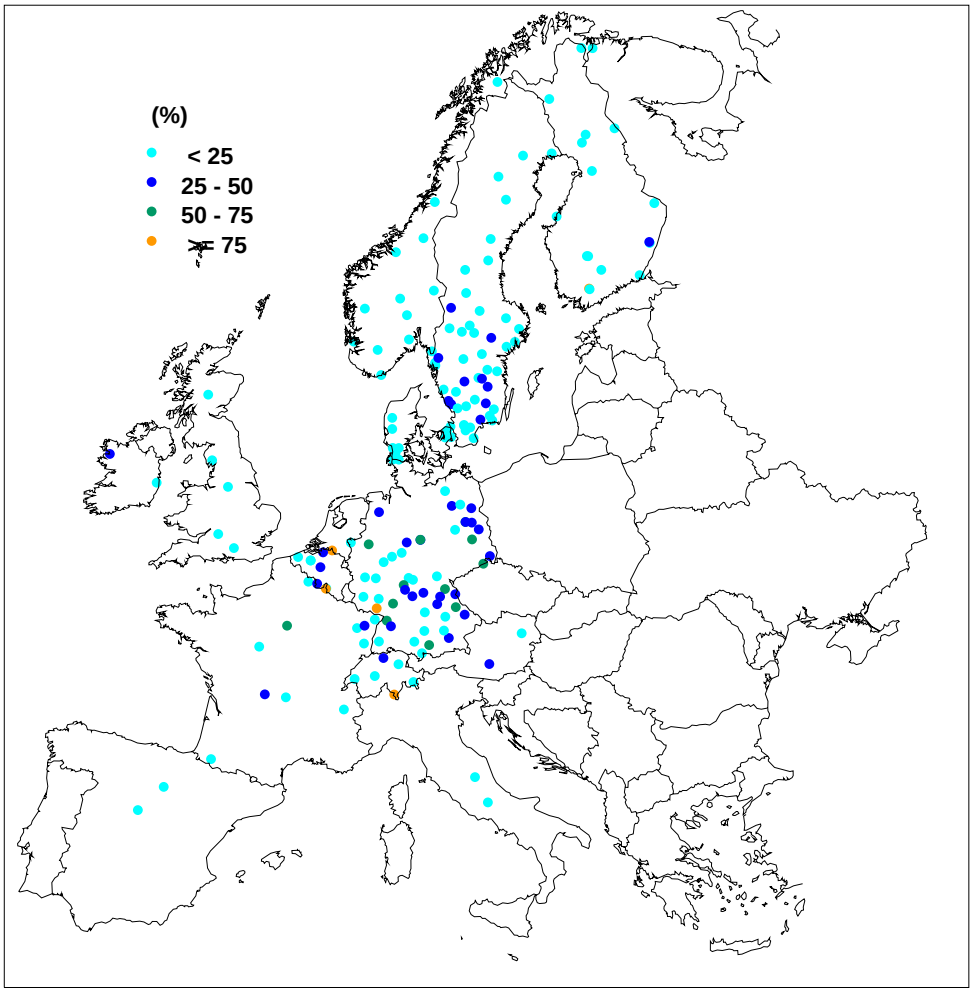

Figure 4.7. Geographical distribution of the percentage of runs where target loads are required to reach ANC=0 in 2050.

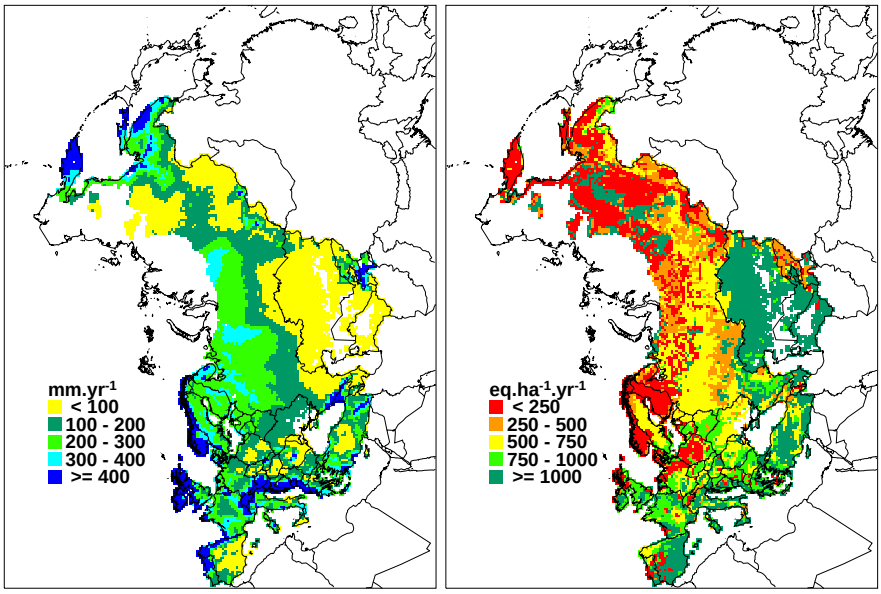

Figure 5.3. A: grid-median leaching flux from root zone (mm yr^{-1}); B: base cation deposition (eq ha^{-1} yr^{-1}).

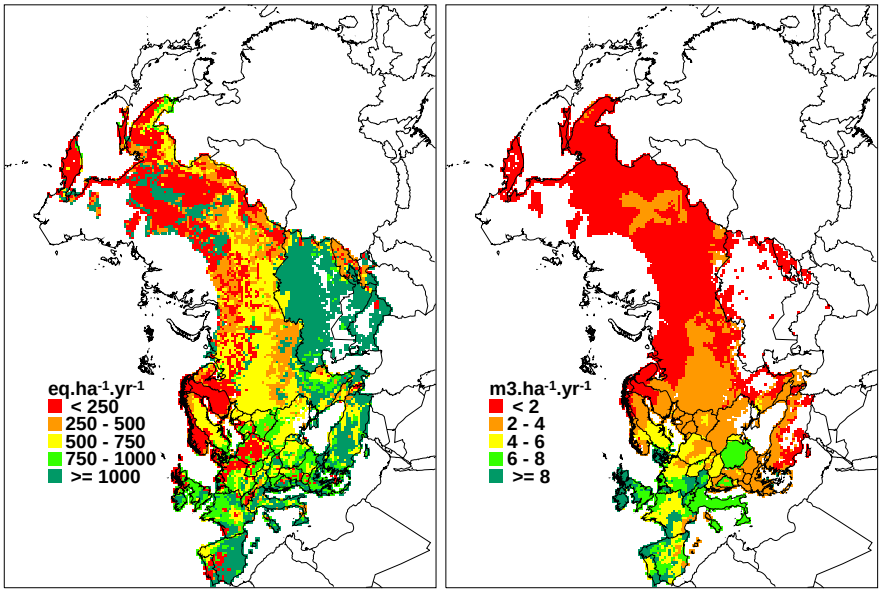

Figure 5.4. A: grid-median base cation weathering (eq ha^{-1} yr^{-1}); B: grid-median forest growth rate (m^3 ha^{-1} yr^{-1}).

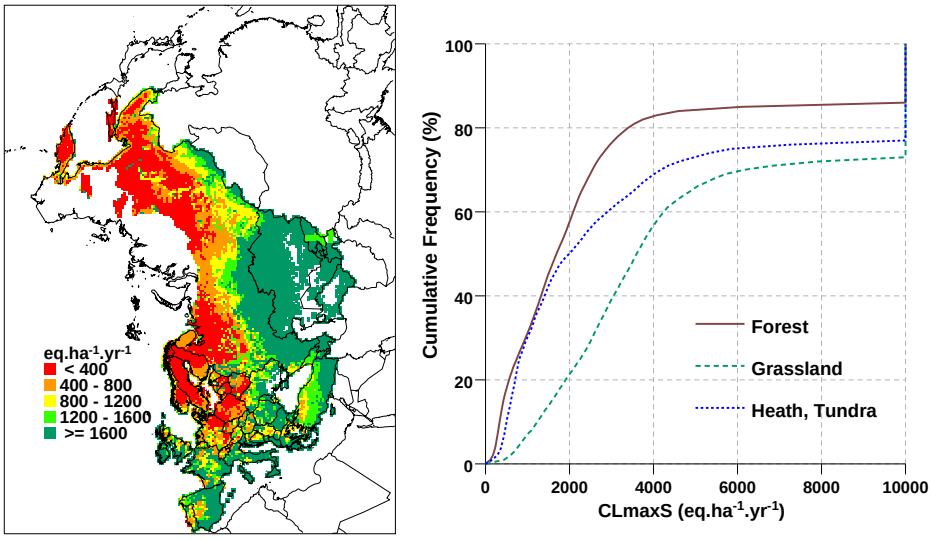

Figure 5.5. A: 5th percentile critical load $CL_{max}(S)$ (eq ha^{-1} yr^{-1}); B: cumulative frequency distribution of $CL_{max}(S)$ for three vegetation classes (eq ha^{-1} yr^{-1}).

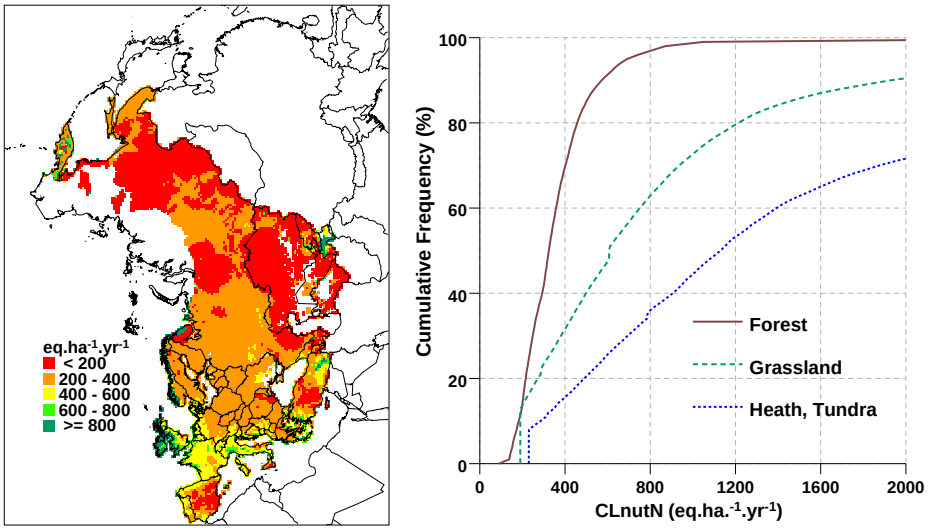

Figure 5.6. A: 5th percentile critical load $CL_{nut}(N)$ (eq ha^{-1} yr^{-1}); B: cumulative frequency distribution of $CL_{nut}(N)$ for three vegetation classes (eq ha^{-1} yr^{-1}).

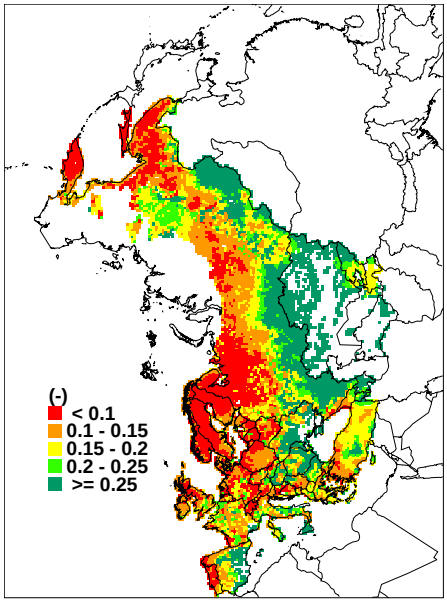

Figure 5.8. Average base saturation (-) per grid cell equivalent to ANC=0 for sensitive ecosystems.

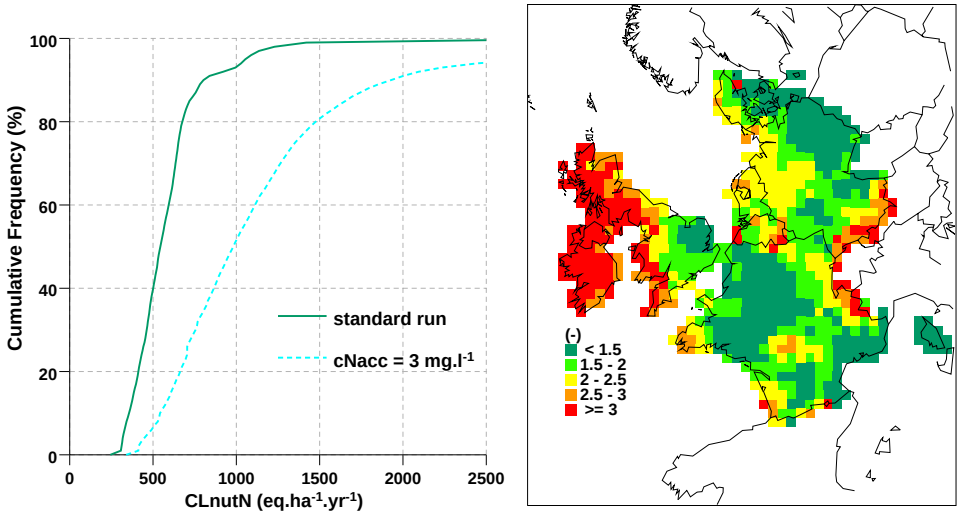

Figure 5.10. A: cumulative frequency distributions of $CL_{nut}(N)$ for forests in western Europe; B: ratio between the 5th percentile $CL_{nut}(N)$ with different values for $[N]_{acc}$.

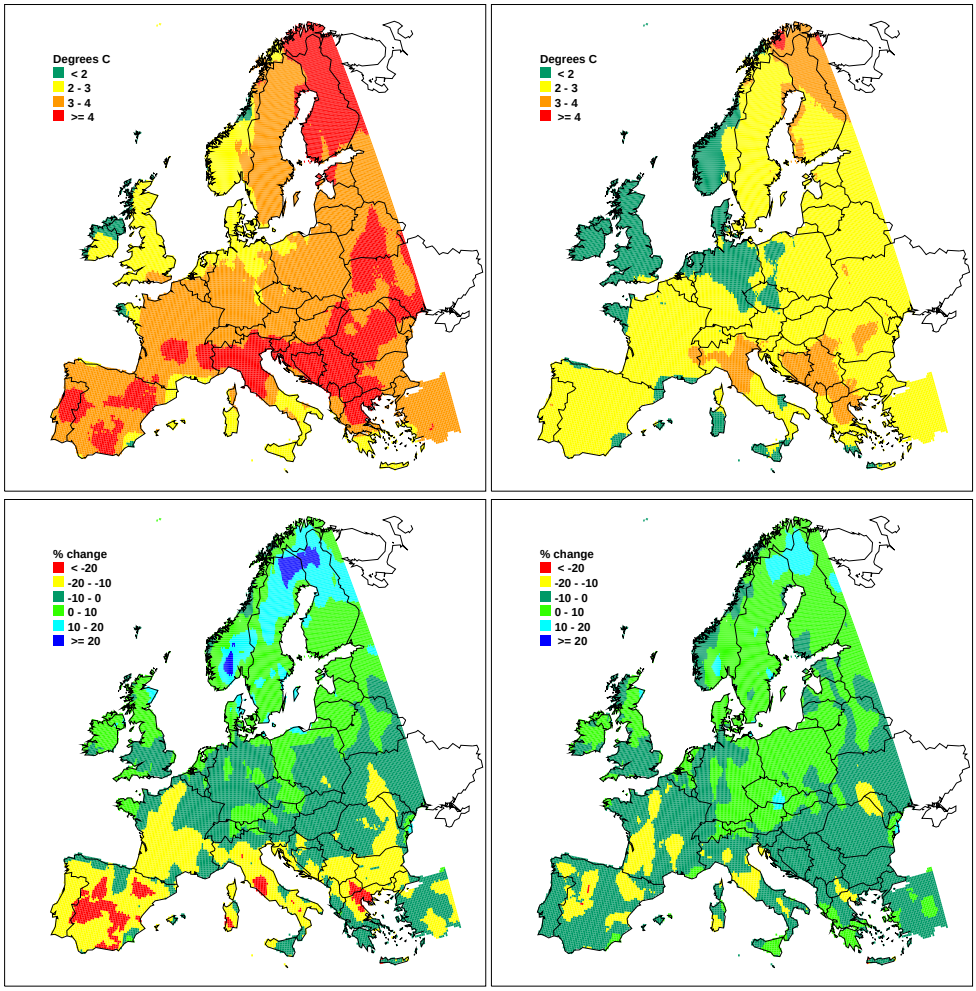

Figure 6.2. Absolute change in mean annual temperature (K) for IPCC SRES scenarios A1 (top left) and B2 (top right) and relative change in precipitation (in percent) for scenarios A1 (lower left) and B2 (lower right) between 1950 (2041-2060) and the reference period (1961-1990)

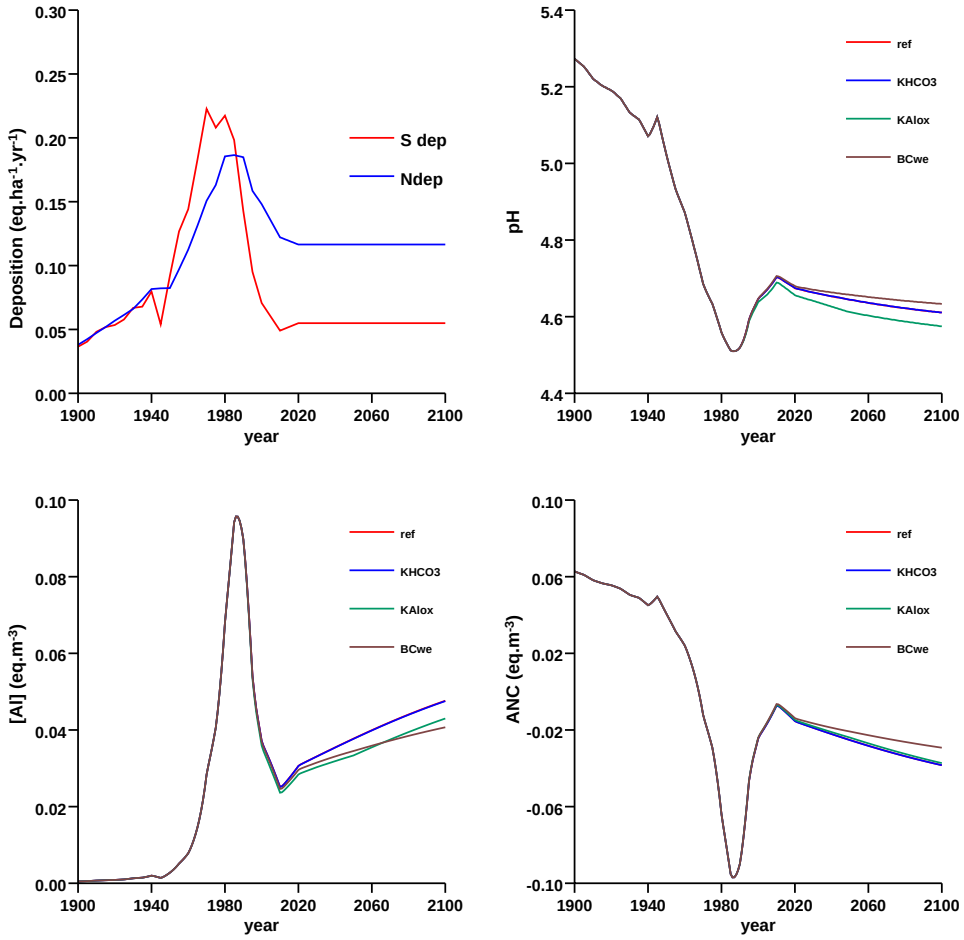

Figure 6.3. Influence of temperature change (upper left figure) from the A1 scenario on soil solution chemistry for a selected plot using the CLE deposition.effects are shown for pH (upper right), [Al] (lower left) and ANC (lower right).

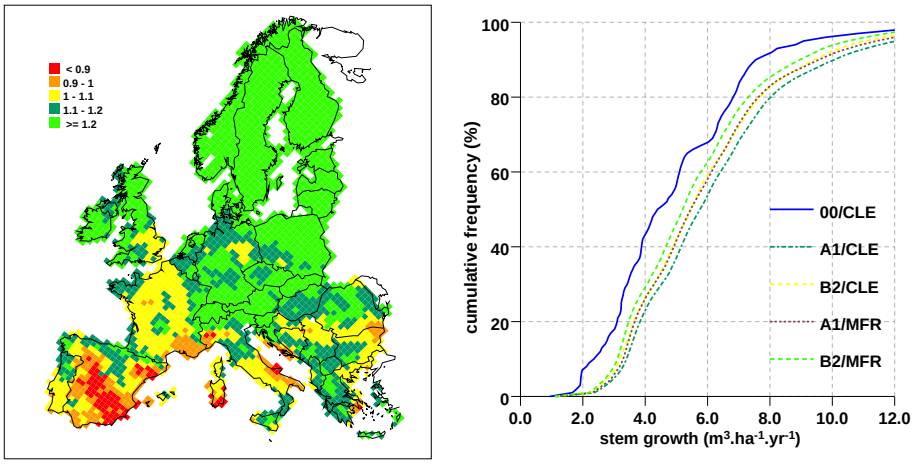

Figure 6.4. Growth under the A1 scenario in 2050 divided by the reference growth 1961-1990 (left) and cumulative frequency of modelled stem growth for two deposition (CLE, MFR) and three climate scenarios (His, A1,B2).

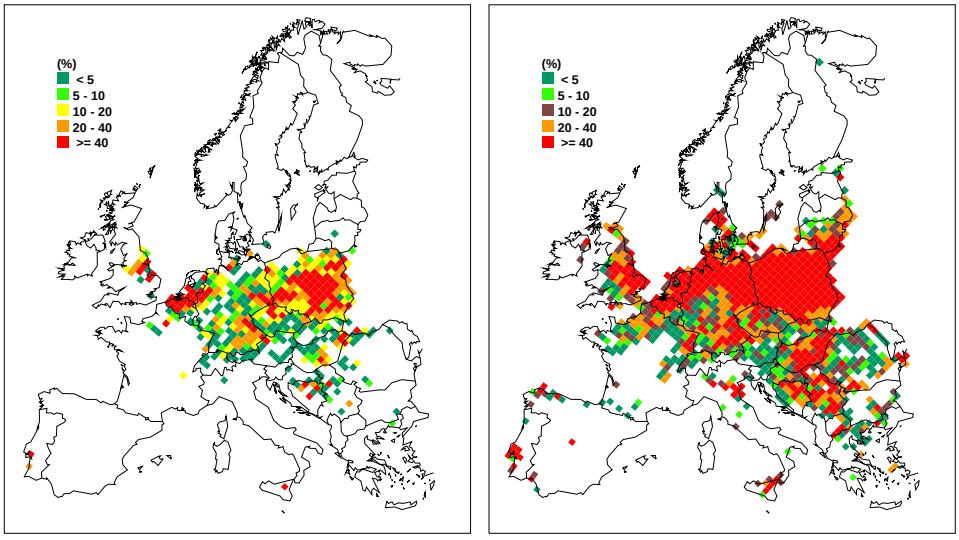

Figure 6.8. Percentage of forested area per EMEP grid cell with target loads < critical load (Case 2) for 2050 for Al/Bc=1 (left) and ANC=0 (right).

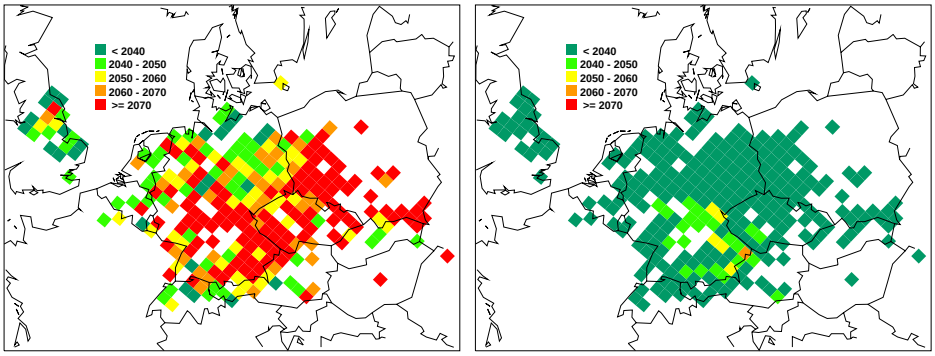

Figure 6.10. Average Recovery Times in central Europe for Al/Bc=1 per EMEP grid cell for the CLE scenario (left) and the MFR scenario (right) for those receptors for which a recovery time exists.